

eman ta zabal zazu



Universidad
del País Vasco

Euskal Herriko
Unibertsitatea



IVERSITÉ
DE PAU ET DES
PAYS DE L'ADOUR

Ecodynamics of metals and metalloids in Pyrenean lakes in relation to climate change and anthropogenic pressure

Bastien Duval

October 2020

***Supervised by:
Alberto de Diego
David Amouroux***

Remerciements

« *Do or do not. There is no try.* »

Et il avait raison le petit bonhomme vert ! La gestation fut longue et compliquée, mais enfin je vais pouvoir ajouter un livre à ~~ma bibliothèque~~ la bibliothèque de ma nouvelle colocataire. Marie, désolé d'avoir passé nos premières journées de vie commune sur mon ordinateur.

Ce manuscrit de thèse est loin d'être uniquement le fruit de mon travail, et des dizaines de personnes y ont contribué, de loin ou de près. Que ce soit d'un point de vue purement scientifique ou tout simplement grâce à un soutien morale et physique, merci à tous de m'avoir accompagné pendant ces quatre années.

Je tiens tout d'abord à remercier mes deux directeurs de thèse, Alberto De Diego et David Amouroux, pour la confiance que vous m'avez accordée. Alberto, merci de m'avoir remonté le moral dans les moments les plus durs grâce à un optimisme à toute épreuve. Merci à toi David, tu m'as appris que l'on pouvait travailler dans la rigueur tout en restant dans la bonne humeur ! L'autonomie que vous m'avez donnée, ajoutée à toutes les connaissances que vous m'avez apportées m'ont permis de grandir d'un point de vue professionnel. Là où je voudrais surtout vous remercier énormément, c'est tout simplement pour m'avoir donné le « goût de la montagne » Sans vous, et donc sans cette thèse, j'aurais probablement passé mes weekend d'été de ces quatre dernières années en mode farniente.

J'aimerais également remercier très fortement Emmanuel Tessier qui m'a constamment accompagné, que ce soit au labo ou sur le terrain. Merci pour ta patience (et il en a fallu !), et ton expertise dans tous les domaines (y compris sur l'ouverture des portes !!!). Les discussions sont toujours passionnantes avec toi.

Merci également à Luis Angel Fernández pour toutes les discussions que l'on a pu avoir sur la science et la vie en général, merci également pour tous tes conseils au laboratoire à l'UPV/EHU, ce fut un vrai plaisir de travailler avec toi.

Je souhaite remercier toutes les personnes du laboratoire IPREM (UPPA) et de l'IBeA (UPV/EHU) que ce soit pour votre aide au laboratoire ou sur le terrain : Kepa, Andrea, Alice, Javier, Nestor, Iciar, Marina, Mireia, Leire, Laura, Marizol. Belen, Thibaut, Gorka, Sylvain, Julien, Josean, Olaia, Silvia, Ainara, Cristina, Jérémy, Asmodée, Thomas etc ...

Spéciales remerciements également à Manue, Mathieu et Marine qui m'ont accueilli comme il se doit à l'Iprem, et à Robin, Cloé et Aurore que je bichonne encore tous les jours comme mes petits bébés *#levieuxc'estmoi*. Merci pour toutes les sorties, les randonnées, les repas, les weekend confinement / Age of Empire / bière (coucou Thomas !)

Merci également à tous ceux qui ont participé à la Mercury Conference 2019, quelle semaine !!!

Merci Gabriella Lobos pour la découverte de ce magnifique pays qu'est le Chili, j'espère pouvoir y revenir très rapidement !

Merci à l'Orchestre Arpège (meilleur orchestre de la Terre entière et même de l'Univers Intersidéral) pour les soirées détentes post-confinement !

Merci à ma famille, l'imputrescible Gégé, la magnifique Julie et ~~la capricieuse~~ sensible Tabtab je vous aime mes chéries adorés de tout mon cœur !!!! Vive les chuletón !!!

Et enfin un immense, incroyable et magnifique merci à l'amour de ma vie, Julia. Merci de ta patience, de ton soutien indéfectible et de ton amour tout simplement. Merci d'avoir toujours été là ses derniers mois, même quand je faisais ma tête de con. L'amour entre nous deux n'est jamais unidirectionnel, sache-le ! Si proto-docteur a su effectuer sa mue avec succès c'est forcément grâce à toi !

Abstract

The Pyrenean high mountain lakes are iconic elements of the landscape and the history of the territory. Their management and conservation, within the current context of climate change and increasing anthropogenic pressure, requires detailed knowledge of the biotic and abiotic processes running on them. This work has been carried out in the framework of a European project (REPLIM) that aims to investigate the past, present and future of lakes and peatbogs in the Pyrenees in a general context of global change. The thesis is the result of a collaboration between the UPV/EHU and the UPPA through a joint call to finance PhD Thesis in co-tutelage. Five sampling campaigns were carried out in 2017-2019 in more than 20 alpine lakes located in the Central Pyrenees. The collection and analysis of subsurface and deep-water samples allowed us to study the occurrence, geographical distribution, depth profiles and seasonal trends of a large array of chemical and physical parameters. Specifically, the fate of Potentially Harmful Trace Elements, the biogeochemistry of mercury species and the cycle of inorganic carbon were investigated in detail. In addition, a new analytical procedure based on the use of graphene nanoparticles for the measurement of mercury in natural waters was also proposed. Finally, two sediment cores from the Pyrenean lakes Marboré and Estanya were analysed to investigate mercury-cycling processes in them using Hg stable isotopic signature as a tracer

Keywords:

Pyrenees; alpine lakes; continental water; trace elements; mercury species; sediments; mercury isotopic analysis; acidification; inorganic carbon cycle

Table of Contents

1. Preface	1
1.1. REPLIM Project	2
1.2. PhD Project	4
2. General Introduction	7
2.1. Climate Change	8
2.2. Mountain Critical Zone: the case of the Pyrenees	11
2.3. High mountain lakes in the Pyrenees as witness of environmental changes	13
2.4. Potential Harmful Trace Elements (PHTEs)	16
2.5. Mercury	18
2.6. Objectives of the present study and experimental design	21
2.7. References	22
3. Sampling and analytical strategy	26
3.1. Studied areas	27
3.2. Sampling strategy	30
3.3. Analytical methods	34
3.3.1. Physicochemical parameters.....	34
3.3.2. Major anions	36
3.3.3. Major and trace cations	38
3.3.4. Organometals (Hg and Sn species).....	43
3.3.5. Dissolved Gaseous Mercury (DGM)	48
3.3.6. Mercury species incubations.....	50
3.3.7. Total selenium (se)	52
3.3.8. Silicate	53
3.3.9. Total Organic Carbon (TOC)	54
3.3.10. Carbon Dioxide (CO ₂) system parameters	56
3.4. References	61
4. Accurate determination of the total alkalinity and the CO₂ system parameters in high altitude lakes from the Western Pyrenees (France – Spain) 64	
4.1. Abstract.....	65
4.2. Introduction	66
4.3. Experimental section	69
4.3.1. Studied area and sampling.....	69
4.3.2. Analytical methods.....	71
4.3.3. Calculation procedures	71
4.4. Results and discussion	73
4.5. Conclusions	80
4.6. References	81
5. A simple determination of trace mercury concentrations in natural waters using Dispersive Micro-Solid Phase Extraction preconcentration based on functionalized graphene nanosheets	85
5.1. Abstract.....	86
5.2. Introduction	87
5.3. Material and methods	89
5.3.1. Preparation of nanoparticles suspension	89
5.3.2. Procedure for mercury preconcentration (optimum conditions).....	90

5.3.3.	Instrumentation and method for mercury analysis.....	91
5.3.4.	Calibration for mercury quantification	91
5.3.5.	Sampling of natural waters	92
5.4.	Results and discussion	93
5.4.1.	Optimisation of the Hg preconcentration method	93
5.4.2.	Optimization of the storage conditions	95
5.4.3.	Potential interferences: matrix effects	97
5.4.4.	Method blank levels and optimization	100
5.4.5.	Analytical performances	100
5.5.	References	103
6.	Occurrence, distribution and characteristics concentrations of Potential Harmful Trace Elements (PHTEs) in Pyrenean lakes and their relation to aquatic biogeochemistry	108
6.1.	Abstract.....	109
6.2.	Introduction.....	110
6.3.	Subsurface lake water geochemistry	112
6.3.1.	Physico-chemical characteristics and PHTEs concentrations	112
6.3.2.	Intra-lake variability	119
6.3.3.	Daily variations	122
6.3.4.	Filtered vs unfiltered trace element concentrations	124
6.4.	Lake classification	126
6.4.1.	Trophic status and water quality	126
6.4.2.	Classification of the lakes according to the water geochemistry	128
6.4.3.	Characteristic concentrations and major sources of Potential Harmful Trace Elements (PHTEs)	136
6.4.4.	Water column dynamic and trace elements distribution in selected alpine lakes	146
6.5.	References	153
7.	Biogeochemistry of mercury species in the water column of high altitude lakes of the Western Pyrenees (France-Spain).....	158
7.1.	Abstract.....	159
7.2.	Introduction.....	160
7.3.	Material and methods	161
7.4.	Results and discussion	161
7.4.1.	Major biogeochemical characteristics and « total » Hg in the aqueous phase	161
7.4.2.	Mercury speciation in subsurface water samples.....	162
7.4.3.	Mercury species distribution in the water column in selected alpine lakes ...	167
7.4.4.	Mercury species transformations in the water column in selected alpine lakes	174
7.5.	References	178
8.	Mercury stable isotopes in lacustrine archives to tracking human pollution and climate variability during the last 2000 years in the southern central Pyrenees (Aragon, Spain)	182
8.1.	Abstract.....	183
8.2.	Introduction	184
8.3.	Material and Methods	186
8.3.1.	Study Site.....	186

8.3.2.	Sediment sequence and age-depth models.....	187
8.3.3.	Mercury concentrations and fluxes	187
8.3.4.	Mercury stable isotopes composition.....	188
8.4.	Results and Discussion.....	190
8.4.1.	Variability of mercury accumulation rates.....	190
8.4.2.	Stable isotopes to refine mercury atmospheric sources and historical pollution in the Pyrenees	193
8.4.3.	Even-MIF isotope reflects Hg deposition pathways and climatic effects in the Pyrenees.....	198
8.4.4.	Comparing Hg stable isotope records in Lake sediment (Marboré) and Peat (Estibere) cores	202
8.5.	References	203

List of Figures

Figure 2.1: Observations and indicators of recent Climate Change induced by human activities. (a) Globally average combined land and ocean surface temperature anomaly; (b) Globally averaged sea level change; (c) Globally averaged greenhouse gas concentrations; (d) Global anthropogenic CO ₂ emissions. <i>From Climate Change 2014 Synthesis Report of the Intergovernmental Panel on Climate Change (IPCC)</i>	10
Figure 2.2: The mountain critical zone processes together with the potential impact of Climate Change (red lightning).....	11
Figure 2.3: Reconstruction of the mining-related pollution legacy in high-altitude lacustrine ecosystems (Lake Marboré) [9]	14
Figure 2.4: Typical mixing pattern for a dimictic lake	15
Figure 2.5: Typical summer thermal stratification. Lake is separated into three separate sections I) Epilimnion II) Metalimnion and III) Hypolimnion	15
Figure 2.6: Periodic table of the elements. Red framed elements are the PHTEs considered in this work	16
Figure 2.7: Global Hg budget in the main environmental compartments and pathways that are of importance in the global mercury cycle. <i>Figure from UNEP 2013 [27]</i>	19
Figure 2.8: The mercury geochemical cycle. Hg is methylated in anoxic environments. The toxic methylmercury accumulates in aquatic species (bioaccumulation), and its concentrations increase with each trophic level (biomagnification), causing a threat to humans whose diets rely on fish [35].....	20
Figure 3.1: Study area together with geological formations; red circle indicates position of the lakes, and colours indicate the elevation of the corresponding lakes.....	29
Figure 3.2: Transport of the material	30
Figure 3.3: Go-Flo sampler.....	32
Figure 3.4: Lake Sabocos (Replim5).....	33
Figure 3.5: Lakes from Ayous area: GEN (Replim5), BER (Replim3) and ROU (Replim5).....	33
Figure 3.6: Lakes from Panticosa area (Replim1): ARN, ORD, PAN, BAC, AZU, XUA, COA and PEC	33
Figure 3.7: Lakes from Cauterets area (Replim1): ARA, BAD, CAM, OPA, PEY, NER, POU and PAR	33
Figure 3.8: EXO2 multiparametric probe.....	36
Figure 3.9: Coefficient of determination R ² and the slope b associated to each linear regression between results obtained by ICP-MS and results obtained by HR-ICP-MS	41
Figure 3.10: Comparison of (a) MMHg concentrations (pg L ⁻¹) obtained in purged and unfiltered samples (Trend line $y = (0.73 \pm 0.06) x$; $r = 0.92$) and (b) iHg concentrations (pg L ⁻¹) obtained in purged and unfiltered samples (Trend line $y = (0.94 \pm 0.07) x$; $r = 0.92$)	48
Figure 3.11: In-field purging system	49
Figure 3.12: FIA manifold used for silicate determination	54
Figure 3.13: Equipment used for the determination of TA and DIC that includes the VINDTA 3C system coupled with a CM5015 coulometer and a 785 DMP Titrino.....	56
Figure 4.1: Location of the Pyrenean lakes considered in this study.....	69
Figure 4.2: Fitting between the experimental curve (black dots) and the calculated curve (red striped dots) for the titration of the lake AZU sample when TA and E ⁰ are refined.....	75
Figure 4.3: Fitting between the experimental curves (black dots) and the calculated curve (red striped dots) for the titration of the lake AZU sample when a) TA, E ⁰ and the a ₀ values in Equation 4.2 are	

refined, b) TA, E^0 and both the pK_a and the total concentration of the new acide-base species were refined and c) all the above mentioned parameters were simultaneously refined	76
Figure 5.1: Transmission Electron Microscopy TEM of (a) Graphene, (b) Graphene + APDC and (c) Graphene + APDC + Hg(II)	90
Figure 5.2: Recovery (n = 4) of Hg (a) as a function of the volume of nanoparticles suspension and (b) as a function of the time in the ultrasonic bath. Theoretical Hg (ng) as a function of the absorbance given by AMA-254 to (c) Rank 1 and (d) Rank 2 for 20 mL and 200 mL of water sample	94
Figure 5.3: Ratio between the recovery of Hg for the testing temperature T (n = 3) and the recovery of Hg for the reference temperature T_{ref}	97
Figure 5.4: Recovery of Hg (a) as a function of the concentration of natural organic matter (NOM) (n = 4) and (b) as a function of the concentration of sodium chloride (NaCl) (n = 5). Ratio (n = 2) between control samples (high purity water) and real samples from (c) Lake Des Carolins (freshwater) and (d) St Jean de Luz (seawater) as a function of the spiked mercury	99
Figure 6.1: (a) Major and trace elements (median concentrations above $1 \mu\text{g L}^{-1}$) and (b) ultra-trace elements (median concentrations below $1 \mu\text{g L}^{-1}$) concentrations in unfiltered subsurface water samples of the 20 studied lakes over the four sampling campaigns. Dots are minimum and maximum, white circles and black crosses are extreme values, bars indicate 10 th and 90 th percentile, boxes indicate 25 th and 75 th , marks within each box are medians and red crosses are mean.	118
Figure 6.2: Relative Standard Deviation (RSD) calculated for each (a) major and trace element and (b) ultra-trace element considered using the results obtained after the analysis of the three samples collected at different parts of each lake. Bars indicate 10 th and 90 th percentile, boxes indicate 25 th and 75 th , marks within each box are medians and red crosses are mean.	121
Figure 6.3: Dissolved Fraction (DF) in subsurface water samples calculated for each major, trace and ultra-trace element considered using the results obtained by ICP-MS. Dots are minimum and maximum, white circles and black crosses are extreme values, bars indicate 10 th and 90 th percentile, boxes indicate 25 th and 75 th , marks within each box are medians and red crosses are mean. For each element, the number n of samples above the LOD for both filtered and unfiltered samples are indicated.	125
Figure 6.4: Trophic State Index (TSI) calculated for all the sampled lakes according to the sampling campaign. TSI below the dashed line (TSI = 40) indicate oligotrophic lakes. Error bars for Lakes ARA, GEN, AZU and SAB are associated to the samples from different times of the day	127
Figure 6.5: Relation between TOC and NO_3^- with ΔTOC corresponding to the increase of TOC between spring value and autumn values, and ΔNO_3^- corresponding to the decrease of NO_3^- between spring value and autumn values	128
Figure 6.6: Loading plots on the PC1-PC2 and PC1-PC3 planes obtained after Principal Component Analysis of the dataset	130
Figure 6.7: Score plots on the PC1-PC2 and PC1-PC3 planes obtained after Principal Component Analysis of the dataset	131
Figure 6.8: Ca concentrations and TA values according to the classification extracted from the PC1, importance of the weathering supplying alkalinity: Low (Lakes CAM, PEY, OPA, NER, POU, GEN, ROU, BER, ARN, BAC, PEC, COA, PAN and XUA), Medium (Lakes ARA, BAD, AZU and ORD) and High (Lake SAB)	132
Figure 6.9: Na and Cl^- concentrations according to the classification extracted from the PC2, importance of the marine influence: Very weak (Lakes ARA, BAD, CAM, PEY, OPA, NER, POU, AZU, ARN, BAC, PEC, COA, XUA and SAB) and Weak (Lakes GEN, ROU, BER, PAN and ORD)	133
Figure 6.10: Negative correlation between elevation and i) Na and ii) Cl^- concentrations (SAB not considered)	134
Figure 6.11: Concentrations of SO_4^{2-} as a function of Mg concentrations. Black dashed line is the threshold set up at 0.7 mg L^{-1} to distinguish between atmospheric and geological supply of SO_4^{2-} : below this limit SO_4^{2-} is mainly originated from atmospheric depositions. Significant correlations between SO_4^{2-} from geological supply and Mg have been found ($r = 0.98$ for Lakes AZU and ARN; $r = 0.77$ for Lakes ARA, BAD, BAC, PEC, PAN and ORD)	135

Figure 6.12: Enrichment factors (EF) for unfiltered subsurface water samples using concentration ratios in the upper continental crust (UCC) and in the Maladeta (MDT) bedrock. Green boxes have been generated using data from low alkaline lakes (Category 1) and blue boxes have been generated using data from medium and high alkaline lakes (Categories 2 and 3). Dots are minimum and maximum, bars indicate 10 th and 90 th percentile, boxes indicate 25 th and 75 th , marks within each box are medians and red crosses are mean.....	143
Figure 6.13: Depth profiles of temperature, percentage of dissolved oxygen saturation, chlorophyll-a (RFU) and the chemical parameters obtained during (a) the third sampling campaign(Spring 2018) and (b) the fourth sampling campaign (Autumn 2018) in Lake Azules	149
Figure 6.14: Depth profiles of temperature, percentage of dissolved oxygen saturation, chlorophyll-a (RFU) and the chemical parameters obtained during (a) the third sampling campaign(Spring 2018) and (b) the fourth sampling campaign (Autumn 2018) in Lake Arratille	150
Figure 6.15: Depth profiles of temperature, percentage of dissolved oxygen saturation, chlorophyll-a (RFU) and the chemical parameters obtained during (a) the third sampling campaign(Spring 2018) and (b) the fourth sampling campaign (Autumn 2018) in Lake Sabocos	151
Figure 6.16: Depth profiles of temperature, percentage of dissolved oxygen saturation, chlorophyll-a (RFU) and the chemical parameters obtained during (a) the third sampling campaign(Spring 2018) and (b) the fourth sampling campaign (Autumn 2018) in Lake Gentau	152
Figure 7.1: Boxplot representations of unfiltered and filtered iHg, MMHg and percentage of MMHg (calculated as ratio between MMHg and Mercury Dissolved Ionic Compound (MDIC = MMHg + iHg), and DGM and percentage of DGM (calculated as ratio between DGM and Total Mercury (THg = MMHg + iHg + DGM)) in subsurface water samples of the 19 studied lakes. Bars indicate 10 th and 90 th percentile, boxes indicate 25 th and 75 th , marks within each box are medians, and red crosses are mean	166
Figure 7.2: Daily variation of DGM in Lakes Arratille, Gentau and Sabocos	167
Figure 7.3: Depth profiles of temperature, percentage of dissolved oxygen saturation, chlorophyll-a (RFU) and some chemical parameters including mercury speciation obtained during (a) the third sampling campaign(Spring 2018), (b) the fourth sampling campaign (Autumn 2018) and (c) the fifth sampling campaign (Spring 2019) in Lake Gentau	170
Figure 7.4: Depth profiles of temperature, percentage of dissolved oxygen saturation, chlorophyll-a (RFU) and some chemical parameters including mercury speciation obtained during (a) the third sampling campaign(Spring 2018), (b) the fourth sampling campaign (Autumn 2018) and (c) the fifth sampling campaign (Spring 2019) in Lake Sabocos.....	171
Figure 7.5: Depth profiles of temperature, percentage of dissolved oxygen saturation, chlorophyll-a (RFU) and some chemical parameters including mercury speciation obtained during (a) the third sampling campaign (Spring 2018) and (b) the fourth sampling campaign (Autumn 2018) in Lake Arratilles.....	172
Figure 7.6: Depth profiles of temperature, percentage of dissolved oxygen saturation, chlorophyll-a (RFU) and some chemical parameters including mercury speciation obtained during (a) the third sampling campaign(Spring 2018) and (b) the fourth sampling campaign (Autumn 2018) in Lake Azules	173
Figure 8.1: Study Sites: Lakes Marboré (42°41'N; 0°2'E, 2612 m asl) and Estanya (42°02'N; 0°32'E, 670 m asl).....	186
Figure 8.2: (a) From bottom to top, variation overtime (same axis x) of $\Delta^{200}\text{Hg}$, $\Delta^{199}\text{Hg}$, $\delta^{202}\text{Hg}$ and Hg Accumulation Rates (HgAR) in Lakes Marboré and Estanya; (b) $\Delta^{199}\text{Hg}$ comparison, starting from 905 CE, between Lake Marboré (This work) and Estibere Peat (Enrico et al., 2017) [33]	192
Figure 8.3: $\delta^{202}\text{Hg}$ vs $\Delta^{199}\text{Hg}$ plot for both Lakes Marboré and Lake Estanya together with literature data: both MDF and odd-MIF increase along with contamination.....	196
Figure 8.4: (a) $\Delta^{199}\text{Hg}$ vs 1/HgAR plot for both Lakes Marboré and Lake Estanya with strong linear relationship for lake Marboré; (b) $\delta^{202}\text{Hg}$ vs 1/HgAR plot for both Lakes Marboré and Lake Estanya	197
Figure 8.5: $\Delta^{201}\text{Hg}$ vs $\Delta^{199}\text{Hg}$ plot for both Lakes Marboré and Lake Estanya together with the theoretical slope for aqueous photoreduction (Bergquist and Blum, 2007) [22].....	197

Figure 8.6: (a) $\delta^{202}\text{Hg}$ vs $\Delta^{200}\text{Hg}$ plot for both Lakes Marboré and Lake Estanya together with typical wet (cloud waters and precipitations) and dry (GEM) deposition Hg isotope signatures in the Central Pyrenees (Enrico et al., 2016 [18]; Fu et al., 2016 [34]); (b) Chronology of Hg wet deposition in Lake Marboré and Estanya; (c) Chronology of Hg wet deposition in Lake Estanya..... 200

Figure 8.7: (a) $\Delta^{204}\text{Hg}$ vs $\Delta^{200}\text{Hg}$ plot for both Lakes Marboré and Lake Estanya together with typical wet and dry deposition Hg isotope signatures in the Central Pyrenees (Enrico et al. 2016 [18]; Fu et al., 2016 [34]): evidence for derived end-member; (b) $\delta^{202}\text{Hg}$ vs $\Delta^{204}\text{Hg}$ plot for both Lakes Marboré and Lake Estanya together with typical wet and dry deposition Hg isotope signatures in the Central Pyrenees (Enrico et al., 2016 [18]; Fu et al., 2016 [34])..... 201

List of Tables

Table 3.1: Some physical characteristics of the sampled lakes.....	29
Table 3.2: Overall of the sampling strategy.....	32
Table 3.3: LOD for major anions analysis	37
Table 3.4: Operating conditions for the ICP-MS and the HR-ICP-MS	39
Table 3.5: LOD and analytical uncertainties for major and trace cations analysed by ICP-MS and HR-ICP-MS	42
Table 3.6: Operating conditions of the GC-ICP-MS	46
Table 3.7: Operating conditions for the incubation experiments	51
Table 3.8: Summary of the parameters analysed together with their associated analytical protocol ...	59
Table 4.1: Values of the $a_0 - a_5$ parameters used in the calculation of the stoichiometric constants of the carbonate system [15]	72
Table 4.2: Salinity, DIC, NPOC and silicate concentrations measured in sub-surface waters of the lakes	73
Table 4.3: Values of the refined parameters as well as the residual sum of squares (RSS), along with their uncertainties, calculated with the help of the Microsoft Excel macro SolverAid when 1) TA and E_0 are refined, 2) TA, E_0 and the a_0 values in Equation 4.2 were refined, 3) TA, E_0 and both the pK_a and the total concentration of the new acid-base species [New-Spe] were refined and 4) when all the above mentioned parameters were refined.....	77
Table 4.4: Values of all the parameters used to characterise the CO_2 system (TA, DIC, pH and fCO_2) as well as the predicted new acid-base species concentration and pK_{new} values of the studied lakes	78
Table 5.1: Storage design for isochronous measurements to evaluate stability of the filters	96
Table 5.2: Methods for analysis of mercury species in natural waters	102
Table 6.1: Main chemical parameters of the studied lakes measured by the multiparametric probe (temperature, conductivity, redox potential), the TOC analyser (TOC as NPOC), Flow Injection Analysis (Silicate), the VINDTA 3C Instrument (DIC, Total Alkalinity) and the ionic chromatograph (Cl^- , NO_3^- and SO_4^{2-}). pH was calculated according to Kortazar et al. (2020) [39]. Chlorophyll-a is not mentioned as it was always below LOD. Dissolved oxygen, as mentioned in Chapter X, was calibrated only once before each sampling campaign and the sensor is sensitive to elevation: the whole lakes were oversaturated in subsurface but the values measured differ among lakes because of elevation. All the methodological details can be found 3.Sampling and analytical strategy.	117
Table 6.2: Temperature, pH and concentrations of several elements measured in water samples collected in four selected lakes at different times of the day.....	123
Table 6.3: Loadings of the variables on PC1, PC2 and PC3 after Principal Component Analysis of the dataset. Bold value are significant at 95 % confidence interval	130
Table 6.4: Scores of the observations on PC1, PC2 and PC3 after Principal Component Analysis of the dataset, together with the proposed classification of these lakes: for PC1, Class 1 (Score < 0) / Class 2 (0 < Score < 3) and Class 3 (Score > 3); for PC2, Class 1 (Score < 0) / Class 2 (Score > 0); for PC3, Class 1 (Score < 0.5) / Class 2 (Score > 0.5).....	131
Table 6.5: Characteristic concentrations for unfiltered subsurface water samples as minimum, median and maximum concentration as well as the calculated threshold for each PHTEs for our study together with data extracted from bibliography (remote and alpine lakes).....	142
Table 6.6: Summary of the results obtained after multiple linear regression of data conducted on each PHTEs using 21 various variables (Catchment influence, Elevation, Maximum depth, Temperature, pH, Ca, Na, Mg, K, Al, Sr, Fe, Mn, Ba, Ti, Cl^- , NO_3^- , SO_4^{2-} , TOC, Silicate and Total Alkalinity) according to the geological classification of the studied lakes (Low Alkaline vs Medium and High Alkaline Lakes). Significant variables with its normalized coefficient associated are shown in this table, together with the equation of the model.....	144

Table 7.1: Comparison of filtered and unfiltered inorganic mercury (iHg), monomethylmercury (MMHg) and Dissolved Gaseous Mercury (DGM) concentrations in the subsurface water samples of the 20 studied lakes with literature data for worldwide pristine areas (oceans, boreal lakes, high altitude lakes) and local areas (freshwaters and estuary). %MMHg is calculated as the ratio between MMHg and Mercury Dissolved Ionic Compound (MDIC = MMHg + iHg). %DGM is calculated as ratio between DGM and Total Mercury (THg = MMHg + iHg + DGM). *THg, **Reactive Hg and ***Surface and Depth samples 165

Table 7.2: Methylation (M), Demethylation (D) and Reduction (R) potentials (mean \pm SD, n=3 for M and D, n=2 for R) in unfiltered waters performed under light and dark conditions at different depths for Lakes Gentau, Sabocos and Arratilles and for sampling campaigns Spring and Autumn 2018 and Spring 2019, together with data from literature. Detection limits are 0.03, 4 and 0.3 % day⁻¹ for Methylation, Demethylation and Reduction yields, respectively. n.d. is not determined. 176

Table 7.3: Methylation (M), Demethylation (D), Mercury Loss (ML) and Reduction (R) potentials (mean \pm SD, n=3 for M, D and ML, n=2 for R) in unfiltered waters performed under light and dark conditions at different depths for Lake Gentau for sampling campaigns Spring and Autumn 2018 and Spring 2019. Detection limits are 0.03, 4 and 0.3 % day⁻¹ for Methylation, Demethylation and Reduction yields, respectively. n.d. is not determined. 177

Table 8.1: Mean values (\pm 2SD) of Hg isotopic composition obtained for reference materials: NIST-8610 (UM-Almadén) and IAEA-405 (estuarine sediment)..... 189

1.Preface

1.1. REPLIM Project

The Pyrenean high mountain lakes and peat bogs are iconic elements of the landscape and the history of the territory. Their management and conservation, within the current context of climate change and increasing anthropogenic pressure, requires a detailed knowledge of the biotic and abiotic processes in these systems, which should include their natural variability and the synergistic effects of the anthropogenic activities on the climate change. The REPLIM project, “Network of observatories of sensitive ecosystems (lakes, wetlands) to Climate Change in the Pyrenees”, aims to establish a monitoring network in lakes and peat bogs of the Pyrenees in order to characterize the impact of climate change on these vulnerable mountain ecosystems, both locally and throughout the territory. The REPLIM network will also make it possible to identify the impacts that occurred before the industrial revolution and the Great Acceleration of the second half of the 20th century, and quantify the most recent ones. Finally, the REPLIM project will attempt to model the effects that the projected climate change will have on these ecosystems in the near future.

REPLIM aims to contribute to the challenge of assessing the impact of climate change in the territory and the development of mitigation and adaptation policies based on scientific knowledge. To this end, REPLIM focuses on increasing the cooperation between scientists, managers and citizens from the Pyrenean area, to establish a network of observatories of lakes and peatlands that make possible to characterize the climate change and its effects along the Pyrenees.

The main objectives of the project are to:

- Establish a monitoring network of lakes and peatlands that brings together scientists and managers specialized in climate change research in high mountain systems
- Define the most appropriate protocols for the characterization of the impacts of CC and human activities in the lakes and peat bogs of the Pyrenees
- Prepare a report on the current situation of the lakes and peat bogs of the Pyrenees, their recent evolution and the possible impacts of the climate change on them
- Encourage and Integrate citizen science activities into the network

With the aims of identifying the most appropriate protocols and indicators to characterize the effects of climate change and on high mountain lakes and peat bogs in the Pyrenees, a multidisciplinary methodology will be applied to the sites of the network. It will include the:

- Installation of temperature sensors at different depths and sediment traps in lakes
- Installation of piezometers to periodically determine the water table depth in peatlands
- Determination of periodic output flow in peatland using permanent weirs
- Seasonal measurements of the chemical composition and some biological properties in waters
- Measurement of greenhouse gas fluxes in peatlands

- Development of common procedures to be followed to carry out the samplings and subsequent analytical determination in the selected lakes and peatlands
- Processing of the monitoring results in order to know the physicochemical and biological state of the selected lakes and peatlands
- Development of participation and citizen science programs that will make the public aware of the impacts of climate change, helping to define a management strategy integrated with the social and economic development of the Pyrenean territory
- Presentation of the final results in an interactive geoportal to allow the dissemination of results to managers and citizens and facilitate the understanding of the effect of the climate change on these sensitive ecosystems

The results of REPLIM will contribute to the development and implementation of the Pyrenean Climate Change Observatory strategy and action plan for the 2016-2019 period.

The main expected results of the project will be the:

- Establishment of a network of climate change observatories located in Pyrenean lakes and peatlands that are sustainable and lasting over time.
- Publication of a methodological manual describing the monitoring protocols in the field applicable to the requirements of the Habitats Directive (HD) and the Water Framework Directive (WFD).
- Development of computer tools for the collection, storage and management of the information generated, in order to assess the impacts of climate change on sensitive high mountain ecosystems.
- Substantial improvement of the knowledge of the current status of the selected Pyrenean peat bogs and lakes, as well as their evolution in recent centuries and their status at the beginning of the 20th century, prior to global warming. Moreover, the project will give valuable information to assess the potential effect of future scenarios of climate change in lakes and peat bogs.
- Promotion of citizen participation for the collection of data in the selected ecosystems thereby increasing awareness of the problems related to climate change.

REPLIM is a cross-border network of research institutions (Spanish National Research Council, Aragon and Catalonia; National Centre for Scientific Research, Occitanie; University of Pau and Pays de l'Adour, Nouvelle-Aquitaine; University of the Basque Country, Basque Country; University of Navarra, Navarra; Centre de Recerca Ecològica i Aplicacions Forestals, Catalonia) whose research area focus specifically on lakes and wetlands, and their relationship with Climate Change.

1.2. PhD Project

Keeping in mind that high altitude lakes are sentinels of global environmental change related to climate variability and anthropogenic pressure, this PhD project aims to evaluate how specific lake ecosystems in the Pyrenees are affected by metal and metalloid contamination and how such contamination can be constrained by climatic, hydrological and local to long-range anthropogenic inputs.

The work presented here is the result of joined actions carried out by two of the research groups involved in the REPLIM: the IBeA (University of the Basque Country, UPV/EHU) and the IPREM (University of Pau and Pays de l'Adour, UPPA). They are fairly complementary in the field of analytical and environmental chemistry. The knowledge and equipment provided by these two groups allow them to get precise information about trace metals and metalloids in particular.

The Basque group (IBeA, Ikerketa eta Berrikuntza Analitikoa) led by Juan Manuel Madariaga is part of the Department of Analytical Chemistry in the University of the Basque Country (UPV/EHU). It counts with a long experience in the analysis of chemicals, both organic and inorganic, in a broad range of environmental samples, from solid (sediment, soil, particulate, vegetal and animal tissues) to liquid ones (natural and sewage water) using both direct non-destructive techniques (Raman, IR, XRF spectroscopy, LIBS) and more conventional destructive ones (GC-MS, GC-MS/MS, LC-MS/MS, ICP-MS and GC-ICP/MS). The group also addresses a deep knowledge of different statistic and chemometric techniques for multivariate data treatment and interpretation. General facilities for sample collection and treatment are hosted in its laboratories, including sediment and water samplers, passive sampling devices, freeze-driers, planetary ball mills, microwave ovens and focused ultrasound sonicators and facilities for long-term sample storage.

The IPREM (Institute of Analytical Sciences and Physico-Chemistry for Environment and Materials) aims to the development of fundamental knowledge in physico-chemistry, analytical chemistry and microbiology, in relation to applications concerning the structure of the living, the management of the environment and the functional properties of different classes of materials. This institute organizes its researches around three different poles: Analytical, Physical and Theoretical Chemistry (CAPT), Physico-chemistry of surfaces and polymer materials (PCM), and Environmental Chemistry and Microbiology (CME). This last has been pioneering the development of innovative methods of speciation analysis since now more than 2 decades to understand biogeochemical cycles and environmental impacts of trace elements and metals in the environment. Part of its work is based in laboratory experiments to better characterize the molecular forms of trace elements and metals, the mechanisms of their transformations and the relative contribution of biotic and abiotic processes. To improve the knowledge on the origin, anthropogenic contribution of chemical forms of trace metals in the environment and, study the environmental mechanisms of isotopic fractionation, analytical methods are also developed to determine the isotopic composition of trace elements and metals "at the molecular level". The CME team leans on various analytical means including several equipment of mass spectrometry for elemental (Q-ICP-MS, HR-ICP-MS), molecular (ESI QTOF, ESI MS/MS), speciation (GC-ICP-MS) and isotopic (MC-ICP-MS) analysis. To improve the knowledge on the contribution of

chemical forms in the environment, this team has an advanced experience in coupling gas-chromatography with MC-ICP-MS to achieve compound specific isotopic analysis (CSIA) of mercury. The group also counts with sampling devices for atmospheric, aquatic and sediment samples, clean labs sample handling and sample preparation techniques (Hotblock, Microwave, High pressure Asher). The PhD project, conducted over four years, has resulted in five sampling campaigns conducted in 20 lakes, with more than 180 water samples collected. This cross-border collaboration brought new insights about high mountain lakes from the Pyrenees, using a physico-chemical point of view. Both laboratories were fully involved and more than 40 people participated in either the sampling campaigns or the analysis of the collected samples. Innovation and knowledge of both laboratories also lead to the creation of a new and simple methodology for the determination of trace mercury in water samples. Finally, collaboration with other cross-border partners contributes to the knowledge of the mercury biogeochemical cycle in lakes using mercury isotopic analysis in lake sediments. All this work has been presented in international conferences (Spectratom 2018 Conference, ISOBAY 18, European Winter Conference 2019, Goldschmidt Conference 2019, ICMGM 2019) and part of this work has been already published in recognized journals (Microchemical Journal, Science of the Total Environment Journal). The following PhD manuscript gather all the methodologies, results and discussions about this four years work.

2. General Introduction

2.1. Climate Change

Climate Change (CC) is an evolution of the climate corresponding to a lasting change (from decades to million years) from statistical parameters of the global Earth's climate or of various regional climates. These changes can be either due to intrinsic processes to the Earth, or more recently to the human activities. Indeed, since the industrial revolution, the climate has increasingly been affected by human activities, mainly as greenhouse gas emission, which are causing global warming and climate change.

Climate Change research has taken additional relevance to the realization that human activities can accelerate Climate Changes. Indeed, warming of the climate is unequivocal, and since the 1950s, many of the observed changes are unprecedented over decades to millennia. The atmosphere and ocean have warmed, the sea level has risen and the greenhouse gas concentrations have increased (**Figure 2.1**). Other direct and/or indirect changes in the global or regional climate parameters have been observed. Regions of high salinity, where evaporation dominates, have become more saline, while regions of low salinity, where precipitation dominates, have become fresher since the 1950s. Uptake of CO₂ by the ocean is also responsible for ocean acidification. Indeed, around 30 % of CO₂ emitted is absorbed by the oceans, lowering its concentration in the atmosphere but making the oceans more acidic: the pH of ocean surface water has decreased by 0.1, corresponding to a 26 % increase in acidity [1]. Worldwide, snow cover decreases under the global warming, highlighted by the melting of the permafrost, of the Arctic sea-ice extent, the glacial retreat.

The primary cause of this global change is the increasing atmospheric concentrations of greenhouse gases, occurring mainly since the pre-industrial era. This has led to atmospheric concentrations of carbon dioxide, methane and nitrous oxide that are unprecedented in at least the last 800,000 years. CO₂ is the primary greenhouse gas. It enters the atmosphere through burning fossil fuels (coal, natural gas, and oil), solid waste, trees and other biological materials, and because of certain chemical reactions (e.g., manufacture of cement). CO₂ is removed from the atmosphere (or "sequestered") when plants absorb it as part of the biological carbon cycle. Apart from forest, oceans [1], and wetlands [2] are also known as sinks of CO₂ and participate actively in the cycle of this important greenhouse gas. The case of lakes is more complex but inland lakes emit CO₂ to the atmosphere [3]. Nevertheless, their low buffer capacity, in particular in high-altitude and remote lakes, threatens this equilibrium between surface lake water and atmosphere.

In recent decades, changes in climate have caused impacts on natural and human systems on all continents and across the oceans. Impacts are due to observed climate change, irrespective of its cause, indicating the sensitivity of natural and human systems to changing climate. The World Health Organization (WHO) estimates that the warming and precipitation trends due to anthropogenic Climate Change in the past 30 years has already caused the death of over 150,000 humans every year. Many prevalent human diseases are linked to climate fluctuations, from cardiovascular mortality and respiratory illnesses due to heatwaves, to altered transmission of infectious diseases and malnutrition from crop failures. A recent study reviewed data to bring to the fore the relationship between Climate Change and health concerns in many regions of the world. The most vulnerable regions to Climate

Change are the temperate latitudes, where the increase in temperature will be the most important, the regions around the Pacific and Indian oceans, where the rainfall variability is expected to be larger, and the cities where the urban heat island (an urban area that is significantly warmer than its surrounding rural areas due to human activities) is important [4].

Continued emission of greenhouse gases will cause further warming and long-lasting changes in all components of the climate system, increasing the likelihood of severe, pervasive and irreversible impacts for people and ecosystems. Limiting climate change would require substantial and sustained reductions in greenhouse gas emissions, which, together with adaptation, can limit climate change risks.

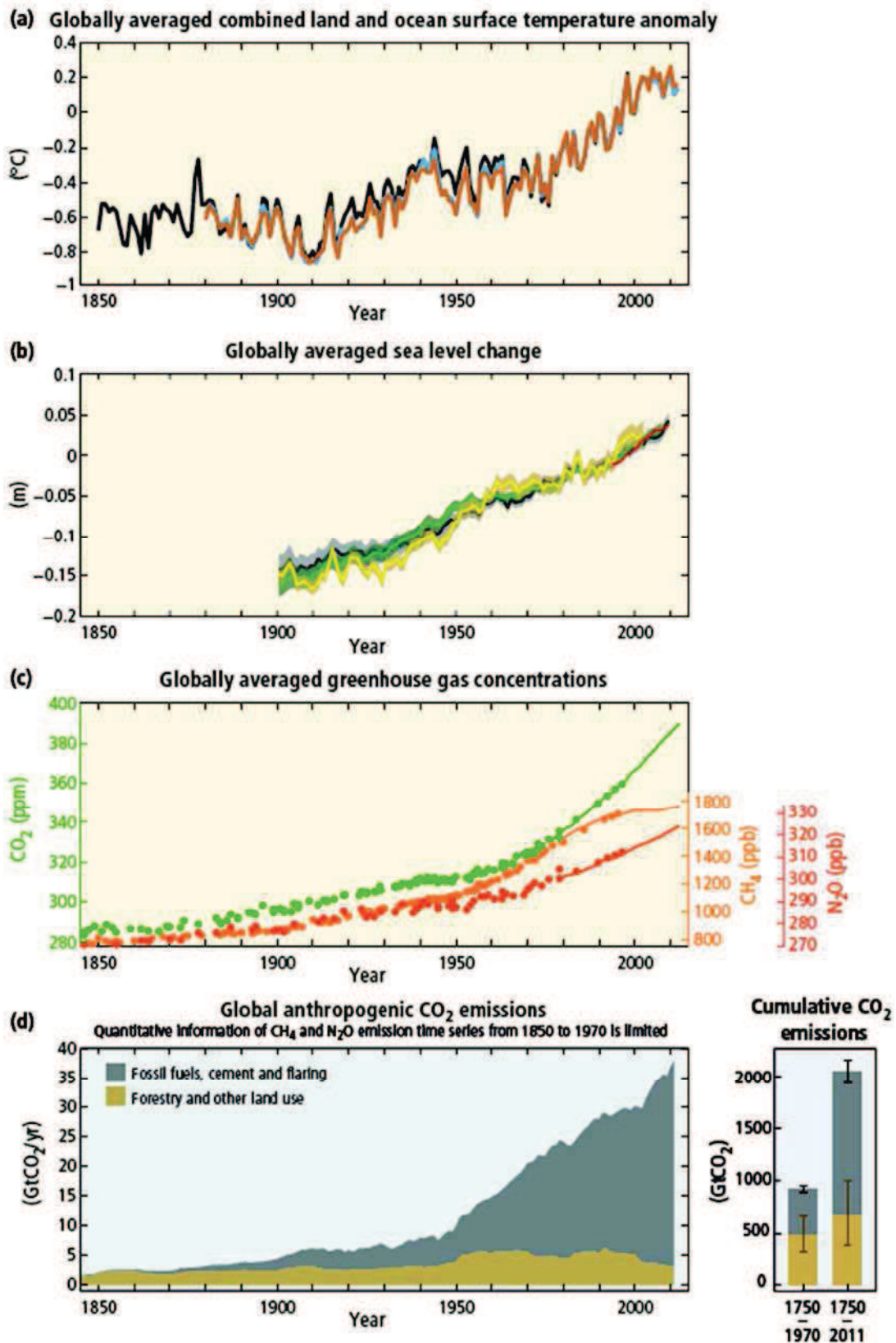


Figure 2.1: Observations and indicators of recent Climate Change induced by human activities. (a) Globally average combined land and ocean surface temperature anomaly; (b) Globally averaged sea level change; (c) Globally averaged greenhouse gas concentrations; (d) Global anthropogenic CO₂ emissions. *From Climate Change 2014 Synthesis Report of the Intergovernmental Panel on Climate Change (IPCC)*

2.2. Mountain Critical Zone: the case of the Pyrenees

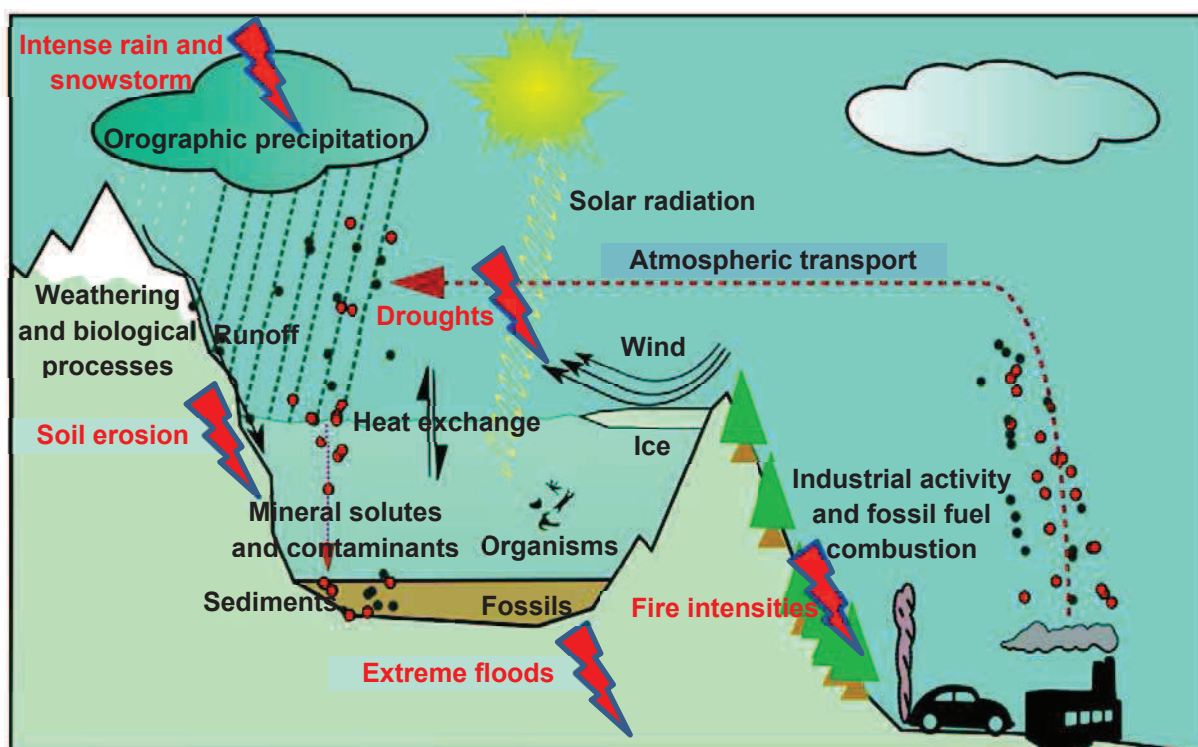


Figure 2.2: The mountain critical zone processes together with the potential impact of Climate Change (red lightning)

High mountain areas are of particular importance in terms of cultural heritage but also in terms of economic issues. Indeed, preservation of the biodiversity of these remote areas is a key point in the development of leisure activities as tourism or mountain sports. Then, the primary importance of these ecosystems has encouraged authorities to take decision in order to protect them by creation of reserves. Nevertheless, high mountain areas are unstable and affected by Climate Change induced by human activities at both local and global scale.

According to *Brantley et al.* [5]: "All life on Earth is supported by the fragile skin of the planet defined from the outer extent of vegetation down to the lower limits of groundwater". *Le Roux et al.* [6] defined the specificities of the mountain as a particular Critical Zone (**Figure 2.1**). Main specificity concerns the high topographic variability, with large slopes increasing the risk of extreme hydrogeochemical events. Orographic precipitation, produced when moist air is lifted as it moves over a mountain range, leads to higher atmospheric depositions than expected. High complexity of the geology in the mountain, such as the presence of young and easily erodible soils, explains potential microscale natural sources of organic matter and specific chemical elements. Weathering and biological processes are also influenced by the high seasonality occurring in the mountain environment (snow deposition, snowmelt, heavy storm rains,

and spring floods) and intense solar radiation. Vegetation, forests and flora are also strongly dependent on the altitude in the Mountain Critical Zone.

These ecosystems are extremely sensitive to environmental change zones: they are anthropically limited, with a short growing season and low warmth. The eventual vulnerability of an ecosystem to some perturbation depends on both the degree of exposure, and the sensitivity to it [7]. Thus, Climate Change may affect strongly the Mountain Critical Zone processes with an increase in rain and snowstorm, in droughts, in soil erosion, in extreme floods, and in fire intensities.

The most noticeable consequences of Climate Change on the Mountain Critical Zone is about the increase in the temperature (+1.2 °C average temperatures rise from 1949 to 2010), the decrease in the precipitations (-2.5 % per decade over the last 50 years) and the decrease of the snow cover (*OPCC1 project* [8]).

Indirect consequences of the Climate Change in the Pyrenees are also numerous. The winter tourism is the main source of income and the driving force of local development in many areas of the Pyrenees. However, in recent years, this sector of the tourism industry have been identified as being extremely vulnerable to the effects of Climate Change. Indeed, the increase in average of maximum and minimum winter temperatures recording during the last century led to a decrease of the number of days with enough snow accumulation for the practice of the various types of alpine skiing. Moreover, the snow line has been in higher altitude in the recent years. Both processes also delayed the season start date leading to economic implications. In order to reduce the impact of the lack of snow, ski resorts are forced to use artificial snow, which has impacts not only in terms of economy but also in terms of environmental issues. Another possible impact of Climate Change on tourism may be linked to landscape changes such as degradation of iconic features of the alpine landscape (peatbogs, lakes, and glaciers), the reduction and/or changes in the biodiversity. The most iconic changes is the unprecedented retreat of the Pyrenean glaciers which survival is compromised beyond a few decades [9]. The extreme weather events, induced by Climate Change, may also affect not only the biodiversity of the mountain zone, but also the infrastructures directly and indirectly related to tourism in the Pyrenees (refuges, telecommunication networks, mountain roads etc ...). Finally, in the tourism sector, Climate Change could also have positive impact with the increase of average temperature in spring and autumn, lengthening the summer tourism season.

Agriculture and livestock, like tourism, are key factors in terms of economy regarding the Pyrenees. Nevertheless, the increase in the concentration of atmospheric CO₂, the consequent increase in air temperature, as well as changes in seasonal precipitation patterns and the greater frequency and intensity of extreme climate events will affect agriculture (less productivity of crop), pastures (less productivity of pastures) and the livestock (thermal stress and risk of spreading of disease) sector in the Pyrenees.

Energy production might be affected by Climate Change, negatively but also positively. Indeed, on the one hand, the decrease in precipitations together with the increase in drought events affects the accumulation capacity of the reservoirs used to produce hydroelectricity. Wind power production might

be also affected as wind speed is decreasing because of Climate Change. On another hand, the increase of the solar radiation index throughout the Pyrenees mountain range could favoured the solar power production.

Flora and fauna in the Pyrenees are also unique and take part of the cultural heritage. Yet, Climate Change that induces a change in the distribution and diversity of high mountain species affects them.

2.3. High mountain lakes in the Pyrenees as witness of environmental changes

High Mountain lakes (i.e. those located above the local tree line) are iconic elements of the Pyrenean landscape and constitute a good candidate to evaluate the impact of Climate Change all along the mountain range. Indeed, their physical, chemical and biological properties respond rapidly to climate-related changes and they are sensitive to even small inputs from diffusive or background atmospheric pollution. However, long-term instrumental records of meteorological parameters (temperature, sea levels etc ...) are scarce. In order to fill this gap, numerous proxies (ice cores, tree rings, pollen etc ...) have been used to reconstruct past climatic fluctuations. As an example, a short sediment core from the small and karstic Lake Estanya (Pyrenees, Spain) provides a detailed record of the complex environmental, hydrological and anthropogenic interactions occurring since medieval times (around 800 years) [10].

Most of the existing alpine lakes originated during the last glaciation due to the action of ice upon the bedrocks: alpine lakes are young ecosystems. Alpine lakes are among the ecosystems with larger similarities throughout the planet. In the Pyrenees, there are about 1000 alpine lakes (> 0.5 ha surface area), located mostly between 2000 and 2500m asl. Considering maximum depth, lakes can be divided into two different categories that will further influence their dynamic: shallow lakes (maximum depth bellow 10-15 m) and deep lakes (maximum depth above 15 m). Depositional dynamic of lakes originating from glacial-related processes are strongly influenced by cryosphere processes in the watersheds (snow accumulation and melting, ice-cover, precipitations). These high altitude ecosystems are characterized by high solar insolation and UV radiation, low temperatures and long ice-cover periods, and very pure waters.

Alpine lakes are characterized by catchment-to-lake-surface-area ratio usually low, as the catchment surface is commonly smaller than lowland lakes. Therefore, atmospheric deposition and catchment weathering are important processes influencing greatly the lake water geochemistry [11]. Thus, mountain lake catchments are viewed and used as excellent proxies of background diffuse contamination. Indeed, high altitude lakes accumulate in their sediments organic and inorganic contaminants. As an example, *Corella et al.* [12] reconstructed the timing and magnitude of trace metal pollutants fluxes over the last 3000 years in the Central Pyrenees by analysing some potential harmful trace elements (Pb, Hg, Zn, As and Cu) in sediment cores retrieved from lake Marboré (2612m asl.) **(Figure 2.3).**

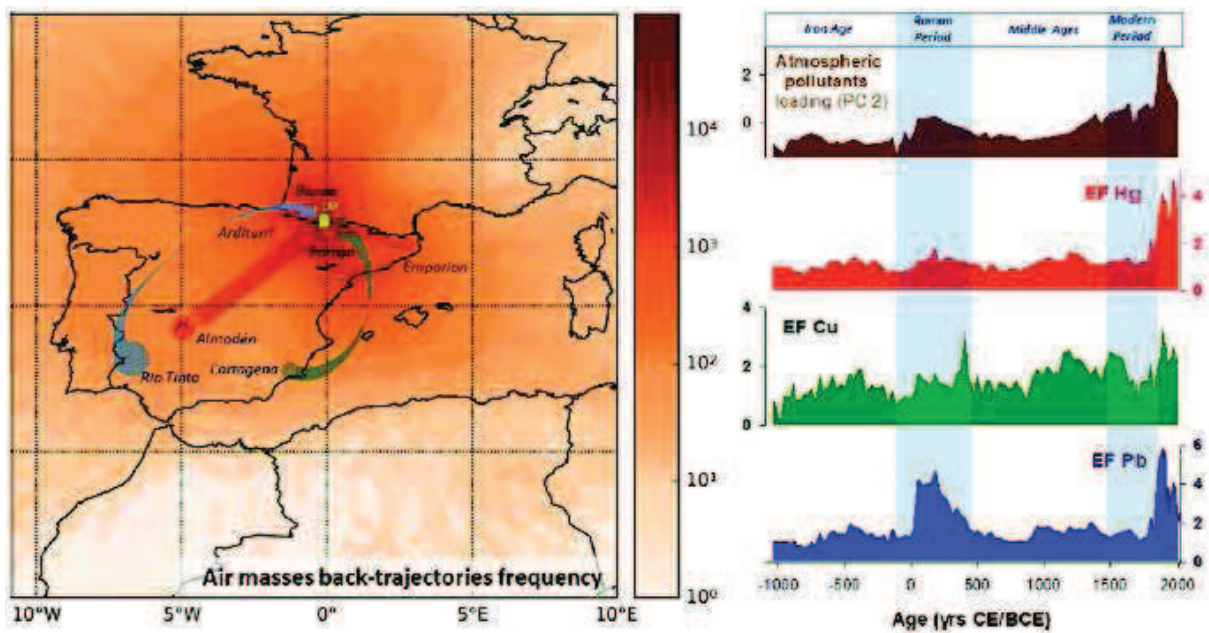


Figure 2.3: Reconstruction of the mining-related pollution legacy in high-altitude lacustrine ecosystems (Lake Marboré) [9]

High mountain lakes in the Pyrenees are pristine areas as indicated by their trophic status. According to the total phosphorus (TP) concentration measured on a survey performed along the Pyrenees in summer year 2000, more than 70 % of the lakes could be classified as ultraoligotrophic ($TP < 4.7 \mu\text{g L}^{-1}$), 22 % as oligotrophic ($4.7 < TP < 9.3 \mu\text{g L}^{-1}$) and 6 % as mesotrophic ($9.3 < TP < 31 \mu\text{g L}^{-1}$) [13]. During the ice-free season, light penetrates until the bottom in more than 75 % of the lakes, so autotrophic biota may develop. UV radiation in these ecosystems can be quite high and may promote the development of microorganisms.

Annual physical cycle in lakes are characterized by a large seasonal variability depending on water availability, thermal regime and length of the ice-covered period. Water stratification is an important phenomenon regarding the dynamics of lakes. It occurs when water masses with different properties – salinity (halocline), oxygenation (chemocline), density (pycnocline), temperature (thermocline) – form layers that act as barriers to water mixing which could lead to anoxia or euxinia. These layers are normally arranged according to density, with the less dense water masses sitting above the more dense layers. Water stratification also creates barriers to nutrient mixing between layers. This can affect the primary production in an area by limiting photosynthetic processes. When nutrients from the benthos cannot travel up into the photic zone, phytoplankton may be limited by nutrient availability. Lower primary production also leads to lower net productivity waters. The most commonly known and studied stratification is the thermal one and concern changes in the temperature profile with depth within a lake system. Different types of lakes exist according to their physical cycle but most of them are holomictic lakes that means they have a uniform temperature and density from top to bottom at a specific time during the year. Polymictic lakes are holomictic lakes that are too shallow to develop thermal

stratification, thus their waters can mix from top to bottom throughout the ice-free period. Dimictic lakes mix from the surface to bottom twice each year (**Figure 2.4**) during spring and fall overturn, and present a summer stratification with warmer surface layers and an inverse winter stratification with colder surface layers. During summer stratification, three distinct sections compose the lake water column: the epilimnion (warmer and more oxygenated top layer), the metalimnion (thermal layer, thermocline) and the hypolimnion (colder and less oxygenated bottom layer) (**Figure 2.5**). Monomictic are lakes where the mixing occur only once per year.

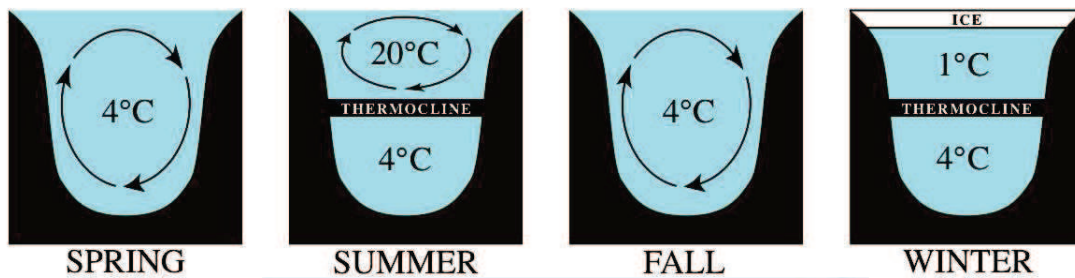


Figure 2.4: Typical mixing pattern for a dimictic lake

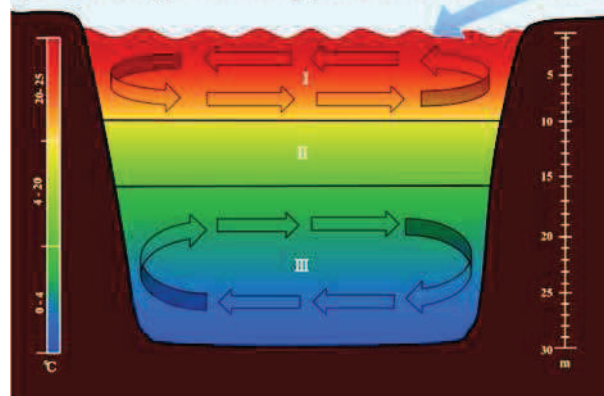


Figure 2.5: Typical summer thermal stratification. Lake is separated into three separate sections I) Epilimnion II) Metalimnion and III) Hypolimnion

Biological cycles follow the same seasonal patterns with phases of variable productivity in phytoplankton communities. Study of Lake Redó [14], a dimictic oligotrophic mountain lake located in the Pyrenees, emphasize four various main production episodes, in relation to the physical functioning of the lake. Indeed, highest chlorophyll-a concentrations, an indicator of the biological productivity, have been measured during spring overturn, in the hypolimnion during summer stratification, during autumn overturn, and under the ice at the beginning of the ice-covered period.

2.4. Potential Harmful Trace Elements (PHTEs)

Potentially Harmful Trace Elements (PHTEs), or more generally trace elements, are considered to be among the most effective environmental contaminants, and their release into the environment is increasing since the last decades. Through many processes and pathways, PHTEs may enter the different environmental compartments [15]. Considering the contributions of soil erosion and eolian dust, *Sen and Peucker-Ehrenbrink* [16] examined the influence of human activities on 77 elements, and it has been found that 62 of them surpass their corresponding natural fluxes. Many of these elements are considered to be PHTEs and the following ones will be studied in this work (**Figure 2.6**): Arsenic (As), Uranium (U), Copper (Cu), Molybdenum (Mo), Vanadium (V), Nickel (Ni), Chromium (Cr), Lead (Pb), Selenium (Se), Antimony (Sb), Cobalt (Co), Cadmium (Cd), Thallium (Tl), Zinc (Zn), Silver (Ag), Titanium (Ti), Tin (Sn) and Mercury (Hg).

1 H Hydrogen (1.008)																	2 He Helium (4.0026)
3 Li Lithium (6.941)	4 Be Beryllium (9.0122)											5 B Boron (10.811)	6 C Carbon (12.011)	7 N Nitrogen (14.007)	8 O Oxygen (15.999)	9 F Fluorine (18.998)	10 Ne Neon (20.180)
11 Na Sodium (22.990)	12 Mg Magnesium (24.305)											13 Al Aluminum (26.982)	14 Si Silicon (28.086)	15 P Phosphorus (30.974)	16 S Sulfur (32.06)	17 Cl Chlorine (35.45)	18 Ar Argon (39.948)
19 K Potassium (39.098)	20 Ca Calcium (40.078)	21 Sc Scandium (44.956)	22 Ti Titanium (47.88)	23 V Vanadium (50.942)	24 Cr Chromium (51.996)	25 Mn Manganese (54.938)	26 Fe Iron (55.845)	27 Co Cobalt (58.933)	28 Ni Nickel (58.693)	29 Cu Copper (63.546)	30 Zn Zinc (65.38)	31 Ga Gallium (69.723)	32 Ge Germanium (72.63)	33 As Arsenic (74.922)	34 Se Selenium (78.96)	35 Br Bromine (79.904)	36 Kr Krypton (83.798)
37 Rb Rubidium (85.468)	38 Sr Strontium (87.62)	39 Y Yttrium (88.906)	40 Zr Zirconium (91.224)	41 Nb Niobium (92.906)	42 Mo Molybdenum (95.94)	43 Tc Technetium (98)	44 Ru Ruthenium (101.07)	45 Rh Rhodium (102.905)	46 Pd Palladium (106.36)	47 Ag Silver (107.868)	48 Cd Cadmium (112.414)	49 In Indium (114.818)	50 Sn Tin (118.710)	51 Sb Antimony (121.757)	52 Te Tellurium (127.6)	53 I Iodine (126.905)	54 Xe Xenon (131.29)
55 Cs Cesium (132.905)	56 Ba Barium (137.327)	57-71 Lanthanoids	72 Hf Hafnium (178.49)	73 Ta Tantalum (180.948)	74 W Tungsten (183.84)	75 Re Rhenium (186.207)	76 Os Osmium (190.23)	77 Ir Iridium (192.222)	78 Pt Platinum (195.084)	79 Au Gold (196.967)	80 Hg Mercury (200.59)	81 Tl Thallium (204.38)	82 Pb Lead (207.2)	83 Bi Bismuth (208.98)	84 Po Polonium (209)	85 At Astatine (210)	86 Rn Radon (222)
87 Fr Francium (223)	88 Ra Radium (226)	89-103 Actinoids	104 Rf Rutherfordium (261)	105 Db Dubnium (262)	106 Sg Seaborgium (263)	107 Bh Bohrium (264)	108 Hs Hassium (265)	109 Mt Meitnerium (266)	110 Ds Darmstadtium (267)	111 Rg Roentgenium (268)	112 Cn Copernicium (269)	113 Nh Nihonium (270)	114 Fl Flerovium (271)	115 Mc Moscovium (272)	116 Lv Livermorium (273)	117 Ts Tennessine (274)	118 Og Oganesson (276)
57 La Lanthanum (138.905)	58 Ce Cerium (140.12)	59 Pr Praseodymium (140.908)	60 Nd Neodymium (144.24)	61 Pm Promethium (145)	62 Sm Samarium (150.36)	63 Eu Europium (151.964)	64 Gd Gadolinium (157.25)	65 Tb Terbium (158.925)	66 Dy Dysprosium (162.50)	67 Ho Holmium (164.930)	68 Er Erbium (167.259)	69 Tm Thulium (168.930)	70 Yb Ytterbium (173.054)	71 Lu Lutetium (174.967)			
89 Ac Actinium (227)	90 Th Thorium (232.038)	91 Pa Protactinium (231.036)	92 U Uranium (238.029)	93 Np Neptunium (237)	94 Pu Plutonium (244)	95 Am Americium (243)	96 Cm Curium (247)	97 Bk Berkelium (247)	98 Cf Californium (251)	99 Es Einsteinium (252)	100 Fm Fermium (257)	101 Md Mendelevium (258)	102 No Nobelium (259)	103 Lr Lawrencium (260)			

Figure 2.6: Periodic table of the elements. Red framed elements are the PHTEs considered in this work

Even if PHTEs constitute less than 0.1 % of the Earth's crust [17], several studies have shown that the contamination by PHTEs is widespread: they can be found in remote areas that are far from contamination sources. Indeed, atmospheric deposition is the main phenomenon controlling Hg, Zn and Pb concentration in the terrestrial compartment of the Svalbard archipelago in the Arctic Ocean [18]. Lichens, used as a good proxy for the assessment of local to long-range atmospheric transport [19], have been collected in James Ross Island, at the north-east of the Antarctica Peninsula, and elemental analysis have been conducted: long-distance transport of some PHTEs such as Co, Hg, Se and As has been demonstrated [20]. The presence of various PHTEs (Pb, Hg, Ag, As, Bi, Cd, Co, Cr, Cs, Cu, Mo, Ni, Sb, Sn, Tl, U, Zn) in ice cores from Polar Regions and high altitude glaciers, evaluated over the past few centuries, suggests that today there are no glaciers on Earth where atmospheric depositions of anthropogenic origin cannot be detected [21]. The occurrence and distribution of PHTEs is worldwide and thus mountain areas are not an exception [12].

PHTEs are naturally present at low concentrations in rocks and bedrocks, and because of physical and chemical weathering, they are thus also naturally present in soil and surface waters. Various natural processes therefore enable their dispersal throughout the environment [22], and from a global point of view the following sources can be distinguished [6]:

- *Terrigenous or lithogenic sources*: dispersal from wind erosion of rocks and soils (i.e., >20 % of natural derived Cu, Ni, Pb, Sb and Zn in the environment).
- *Volcanic sources*: dispersal through volcanic activities discharging emission of a significant amount of PHTEs (i.e., ~ 20 % of As, Cd, Cr, Cu, Hg, Ni, Pb and Sb) up to the stratosphere.
- *Sea spray*:
- *Biogenic sources*: biomass fires driven either by natural or anthropogenic processes acts as point sources of PHTEs

Anthropogenic sources of PHTEs are mainly due to high-temperature combustion activities resulting in volatilization of trace elements or their release in the form of very fine aerosols (<μm). In the case of erosion or dust emission, without any underlying high-temperature process, emissions tend to be much more localized (i.e., mining activities). Broadly speaking, the activities can be categorized into the following different sources/activities [6]:

- *Energy production by combustion*: the dominating anthropogenic source of PHTEs emission, entailing burning of wood, coal, and oil (As, Cd, Cu, Hg, Ni, Pb, Sb, Se, V, and Zn).
- *The metallurgical industry*: emission of dust near the extraction and point of exploitation, high-temperature processing of ores emit aerosols rich in trace elements (Cd, Cu, Ni, Pb, V, and Zn). The proportion of individual elements emitted in the aerosols depends on the type of ore processed.
- *Other industrial processes*: high-temperature processing and manufacturing (As, Cr, Cu, Ni, Pb, and Zn).
- *Transport*: road traffic (Cd, Cu, Fe, Ni, Pb, and Zn), erosion of brake pads (Cu, and Sb), erosion of train rails (Cu).
- *Waste treatment*: incineration of household waste (As, Cr, Cu, Ni, Pb, Sb, Se, V, and Zn)
- *Livestock and, especially, agricultural activities*

The responsibility of humans regarding the dispersion of aerosols and PHTEs by anthropogenic activities is undeniable, but it is important to take into account the intensification of natural processes in the biogeochemical cycle of PHTEs. On one part, human activities are modifying the natural atmospheric transport of substances in a direct way: agricultural practices and deforestation may enhance production of dust and Aeolian transport from land; changes in the wild fires regime affect the emission of ashes and gases from burning biomass. On another part, Climate Change also accelerates many of these processes: droughts and losses of snow cover that enhance dust production, melting of organic

permafrost that increases CO₂ and methane emissions from soil, changes in the prevailing winds and patterns of circulation of air masses that carry airborne substances.

2.5. Mercury

Mercury is a chemical element taking part of the PHTEs. The symbol of mercury, Hg, is coming from the Latin, itself derived from the Greek *hydrargyrum* that means silver water. Hg atomic number is 80 and its average atomic mass is 200.59 g mol⁻¹. Hg has a low melting point ($T_{\text{melting}} = 38.84 \text{ }^{\circ}\text{C}$), therefore it appears under its liquid form at normal conditions of temperature and pressure. Moreover, mercury is highly volatile because of its relatively high vapour pressure (0.180 Pa à 293 K). Mercury has seven various stable isotopes (*abundances in SRM 3133 NIST*): ¹⁹⁶Hg (0.155 %), ¹⁹⁸Hg (10.04 %), ¹⁹⁹Hg (16.94 %), ²⁰⁰Hg (23.14 %), ²⁰¹Hg (13.17 %), ²⁰²Hg (29.73 %) and ²⁰⁴Hg (6.83 %) [23]. Regarding its electronic structure ([Xe] 4f¹⁴ 5d¹⁰ 6s²), mercury is classified as a transition metal IIB presenting an unsaturated “d” layer hence it is easily polarizable. The global annual mean lifetime of Hg(0) against the net photochemical oxidation is estimated to be about 1 year [24], and recent findings on the rapid photochemistry of oxidized mercury have postulated that global atmospheric Hg lifetime could increase by a factor of 2 [25,26]. Therefore, mercury is a ubiquitous element and can appear in all environmental compartments (atmosphere, soils and sediments, and aquatic environment) under different chemical forms: elemental mercury (Hg(0)), divalent inorganic form (Hg²⁺ or iHg), and organic forms including monomethylmercury (MMHg), dimethylmercury ((DMHg) and ethylmercury (C₂H₅Hg). It is possible to define three various steps regulating the biogeochemical cycle of Hg:

- Emission from natural and/or anthropogenic sources or reemission
- Transport and deposition in aquatic and terrestrial environments
- Chemical transformations and accumulation in living organisms

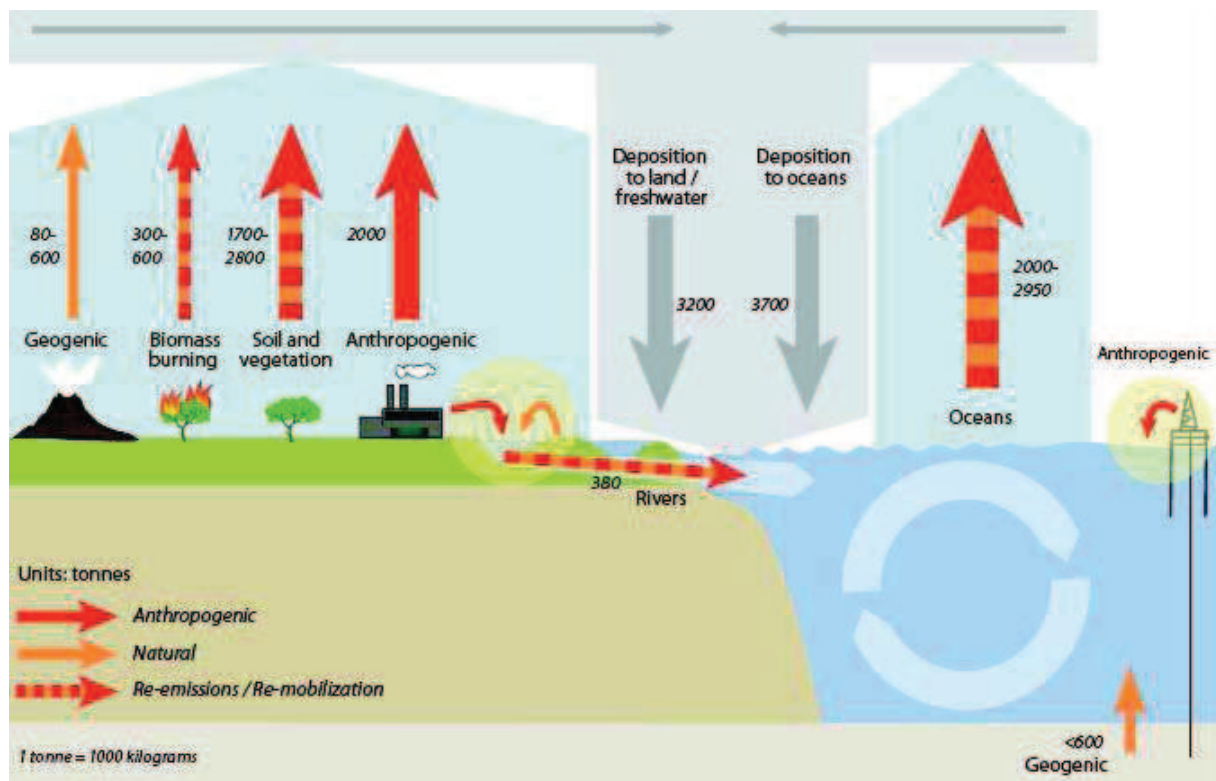


Figure 2.7: Global Hg budget in the main environmental compartments and pathways that are of importance in the global mercury cycle. *Figure from UNEP 2013 [27]*

Sources of Hg (**Figure 2.7**) [27] can be either from natural or anthropogenic origins.

Natural sources of Hg are geogenic and consist in the direct release of Hg present at trace levels in the earth's crust (between 21 and 56 $\mu\text{g kg}^{-1}$ [28], mainly as cinnabar HgS). Thus, natural erosion (water, wind) of these ores in rocks and soils [29], natural fires and volcanic degassing [30], and hydrothermal activities [31] allow Hg to enter the different environmental compartments. These natural sources of Hg account for about 10 % of the 5500-8900 tons of Hg actually emitted and re-emitted in the atmosphere every year [27].

But nowadays, anthropogenic emissions are about three times higher than the natural ones [27,32,33]. It is important to distinguish between the "unintentional" (or "by-product") discharge of mercury (coal burning, mining, industrial activities that process ores to produce various metals or process other raw materials to produce cement) from the intentional discharge of mercury. In the latest, artisanal and small-scale gold mining is the largest of these: gold is extracted from rocks, soils and sediments by amalgamation with Hg.

Finally, re-emission of mercury account for about 60 % of emitted and re-emitted Hg in the atmosphere [27]. Indeed, Hg derived from atmospheric emissions (natural or anthropogenic) is deposited in terrestrial and aquatic compartments (soils, surface waters, plants), thus can be re-emitted into the air.

This re-emission is the result of natural processes that transform organic and inorganic mercury forms into elemental Hg, which is volatile [34].

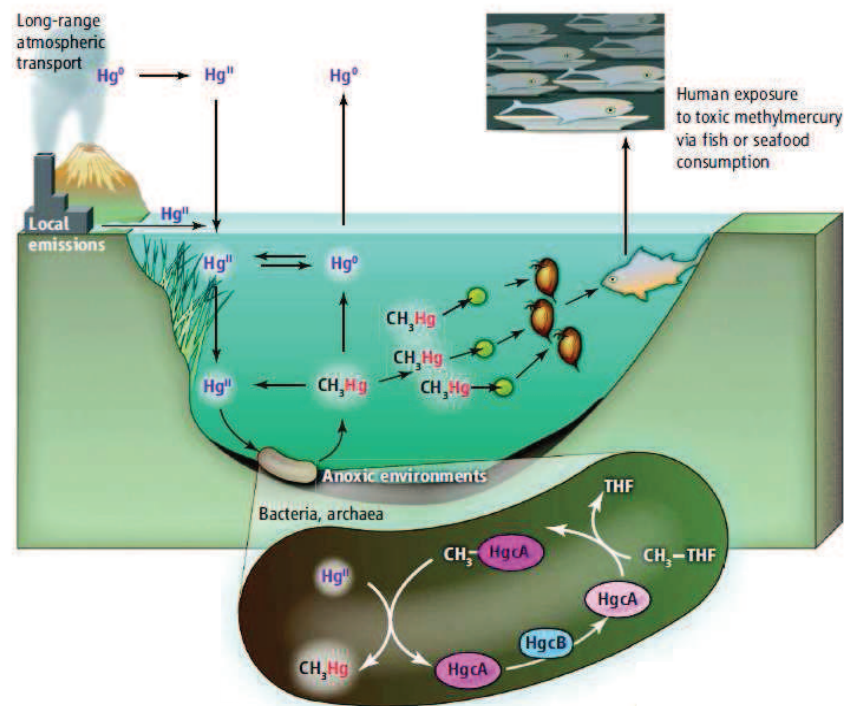


Figure 2.8: The mercury geochemical cycle. Hg is methylated in anoxic environments. The toxic methylmercury accumulates in aquatic species (bioaccumulation), and its concentrations increase with each trophic level (biomagnification), causing a threat to humans whose diets rely on fish [35]

In marine environment (**Figure 2.8**), presence of Hg may represent an important source of pollution for the atmosphere (volatilization of $Hg(0)$), for the sediments ($Hg(II)$) as well as for the food web (accumulation of MeHg). Therefore, it is important to understand better the biogeochemical cycle of mercury in the aquatic compartment. Hg can reach this compartment by many ways. First of all, in the atmosphere, more than 95 % of the Hg is under elemental form $Hg(0)$ [36]. Thus, as mentioned previously, $Hg(0)$ lifetime is important in the atmosphere but once it is oxidized, Hg becomes reactive and can be rapidly deposit at the surface of oceans. This atmospheric deposition, either by dry or wet processes is also important in lakes with large surface area-to-volume ratios and small catchment-to-lake surface areas [33]. Moreover, lixiviation processes releases Hg present in the soil compartment into the marine environment.

The various Hg forms are subject to numerous reactions in the aquatic compartment (redox reactions, methylation/demethylation, and photochemical reactions) (**Figure 2.8**). First of all, volatilization of $Hg(0)$ into the atmosphere is mainly occurring while iHg is transferred from water to sediments and vice-versa through sedimentation and remobilization phenomena. In deepest water, biological activity (bacteria, phytoplankton) is responsible of numerous reactions involving mercury, while at the surface water, abiotic reactions (photoreduction, photodemethylation) are mainly occurring [37,38]. Methylmercury

(MeHg) production is a critical process that occurs within aquatic ecosystems. The largest source of MeHg to freshwater lakes and wetlands is in situ microbial production. Indeed, microorganisms such as Sulphate and Iron Reducing Bacteria (SRB and IRB, respectively) can methylate iHg into MeHg. SRB are known as the main responsible of methylation in anoxic aquatic environment, but yield of this reaction vary strongly depending on the involving bacteria [39]. Nevertheless, it is important to note that abiotic methylation can also occur [40], but this phenomenon is photochemically reversible. The activity of methylating microbes is controlled by temperature, redox conditions, pH, and the presence of suitable electron donors (i.e., sulphate, Fe^{III}, methane). Once produced, MeHg is bioaccumulated and biomagnified within the food web, and can reach dangerous levels in fishes, birds and mammals [41].

2.6. Objectives of the present study and experimental design

This work has been carried out in the framework of REPLIM that aims to investigate the past, present and future of lakes and peatbogs in the Pyrenees in a general context of global change.

In part **3 Sampling and analytical strategy**, the analytical procedure for an effective and accurate assessment of the water geochemistry in alpine lake waters was described. A special care has been taken during all the analysis process starting by a thorough cleaning of all the material in the laboratory, a careful and homogenous treatment of the samples on field and a proper storage prior the return to the laboratory. To fulfil this objective, the methodology for an **4 Accurate determination of the total alkalinity and the CO₂ system parameters in high altitude lakes from the Western Pyrenees (France – Spain)** and a **5 A simple determination of trace mercury concentrations in natural waters using Dispersive Micro-Solid Phase Extraction preconcentration based on functionalized graphene nanosheets** were developed.

Results for the sampling described allowed us to study **6 Occurrence, distribution and characteristics concentrations of Potential Harmful Trace Elements (PHTEs) in Pyrenean lakes and their relation to aquatic biogeochemistry** as well as **7 Biogeochemistry of mercury species in the water column of high altitude lakes of the Western Pyrenees (France-Spain)**.

Finally, thanks to the REPLIM network, **8 Mercury stable isotopes in lacustrine archives to tracking human pollution and climate variability during the last 2000 years in the southern central Pyrenees (Aragon, Spain)**.

2.7. References

- [1] K. Caldeira, M.E. Wickett, Anthropogenic carbon and ocean pH, *Nature*. 425 (2003) 365–365. <https://doi.org/10.1038/425365a>.
- [2] W.J. Mitsch, B. Bernal, A.M. Nahlik, Ü. Mander, L. Zhang, C.J. Anderson, S.E. Jørgensen, H. Brix, Wetlands, carbon, and climate change, *Landscape Ecology*. 28 (2013) 583–597. <https://doi.org/10.1007/s10980-012-9758-8>.
- [3] N.R. Urban, A. Desai, Are the Great Lakes a significant net source or sink of CO₂?, *SIL Proceedings*, 1922-2010. 30 (2009) 1283–1288. <https://doi.org/10.1080/03680770.2009.11923931>.
- [4] J.A. Patz, D. Campbell-Lendrum, T. Holloway, J.A. Foley, Impact of regional climate change on human health, *Nature*. 438 (2005) 310–317. <https://doi.org/10.1038/nature04188>.
- [5] S.L. Brantley, M.B. Goldhaber, K.V. Ragnarsdottir, Crossing Disciplines and Scales to Understand the Critical Zone, *Elements*. 3 (2007) 307–314. <https://doi.org/10.2113/gselements.3.5.307>.
- [6] G. Le Roux, S.V. Hansson, A. Claustres, Inorganic Chemistry in the Mountain Critical Zone, in: *Developments in Earth Surface Processes*, Elsevier, 2016: pp. 131–154. <https://doi.org/10.1016/B978-0-444-63787-1.00003-2>.
- [7] F. Lloret, Trade-offs in High Mountain Conservation, in: J. Catalan, J.M. Ninot, M.M. Aniz (Eds.), *High Mountain Conservation in a Changing World*, Springer International Publishing, Cham, 2017: pp. 37–59. https://doi.org/10.1007/978-3-319-55982-7_2.
- [8] OPCC-CTP, *Climate change in the Pyrenees: Impacts, vulnerabilities and adaptation.*, 2018.
- [9] A. Moreno, M. Bartolomé, J.I. López-Moreno, J. Pey, P. Corella, J. García-Orellana, C. Sancho, M. Leunda, G. Gil-Romera, P. González-Sampériz, C. Pérez-Mejías, F. Navarro, J. Otero-García, J. Lapazarán, E. Alonso-González, C. Cid, J. López-Martínez, B. Oliva-Urcia, S.H. Faria, M.J. Sierra, R. Millán, X. Querol, A. Alastuey, J.M. García-Ruiz, The case of a southern European glacier disappearing under recent warming that survived Roman and Medieval warm periods, *Glaciers/Paleoclimate*, 2020. <https://doi.org/10.5194/tc-2020-107>.
- [10] M. Morellón, B. Valero-Garcés, P. González-Sampériz, T. Vegas-Vilarrúbia, E. Rubio, M. Rieradevall, A. Delgado-Huertas, P. Mata, Ó. Romero, D.R. Engstrom, M. López-Vicente, A. Navas, J. Soto, Climate changes and human activities recorded in the sediments of Lake Estanya (NE Spain) during the Medieval Warm Period and Little Ice Age, *J Paleolimnol*. 46 (2011) 423–452. <https://doi.org/10.1007/s10933-009-9346-3>.
- [11] L. Camarero, M. Rogora, R. Mosello, N.J. Anderson, A. Barbieri, I. Botev, M. Kernan, J. Kopáček, A. Korhola, A.F. Lotter, G. Muri, C. Postolache, E. Stuchlík, H. Thies, R.F. Wright, Regionalisation of chemical variability in European mountain lakes: *Regionalisation of mountain lakes chemistry*, *Freshwater Biology*. 54 (2009) 2452–2469. <https://doi.org/10.1111/j.1365-2427.2009.02296.x>.
- [12] J.P. Corella, M.J. Sierra, A. Garralón, R. Millán, J. Rodríguez-Alonso, M.P. Mata, A.V. de Vera, A. Moreno, P. González-Sampériz, B. Duval, D. Amouroux, P. Vivez, C.A. Cuevas, J.A. Adame, B. Wilhelm, A. Saiz-Lopez, B.L. Valero-Garcés, Recent and historical pollution legacy in high altitude Lake Marboré (Central Pyrenees): A record of mining and smelting since pre-Roman times in the Iberian Peninsula, *Science of The Total Environment*. 751 (2021) 141557. <https://doi.org/10.1016/j.scitotenv.2020.141557>.
- [13] J. Catalan, L. Camarero, M. Felip, S. Pla, M. Ventura, T. Buchaca, F. Bartumeus, G. de Mendoza, A. Miró, E.O. Casamayor, J.M. Medina-Sánchez, M. Bacardit, M. Altuna, M. Bartrons, D.D. de Quijano, High mountain lakes: extreme habitats and witnesses of environmental changes, (n.d.) 35.
- [14] M. Ventura, L. Camarero, T. Buchaca, F. Bartumeus, D.M. Livingstone, J. Catalan, The main features of seasonal variability in the external forcing and dynamics of a deep mountain lake (Redó, Pyrenees), *Journal of Limnology*. 59 (2000). <https://doi.org/10.4081/jlimnol.2000.s1.97>.

- [15] C. Bini, M. Wahsha, Potentially Harmful Elements and Human Health, in: C. Bini, J. Bech (Eds.), PHEs, Environment and Human Health, Springer Netherlands, Dordrecht, 2014: pp. 401–463. https://doi.org/10.1007/978-94-017-8965-3_11.
- [16] I.S. Sen, B. Peucker-Ehrenbrink, Anthropogenic Disturbance of Element Cycles at the Earth's Surface, *Environmental Science & Technology*. 46 (2012) 8601–8609. <https://doi.org/10.1021/es301261x>.
- [17] H.B. Bradl, Chapter 1 Sources and origins of heavy metals, in: *Interface Science and Technology*, Elsevier, 2005: pp. 1–27. [https://doi.org/10.1016/S1573-4285\(05\)80020-1](https://doi.org/10.1016/S1573-4285(05)80020-1).
- [18] S.N. Aslam, C. Huber, A.G. Asimakopoulos, E. Steinnes, Ø. Mikkelsen, Trace elements and polychlorinated biphenyls (PCBs) in terrestrial compartments of Svalbard, Norwegian Arctic, *Science of The Total Environment*. 685 (2019) 1127–1138. <https://doi.org/10.1016/j.scitotenv.2019.06.060>.
- [19] J.P.G. Barre, G. Deletraz, J. Frayret, H. Pinaly, O.F.X. Donard, D. Amouroux, Approach to spatialize local to long-range atmospheric metal input (Cd, Cu, Hg, Pb) in epiphytic lichens over a meso-scale area (Pyrénées-Atlantiques, southwestern France), *Environmental Science and Pollution Research*. 22 (2015) 8536–8548. <https://doi.org/10.1007/s11356-014-3990-5>.
- [20] S.P. Catán, D. Bubach, M. Arribere, M. Ansaldo, M.J. Kitaura, M.C. Scur, J.M. Lirio, Trace elements baseline levels in *Usnea antarctica* from Clearwater Mesa, James Ross Island, Antarctica, *Environmental Monitoring and Assessment*. 192 (2020). <https://doi.org/10.1007/s10661-020-8212-7>.
- [21] P. Gabrielli, P. Vallelonga, Contaminant Records in Ice Cores, in: J.M. Blais, M.R. Rosen, J.P. Smol (Eds.), *Environmental Contaminants*, Springer Netherlands, Dordrecht, 2015: pp. 393–430. https://doi.org/10.1007/978-94-017-9541-8_14.
- [22] J.M. Pacyna, E.G. Pacyna, An assessment of global and regional emissions of trace metals to the atmosphere from anthropogenic sources worldwide, *Environmental Reviews*. 9 (2001) 269–298. <https://doi.org/10.1139/er-9-4-269>.
- [23] J.D. Blum, B.A. Bergquist, Reporting of variations in the natural isotopic composition of mercury, *Analytical and Bioanalytical Chemistry*. 388 (2007) 353–359. <https://doi.org/10.1007/s00216-007-1236-9>.
- [24] P.A. Ariya, M. Amyot, A. Dastoor, D. Deeds, A. Feinberg, G. Kos, A. Poulain, A. Ryjkov, K. Semeniuk, M. Subir, K. Toyota, Mercury Physicochemical and Biogeochemical Transformation in the Atmosphere and at Atmospheric Interfaces: A Review and Future Directions, *Chemical Reviews*. 115 (2015) 3760–3802. <https://doi.org/10.1021/cr500667e>.
- [25] A. Saiz-Lopez, S.P. Sitkiewicz, D. Roca-Sanjuán, J.M. Oliva-Enrich, J.Z. Dávalos, R. Notario, M. Jiskra, Y. Xu, F. Wang, C.P. Thackray, E.M. Sunderland, D.J. Jacob, O. Travnikov, C.A. Cuevas, A.U. Acuña, D. Rivero, J.M.C. Plane, D.E. Kinnison, J.E. Sonke, Photoreduction of gaseous oxidized mercury changes global atmospheric mercury speciation, transport and deposition, *Nature Communications*. 9 (2018). <https://doi.org/10.1038/s41467-018-07075-3>.
- [26] A. Saiz-Lopez, A.U. Acuña, T. Trabelsi, J. Carmona-García, J.Z. Dávalos, D. Rivero, C.A. Cuevas, D.E. Kinnison, S.P. Sitkiewicz, D. Roca-Sanjuán, J.S. Francisco, Gas-Phase Photolysis of Hg(I) Radical Species: A New Atmospheric Mercury Reduction Process, *Journal of the American Chemical Society*. 141 (2019) 8698–8702. <https://doi.org/10.1021/jacs.9b02890>.
- [27] UNEP, 2013, *Global Mercury Assessment 2013: Sources, Emissions, Releases and Environmental Transport*, (n.d.).
- [28] K.H. Wedepohl, *The composition of the continental crust*, (n.d.) 16.
- [29] J.O. Nriagu, A global assessment of natural sources of atmospheric trace metals, *Nature*. 338 (1989) 47–49. <https://doi.org/10.1038/338047a0>.
- [30] D.M. Pyle, T.A. Mather, The importance of volcanic emissions for the global atmospheric mercury cycle, *Atmospheric Environment*. 37 (2003) 5115–5124. <https://doi.org/10.1016/j.atmosenv.2003.07.011>.
- [31] J.C. Varekamp, P.R. Buseck, Global mercury flux from volcanic and geothermal sources, *Applied Geochemistry*. 1 (1986) 65–73. [https://doi.org/10.1016/0883-2927\(86\)90038-7](https://doi.org/10.1016/0883-2927(86)90038-7).

- [32] N. Pirrone, S. Cinnirella, X. Feng, R.B. Finkelman, H.R. Friedli, J. Leaner, R. Mason, A.B. Mukherjee, G.B. Stracher, D.G. Streets, K. Telmer, Global mercury emissions to the atmosphere from anthropogenic and natural sources, *Atmospheric Chemistry and Physics*. 10 (2010) 5951–5964. <https://doi.org/10.5194/acp-10-5951-2010>.
- [33] D. Obrist, J.L. Kirk, L. Zhang, E.M. Sunderland, M. Jiskra, N.E. Selin, A review of global environmental mercury processes in response to human and natural perturbations: Changes of emissions, climate, and land use, *Ambio*. 47 (2018) 116–140. <https://doi.org/10.1007/s13280-017-1004-9>.
- [34] M.S. Gustin, S.E. Lindberg, P.J. Weisberg, An update on the natural sources and sinks of atmospheric mercury, *Applied Geochemistry*. 23 (2008) 482–493. <https://doi.org/10.1016/j.apgeochem.2007.12.010>.
- [35] A.J. Poulain, T. Barkay, Cracking the Mercury Methylation Code, *Science*. 339 (2013) 1280–1281. <https://doi.org/10.1126/science.1235591>.
- [36] W.F. Fitzgerald, D.R. Engstrom, R.P. Mason, E.A. Nater, The Case for Atmospheric Mercury Contamination in Remote Areas, *Environmental Science & Technology*. 32 (1998) 1–7. <https://doi.org/10.1021/es970284w>.
- [37] M. Monperrus, E. Tessier, D. Point, K. Vidimova, D. Amouroux, R. Guyoneaud, A. Leynaert, J. Grall, L. Chauvaud, G. Thouzeau, O.F.X. Donard, The biogeochemistry of mercury at the sediment–water interface in the Thau Lagoon. 2. Evaluation of mercury methylation potential in both surface sediment and the water column, *Estuarine, Coastal and Shelf Science*. 72 (2007) 485–496. <https://doi.org/10.1016/j.ecss.2006.11.014>.
- [38] M. Monperrus, E. Tessier, D. Amouroux, A. Leynaert, P. Huonnic, O.F.X. Donard, Mercury methylation, demethylation and reduction rates in coastal and marine surface waters of the Mediterranean Sea, *Marine Chemistry*. 107 (2007) 49–63. <https://doi.org/10.1016/j.marchem.2007.01.018>.
- [39] R. Bridou, M. Monperrus, P.R. Gonzalez, R. Guyoneaud, D. Amouroux, Simultaneous determination of mercury methylation and demethylation capacities of various sulfate-reducing bacteria using species-specific isotopic tracers, *Environmental Toxicology and Chemistry*. 30 (2011) 337–344. <https://doi.org/10.1002/etc.395>.
- [40] V. Celso, D.R.S. Lean, S.L. Scott, Abiotic methylation of mercury in the aquatic environment, *Science of The Total Environment*. 368 (2006) 126–137. <https://doi.org/10.1016/j.scitotenv.2005.09.043>.
- [41] D.C. Evers, Y.-J. Han, C.T. Driscoll, N.C. Kamman, M.W. Goodale, K.F. Lambert, T.M. Holsen, C.Y. Chen, T.A. Clair, T. Butler, Biological Mercury Hotspots in the Northeastern United States and Southeastern Canada, *BioScience*. 57 (2007) 29–43. <https://doi.org/10.1641/B570107>.

3. Sampling and analytical strategy

3.1. Studied areas

Water samples were collected from 20 different high mountain lakes in the Central Pyrenees, most of them at an altitude higher than 2000 m above the sea level (asl): 11 in the French areas of Cauterets and Ayous and 9 in the Spanish areas of Panticosa and Sabocos. Those in Cauterets were Lac d'Arratille (**ARA**), Lac de la Badète (**BAD**), Grand lac de Cambalès (**CAM**), Lac de Peyregnets de Cambalès (**PEY**), Lac de Petite Opale (**OPA**), Lac de Pourtet (**POU**), Lac Nere (**NER**) and Lac du Paradis (**PAR**); while those in Ayous were Lac Gentau (**GEN**), Lac Roumassot (**ROU**) and Lac Bersau (**BER**). The sampled lakes in Panticosa were Ibón de Coanga (**COA**), Ibón de los Arnales (**ARN**), Ibón Azul Alto (**AZU**), Embalse de Bachimaña Bajo (**BAC**), Ibón de los Baños de Panticosa (**PAN**), Ibón de Ordicuso Inferior (**ORD**), Ibón de Xuans (**XUA**) Ibón de Pecico de la Canal (**PEC**) and, finally, Ibón de Sabocos (**SAB**) was also sampled. These small lakes show similar physical properties (i.e. size, depth) but differ from their catchment characteristics and geological background (i.e. mainly granitic vs sedimentary rocks) (**Figure 3.1**). The lakes are located at different altitudes, from around 1600 m asl (PAN and PAR) to around 2600 m asl (XUA). Bioclimatic conditions are also substantially different with a decrease in the temperature and an increase in the precipitations at higher altitude. It is worth noting that most of the physical parameters listed in **Table 3.1** are season-dependent, meaning that temperature, precipitation and ice cover duration will have a strong influence, especially on the water level.

Firstly, the eight lakes of the Cauterets Area (**Figure 3.7**) are covering a 900 m altitudinal gradient and spanning about 7 km distance. This zone of the Pyrenees, historical passage for French-Spanish exchange, is a mosaic of crystalline, granitic and sedimentary rocks [1]. All these lakes are within the Parc National des Pyrénées (PNP), so the anthropogenic inputs are limited and restricted to pastoralism, fishing and hiking. PEY, CAM and OPA are directly connected and the same observation can be made for ARA and BAD, and NER and POU. On one side, the lakes CAM, PEY, NER and POU have a granitic basin (igneous rocks containing mainly quartz and feldspar) while OPA, besides the same type of basin, can be influenced by Devonian sedimentary rocks (limestone, sandstone, shale) in its surroundings. On the other side, the basin and/or catchment of the lakes ARA, BAD and PAR are mainly composed by Devonian sedimentary rocks, but granitic rocks are also present in their surroundings. While all the other lakes are showing similar characteristics, PAR (1620 m asl) differs for many reasons. It is the only lake below 2000 m asl, located in a small forest close to a Park service road. It is also the smaller lake with a surface of 0.4 ha and a maximum depth of 3 m, which encourage the constant resuspension of sediments. Adding the strong vegetation surrounding the lake to these physical characteristics, and this lake is gradually transforming into a wetland: high content of organic matter is expected. BAD also has a specificity regarding its water level. Indeed, a buried pipe links this lake with electricity facilities down the valley so the water of BAD can be freely dragged. As an example, the water level in October 2017 (Replim2) was a few meters lower than in June 2017 (Replim1).

In the Ayous area (**Figure 3.5**), BER is located in the PNP while the other two lakes (ROU and GEN) are located close to it. The three lakes are directly connected and lie on Permo-Triassic volcanic rocks

(conglomerate, sandstone, lutite, and andesite) while Carboniferous rocks are mainly present in the environment. Even if they are protected areas, the agropastoralism, present for centuries, and, therefore, the presence of gaggles, represents an important source of organic matter and nutrients, especially in GEN (1942 m asl). Moreover, the mineral contributions from the pic d'Ayous, essentially iron, turn the bottom of the lake GEN into an anoxic zone so this lake can be considered as more eutrophic in comparison with the other ones. It is worth noting that recreational fishing is also one of the main activities in all the French lakes, and can influence the water quality of the studied lakes.

The eight lakes of the Panticosa area (**Figure 3.6**) are covering a 1000 m altitudinal gradient and spanning about 10 km. Even if the geological structure on this side of the Pyrenees is similar to the Cauterets area, mostly granitic [2], climatic conditions in the Panticosa area differ, leading to visible changes in the vegetation. PAN, XUA, COA, ARN and BAC have a basin mainly composed by granite while PEC, AZU and ORD lie on Devonian rocks. Three of these lakes can be directly influenced by local human activity because of the production of electricity coming from hydroelectric dams. Indeed, the flow of water is controlled upstream of BAC (2178 m asl), PAN (1640 m asl) and PEC (2460 m asl). It is also worth noting that PAN and BAC are connected to other lakes upstream so they will directly influence the geochemistry of PAN and BAC by dragging any mobile elements into these lakes. Finally, PAN is directly located in the small town of Baños de Panticosa where tourism is the main activity (hotels, thermal baths, fishing, hiking) and can eventually influence the water geochemistry of the lake.

On its side, the basin of SAB (1900 m asl) (**Figure 3.4**) is dominated by sedimentary rocks (Devonian and Cretaceous) and the lake is located close to a ski resort. All facilities of this touristic activity, which are operational the whole year, contribute to the presence of hikers and skiers nearby this lake. Moreover, in analogy to Gentau, agropastoralism with bovine and equine cattle and fishing are important activities in this area [3], showing also an anoxic zone at its bottom.

Table 3.1: Some physical characteristics of the sampled lakes

ID Lake	Latitude	Longitude	Elevation (m asl)	Size (Ha)	Catchment (Ha)	Max depth (m) (*calculated)	Volume (m ³) (calculated)	Geological background
ARA	42.8009	-0.1748	2256	5.87	296.4	12	264307	Devonian (+ Granite)
BAD	42.7938	-0.1820	2341	6.97	79.9	7	243990	Devonian (+ Granite)
CAM	42.8297	-0.2251	2344	3.46	179.7	15	208745	Granite
PEY	42.8324	-0.2379	2493	1.17	15.2	9	52987	Granite
OPA	42.8284	-0.2177	2290	0.64	129.3	6*	25788	Granite (+ Devonian)
NER	42.8350	-0.2029	2304	2.91	94.8	12	178522	Granite
POU	42.8432	-0.2031	2403	5.95	48.7	13	387705	Granite
PAR	42.8487	-0.1603	1620	0.43	25.4	3	16570	Devonian (+ Granite)
GEN	42.8482	-0.4874	1942	8.62	186.2	20	993736	Permo-Triassic
ROU	42.8480	-0.4793	1843	5.15	268.2	16	424200	Permo-Triassic
BER	42.8392	-0.4952	2080	12.82	61.4	35	2266475	Permo-Triassic
ARN	42.7738	-0.2435	2320	2.60	93.5	9	84579	Granite
ORD	42.7571	-0.2478	2100	0.37	14.9	3	14171	Devonian (+ Granite)
PAN	42.7589	-0.2370	1620	5.50	3229	15	470072	Granite
AZU	42.7898	-0.2461	2420	3.89	151.4	8	273527	Devonian (+ Granite)
PEC	42.7992	-0.2251	2460	0.91	167.5	9*	38954	Devonian (+ Granite)
XUA	42.7773	-0.2090	2600	2.97	41.3	15	183875	Granite
COA	42.7774	-0.2199	2304	0.58	27.9	5	23208	Granite
BAC	42.7813	-0.2266	2178	3.08	1470.1	13*	193335	Granite
SAB	42.6926	-0.2574	1900	9.56	231.7	25	1183798	Devonian + Cretaceous

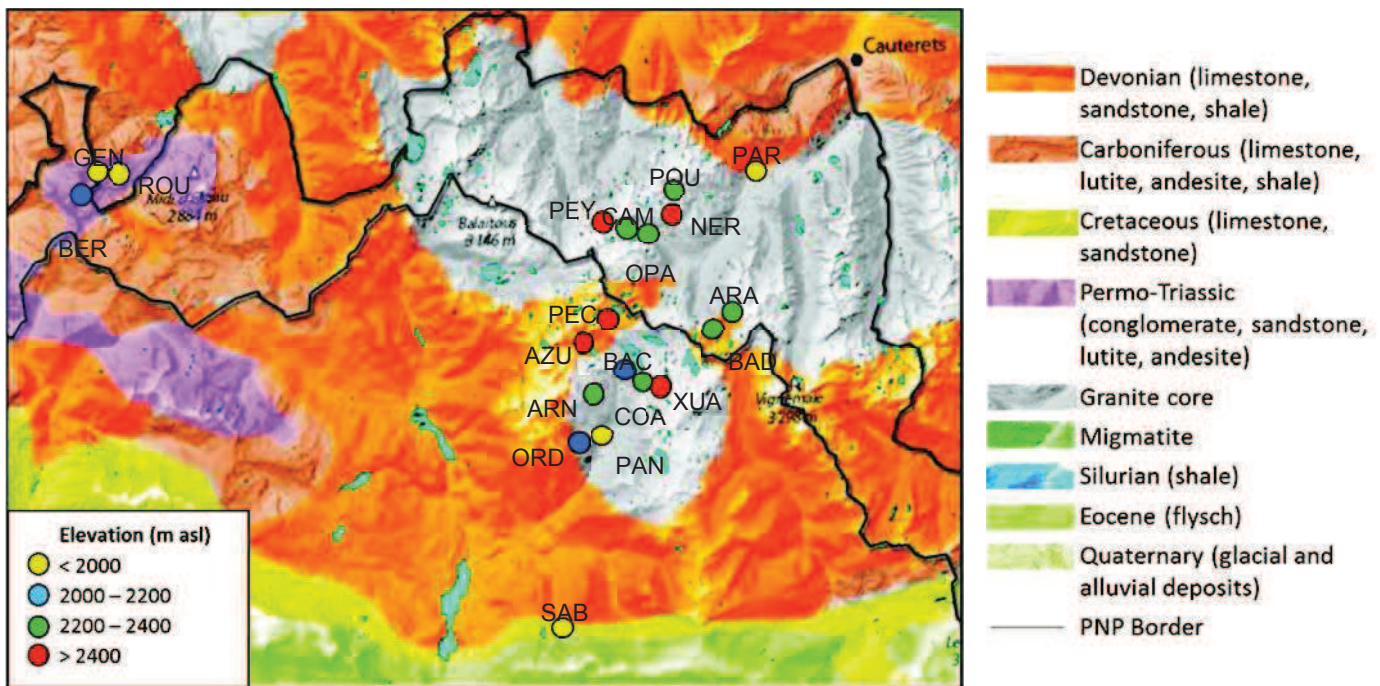


Figure 3.1: Study area together with geological formations; red circle indicates position of the lakes, and colours indicate the elevation of the corresponding lakes

3.2. Sampling strategy

Water samples, either unfiltered and/or filtered, were collected in June 2017 (**Replim1**), October 2017 (**Replim2**), June 2018 (**Replim3**), October 2018 (**Replim4**) and June 2019 (**Replim5**) (**Table 3.2**). For the area of Cauterets, the necessary material for all the lakes was first transported in hiking backpacks, with the help of donkeys only for the first sampling campaign, to the Wallon Refuge (1865 m asl) where the field laboratory was settled up (**Figure 3.2**). Then the sampling was performed in 3-4 consecutive days. In the same way, the Refugio de Casa de Piedra (1636 m asl) and the Refugio de los Ibones de Bachimaña (2200 m asl) were used as field laboratories for the 3-4 days of samplings in the area of Panticosa. Finally, the Refugio de Sabocos (1900 m asl) and the Refuge d'Ayous (1980 m asl), respectively located next to the lakes SAB and GEN, were used as field laboratories. Each lake was reached by foot so at least eight people were involved for each sampling for a total of 26 people for all the sampling campaigns.



Figure 3.2: Transport of the material

Subsurface (~0.5 m depth) water samples were collected during all the sampling campaigns (Replim1, 2, 3, 4 and 5) to investigate possible spatial and seasonal variations in the water hydrological and geochemical characteristics (temperature, dissolved oxygen, silicates, TOC, DIC, total alkalinity, anions, major and trace cations). Thus, in details, intra-lake variability has been evaluated in 2017 (Replim1 and 2) performing a triplicate sampling in each lake, at upstream, centre and downstream. During the other sampling campaigns, only one subsurface sampling was conducted at the deepest point of each lake. Moreover, during Replim3, 4 and 5 (2018-2019), a more in-depth study was performed in GEN, ARA, SAB and AZU, by sampling at different depths along the day. Besides, in situ incubation experiments using isotopically enriched Hg species (^{199}iHg , $^{201}\text{MMHg}$) were conducted in GEN, ARA and SAB to investigate Hg transformation mechanisms in the water column (methylation, demethylation, reduction). All the sampling strategy is summarized in **Table 3.2**.

A key point in the determination of trace elements is the rigour. Every step of the analytical protocol has to be done uniformly and very carefully with material as clean as possible to obtain results comparable over time. Thus, thorough cleaning of all the material in the laboratory, a careful and homogenous treatment of the samples on field and a proper storage prior to the laboratory return are the main critical steps involved in the analytical protocol.

After the transport by walking of all the material needed up to the lake, the boat (*Fish Hunter™ FH280, Decathlon, France*) was inflated to reach the sampling point. Then, the operator, always wearing wear powder-free gloves, has to operate manually the ultra-clean sampler (*Go-Flo Water Sampler 5L Teflon Coated, General Oceanics, USA*) (**Figure 3.3**) to collect the subsurface water sample, avoiding the surface microlayer. For depth sampling, it is necessary to equip the Go-Flo sampler with a rope and a weight and operate the sampler at the desired depth with a messenger. Back ashore, after connecting a clean silicone tubing to the outlet of the sampler, the water sample is distributed in various flasks according to the parameter to be analysed.

Note:

Due to time constraints, for Replim5, only results for mercury speciation are available and will be discussed in this manuscript.

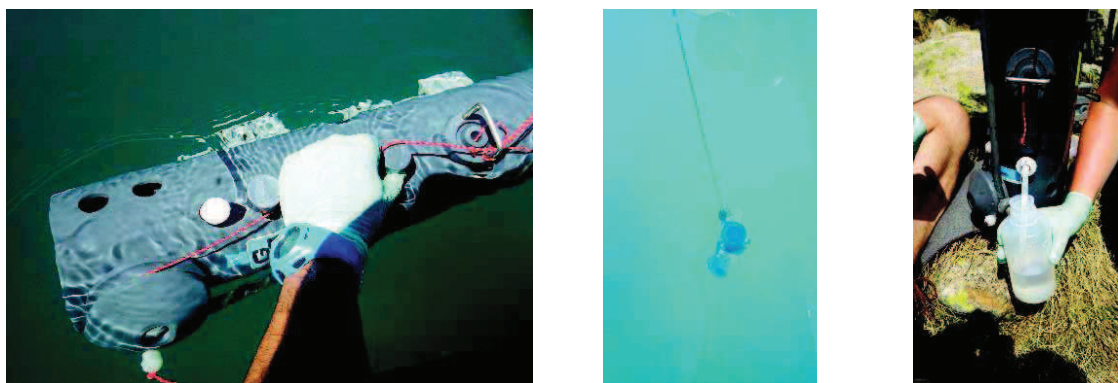


Figure 3.3: Go-Flo sampler

Table 3.2: Overall of the sampling strategy

Lake	Replim1 (June 2017)	Replim2 (October 2017)	Replim3 (June 2018)	Replim4 (October 2018)	Replim5 (June 2019)
ARA	Subsurface (triplicate)	Subsurface (triplicate)	In-depth study	In-depth study	-
BAD	Subsurface (triplicate)	Subsurface (triplicate)	Subsurface (singlicate)	Subsurface (singlicate)	-
CAM	Subsurface (triplicate)	Subsurface (triplicate)	Subsurface (singlicate)	Subsurface (singlicate)	-
PEY	Subsurface (triplicate)	Subsurface (triplicate)	Subsurface (singlicate)	Subsurface (singlicate)	-
OPA	Subsurface (triplicate)	Subsurface (triplicate)	Subsurface (singlicate)	Subsurface (singlicate)	-
NER	Subsurface (triplicate)	-	-	-	-
POU	Subsurface (triplicate)	-	-	-	-
PAR	Subsurface (triplicate)	Subsurface (triplicate)	Subsurface (singlicate)	Subsurface (singlicate)	-
GEN	-	-	In-depth study	In-depth study	In-depth study
ROU	-	-	Subsurface (singlicate)	Subsurface (singlicate)	Subsurface (singlicate)
BER	-	-	Subsurface (singlicate)	Subsurface (singlicate)	Subsurface (singlicate)
ARN	Subsurface (triplicate)	Subsurface (triplicate)	Subsurface (singlicate)	Subsurface (singlicate)	Subsurface (singlicate)
ORD	Subsurface (triplicate)	-	Subsurface (singlicate)	Subsurface (singlicate)	Subsurface (singlicate)
PAN	Subsurface (triplicate)	Subsurface (triplicate)	Subsurface (singlicate)	Subsurface (singlicate)	Subsurface (singlicate)
AZU	Subsurface (triplicate)	Subsurface (triplicate)	In-depth study	In-depth study	Subsurface (singlicate)
PEC	Subsurface (triplicate)	-	Subsurface (singlicate)	Subsurface (singlicate)	Subsurface (singlicate)
XUA	Subsurface (triplicate)	-	-	-	-
COA	Subsurface (triplicate)	Subsurface (triplicate)	Subsurface (singlicate)	Subsurface (singlicate)	Subsurface (singlicate)
BAC	Subsurface (triplicate)	Subsurface (triplicate)	Subsurface (singlicate)	Subsurface (singlicate)	Subsurface (singlicate)
SAB	-	-	In-depth study	In-depth study	In-depth study



Figure 3.7: Lakes from Cauterets area (Replim1): ARA, BAD, CAM, OPA, PEY, NER, POU and PAR



Figure 3.5: Lakes from Ayous area: GEN (Replim5), BER (Replim3) and ROU (Replim5)



Figure 3.6: Lakes from Panticosa area (Replim1): ARN, ORD, PAN, BAC, AZU, XUA, COA and PEC



Figure 3.4: Lake Sabocos (Replim5)

3.3. Analytical methods

Table 3.8 resume all the parameters analysed together with their associated analytical protocol.

3.3.1. Physicochemical parameters

Determination of several physicochemical parameters, that directly influence the chemical composition of the lake, was carried out using an EXO2 multiparametric probe (*YSI Inc., USA*) (**Figure 3.8**), and only the following ones will be discussed: depth, temperature, conductivity, salinity, dissolved oxygen (DO), pH, oxidation-reduction potential (ORP) and chlorophyll-a (Chl-a).

The probe determines the depth with a non-vented strain gauge, which measures the pressure exerted by the water column. As the atmospheric pressure changes with altitude, it is important to calibrate the depth sensor before each measurement.

The probe is equipped with a combination temperature/conductivity sensor. The temperature sensor uses a thermistor whose resistance changes with temperature: an algorithm is used to perform the conversion. No calibration or maintenance of the temperature sensor is required and the accuracy is ± 0.01 °C from -5 to 35 °C. The conductivity sensor uses four internal, pure-nickel electrodes to measure solution conductance. Two of the electrodes are current driven, and two are used to measure the voltage drop. The measured voltage drop is then converted into a conductance value in milliSiemens. Thus, the conductance is multiplied by the cell constant (approximately 5.1 cm^{-1}) to obtain the conductivity value in millisiemens per cm (mS cm^{-1}). Calibration is performed with a 12.88 mS cm^{-1} (at 25 °C) standard solution (*Crison Instruments S.A., Spain*) which allows adjusting the value of the cell constant, and the accuracy is ± 0.5 % for 0 to 100 mS cm^{-1} and 1 % for 100 to 200 mS cm^{-1} . Salinity is determined automatically from the conductivity and temperature sensor according to algorithms found in Standard Methods for the Examination of Water and Wastewater (23rd edition, 2015) [4]. The use of the Practical Salinity Scale results in unitless values since the measurements are carried out in reference to the conductivity of standard seawater at 15 °C.

The optical Dissolved Oxygen (DO) sensor works based on the influence of DO on an indicator dye. When there is no oxygen present, the lifetime (T) and intensity (I) of the signal, measured via a photodiode, is maximal. As oxygen is introduced to the membrane surface of the sensor, the lifetime becomes shorter and intensity decreases. Thus, the lifetime and the intensity of the luminescence are inversely proportional to the amount of oxygen present, and oxygen can be quantified by the Stern-Volmer equation:

Equation 3.1

$$\frac{I_0}{I} = \frac{T_0}{T} = 1 + K_{SV} \times [O_2]$$

where I_0 and I are the luminescence intensities in absence and presence of oxygen, T_0 and T the luminescence lifetime in absence and presence of oxygen, K_{SV} the Stern-Volmer constant (quantifies the quenching efficiency and therefore the sensitivity of the sensor) and $[O_2]$ the oxygen content

The sensor gives the DO as oxygen saturation (%) or concentration (mg L^{-1}), and the accuracy is $\pm 1\%$ from 0 to 200 % oxygen saturation and $\pm 5\%$ from 200 to 500 % oxygen saturation. One calibration was performed at the beginning of each sampling campaign with water. The problem is that the DO measurement will be affected by the atmospheric pressure, and this parameter decreases with altitude. Thus, calibration should have been done in each sampling location, which is complicated to set up due to time constraints. The results of DO, discussed in this manuscript, have to be taken carefully and are reflected semi-quantitative values rather than quantitative values: precise but not fully accurate.

A combination pH/ORP sensor is used for the determination of these two parameters. The probe measures the pH with two electrodes, one for hydrogen ions and one as reference. The sensor is a glass bulb filled with a solution of stable pH and the inside of the glass surface experiences constant binding of H^+ ions. Before each sampling campaign, calibration was performed with three different buffer solutions (pH = 4.01, 7.00 and 10.00; *Hamilton Bonaduz AG, Switzerland*). These measurements can reach accuracies of ± 0.1 pH units within $\pm 10^\circ\text{C}$ of calibration temperature and ± 0.2 pH units for the entire temperature range. The ORP is measured by the difference in potential between an electrode, which is relatively chemically inert, and a reference electrode. The ORP sensor consists of a platinum button found on the tip of the probe. The potential associated with this metal is read versus the Ag/AgCl reference electrode of the combination sensor that uses a gelled electrolyte. A one-point calibration was performed with a 425 mV (at 25°C) buffer solution (*Hamilton Bonaduz AG, Switzerland*). ORP values are presented in millivolts, with an accuracy of ± 20 mV in Redox standard solution, and are not compensated for temperature. The pH/ORP sensor is stored in acetate/acetic acid buffer of pH = 4 while not used.

The Total Algae (TAL) sensor unit includes a dual-channel fluorescence sensor that allows the determination of chlorophyll a (Chl-a) (excitation with a blue-emitting LED at 470 ± 15 nm) and phycoerythrin (BGA-PE) (excitation with a blue-shifted beam at 525 ± 15 nm). This manuscript will only focus on Chl-a results. The probe generates data in either RFU (Relative Fluorescence Units) or $\mu\text{g L}^{-1}$ of pigment. However, RFU is recommended as the default unit rather than $\mu\text{g L}^{-1}$ of pigment. Indeed, on one hand, RFU (0 to 100 %) is obtained by normalisation of the sensor's output with a secondary standard, rhodamine WT dye (*Acros Organics, Belgium*). It allows the correction of the sensor's drift such as biofouling and declining sensitivity over time, and improve the accuracy of the measurements with better linearity. On the other hand, the $\mu\text{g L}^{-1}$ of pigment unit is just an estimation of pigment concentration based on the correlation between sensor outputs and extracted pigments from laboratory-grown blue-green algae. Thus, this unit is very dependent upon the composition of the algal population, the time of the day, the physiological health of the algae, and other environmental factors. Chlo-a results will be discussed as RFU units and as a semi-quantitative variable.

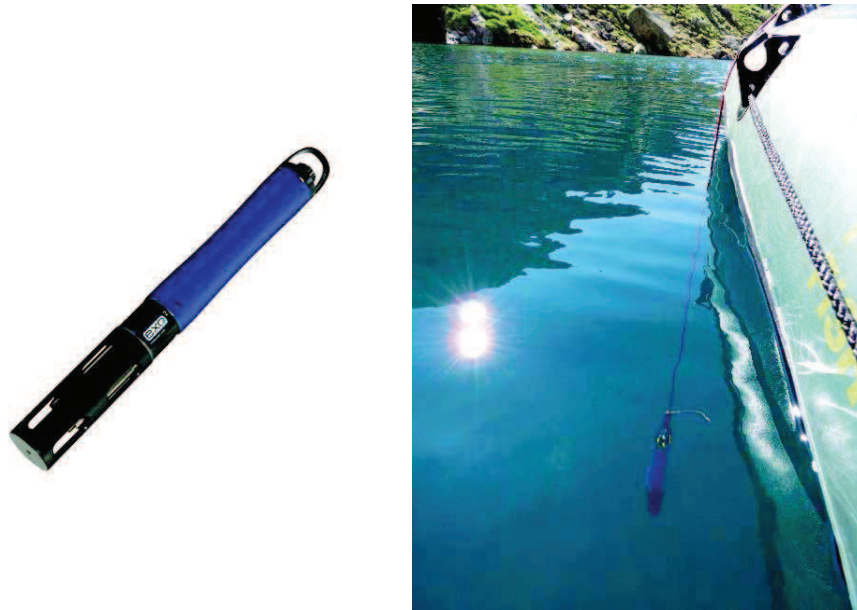


Figure 3.8: EXO2 multiparametric probe

3.3.2. Major anions

1. Sampling

Only filtrated samples were collected and analysed, and no cleaning of the material is needed. Indeed, the plastic material used in this case (containers, syringes and filters) were directly used as received from the supplier, without a previous specific cleaning procedure. On field, after collecting a water sample using Go-Flo sampler (**3.2 Sampling strategy**), the filter and the syringe connected together were rinsed with the water sample. Approximately 50 mL of water were used to rinse the filter and the plastic container. Then, 40 mL of the water sample using the previously rinsed syringe-filter unit. About 10 mL of headspace was kept in the container to prevent an eventual collapse due to swelling of the sample if frozen during storage. The samples dedicated to major anions analysis were kept in a portable cooler (5-10 °C), protected from light, during transportation to the laboratory where they were stored in the fridge (4 °C).

2. Analysis

The analysis of major anions (Fluoride F^- , Chloride Cl^- , Nitrite NO_2^- , Bromide Br^- , Nitrate NO_3^- , Phosphate PO_4^{3-} , and Sulphate SO_4^{2-}) has been carried out using ionic chromatography by external standard calibration according to the EPA Method 300.1 [5,6]. Globally, a small volume of sample (20 μ L) was injected into the ion chromatograph. Then, analytes were separated and measured using a system comprised of a guard column, analytical column, suppressor device and conductivity detector. For the introduction of the sample, the AS40 autosampler (*Dionex Corporation, USA*) was used. Together with an ASRS 300 (4 mm) suppressor, an IonPac AS23 (4 \times 250 mm) column and IonPac AG23 (4 \times 50 mm) precolumn (*Dionex Corporation, USA*) were used for the separation, whereas quantification was performed with a ICS 2500 ionic chromatograph with an ED50 suppressed conductivity detector (*Dionex*

Corporation, USA). Finally, 4.5 mmol L⁻¹ sodium carbonate (Na₂CO₃) / 0.8 mmol L⁻¹ sodium bicarbonate (NaHCO₃) solution was used as mobile phase. 25 mA of suppression current and 1 mL min⁻¹ flow rate were the chromatographic conditions. The program employed for data acquisition was Chromeleon 6.60 (Dionex Corporation, USA).

Analysis batch consists primarily in calibration check standard with eight solutions made up with 1000 mg L⁻¹ commercial solutions (Sigma-Aldrich, USA) diluted in high purity water obtained from a Millipore water purification system (Millipore Co., USA; 18.2MΩ cm). Laboratory and in-field blanks were also analysed regularly all along the process to check for contamination issues.

3. Limit of detection (LOD)

The limit of detection (LOD), associated to a specific technique, is the minimum concentration of an analyte in a sample that can be detected. In the case of the analysis of major anions, the in-field blanks did not display any signal on the chromatogram. Therefore, the calibration curve was used to calculate the LOD as follow:

Equation 3.2

$$LOD = b + (3 \times \sigma_b)$$

where b is the intercept of the regression line and σ_b is its corresponding standard deviation.

Analysis of the samples has been done during four different analytical sessions, corresponding to the four sampling campaigns, and the LODs together with the number of samples analysed on each case are listed in the **Table 3.3**. Chloride (100%), Nitrate (88%) and Sulphate (96%) have been detected in almost all the samples whereas Fluoride (22%), Nitrite (0%), Bromide (3%), and Phosphate (0%) were mainly below the LOD.

Table 3.3: LOD for major anions analysis

	F ⁻	Cl ⁻	NO ₂ ⁻	Br ⁻	NO ₃ ⁻	PO ₄ ³⁻	SO ₄ ²⁻	n
LOD_{Replim1} (µg L⁻¹)	33	24	19	38	50	81	35	47
n > LOD	0	47	0	0	45	0	47	
LOD_{Replim2} (µg L⁻¹)	11	25	27	43	142	52	102	34
n > LOD	16	34	0	0	27	0	34	
LOD_{Replim3} (µg L⁻¹)	1	22	-	6	12	41	213	40
n > LOD	13	40	-	4	40	0	39	
LOD_{Replim4} (µg L⁻¹)	2	9	-	54	65	90	292	34
n > LOD	5	34	-	0	24	0	29	

3.3.3. Major and trace cations

1. Sampling

Two different kinds of samples were collected and analysed: filtered and unfiltered.

Considering the very low concentrations expected in the samples and the potential contaminations, working with clean material is required. In that sense, an acid nitric bath at 10 % was prepared with a mix of nitric acid at 65 % (*PanReac, Spain*) and Elix quality water (*Merck Millipore, USA*) and plastic containers were kept in that bath for 24 hours. Then, they were rinsed twice with Milli-Q water and dried in a clean atmosphere before being stored in Zip-lock bags. For syringes and syringe-filters were also cleaned using 10 % HNO₃ solution prepared with sub-boiling twice-distilled 69 % nitric acid and Milli-Q quality water (*Millipore Co., USA*; 18.2MΩ cm). First, the syringe is filled with 10 % HNO₃, the filter is connected and the acid is pushed through the latter. Then, this step was repeated using Milli-Q water instead of 10 % HNO₃. Both materials (filters and syringes) were dried in a clean atmosphere and stored in Zip-lock bags until their use.

Sampling was done following the recommendations of EPA Method 1669 [7].

For the filtered samples, the water sample collected with the Go-Flo sampler (**3.2 Sampling strategy**) was used to fill the syringe, previously connected to the filter. That portion of the sample was passed through the filter and used to rinse one plastic container before being discarded. Then, about 40 mL of the water sample was filtered and used to fill the plastic container. It is important to leave a headspace of about 10 mL in the plastic container to prevent an eventual collapse of the container due to swelling of the sample if frozen before analysis.

For the unfiltered samples, after rinse of the plastic container using the water sample, it was directly filled with about 40 mL of the water sample.

To prevent eventual adsorption on the wall, losses and/or transformations during storage, all samples were acidified using about 580 µL of sub-boiling twice-distilled HNO₃ 69 %. The plastic container was closed, transported to the laboratory as fresh as possible (4 °C) and protected from light, and finally stored in a freezer (-20 °C) until analysis.

2. Analysis

Quantification has been done with ICP-MS by internal standard calibration according to EPA Method 1640 [8], using two types of equipment: one classical quadrupole ICP-MS with Collision/Reaction Cell (filtered and unfiltered samples) (NexION 300, Perkin Elmer Inc., USA) and one High Resolution (HR) ICP-MS (unfiltered samples only) (Element XR, Thermo Scientific, Germany), thus enabling future intercomparison of the results. Operating conditions for both equipment are summarized in **Table 3.4**.

For both methods, no additional sample treatment was needed and the samples were analysed directly from the plastic container used for sampling. Indeed, given the remote location of the sampling lakes, resulting in ultra-clear water, the matrix of the samples was not considered complex, and possible interferences due to the matrix were negligible: no need for digestion of the samples. Besides, salt

concentrations in the water samples were expected to be very low so problems related to the potential presence of salts in the analysis by ICP-MS were negligible: no need for dilution steps.

For the analysis by classical ICP-MS, quality control was insured by analysis of all the calibration standards several times per session, replication of one sample every ten samples to correct for drift in the sensitivity of the equipment, analysis of reference material (SRM 1640a, Trace Elements in Natural Water; *Sigma-Aldrich, USA*), and laboratory and in-field blanks analysis. To reduce potential polyatomic interferences for some elements (Na, Mg, K, Ca, Ti, V, Cr, Mn, Fe, Co, Ni, Cu, Zn, As and Cd), Helium (He) was used to fill the Collision/Reaction cell device (collision mode with kinetic energy discrimination KED).

With the HR-ICP-MS, resolution was adapted to each element likely to be affected by spectral overlaps. However, physical correction of this problem has an inherent disadvantage in that the higher resolving capability will go along with lower sensitivity (decrease in the transmission). Quality control was insured by analysis of all the calibrations standards several times per session, and laboratory and in-field blanks analysis.

Table 3.4: Operating conditions for the ICP-MS and the HR-ICP-MS

	ICP-MS NexION 300 (Perkin Elmer)		HR-ICP-MS Element XR (Thermo Scientific)
Forward power	1600 W	Forward power	1200 W
Plasma gas flow (Ar)	18 L min ⁻¹	Plasma gas flow (Ar)	15.90 L min ⁻¹
Auxiliary gas flow (Ar)	1.2 L min ⁻¹	Auxiliary gas flow (Ar)	1 L min ⁻¹
Nebulizer gas flow (Ar)	0.90-1.00 L min ⁻¹	Nebulizer gas flow (Ar)	0.745 L min ⁻¹
Sample flow	0.4 mL min ⁻¹	Sample flow (Azote)	10 L min ⁻¹
Cell gas flow (He) (depending on elements)	2.0 mL min ⁻¹ 4.0 mL min ⁻¹		
Integration time	1000 ms	Integration time	100 ms
Dwell time	50 ms	Dwell time	10 ms
Sweeps	20	Sweeps	10
Reading	1	Reading	5
Replicates	3	Replicates	5
Internal Standard	⁹ Be, ⁴⁵ Sc, ⁷⁴ Ge, ⁸⁹ Y, ¹¹⁵ In, ²⁰⁹ Bi	Internal Standard	¹⁰³ Rh
Isotopes measured	²³ Na, ²⁴ Mg, ²⁷ Al, ³⁹ K, ⁴⁴ Ca, ⁴⁷ Ti, ⁵¹ V, ⁵² Cr, ⁵⁵ Mn, ⁵⁶ Fe, ⁵⁹ Co, ⁶⁰ Ni, ⁶³ Cu, ⁶⁶ Zn, ⁷⁵ As, ⁸⁸ Sr, ⁹⁸ Mo, ¹⁰⁷ Ag, ¹¹¹ Cd, ¹²⁰ Sn, ¹²¹ Sb, ¹³⁷ Ba, ¹⁸⁴ W, ²⁰⁵ Tl, ²⁰⁸ Pb	Isotopes measured	Low Resolution ⁴³ Ca, ⁷⁵ As, ⁸⁸ Sr, ⁹⁵ Mo, ¹⁰⁹ Ag, ¹¹¹ Cd, ¹¹⁸ Sn, ¹²¹ Sb, ¹³⁸ Ba, ¹⁸² W, ²⁰⁵ Tl, ²⁰⁸ Pb, Medium Resolution ²³² Th, ²³⁸ U ²³ Na, ²⁶ Mg, ²⁷ Al, ³⁹ K, ⁴⁷ Ti, ⁵¹ V, ⁵² Cr, ⁵⁵ Mn, ⁵⁶ Fe, ⁵⁹ Co, ⁶² Ni, ⁶³ Cu, ⁶⁶ Zn

3. Validation of the results

Analytical uncertainties for both methodologies have been evaluated using replicate analysis of the same sample. The LOD associated to each element was calculated according to two different ways. For the results obtained by the ICP-MS, the calibration curve was used with the same formula as for the determination of instrumental LODs for major anions:

Equation 3.3

$$LOD = b + (3 \times \sigma_b)$$

where b is the intercept of the regression line and σ_b is its corresponding standard deviation.

While the major cations (Na, Mg, K and Ca) were detected in all the samples and other trace cations (Al, Ti, V, Mn, Fe, As, Sr, Mo, Sb and Ba) in more than 75% of the samples, most of the ultra-trace cations (Cr, Co, Ni, Cu, Zn, Ag, Cd, Sn, W, Tl and Pb), potentially harmful to human health or the environment, were below the limit of detection.

Laboratory blanks were used in the case of the HR-ICPMS for the calculation of the LOD, using the following formula:

Equation 3.4

$$LOD = 3 \times \sigma_{blank}$$

where σ_{blank} is the standard deviation associated to the laboratory blank analysis.

The HR-ICP-MS provided better results because main of the elements analysed, either trace or major, have shown lower limit of detection. Only two elements have not been detected in most of the samples: Ag and Sn. In pristine natural waters, Ag occurs at low ng L^{-1} levels ($0.1 - 5 \text{ ng L}^{-1}$) [9] not detectable with classical methodologies such as detection by ICP-MS and quantification by external calibration. Regarding Sn, it is an ubiquitous contaminant in laboratory vessels (including quartz and many plastics), which may explain the relative high limit of detection in comparison with other trace elements.

Another trace element showed a high limit of detection, for both techniques: Zn. This was probably due to laboratory contamination that may occur in both the material and Milli-Q water used for the preparation of the calibration curve and the blank solutions. Other lab manipulations also increase the contamination by Zn in water samples. For example, when filtering the samples with PVDF filters, the contamination by Zn was higher, and the results obtained when comparing filtered and non-filtered samples supported this fact. This contamination occurs randomly so even if it has been detected in more than 90 % of the samples, Zn levels will not be discussed further more in this manuscript.

In order to compare the efficiency and suitability of the two methods, a linear regression analysis has been performed with the results obtained. The coefficient of determination R^2 and the slope b , together with its associated standard error $\pm b$, are displayed in the **Figure 3.9**. Except for Al, Co, Cu, Zn and W, most of the elements well detected using ICP-MS display a strong linear relationship with the ones obtained by HR-ICP-MS. Nevertheless, when looking at the slopes associated to each regression, which

is under the value of one, it seems obvious that using the ICP-MS methodology will lead to an underestimation of the results. This is probably due to the quantification process. Indeed, the standard solutions used for the ICP-MS could be stored for a maximum of one month whereas the ones for HR-ICP-MS were prepared daily. Moreover, we have used the results obtained firstly by ICP-MS to adjust more properly the calibration curves for the HR-ICP-MS, thereby avoiding that some points appear out of the curve (extreme values). Only one element, Sr, display results always higher with the ICP-MS, this is due to some manipulation problems with the commercial solution used for the HR-ICP-MS methodology.

As a resume, the ICP-MS methodology, used daily for various analysis (sediments, waters, plants etc ...), will be qualified as a semi-quantitative method. With an estimation of the concentrations, its results allow us to compare the variation of each elements within the samples, either unfiltered or filtered. For a better accuracy and precision regarding the unfiltered samples, results coming from the HR-ICP-MS methodology will be used within this manuscript (except for Sr).

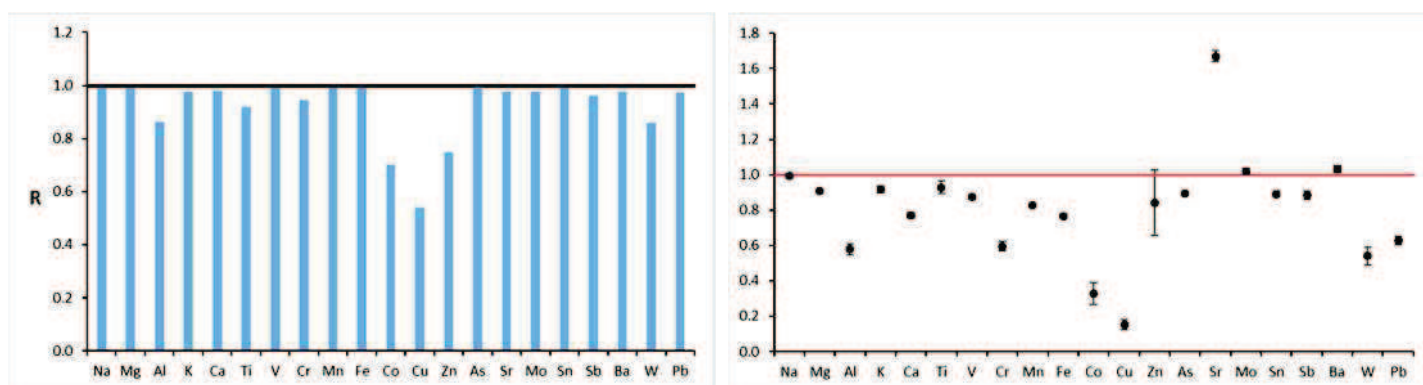


Figure 3.9: Coefficient of determination R^2 and the slope b associated to each linear regression between results obtained by ICP-MS and results obtained by HR-ICP-MS

Table 3.5: LOD and analytical uncertainties for major and trace cations analysed by ICP-MS and HR-ICP-MS

	Na	Mg	Al	K	Ca	Ti	V	Cr	Mn	Fe	Co	Ni	Cu	Zn	As	Sr	Mo	Ag	Cd	Sn	Sb	Ba	W	Tl	Pb	U	n	
ICP-MS	LOD ₁ (ng L ⁻¹)	18765	2661	2256	3066	6700	3	10	7	8	726	4	20	15	493	46	140	6	9	9	5	10	6	4	3	4	-	45
	<i>n</i> > LOD	45	45	32	45	45	45	43	36	45	45	33	0	37	10	44	45	35	18	1	2	31	45	40	4	36	-	
	LOD ₂ (ng L ⁻¹)	26308	4482	450	11515	6289	66	39	40	45	617	26	62	66	2367	93	36	9	18	9	8	4	22	4	5	45	-	34
	<i>n</i> > LOD	34	34	34	34	34	30	34	6	34	34	1	0	34	2	34	34	34	0	0	14	34	34	34	0	3	-	
	LOD ₃ (ng L ⁻¹)	17597	14753	2313	4396	15238	13	41	33	390	8124	111	82	83	165	131	216	22	-	90	20	6	230	11	19	117	-	40
	<i>n</i> > LOD	40	40	34	40	40	40	28	12	37	19	0	1	2	6	39	40	32	-	0	18	39	37	19	0	0	-	
	LOD ₄ (ng L ⁻¹)	1168	1975	1332	623	15320	30	27	37	354	745	51	77	41	836	68	225	8	-	30	5	17	107	17	11	15	-	34
	<i>n</i> > LOD	34	34	15	34	34	34	30	14	34	34	1	2	7	2	31	34	34	-	0	9	23	32	10	0	9	-	
	<i>n</i> > LOD	153	153	115	153	153	149	135	68	150	132	35	3	80	20	148	153	135	18	1	43	127	148	103	4	48	-	153
	(%)	100	100	75	100	100	97	88	44	98	86	23	2	52	13	97	100	88	12	1	28	83	97	67	3	31	-	
HR-ICP-MS	LOD (ng L ⁻¹)	977	348	339	9457	6690	2	0.1	3	4	66	0.1	11	18	264	0.5	2	2	6	0.5	19	2	2	44	0.2	2	0.1	143
	<i>n</i> > LOD	143	143	143	143	143	143	143	143	143	143	143	143	143	129	143	143	143	2	143	35	143	143	143	142	143	143	
	(%)	100	100	100	100	100	100	100	100	100	100	100	100	100	90	100	100	100	1	100	24	100	100	100	99	100	100	
ICP-MS Analytical																												
Uncertainties (%)		6	5	8	3	5	9	8	19	3	4	8	4	6	4	5	3	4	22	17	8	4	2	9	5	5	-	
HR-ICP-MS Analytical																												
Uncertainties (%)		2	2	9	2	2	3	2	3	2	2	2	9	10	35	2	2	2	8	2	6	2	2	6	2	3	3	

3.3.4. Organometals (Hg and Sn species)

1. Sampling

Working with ultra-clean material is essential for determination of mercury and tin content, especially in water samples from remote areas. In that sense, time and effort have been dedicated for the cleaning of material used during the analytical process. Teflon containers were filled with nitric acid (HNO_3 , *Fisher Scientific, USA*) solution (10% v/v, deionized water), sonicated for 2h, and deionized water was used to rinse them. Then a second cleaning has been processed by filling the Teflon containers with a second solution of HNO_3 (10% v/v, deionized water). They have been sonicated 2h and rinsed with deionized water. Finally a last cleaning using a solution of HCl (*Fisher Scientific, USA*) (10% v/v, deionized water) to fill the Teflon containers has been done. After a last sonication of 2h, Teflon containers have been rinsed three times with deionized water and dried in a clean atmosphere, under a laminar flow hood. Concerning the syringe, silicone and Teflon tubings, cleaning has been processed in a similar way. All this material has been soaked in a first HNO_3 solution (10% v/v, deionized water), sonicated for 2h and rinsed with deionized water. This procedure has been repeated twice with a second solution of HNO_3 (10% v/v, deionized water), and with a solution of HCl (10% v/v, deionized water). Finally, all components were dried in a clean atmosphere, under a laminar flow hood. Sterivex units do not required any cleaning protocol and can be used directly from their original package.

Two different kinds of samples were collected and analysed: filtered and unfiltered.

For the filtered samples, after collecting a water sample using Go-Flo sampler (**3.2 Sampling strategy**), a Teflon container of 250 mL has to be rinsed three times with an aliquot of the water sample and filled with around 250 mL of the water sample. Then, a Teflon tube is connected to the syringe, and both are rinsed three times using the water sample from the 250 mL Teflon container. This last is also used to fill the syringe at the half before connecting the Sterivex Filter unit in place of the Teflon tube. The water sample collected in the syringe is passed through the filter and used to rinse three times a 125 mL Teflon container. Finally, according to this protocol the 125 mL Teflon is filled with 125 mL of the water sample.

For the unfiltered samples, a 125 mL Teflon container is directly rinsed three times with the water sample from the sampler and then filled with 125 mL of the water sample. In-field, all samples, filtered and unfiltered, were acidified at 0.5% v/v adding 625 μL of acetic acid (CH_3COOH 99%, Trace metal grade, *Fisher Scientific, USA*). Teflon containers were closed tightly and stored in double PE Zip-lock bags in a portable cooler (5-10 °C), protected from light, during transportation to the fridge laboratory (5-10 °C).

2. Isotopic Dilution Analysis (IDA)

The quantification by Isotopic Dilution Analysis (IDA) [10] is based on the measurement of the isotopic ratio in a sample where the natural isotopic abundance has been altered by the spike of an isotope tracer's solution. Isotopic dilution allows being free from the intensity variations that could be observed on the chromatogram (loss, dilution, transformations etc ...), thus, increasing significantly accuracy and precision of the measure. Moreover, the enrichment of samples in stable isotopes at the beginning of the analytical protocol also makes possible the evaluation of interconversion reactions (methylation, demethylation).

Two different modes of IDA application exist: species-unspecific (SU) and species-specific (SS).

The SU spiking mode was usually used because of a lack of mercury isotopically enriched spikes (MMHg, iHg) commercially available. This mode only allows correcting the errors derived from the detection step. Indeed, the isotopically enriched spikes are introduced online in the equipment, before the ionisation and detection process. The SU spiking mode does not make possible to correct the loss or transformations that occur during the analytical process.

With the SS spiking mode, isotopically enriched spikes are added during the analytical protocol, and IDA is applied specifically to one or more species, depending on whether the single or multiple IDA technique is used.

With classical or simple isotope dilution analysis (S-IDA), only one species enriched in one isotope is added to the sample. Loss or non-quantitative extraction during the analytical protocol are corrected, but not the inter-conversions (MMHg to iHg and vice versa) because each analyte is quantified independently of the others.

In double isotope dilution analysis (D-IDA), two isotope tracer's solutions, with known abundance, are spiked to the sample (e.g. ^{199}iHg and $^{201}\text{MMHg}$) and will react the same way that the studied species (e.g. ^{202}iHg and $^{202}\text{MMHg}$). The natural isotopic composition of the sample is altered, and the quantification is based on the measurement of the mixed isotope ratios. Data obtained by D-IDA can be processed specifically for two species (i.e. double species-specific isotope dilution analysis, D-SS-IDA) or for the whole system (i.e. isotope pattern deconvolution, IPD). D-SS-IDA model consists of the specific measurement of Hg species separately, and only two isotopes are considered for the quantification of each Hg species (e.g. $^{199}\text{iHg}/^{202}\text{iHg}$ for iHg and $^{201}\text{MMHg}/^{202}\text{MMHg}$ for MMHg). Both D-SS-IDA and IPD allow correcting losses and inter-conversions that occur during the whole analytical process. However, IPD takes into account all the different isotopic patterns of both spikes and endogenous species so it is more reliable than the D-SS-IDA. It also provides the determination of methylation and demethylation rates from the inter-conversions.

3. Analysis

Back to the laboratory, quantification is carried out by double species-specific isotopic dilution analysis (D-SS-IDA) and analysis by capillary GC-ICP-MS [11,12]. The operating conditions are listed in **Table 3.6**.

For that purpose, a derivatization step is needed. The sample in the 125 mL Teflon container is sonicated for 10 min to desorb potential surface-wall mercury. About 100 mL of that sample is weighted in a Boston clear glass vial followed by the addition of 5 mL of acetic acid/acetate buffer (0.1 mol L⁻¹, pH = 4.9) (*Fisher Scientific, USA*). The sample is spiked with weighted amounts of isotope tracer's solution (¹⁹⁹iHg inorganic mercury, ²⁰¹MMHg methylmercury, and ¹¹⁹BuSn mix of Mono-, Di- and Tributyltin; *ISC-Science, Spain*). Then, the sample is stored at room temperature, protected from light, in a laminar flow hood at least for 12 hours. After this equilibrium step, the pH has to be adjusted between 4.85 and 5.05 using additions of ultrapure HCl and/or NH₃ solutions (*Optima Grade, Fisher Scientific, USA*). 70 µL of derivatizing agent, sodium tetraethylborate (NaBEt₄, 5% v/v in Milli-Q water) (*Merseburger Spezialchemikalien, Germany*) and 250 µL of GC organic solvent (Isooctane, *Sigma-Aldrich*) is added to the mixture. After an agitation step of 20 min using an orbital shaker, the organic phase containing Hg species is recovered and transferred in a GC vial equipped with a 200 µL micro insert. Finally, it is stored at -20 °C until analysis.

For quality control purpose, laboratory and in-field blanks were processed regularly. An internal standard solution (0.5 µg L⁻¹ ²⁰³Tl and ²⁰⁵Tl, mass close to Hg) is also introduced together with the sample in the nebulizer chamber for mass bias correction.

Table 3.6: Operating conditions of the GC-ICP-MS

Gas Chromatograph	
Trace Ultra GC (Thermo Scientific, USA)	
Column	
Injector temperature	250 °C
Injection volume	2 µL (splitless)
Temperature program	Start at 80 °C (30 sec), 60 °C min ⁻¹ until 260 °C (60 sec)
Carrier gas flow (He)	5 mL min ⁻¹
Interface	
Interface temperature	280 °C
Interface length	0.50 m
ICP-MS	
XSeries II (Thermo Scientific, USA)	
Forward power	1250 W
Plasma gas flow (Ar)	15 L min ⁻¹
Auxiliary gas flow (Ar)	0.9 L min ⁻¹
Nebulizer gas flow (Ar)	0.27 L min ⁻¹
Make up gas flow (Ar)	300 mL min ⁻¹
Acquisition mode	Transient Time resolved analysis
Acquisition time	550 sec
Dwell time	20 ms
Detection mode	Pulse
Isotopes measured	¹¹⁷ Sn, ¹¹⁸ Sn, ¹¹⁹ Sn, ¹²⁰ Sn, ¹⁹⁹ Hg, ²⁰⁰ Hg, ²⁰¹ Hg, ²⁰² Hg, ²⁰⁴ Hg, ²⁰³ Tl, ²⁰⁵ Tl

4. Validation of the results

For iHg, laboratory blanks were used for the calculation of the LOD using the following formula:

Equation 3.5

$$LOD = 3 \times \sigma_{blank}$$

where σ_{blank} is the standard deviation associated to the blank analysis, either laboratory and/or in-field blanks.

iHg was detected in all the samples from Replim1 to Replim5 with LOD of respectively 26, 27, 57, 9 and 34 pg L⁻¹. It is in adequacy with recent publications from *Monperrus et al.* [11] and *Cavalheiro et al.* [12] where the LOD, calculated using the same formula mentioned above, were respectively of 53 and 42 pg L⁻¹.

It is worth noting that to obtain more accurate results, blanks levels (90, 50, 170, 100 and 104 pg L⁻¹ for respectively Replim1, 2, 3, 4 and 5), were subtracted from the results obtained by D-SS-IDA.

In the case of MMHg, the analysis of all the laboratory and in-field blanks did not display any signal at the corresponding retention time: it was below LOD. Thus, the LOD was estimated graphically from the background signal using one chromatogram extracted from one blank analysis. The following formula was used:

Equation 3.6

$$LOD = \frac{3 \times \sigma_{background} \times R}{m}$$

where $\sigma_{background}$ is the standard deviation associated to the mean of the background signal amplitude close to the retention time, R the response factor concentration/signal, and m the average mass of sample weighted at the beginning of the analytical process.

LOD for MMHg were 3 pg L⁻¹ for Replim1, Replim2 and Replim3, and 4 pg L⁻¹ for Replim4 and Replim5. As an analogy with iHg, these LOD are consistent with already published works: 16 pg L⁻¹ [11] and 12 pg L⁻¹ [12].

Except for Replim1 (n=93) and Replim2 (n=69) where 31 and 9 of the samples analysed have shown results <LOD, MMHg was detected in all the samples from Replim3 (n=80), Replim4 (n=68) and Replim5 (n=43). Detection of MMHg in these pristine ecosystems is very tricky as only a few thousands of count per second (cps) are finally detected on the chromatogram. Thus, a slight decrease in the sensitivity of the equipment and/or losses of mercury compounds during the analytical protocol will imply a decrease in the signal observed on the chromatogram: the more the user practice, the better are the results.

Another concern drove our attention regarding the results for organomercury species. Indeed, the total mercury (Hg_{tot}), calculated as the sum of iHg and MMHg, ranges from 121 to 2906 pg L⁻¹ in the subsurface water samples with a median value of 402 pg L⁻¹, while dissolved gaseous mercury (DGM) ranges from 20 to 10792 pg L⁻¹ with a median value of 119 pg L⁻¹. Therefore, the question was: is it possible that a fraction of the DGM was reduced into iHg during the sampling thus leading to an overestimation of the concentrations of iHg?

To answer properly to that question, in the last sampling campaigns Replim5, we collected in 125 mL Teflon container the water sample that has been previously purged to collect DGM species on gold-coated sand trap. These “purged samples” were acidified at 0.5% v/v adding 625 µL of CH₃COOH 99%(Trace metal grade) and analysed by GC-ICP-MS. Erreur ! Source du renvoi introuvable. shows a comparison between results obtained in purged and unfiltered samples for both MMHg and iHg. With good coefficient of determination r, and a slope not significantly different from 1, the results for iHg analysis confirm the fact that no reduction occur between the sampling and the analysis.

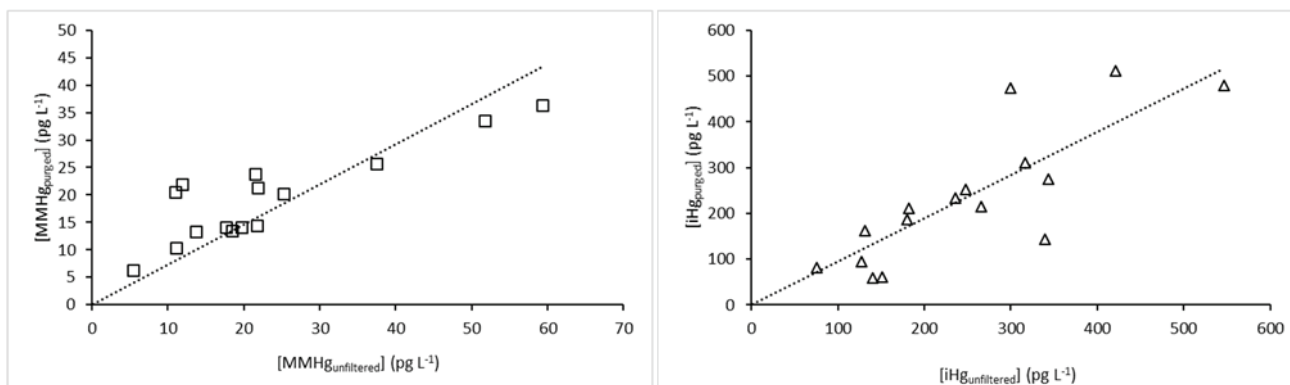


Figure 3.10: Comparison of (a) MMHg concentrations (pg L^{-1}) obtained in purged and unfiltered samples (Trend line $y = (0.73 \pm 0.06)x$; $r = 0.92$) and (b) iHg concentrations (pg L^{-1}) obtained in purged and unfiltered samples (Trend line $y = (0.94 \pm 0.07)x$; $r = 0.92$)

3.3.5. Dissolved Gaseous Mercury (DGM)

1. Sampling

In analogy with the protocol for organometals, specific cleaning procedure has been applied to the material used for DGM analysis. All plastic and glassware (containers, tubing, fittings, and moisture trap) were soaked in a HNO_3 solution (10% v/v, deionized water), sonicated for 2h and rinsed with deionized water. A second HNO_3 solution (10% v/v, deionized water) was used to soak the material. This second acid bath was sonicated 2h and all material was rinsed with deionized water. Finally, all components were soaked in a HCl solution (10% v/v, deionized water), sonicated for 2h and rinsed three times with deionized water. Drying was processed in a clean atmosphere, under a laminar flow hood. Regarding the gold-coated sand traps, they were heated three times at 600°C during 1 min, under argon flow (100 mL min^{-1}). They have been cooled down under a laminar flow hood and closed tightly with caps.

After collecting a water sample using Go-Flo sampler (**3.2 Sampling strategy**), the Teflon 250 mL container is rinsed three times with an aliquot of the water sample. Then, the Teflon container is filled overflow without headspace and following the Winkler method (introducing the silicone tubing down to the bottom remove all bubbles). Teflon containers were closed tightly and stored in double PE Zip-lock bags in a portable cooler ($5\text{-}10^\circ\text{C}$).

Samples have to be analysed as soon as possible. The first step consists of a specific purging treatment for the samples collected [13] (**Figure 3.11**). Nitrogen (N_2) cylinder or Pump-Rotameter, gas washing bottle, moisture trap and labelled gold-coated sand trap compose the purging line. Eight ice cubes and around 200 mL of ethanol or acetone have to be mixed in the dewar vessel to prepare the moisture trap bath. Then, the moisture trap is introduced in the mixture: the temperature has to reach -20 to -25°C . The water sample is poured out of the 250 mL Teflon container to reach a remaining volume of 200 mL, and the container is connected immediately to the gas washing bottle head. The water sample is flushed under nitrogen flow at 500 mL min^{-1} . After 20 min, the purge is stopped and the gold-sand trap

disconnected. To get a purge blank control, a new trap is connected and another 20 min of the purge is processed. Finally. Both gold-coated sand traps are closed with caps, stored in double zip-lock bags, and the gas washing bottle is rinsed with Milli-Q water.

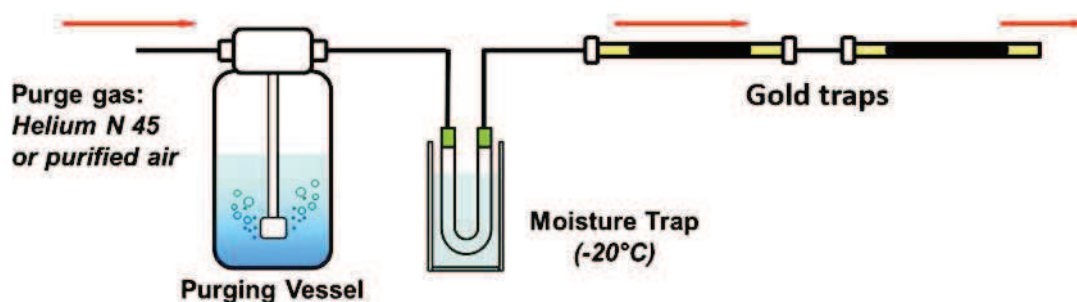


Figure 3.11: In-field purging system

2. Analysis

The analysis is done by double amalgamation on gold-AFS (DA/Au-AFS) [14]. Briefly, gold-coated sand traps are thermodesorbed (1 min at 600°C followed by 1 min cooling) under argon flow (100 mL min⁻¹) to transfer and amalgamate the mercury onto an analytical preconcentration pure gold trap (gold wool, *Brooks rand Labs, USA*). Then, a 30-sec flash heating at 800 °C is applied to the analytical trap to transfer the mercury to the detector.

Thermodesorption efficiency is controlled by carrying out two consecutive analyses of the gold-coated sand trap. Gaseous mercury quantification is done by external calibration of the DA/Au-AFS device using a controlled Hg⁰ source. Finally, the analysis of purge blanks allows estimating the efficiency of the sample treatment procedure.

3. Validation of the results

Analysis of the purge blanks allows estimating the efficiency of the sample treatment procedure. On the whole sampling campaigns, efficiency of the purging treatment was $(95\pm 3)\%$ ($n=12$) and allow validation of the method.

Regarding the limit of detection, it was calculated either with the results from a second analysis of a trap associated to a sample (sample blanks) or the results from the analysis of traps that were only transported during the sampling campaigns (storage blanks). The following formula was used:

Equation 3.7

$$LOD = 3 \times \sigma_{blank}$$

where σ_{blank} is the standard deviation associated to the blank analysis, either sample or storage blanks.

LOD were quiet constant over the sampling campaigns with values of 0.4, 0.1, 0.5, 0.2 and 0.2 pg L^{-1} respectively for Replim1, Replim2, Replim3, Replim4 and Replim5, which is consistent with the LOD of 0.4 pg L^{-1} expressed in *Bouchet et al.* [14].

3.3.6. Mercury species incubations

As mentioned **3.2 Sampling strategy**, intensive monitoring have been performed in ARA, GEN, SAB and AZU in order to better understand the dynamic of these lakes. In that sense, mercury species transformation potentials were determined through in situ incubations performed using isotopically enriched mercury species (^{199}iHg and $^{201}\text{MMHg}$) according to procedure published elsewhere [15,16].

1. Sampling

Two sets of unfiltered water samples were collected to perform the incubation experiments. All material used for this methodology underwent the same cleaning procedure described for **3.3.4 Organometals (Hg and Sn species)** and **3.3.5 Dissolved Gaseous Mercury (DGM)**. Different conditions of incubation have been tested depending on the sampling depth (subsurface S, middle M, and bottom B) or the light exposure (Light L vs Dark D) (**Table 3.7**), and the following protocol describes the sampling for only one condition.

After collecting a water sample using Go-Flo sampler (**3.2 Sampling strategy**), three 125 mL Teflon container (triplicate) per condition were directly filled with the water sample up to the top. Isotopically enriched spikes were added to each of the replicate to obtain concentrations in ^{199}iHg and $^{201}\text{MMHg}$ of respectively 2 and 0.2 ng L^{-1} . It corresponds to about 10 times the natural concentrations observed in the studied ecosystems: high enough to overlap the natural concentrations and low enough to avoid overestimation of the transformation rates. Using a rope and a weight, a line is setting up at the sampling point of the lake. Teflon containers either protected from the light or not, were placed at the corresponding depth using mounting plate fixed on the line. After 7 hours, the Teflon containers were collected and the incubation processes were stopped by adding high-purity HCl (1 % v/v). Teflon

containers were closed tightly and stored in double PE Zip-lock bags in a portable cooler (5-10 °C), protected from light, during transportation to the fridge laboratory (5-10 °C).

While the first set of samples will allow the determination of methylation and demethylation rates, the second set was collected to determine mercury reduction rates. After collecting the water samples for the first set of samples, two 250 mL Teflon containers (duplicate) per condition were filled overflow without headspace and following the Winkler method (introducing the silicone tubing down to the bottom remove all bubbles). They were incubated with the same Hg isotopic tracers concentration levels (2 ng L⁻¹ ¹⁹⁹iHg and 0.2 ng L⁻¹ ²⁰¹MMHg) and under similar conditions. The difference is that, at the end of the 7 hours, the elemental mercury (¹⁹⁹Hg₀) was immediately recovered in gold-coated sand traps by purging the water samples.

Table 3.7: Operating conditions for the incubation experiments

ID	Replim3	Replim4	Replim5
Lac Gentau	Subsurface (Light and Dark)	Subsurface (Light and Dark)	Subsurface (Light and Dark)
	Middle (Light and Dark)	Middle (Light and Dark)	Middle (Light and Dark)
	Bottom (Dark)	Bottom (Dark)	Bottom (Dark)
Ibón de Sabocos	Subsurface (Light and Dark)	Subsurface (Light and Dark)	Subsurface (Light and Dark)
	Bottom (Dark)	Bottom (Dark)	Middle (Light and Dark)
			Bottom (Dark)
Lac d'Arratille	Subsurface (Light and Dark)	Subsurface (Light and Dark)	
	Bottom (Dark)	Bottom (Dark)	-

2. Analysis

Back to the laboratory, quantification is carried out by isotope pattern deconvolution (IPD) isotope dilution analysis (IDA) and analysis by capillary GC-ICP-MS for the water samples following the same protocol that for the determination of organomercury species. The particularity is that the samples have to be spiked with other isotope tracer's solution (¹⁹⁸iHg and ²⁰²MMHg) as we already used ¹⁹⁹iHg and ²⁰¹MMHg in field.

The gaseous species trapped in the gold-coated sand traps were quantified by IPD and analysed by thermal desorption cryogenic trapping (CT) followed by GC-ICP-MS.

3.3.7. Total selenium (se)

1. Sampling

New Falcon tubes and Polypropylene containers do not need any cleaning step: they are fully suitable for Se analysis.

Two different kinds of samples were collected and analysed: filtered and unfiltered.

For the filtered samples, after collecting a water sample using Go-Flo sampler (**3.2 Sampling strategy**), a Teflon container of 250 mL has to be rinsed three times with an aliquot of the water sample and filled with around 250 mL of the water sample. Then, a Teflon tube is connected to the syringe, and both are rinsed three times using the water sample from the 250 mL Teflon container. This last is also used to fill the syringe at the half before connecting the Sterivex Filter unit in place of the Teflon tube. The water sample collected in the syringe is passed through the filter and used to rinse three times a 15 mL Falcon tube. Finally, according to this protocol the 15 mL Falcon tube is filled with 15 mL of the water sample. For the unfiltered samples, a 15 mL Falcon tube is directly rinsed three times with the water sample from the sampler and then filled with 15 mL of the water sample. In-field, all samples, filtered and unfiltered, were acidified at 1% v/v adding 150 μL of nitric acid (HNO_3 , *Optima Grade, Fisher Scientific, USA*). Falcon tubes were closed tightly and stored in double PE Zip-lock bags in a portable cooler (5-10 °C), protected from light, during transportation to the fridge laboratory (5-10 °C).

2. Analysis

Back to the laboratory, unfiltered samples have to be digested. The 15 mL sample are weighted, and addition of 300 μL of HNO_3 and 150 μL of HCl (final concentration of respectively 3% v/v and 1% v/v) is done prior to digestion using a DigiPrep (*SCP Science, Canada*). Facility method consists in a temperature gradient for 30 min (0-90 °C), followed by a constant heating at 90°C for 3 hours. Finally, unfiltered digested samples have to be weighted and filtered using Sterivex filter unit prior to their analysis.

Analysis of both filtered and unfiltered samples is carried out by ICP-MS (Agilent 7900) using H_2 as cell gas to reduce argon-based polyatomic interferences. Quality of the analytical protocol is assured by replicate analysis ($n \geq 2$), and multiple analysis of laboratory and in-field blanks ($n \geq 6$).

3.3.8. Silicate

1. Sampling

The sample used for silicate determination were the same as for major anions determination. Therefore, all details on the sampling are described in **3.3.2 Major anions**.

2. Analysis

Analysis is carried out by means of Flow Injection Analysis (FIA) [17] using the manifold depicted in **Figure 3.12**. The method employed is based on the classical Molybdenum Blue method but injecting the molybdate reagent (MR) on a sample carrier stream to improve sensibility, and detection is carried out spectrophotometrically at 810 nm. A molybdate reagent was prepared by dissolving 4.5 g of ammonium molybdate tetrahydrate ($(\text{NH}_4)_6\text{Mo}_7\text{O}_{24}\cdot 4\text{H}_2\text{O}$, *Merck KGaA, Germany*) in 400 mL of Milli-Q water and adding 3.7 mL of concentrated sulphuric acid (H_2SO_4 , *Merck KGaA, Germany*). Then, Oxalic acid (OA) was prepared by dissolving 25 g of oxalic acid ($\text{C}_2\text{H}_2\text{O}_4$, *Merck KGaA, Germany*) in 400 mL of Milli-Q water. Finally, Ascorbic acid (AA) was prepared by dissolving 12.5 g of ascorbic acid ($\text{C}_6\text{H}_8\text{O}_6$, *Merck KGaA, Germany*) in 400 mL of Milli-Q water. All three solutions were adjusted up to 500 mL using Milli-Q water.

The FIA system used for the analysis consists in a 4-channel MiniPuls 2 peristaltic pump (*Gilson Inc., USA*) and an E60-CE model injection valve (*Valco Instruments Co. Inc., USA*) with an automated single injection port. All the Teflon tubings have an inner diameter of 0.8 mm. As a detector, an Ultrospec III model spectrophotometer (*Pharmacia LKB Biotechnology AB, Sweden*) with a nominal precision of 0.001 absorbance units was used. The analogue signal from the detector was sent to the computer using a PowerChrom 280 analogue to digital convertor (*eDAQ Pty Ltd, Australia*) with a precision of 0.001 mV.

For silicate content determination, external calibration was used with silicon standard solutions (CertiPUR, 1000 mg(Si) L⁻¹, *Sigma-Aldrich, USA*) in a matrix similar to the samples in salinity, here with Milli-Q water as the salinity in the samples was very low or insignificant. According to the expected concentration in the samples, three different calibration ranges were prepared (0.05 to 0.3 mg(Si) L⁻¹; 0.3 to 1.5 mg(Si) L⁻¹; 1.5 to 6 mg(Si) L⁻¹). For each of these calibration ranges, three laboratory blank solutions were also measured. All samples, together with the calibration solutions, were analyzed once.

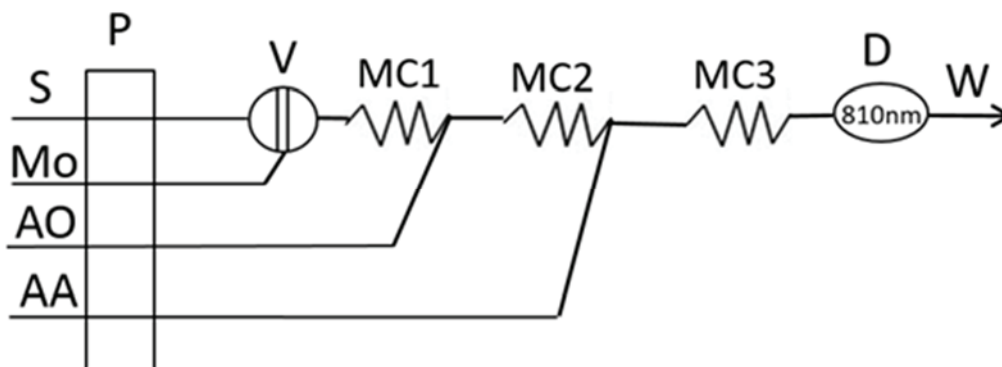


Figure 3.12: FIA manifold used for silicate determination

P: Peristaltic pump / V: Injection valve (500 μL) / D: Detector / MC1, MC2 and MC3: Mixing coils (100, 25 and 45 cm, respectively) / S: Sample (750 $\mu\text{L min}^{-1}$) / Mo: Molybdate reagent (750 $\mu\text{L min}^{-1}$) / AO: Oxalic acid reagent (750 $\mu\text{L min}^{-1}$) / AA: Ascorbic acid reagent (750 $\mu\text{L min}^{-1}$) / W: Waste

3.3.9. Total Organic Carbon (TOC)

1. Sampling

100 mL narrow neck glass bottles were rinsed successively with tap, deionized and Milli-Q water, and then dried in an oven. The glass caps were first cleaned from sealant vacuum grease with the help of a paper tissue before being cleaned with a detergent and rinsed with water in the same way as the bottles. Once dry, a thin layer of vacuum grease was applied to them again.

With the help of the silicon tubing connected to the Go-Flo sampler, the glass bottle was filled from the bottom, letting the water overflow until an approximate volume similar to that of the bottle was removed. Then, once the bottle is filled, a plastic pipette was used to leave a headspace of 1 % the volume of the bottle to allow the water expansion. For chemical preservation, 50-125 μL of the saturated HgCl_2 solution was added to the bottle using a micropipette and a new tip each time (0.02-0.05 % v/v) to stop biological activity from altering the carbon distributions in the sample. The bottle was closed with its glass cap, the cap was wrapped tightly using sealant tape, and the bottle was mixed gently. As fresh as possible and protected from light, the bottles wrapped in air bubble plastic bags were transported to the fridge laboratory (5-10 $^{\circ}\text{C}$).

2. Analysis

Total Organic Carbon was determined by catalytic combustion of the sample at 680 °C using a special analyser, Shimadzu TOC-V (*Shimadzu Corporation, Japan*). 20 mL of the samples were placed into the automatic sampler. As the organic carbon concentrations are very low in these samples, the inorganic carbon was first stripped from the sample using 20 µL of a 2 mol L⁻¹ HCl solution (*Bernd Kraft GmbH, Germany*), which transforms it to carbon dioxide (CO₂) in a quantitative way, and was purged away for 90 sec with the carrier gas, a synthetic air mixture (Zero K50S) 99.999 % free of CO₂ (*Carburos Metálicos, Spain*). Then, 100 µL of the acidified sample was injected in the combustion column. The organic carbon was converted to CO₂ and it was quantitatively determined with the help of a high sensitivity Non Dispersive InfraRed (NDIR) detector. If volatile organic compounds are present, then the method yields the Non Purgeable Organic Carbon (NPOC) instead.

External calibration, prepared daily with Milli-Q water up to 6 mg(C) L⁻¹, was carried out using a NIST traceable potassium hydrogen phthalate solution (*Panreac Química SLU, Spain*). To ensure precision of the results, replicate analysis were processed for laboratory blanks (n=10), standard solutions (n=5) and samples (n=3).

3. Limit of detection (LOD)

The limit of detection (LOD), associated to a specific technique, is the minimum concentration of an analyte in a sample that can be detected and it has been calculated as follow:

Equation 3.8

$$LOD = 3 \times \sigma_{blank}$$

where σ_{blank} is the standard deviation associated to the laboratory blank analysis

Analysis of the four sampling campaigns samples has been done during three different analytical sessions. The LODs obtained for these three analytical sessions were 0.12, 0.25 and 0.17 mg(C) L⁻¹, and all the results obtained were above the LOD associated to their analytical session.

3.3.10. Carbon Dioxide (CO₂) system parameters

1. Sampling

250 mL narrow neck glass bottles were rinsed successively with tap, deionized and Milli-Q water, and then dried in a clean atmosphere. The glass caps were first cleaned from sealant vacuum grease with the help of a paper tissue before being cleaned with a detergent and rinsed with water in the same way as the bottles. Once dry, a thin layer of vacuum grease was applied to them again.

With the help of the silicon tubing connected to the Go-Flo sampler, the glass bottle was filled from the bottom, letting the water overflow until an approximate volume similar to that of the bottle has been delivered. Then, once the bottle was filled, the use of a plastic pipette allow to leave a headspace of 1 % the volume of the bottle. For chemical preservation, 50-125 μL of the saturated HgCl_2 (*Merck, Germany*) solution was added to the bottle using a micropipette and a new tip each time (0.02-0.05 % v/v). The bottle was closed with its glass cap, the cap was wrapped tightly using the sealant tape, and the bottle was mixed gently. As fresh as possible and protected from light, the bottles wrapped in air bubble plastic bags were transported to the fridge laboratory (5-10 °C).

2. Analysis

Total Alkalinity and Dissolved Inorganic Carbon were measured using a VINDTA 3C instrument (Versatile Instrument for the Determination of Total inorganic carbon and titration Alkalinity) (*Marianda, Germany*) (**Figure 3.13**). The method for their determination in the high altitude lakes has been adapted from *Kortazar et al* who determined TA and DIC in estuarine waters [18], and has been already published [19]. It is fully described in the next chapter of this manuscript. Here we describe a short resume of the procedure.

Some future adjustment will be done in the calculation process for TA and DIC determination, so it is important working at constant temperature of 25 °C. For that purpose, samples were placed in a Julabo CORIO CD-BC26 Heating Circulator (*Julabo GmbH, Germany*) also connected to the VINDTA system to guarantee a temperature of 25 °C.

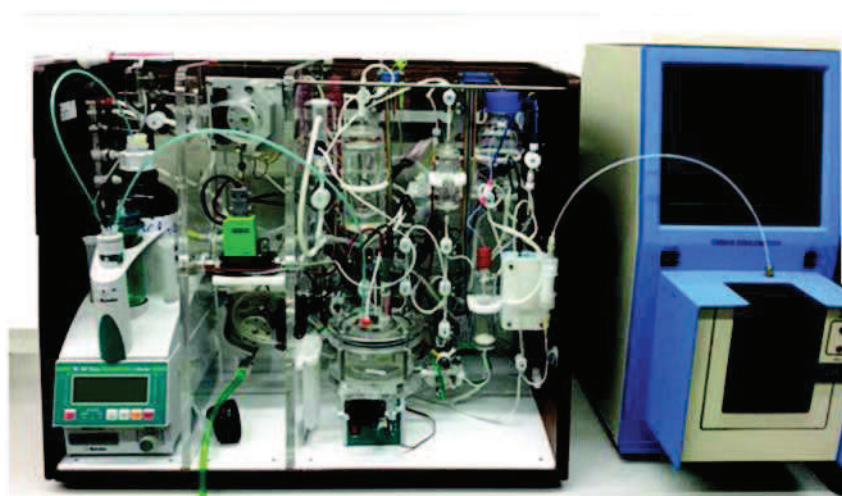


Figure 3.13: Equipment used for the determination of TA and DIC that includes the VINDTA 3C system coupled with a CM5015 coulometer and a 785 DMP Titrino

3. Dissolved Inorganic Carbon (DIC)

Dissolved Inorganic Carbon was quantified first in the samples by means of a coulometric determination [20] using the VINDTA 3C instrument fitted with a CM5015 Coulometer with the CM5011 emulator (*UIC Inc., USA*). The inorganic carbon is stripped from the sample pumped by the VINDTA 3C (20 mL using the small pipette) system using 10% v/v phosphoric acid (H_3PO_4) solution (*PanReac, Spain*), which transforms it to CO_2 in a quantitative way. The gas carrier, 99.999% nitrogen (N_2) (*Messer Group GmbH, Germany*), was filtrated ahead the equipment with a CO_2 trap (*Supelco, Sigma Aldrich, USA*). After, the CO_2 transported is titrated coulometrically in a special cell with cathode solution, anode solution and KI (*UIC Inc., USA*). Counts are measured every minute until the increment goes four times below the blank, measured at the beginning of the analytical session. A moisture trap made up with a few grams of granulated anhydrous magnesium perchlorate (*Alfa Aesar, Thermo Fisher (Kandel) GmbH, Germany*) is also placed before the cell to remove water. It is worth noting that the VINDTA system cleans the tubes and the small pipette with a few millilitres of the sample to be analysed at the beginning of the experiment.

To ensure the accuracy of the DIC measurements, Certified Reference Material for oceanic CO_2 measurements (*A. Dickson, Scripps Institution of Oceanography, USA*) is analysed. A correction factor was calculated by dividing the average experimentally obtained CRM values by the certified one. This factor was applied to the DIC values obtained experimentally for the samples collected for better accuracy of the results.

4. Total Alkalinity (TA)

Total Alkalinity was determined in the samples by means of an open cell potentiometric titration using the VINDTA 3C instrument. The titration is carried out with hydrochloric acid (HCl, Tracepur) (*Merck KGaA, Germany*) until a pH value around 4 is reached, corresponding to the carbonic acid end-point. Since the values of the DIC and TA are very similar in these samples, the previously determined DIC values were used to predict the concentration of HCl needed to titrate each sample. Four different HCl solutions were prepared (0.03, 0.015, 0.036 and 0.1 mol L^{-1}). To ensure the cleanliness of the system, a milli-Q water solution is used to remove the acid residue in the titration cell. Moreover, a few millilitres of samples are passed through the tubes and the pipettes to rinse them before the TA determination.

An extremely accurate determination of the titrant HCl concentration is mandatory. For that, a potentiometric standardisation with tris(hydroxymethyl)aminomethane (Tris) (*Panreac Química SLU, Spain*) is performed and the equivalence volume is calculated using Gran's equations [21].

Once the titration has been completed, TA was determined by non-linear least squares procedure with volume fitting using the Levenberg-Marquardt Algorithm (LMA) using the Microsoft Office Excel spreadsheet. The added volume values were theoretically calculated with the following equation:

Equation 3.9

$$V_{\text{calc},i} = \frac{m_0 \cdot (\text{term} - \text{TA})}{(C_{\text{H}}^0 - \text{term}) \cdot \delta_{\text{sample}}}$$

where C_H^0 is the concentration of the HCl titrant, $\bar{\delta}_{\text{sample}}$ is the density of the sample, m_0 the sample mass and *term* is defined as:

Equation 3.10

$$\begin{aligned} \textit{term} = & [\text{H}^+]_{\text{F}} + [\text{HSO}_4^-] + [\text{HF}] + [\text{H}_3\text{PO}_4] + [\textit{organic acids}] - [\text{HCO}_3^-] - 2[\text{CO}_3^{2-}] - [\text{B}(\text{OH})_4^-] - [\text{OH}^-] \\ & - [\text{HPO}_4^{2-}] - 2[\text{PO}_4^{3-}] - [\text{SiO}(\text{OH})_3^-] - [\text{NH}_3] - [\textit{organic bases}] \end{aligned}$$

The difference between the calculated volume and the experimental volume is minimised using the Solver complement available in the Microsoft Office Excel software by refining the standard potential of the electrode (E^0), TA and the total concentration and acidity constant of the organic alkalinity. In reality, the organic alkalinity would be the sum of all the acid-base species that are not considered in the classical equation for TA determination (i.e. without [organic acids] and [organic bases]).

5. pH and fugacity of CO_2 ($f\text{CO}_2$)

Using DIC and TA values, other parameters that characterise the CO_2 system such as the pH and the fugacity ($f\text{CO}_2$) were calculated with the help of the CO2SYS software [19]. Since this program has been developed for marine measurements, The MATLAB script version used in this work was modified to implement the set of stability constants for the carbonate system published by *Kortazar et al.* [18] and the organic alkalinity contribution (concentration and associated pK_a) determined previously with the TA.

Table 3.8: Summary of the parameters analysed together with their associated analytical protocol

Parameter	Matrix	Method	Material	Reagents
Physicochemical parameters (depth, temperature, conductivity, salinity, dissolved oxygen, pH, oxidation-reduction potential and chlorophyll-a)	Unfiltered water	Multiparametric probe (in-situ measurements)	-	-
Major anions (Fluoride F ⁻ , Chloride Cl ⁻ , Nitrite NO ₂ ⁻ , Bromide Br ⁻ , Nitrate NO ₃ ⁻ , Phosphate PO ₄ ³⁻⁻ , and Sulphate SO ₄ ²⁻)	Filtered water	Ionic chromatography	Plastic containers (50 mL); syringes; syringe-filters (polyamide, 0.45 µm); Zip-lock bags	<u>Cleaning:</u> none <u>In-situ treatment:</u> none <u>Analysis:</u> Milli-Q water (18.2 MΩ cm); 4.5 mmol L ⁻¹ Na ₂ CO ₃ / 0.8 mmol L ⁻¹ NaHCO ₃ ; Standards commercial solutions of the anions of interest
Major and trace cations	Filtered and unfiltered water	ICP-MS or HR-ICP-MS	Plastic containers (50 mL); syringes; syringe-filters (PVDF, 0.45 µm); Zip-lock bags	<u>Cleaning:</u> Elix water (10-15 MΩ cm); Milli-Q water (18.2 MΩ cm); HNO ₃ (Analytical grade) <u>In-situ treatment:</u> sub-boiling twice-distilled HNO ₃ (Tracepur grade) for acidification <u>Analysis:</u> Milli-Q water (18.2 MΩ cm); Standards commercial solutions of the cations of interest; Internal standards (usually Sc, Y, In, Bi, Ge or similar); Argon
Organometals (Inorganic mercury iHg, Monomethylmercury MMHg and Butyltin BuSn)	Filtered and unfiltered water	GC-ICP-MS using isotope dilution analysis	Teflon containers (125 or 250 mL + one single 250 mL for filtration operation); Luer-lock Teflon or PP syringes (plunger without rubber); Sterivex Filter units (PVDF, 0.22µm); Teflon tubings (10 cm length, ¼ inch OD, for filtration operation); PE Wash bottle; Zip-lock bags	<u>Cleaning:</u> deionized water (13 MΩ cm); HNO ₃ (Analytical grade); HCl (Analytical grade) <u>In-situ treatment:</u> CH ₃ COOH (Trace metal grade) for acidification <u>Analysis:</u> Milli-Q water (18.2 MΩ cm); CH ₃ COOH (Trace metal grade) and Sodium acetate trihydrate (ACS grade) for buffer preparation; NH ₃ and HCl (Optima grade) for pH adjustment; NaBEt ₄ as derivatizing agent; Isooctane (HPLC grade) as organic solvent; Thallium (Claritas PPT® Grade) as internal standard; ²⁰¹ Hg-enriched Monomethylmercury, ¹⁹⁹ Hg-enriched Inorganic mercury and ¹¹⁹ Sn-enriched Butyltin mix standard solutions; Argon and Helium
Dissolved Gaseous Mercury (DGM)	Unfiltered water	Preconcentration on gold trap and detection by Double amalgamation on gold-AFS (DA/Au-AFS)	Teflon containers (250 mL); Nitrogen cylinder or Pump-Rotameter; Gas washing bottle; dewar vessel; gold-coated sand trap; Zip-lock bags	<u>Cleaning:</u> deionized water (13 MΩ cm); HNO ₃ (Analytical grade); HCl (Analytical grade) <u>In-situ treatment:</u> Ice cubes and ethanol or acetone (Analytical or technical grade) for moisture trap preparation <u>Analysis:</u> Pure metallic mercury standard for quantification by Headspace injection/Double amalgamation on gold-AFS (DA/Au-AFS); Argon

Total selenium	Filtered and unfiltered water	ICP-MS	Polypropylene (PP) Falcon tubes (15 mL) and a PP or Teflon 250 mL for filtration operation; Luer-lock Teflon or PP syringes (plunger without rubber); Sterivex Filter units (PVDF, 0.22µm); Teflon tubings (10 cm length, ¼ inch OD, for filtration operation); PE Wash bottle; Zip-lock bags	<p><u>Cleaning:</u> none</p> <p><u>In-situ treatment:</u> HNO₃ (Optima grade) for acidification</p> <p><u>Analysis:</u> HNO₃ and HCl (Trace metal grade) for digestion; Single element calibration standard for ICP-MS for total selenium determination</p>
Silicate	Filtered and unfiltered water	Flow Injection Analysis (FIA)	Plastic containers (50 mL); syringes; syringe-filters (polyamide, 0.45 µm); Zip-lock bags	<p><u>Cleaning:</u> Tap water, Elix water (10-15 MΩ cm) and Milli-Q water (18.2 MΩ cm)</p> <p><u>In-situ treatment:</u> none</p> <p><u>Analysis:</u> Milli-Q water (18.2 MΩ cm); ammonium molybdate tetrahydrate; H₂SO₄; oxalic acid; ascorbic acid; Silicon standard solution for external calibration</p>
Total organic carbon	Unfiltered water	TOC analyser	100 mL narrow neck glass bottles provided with glass caps; protective air bubble plastic bags; silicon rubber tubing; plastic pipette; sealant tape; micropipette; tips	<p><u>Cleaning:</u> Tap water, Elix water (10-15 MΩ cm) and Milli-Q water (18.2 MΩ cm)</p> <p><u>In-situ treatment:</u> Saturated HgCl₂ solution for sample preservation</p> <p><u>Analysis:</u> Milli-Q quality water (18.2 MΩ cm); HCl (p.a. tracepur); HK-Phtalate (NIST traceable standard); carrier gas Zero K50S 99.999 % free of CO₂</p>
Dissolved inorganic carbon (DIC) and Total alkalinity (TA)	Unfiltered water	VINDTA	250 mL narrow neck glass bottles provided with glass caps; protective air bubble plastic bags; silicon rubber tubing; plastic pipette; sealant tape; micropipette; tips	<p><u>Cleaning:</u> Tap water, Elix water (10-15 MΩ cm) and Milli-Q water (18.2 MΩ cm)</p> <p><u>In-situ treatment:</u> Saturated HgCl₂ solution for sample preservation</p> <p><u>Analysis:</u></p> <ul style="list-style-type: none"> - DIC: H₃PO₄ (p.a. tracepur); Anode and Cathode solutions; KI (p.a.) - TA: HCl (Tracepur); NaCl rinsing solution; Tris

3.4. References

- [1] D.G. Zaharescu, P.S. Hooda, C.I. Burghilea, A. Palanca-Soler, A Multiscale Framework for Deconstructing the Ecosystem Physical Template of High-Altitudes Lakes, (n.d.) 30.
- [2] E. Serrano-Cañadas, Glacial evolution of the upper Gallego Valley (Panticosa mountains and Ribera de Biescas, Aragonese Pyrenees, Spain), (n.d.) 23.
- [3] Z. Santolaria, T. Arruebo, J.S. Urieta, F.J. Lanaja, A. Pardo, J. Matesanz, C. Rodriguez-Casals, Hydrochemistry dynamics in remote mountain lakes and its relation to catchment and atmospheric features: the case study of Sabocos Tarn, Pyrenees, Environmental Science and Pollution Research. 22 (2015) 231–247. <https://doi.org/10.1007/s11356-014-3310-0>.
- [4] L.L. Bridgewater, R.B. Baird, A.D. Eaton, E.W. Rice, American Public Health Association, American Water Works Association, Water Environment Federation, eds., Standard methods for the examination of water and wastewater, 23rd edition, American Public Health Association, Washington, DC, 2017.
- [5] J.D. Pfaff, D.P. Hautman, DETERMINATION OF INORGANIC ANIONS IN DRINKING WATER BY ION CHROMATOGRAPHY, (n.d.) 40.
- [6] N. Prieto-Taboada, O. Gómez-Laserna, I. Martínez-Arkarazo, M.A. Olazabal, J.M. Madariaga, Optimization of two methods based on ultrasound energy as alternative to European standards for soluble salts extraction from building materials, Ultrasonics Sonochemistry. 19 (2012) 1260–1265. <https://doi.org/10.1016/j.ultsonch.2012.03.002>.
- [7] Method 1669: Sampling Ambient Water for Trace Metals at EPA Water Quality Criteria Levels, (n.d.) 39.
- [8] Method 1640: Determination of Trace Elements in Water by Preconcentration and Inductively Coupled Plasma-Mass Spectrometry, (n.d.) 65.
- [9] C.M. Wood, Silver, in: Fish Physiology, Elsevier, 2011: pp. 1–65. [https://doi.org/10.1016/S1546-5098\(11\)31023-0](https://doi.org/10.1016/S1546-5098(11)31023-0).
- [10] S. Clémens, M. Monperrus, O.F.X. Donard, D. Amouroux, T. Guérin, Mercury speciation in seafood using isotope dilution analysis: A review, Talanta. 89 (2012) 12–20. <https://doi.org/10.1016/j.talanta.2011.12.064>.
- [11] M. Monperrus, E. Tessier, S. Veschambre, D. Amouroux, O. Donard, Simultaneous speciation of mercury and butyltin compounds in natural waters and snow by propylation and species-specific isotope dilution mass spectrometry analysis, Analytical and Bioanalytical Chemistry. 381 (2005) 854–862. <https://doi.org/10.1007/s00216-004-2973-7>.
- [12] J. Cavalheiro, C. Sola, J. Baldanza, E. Tessier, F. Lestremau, F. Botta, H. Preud'homme, M. Monperrus, D. Amouroux, Assessment of background concentrations of organometallic compounds (methylmercury, ethyllead and butyl- and phenyltin) in French aquatic environments, Water Research. 94 (2016) 32–41. <https://doi.org/10.1016/j.watres.2016.02.010>.
- [13] D. Amouroux, E. Tessier, C. Pécheyran, O.F.X. Donard, Sampling and probing volatile metal(loid) species in natural waters by in-situ purge and cryogenic trapping followed by gas chromatography and inductively coupled plasma mass spectrometry (P-CT-GC-ICP/MS), Analytica Chimica Acta. 377 (1998) 241–254. [https://doi.org/10.1016/S0003-2670\(98\)00425-5](https://doi.org/10.1016/S0003-2670(98)00425-5).
- [14] S. Bouchet, E. Tessier, M. Monperrus, R. Bridou, J. Clavier, G. Thouzeau, D. Amouroux, Measurements of gaseous mercury exchanges at the sediment–water, water–atmosphere and sediment–atmosphere interfaces of a tidal environment (Arcachon Bay, France), Journal of Environmental Monitoring. 13 (2011) 1351. <https://doi.org/10.1039/c0em00358a>.
- [15] M. Monperrus, E. Tessier, D. Amouroux, A. Leynaert, P. Huonnic, O.F.X. Donard, Mercury methylation, demethylation and reduction rates in coastal and marine surface waters of the Mediterranean Sea, Marine Chemistry. 107 (2007) 49–63. <https://doi.org/10.1016/j.marchem.2007.01.018>.

- [16] P. Rodriguez-Gonzalez, S. Bouchet, M. Monperrus, E. Tessier, D. Amouroux, In situ experiments for element species-specific environmental reactivity of tin and mercury compounds using isotopic tracers and multiple linear regression, *Environmental Science and Pollution Research*. 20 (2013) 1269–1280. <https://doi.org/10.1007/s11356-012-1019-5>.
- [17] J. Ma, R.H. Byrne, Flow injection analysis of nanomolar silicate using long pathlength absorbance spectroscopy, *Talanta*. 88 (2012) 484–489. <https://doi.org/10.1016/j.talanta.2011.11.019>.
- [18] L. Kortazar, D. Milea, O. Gómez-Laserna, L.A. Fernández, Accurate determination of total alkalinity in estuarine waters for acidification studies, *TrAC Trends in Analytical Chemistry*. 114 (2019) 69–80. <https://doi.org/10.1016/j.trac.2019.01.010>.
- [19] L. Kortazar, B. Duval, O. Liñero, O. Olamendi, A. Angulo, D. Amouroux, A. de Diego, L.A. Fernandez, Accurate determination of the total alkalinity and the CO₂ system parameters in high-altitude lakes from the Western Pyrenees (France – Spain), *Microchemical Journal*. 152 (2020) 104345. <https://doi.org/10.1016/j.microc.2019.104345>.
- [20] A.G. Dickson, C.L. Sabine, J.R. Christian, C.P. Barger, North Pacific Marine Science Organization, eds., *Guide to best practices for ocean CO₂ measurements*, North Pacific Marine Science Organization, Sidney, BC, 2007.
- [21] G. Gran, Determination of the equivalence point in potentiometric titrations. Part II, *The Analyst*. 77 (1952) 661. <https://doi.org/10.1039/an9527700661>.

**4. Accurate determination of the total alkalinity
and the CO₂ system parameters in high
altitude lakes from the Western Pyrenees
(France – Spain)**

4.1. Abstract

Studies on the CO₂ system in alpine lakes are performed by scientists of different areas and, therefore, it is crucial to establish common procedures to investigate the chemical properties of these ecosystems to reach comparable results and perform meaningful long-term studies. In this work, a robust procedure was developed to determine the total alkalinity in high altitude mountain lakes which allows the determination of the CO₂ system parameters with improved precision and accuracy. In the potentiometric titration of the samples with HCl, used for the Total Alkalinity determination, the fitting between experimental and calculated titration points was greatly improved by incorporating the contribution of new acid-base species, which had not been accounted for in previous works. This methodology can be used not only for alpine lakes but also for other natural water systems where the contribution of an extended set of acid-base species is normally not considered. A modified script has been also developed for the Matlab version of the CO₂SYST program, which allows an adequate calculation of the rest of the CO₂ system parameters. The calculated pK_a values of the new acid-base species are consistent in nearly all the lakes, ranging from 6.5 to 7, suggesting the similar nature of the acid-base species in all the lakes and that in the Ayous area a different number and/or type of species could be present. Furthermore, the values of all the chemical parameters studied were explained considering the geochemistry of the bedrock.

Keywords:

Total Alkalinity; Data analysis; CO₂ system; High altitude mountain lakes; Pyrenees

L. Kortazar, B. Duval, O. Liñero, O. Olamendi, A. Angulo, D. Amouroux, A. de Diego, L.A. Fernandez, Accurate determination of the total alkalinity and the CO₂ system parameters in high-altitude lakes from the Western Pyrenees (France – Spain), *Microchemical Journal*. 152 (2020) 104345. <https://doi.org/10.1016/j.microc.2019.104345>.

4.2. Introduction

Alpine lakes are iconic landscapes in mountain regions, where they frequently play an important role as economic and touristic resources. From an environmental point of view, as these ecosystems are usually far from local sources of pollution, they are particularly sensitive to the atmospheric deposition of pollutants and climate change due to climatic factors, shallow soil cover, the modest dimension of the watershed and rapid flushing rates. Alpine lakes are often located in crystalline bedrocks, which implies low ionic strength waters with a poor buffer capacity. It has been reported that physical, chemical, and biological lake properties respond rapidly to climate-related changes [1–5]. Studies performed in lakes can provide some of the early indications of the effects of climate change on the ecosystem's structure and function as well as the consequences for ecosystem services [5]. Particularly, the study of the Pyrenean lakes is of special interest due to their geographical situation, which makes the chemistry of precipitation to be influenced by the air masses with different origins: Mediterranean, Atlantic, Saharan and Continental [1].

Since the industrial revolution times, CO₂ is being produced and emitted to the atmosphere in important quantities. The CO₂ concentration in the atmosphere has increased from pre-industrial levels of around 280 parts per million (ppm) up to 415 ppm in May 2019 [6,7] (updated regularly at: <https://www.esrl.noaa.gov/gmd/ccgg/trends/>), which means about a 50% increment. The CO₂ concentration is predicted to keep rising and may reach levels of around 936 ppm by the year 2100 according to the Representative Concentration Pathway (RCP) 8.5 of the IPCC which is the “high emission scenario” [6], and could have negative effects in different ecosystems.

For instance, a large part of the excess of the emitted CO₂ is absorbed by various natural sinks, the most well-known being oceans, which absorb the excess of CO₂, lowering its concentration in the atmosphere but making the oceans more acidic [6,8,9]. This phenomenon is known as ocean acidification. The pH of the ocean has lowered about 0.1 units from pre-industrial levels [10] and by the end of the century, the average surface ocean pH could be 0.2 - 0.4 units lower than it is today [6,11]. Although this phenomenon is referred to oceanic waters, every natural water system is being affected by this excess of atmospheric CO₂ in different ways and its study in different natural water bodies is of great interest. Since the effects of the increase of the atmospheric CO₂ concentration will be appreciated with difficulty in short periods, it is crucial to use a proper methodology to study the CO₂ system to obtain results with the highest possible accuracy and precision. This has been the highest priority for oceanographers in the last decades.

When the “quality” of analytical measurements is being tested, it is very important to consider the scientific application that they are required for, and the maximum uncertainty that is considered appropriate for that application. A quite recent report describing plans for a Global Ocean Acidification Observing Network (GOA-ON) articulates two such applications: a “weather” goal and a “climate” goal [12]. The former is defined as a set of measurements of a quality that is sufficient to identify relative spatial patterns and short-term variations, supporting mechanistic responses to the impact on local, immediate ocean acidification dynamics. This implies an uncertainty of ~10 μmol kg⁻¹ in measurements

of total alkalinity (TA) and dissolved inorganic carbon (DIC) (~0.5 %). The “climate” goal is defined as a set of measurements of a quality that is enough to assess long-term trends with a defined level of confidence, supporting detection of the long-term anthropogenically driven changes in hydrographic conditions. This objective is much more demanding and implies an uncertainty of ~2 μmol kg⁻¹ in measurements of TA and DIC (~0.1 %). These “weather” and “climate” goals were used by Bockmon and Dickson [13] at their interlaboratory comparison studies.

To characterise the CO₂ chemistry, four measurable parameters can be used: TA, (DIC), pH and partial pressure of CO₂ (pCO₂) or fugacity (fCO₂) [14]. Given the thermodynamic relation between all of them, it is only necessary to experimentally measure two of them to calculate the other two if the temperature, ionic strength, pressure and the concentrations of other acid-base species are known [9,14–16]. The equations used to obtain a complete description of the carbon dioxide system are the mass-conservation equations and the equilibrium constants, which are gathered in the book “Guide to Best Practices for Ocean CO₂ Measurements” [17]. These four parameters are described in the following.

TA is a mass-conservation expression for the hydrogen ion. The most used definition for alkalinity nowadays is that formulated by Andrew Dickson [18]. According to him: “The total alkalinity of a natural water is thus defined as the number of moles of hydrogen ion equivalent to the excess of proton acceptors (bases formed from weak acids with a dissociation constant $K \leq 10^{-4.5}$, at 25 °C and zero ionic strength) over proton donors (acids with $K > 10^{-4.5}$) in one kilogram of sample.”

The total alkalinity is expressed according to **Equation 4.1**:

Equation 4.1

$$\begin{aligned} \text{TA} = & [\text{HCO}_3^-] + 3[\text{CO}_3^{2-}] + [\text{B}(\text{OH})_4^-] + [\text{OH}^-] + [\text{HPO}_4^{2-}] + 2[\text{PO}_4^{3-}] + [\text{SiO}(\text{OH})_3^-] \\ & + [\text{HS}^-] + 2[\text{S}^{2-}] + [\text{NH}_3] - [\text{H}^+] - [\text{HSO}_4^-] - [\text{HF}] \\ & - [\text{H}_3\text{PO}_4] + [\text{organic bases}] - [\text{organic acids}] \end{aligned}$$

The contribution from organic species such as the bases of humic and fulvic acids is usually assumed to be negligible in systems like seawater. However, several studies have shown that the TA contribution from dissolved organic carbon (DOC) can be significant, especially in river, estuary and coastal waters, where the concentration of DOC is usually higher [19–22]. Conversely, since neither the detailed nature of DOC nor the dissociation constants for these organic species are well known, the effect of organic acids and bases on the alkalinity is very difficult to estimate [23]. However, ignoring the contribution of these systems would produce important errors when determining TA and, subsequently, the rest of the parameters for studying the CO₂ system.

DIC is the sum of the three species of the carbonate system in water: dissolved CO₂, HCO₃⁻ and CO₃²⁻. The pH of the water will determine the relative proportion of each of them. pH is the minus logarithm of the hydrogen ion concentration and, finally, pCO₂ is the partial pressure of CO₂ in air in equilibrium with a water sample, which is a measure of the degree of saturation of the sample with CO₂ gas. In thermodynamics, the fCO₂ of a real gas replaces the mechanical partial pressure used for ideal gases.

This chemical system has been widely studied in seawater and lately it is being studied in estuary waters as well [15], where accurate measurements of the carbonate system have become a high priority in the

last decades. Regarding high-altitude mountain systems, it has been found that CO₂ release from inland waters contribute significantly to the global carbon budget [24–28], although they have not been widely studied yet. This means that inland lakes are not CO₂ sinks, but instead, they emit this gas to the atmosphere. However, an anthropogenic increase of the atmospheric CO₂ concentration will affect the equilibrium between the atmosphere and the surface of the lakes. The concentration of CO₂ in water would increase, whereas the pH would still decrease. Considering the usually low buffer capacity of high-altitude mountain lakes, small changes in the proton concentration will be more noticeable than in other natural waters with a higher buffer capacity, such as seawater. An important decrease on the pH would be harmful for all the organisms that inhabit these ecosystems.

Even if the lakes are very important for the global CO₂ budget, the methodology employed up to now is far from being acceptable for this kind of studies, considering the weather and climate goals mentioned before. For instance, *Finlay et al.* [27] studied the seasonality of pCO₂ in some lakes with data collected over 36 years. They estimated the pCO₂ and the CO₂ flux from conductivity, temperature and pH measurements. Moreover, they estimated the DIC from a previously derived relationship between DIC and conductivity. Whereas these methodologies may be valid to obtain approximate values, they cannot be considered acceptable for accurate studies of the CO₂ system. *Wen et al.* [29] studied the CO₂ emissions from lakes and reservoirs of China based on the pCO₂ values. These values were estimated from pH, TA, salinity and temperature, where pH was measured using a multiparametric probe with an uncertainty of 0.01 units in pH and TA was measured following an old-fashioned standard procedure [30] with a measurement error of 100 μmol L⁻¹. Moreover, the dissociation constants they used for the CO₂ system are intended to be used in seawater and are not suitable for freshwater [31,32]. According to up to date standards, these methodologies would be deemed unacceptable to study the CO₂ system in other natural water systems such as seawater, and, therefore, they should not be considered adequate for inland waters either.

Taking into account everything mentioned before, we have considered necessary to establish a proper calculation strategy for the determination of TA with high accuracy and precision to study the effects of the increased emissions of CO₂ in the carbonate system of high-altitude mountain lakes. The developed methodology was tested in alpine lakes from the Pyrenees, although it could be used in other natural water systems. Furthermore, a preliminary analysis of the results was performed by linking them with the bedrock of the area.

4.3. Experimental section

4.3.1. Studied area and sampling

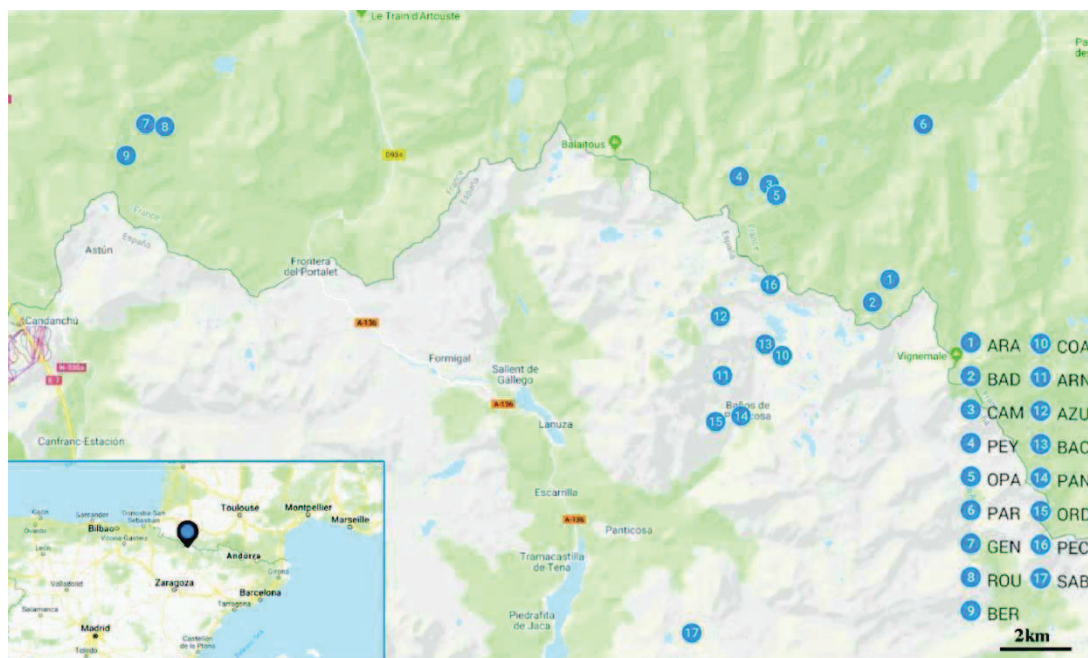


Figure 4.1: Location of the Pyrenean lakes considered in this study

Water samples were collected from 17 different high mountain lakes in the Pyrenees, most of them at an altitude higher than 2000 m: 9 in the French areas of Cauterets and Ayous and 8 in the Spanish areas of Panticosa and Sabocos (**Figure 4.1**). Those in Cauterets were Lac d'Arratille (ARA), Lac de la Badete (BAD), Grand lac de Cambales (CAM), Lac de Peyregnets de Cambales (PEY), Lac de Petite Opale (OPA) and Lac du Paradis (PAR); while those in Ayous were Lac Gentau (GEN), Lac Roumassot (ROU) and Lac Bersau (BER). The sampled lakes in Panticosa were Ibon de Coanga (COA), Ibon de los Arnales (ARN), Ibon Azul Alto (AZU), Embalse de Bachimana Bajo (BAC), Ibon de los Banos de Panticosa (PAN), Ibon de Ordicuso Inferior (ORD) and Ibon de Pecico de la Canal (PEC) and, finally, Ibon de Sabocos (SAB) was also sampled.

The lakes are located at different altitudes, from around 1600m above the sea level (asl) (PAN and PAR) to around 2500m asl (PEY).

Firstly, the six lakes of the Cauterets Area are covering a 900m altitudinal gradient and span about 7 km distance. This zone of the Pyrenees is a mosaic of crystalline, granitic and sedimentary rocks [33]. All these lakes are within the Parc National des Pyrenees (PNP), so the anthropogenic inputs are limited and restricted to pastoralism, fishing and hiking. PAR (1620m asl) is the only lake below 2000m asl. and close to a Park service road. It is also the smaller lake (0.4 Ha) showing a high content of organic matter

so a probable future transformation into a wetland cannot be discarded. In the Ayous area, ROU, GEN and BER are located close to the PNP. However, the agro pastoralism, and, therefore, the presence of gaggles, represents an important source of organic matter and nutrients, especially in GEN (1942m asl). Moreover, the mineral contributions from the pic d'Ayous, essentially iron, turn the bottom of lake GEN into an anoxic zone so this lake can be considered as eutrophic. It is worth noting that recreational fishing is also one of the main activities in all the French lakes.

The six lakes of the Panticosa area cover a 1000m altitudinal gradient and span about 10 km. Even if the geological structure on this side of the Pyrenees is similar, mostly granitic [34], climatic conditions in the Panticosa area differ from the Caunterets area, leading to visible changes in the vegetation. Three of these lakes can be influenced by local human activity because of the production of electricity coming from hydroelectric dams. Indeed, the flow of water is controlled upstream of BAC (2178m asl), PAN (1640m asl) and PEC (2460m asl). On its side, basin of SAB (1900m asl) is dominated by sedimentary rocks (Devonian and Cretaceous) and the lake is located close to a ski resort. All facilities of this touristic activity, which are operational the whole year, contribute to the presence of hikers and skiers nearby this lake. Moreover, by analogy to Gentau, agropastoralism with bovine and equine cattle and fishing are important activities in this area [35], showing also an anoxic zone at its bottom.

The sampling campaign addressed in this work took place in October 2018. The areas of Caunterets and Panticosa were sampled in 3 - 4 consecutive days. The samplings in Ayous and Sabocos were performed in a full working day each, where several samples were taken along the day in the same spot to study daily variations. All the lakes were reached by foot and the necessary material was transported in hiking backpacks. Sub-surface water samples (~0.5 m) were collected at the deepest point of each lake, which was reached with an inflatable boat. Physico-chemical parameters were also measured at each lake using an EXO2 multiparametric probe (YSI Inc., OH, USA). The measured parameters were conductivity (and its derived parameters, like salinity), temperature, pH, oxidation–reduction potential (ORP), Optical Dissolved Oxygen (ODO), Fluorescent Dissolved Organic Matter (fDOM) and depth. The water samples were taken using a 5 L capacity GO-FLO Teflon Trace Metal Bottle (General Oceanics, FL, USA). At the lake shore, the sample was divided in different sub-samples for specific parameters analysis. Sub-samples for the analysis of alkalinity and dissolved inorganic carbon were collected in 250 mL borosilicate brown glass bottles fitted with glass stoppers. Then, a headspace of 1 % of the bottle volume was left to allow for water expansion and a 100 μL spike of a saturated HgCl_2 solution (60 g L^{-1}) was added to stop biological activity from altering the carbon distribution in the samples, as recommended by the standard operating procedures (SOPs) [17]. Besides, sub-samples for the analysis of organic carbon were collected in 100 mL borosilicate glass bottles fitted with glass stoppers in which HgCl_2 spikes were also added. Finally, samples used for silicate and major anions (phosphate, fluoride and sulphate) analysis were collected in 50 mL polypropylene bottles. All these samples were kept at 4 °C until measurement.

4.3.2. Analytical methods

Silicate was measured by means of flow injection analysis (FIA) using the molybdenum blue method proposed by *Ma et al.* [36] and using the equipment described by *Kortazar et al.* [37], while phosphate was measured using ion chromatography (IC) [38] along with fluoride and sulphate. Total organic carbon (TOC) was measured as nonpurgeable organic carbon (NPOC) using a TOC-VCSH system with an automatic sampler (Shimadzu Corporation, Kyoto, Japan).

TA and DIC were measured using a VINDTA 3C system (Marianda, Kiel, Germany) [15]. TA was determined using a potentiometric titration while DIC determination was performed coulometrically [17] with a CM5015 Coulometer with the CM5011 emulator supplied by UIC Inc. (UIC Inc., Rockdale, IL, USA).

Since the TA values of these samples differ widely, it was deemed necessary to perform first the determination of the DIC in all the samples. Afterwards, considering that the TA values are usually very similar to DIC, samples were separated into 4 - 5 different groups and HCl titrant solutions of adequate concentration were prepared for each group. This working procedure assured a proper quality of the potentiometric titrations. The used HCl concentrations were 0.003, 0.015, 0.036 and 0.1 mol L⁻¹. HCl was standardised by potentiometric titration using Tris (tris(hydroxymethyl)aminomethane), and the equivalence volume was calculated using Gran II equations [39]. The HCl 0.1 mol L⁻¹ solution was titrated both with a Certified Reference Material (CRM) provided by Andrew Dickson's laboratory (A. Dickson, Scripps Institution of Oceanography, San Diego) and with Tris in order to verify the usefulness of Tris and Gran II equations for this purpose.

4.3.3. Calculation procedures

Silicate was measured using flow injection analysis (FIA) using the molybdenum blue method proposed by *Ma et al.* [36] and using the equipment. In the case of DIC, correction factors were calculated, using the CRMs, by dividing the average experimentally obtained CRM values of the day with the certified ones. These correction factors were then applied to the experimental results to obtain traceable DIC values. For the determination of TA this procedure was not applicable due to the CRM's high TA concentration and matrix difference. Instead, a nonlinear least squares procedure with volume fitting using the Levenberg-Marquardt Algorithm (LMA) was used to calculate the TA using the Microsoft Office Excel program. The calculation procedure was previously published by *Kortazar et al.* [15] for estuarine waters but had to be modified for alpine lakes due to the matrix difference. All the equations to determine the stoichiometric constants used were in the total proton and in the mol kg_{solution}⁻¹ scales. The equations for the calculation of the dissociation constants of sulphuric acid and the self-ionisation of water were taken from the book "CO₂ in Seawater: Equilibrium, Kinetics, Isotopes" [16]. The pK₁ and pK₂ values for the carbonate system were published by *Kortazar et al.* [15]. These constants are based in those proposed by *Millero* [40]:

Equation 4.2

$$pK = pK_1^0 + a_0 \cdot S^{0.5} + a_1 \cdot S + a_2 \cdot S^{1.5} + \frac{(a_3 \cdot S^{0.5} + a_4 \cdot S)}{T} + a_5 \cdot S^{0.5} \cdot \ln T$$

where $i = 1$ or 2 , correspond to the first or the second dissociation equilibria of the carbonate system, respectively, and pK_0 refers to the thermodynamic constant that was calculated according to the equations proposed by *Millero*:

Equation 4.3

$$pK_1^0 = -126.34048 + \frac{6320.813}{T} + 19.568224 \ln T$$

Equation 4.4

$$pK_2^0 = -90.18333 + \frac{5143.692}{T} + 14.613358 \ln T$$

The values of the parameters a_0 to a_5 can be found in *Kortazar et al.* [15] and are gathered in **Table 4.1**.

Table 4.1: Values of the $a_0 - a_5$ parameters used in the calculation of the stoichiometric constants of the carbonate system [15]

	For pK_1	For pK_2
a_0	15 (kept fixed)	21 (kept fixed)
a_1	0.0450 ± 0.0047	0.1453 ± 0.0072
a_2	-0.000852 ± 0.000042	-0.00517 ± 0.000064
a_3	-594.5 ± 6.5	-768.5 ± 9.9
a_4	-8.4 ± 1.4	-19.4 ± 2.1

As mentioned before, TA was determined by means of non-linear least-squares regression with volume fitting. This means that the added volume values were theoretically calculated, v_{calc} , and their differences with the experimental ones, v_{exp} , were minimised by refining certain parameters. In the present work, several models with different refined parameters were essayed in order to choose the most suitable ones.

For each titration point v_{calc} was calculated with the following equation:

Equation 4.5

$$v_{calc,i} = \frac{m_0 \cdot (\text{term} - TA)}{(C_H^0 - \text{term}) \cdot \delta_{sample}}$$

where C_H^0 is the concentration of the HCl titrant, δ_{sample} is the density of the sample and term is defined as:

Equation 4.6

$$\begin{aligned} \text{term} = & [\text{H}^+]_{\text{F}} + [\text{HSO}_4^-] + [\text{HF}] + [\text{H}_3\text{PO}_4] + [\text{organic acids}] \\ & - [\text{HCO}_3^-] - 2[\text{CO}_3^{2-}] - [\text{B}(\text{OH})_4^-] - [\text{OH}^-] - [\text{HPO}_4^{2-}] \\ & - 2[\text{PO}_4^{3-}] - [\text{SiO}(\text{OH})_3^-] - [\text{NH}_3] - [\text{organic bases}] \end{aligned}$$

Once TA and DIC were calculated, the rest of the parameters that characterise the CO₂ system, such as, pH or fCO₂ were calculated with the help of the CO2SYS software [41,42]. In this work, the MATLAB script version modified by *Orr. et al.* [43] was used and further modified as will be explained below. The script was executed in the GNU Octave software environment (John W. Eaton.,FSF, Inc).

4.4. Results and discussion

Among the measured anions that could contribute to the TA, fluoride (< 0.002 mg L⁻¹) and phosphate (< 0.090 mg L⁻¹) were under the limit of detection (LOD) and, therefore, their contribution was considered negligible. **Table 4.2** collects the concentrations of DIC, NPOC and silicate along with the salinity found in the investigated lakes.

Table 4.2: Salinity, DIC, NPOC and silicate concentrations measured in sub-surface waters of the lakes

ID Lake	Salinity	DIC ($\mu\text{mol kg}^{-1}$)	NPOC ($\mu\text{mol kg}^{-1}$)	SiO(OH) ₃ ⁻ ($\mu\text{mol kg}^{-1}$)
ARA	0.028	776.94	149.87	50.17
BAD	0.029	778.48	105.32	43.35
CAM	0.006	162.29	90.44	19.74
PEY	0.003	79.41	136.97	8.52
OPA	0.011	306.91	93.26	25.10
PAR	0.022	641.62	191.84	67.77
GEN	0.014	367.98	108.90	14.75
ROU	0.014	358.60	155.49	12.17
BER	0.008	237.32	132.21	9.24
AZU	0.029	803.34	78.66	28.63
ARN	0.011	308.67	–	26.02
BAC	0.013	357.95	87.87	15.64
PEC	0.016	443.61	89.90	23.31
COA	0.004	124.64	156.51	12.28
PAN	0.013	371.60	169.20	31.40
ORD	0.020	572.54	386.39	30.12
SAB	0.058	1691.23	252.41	11.65

As can be appreciated, DIC values are much lower than those values usually found in other natural waters such as seawater, where DIC is around 2400 $\mu\text{mol kg}^{-1}$. Besides that, values differ substantially among lakes, which corresponds, mainly, to differences in the bedrock composition. The higher values are found in SAB whose basin lies on Devonian sedimentary rocks (limestone, sandstone, shale), and Cretaceous sedimentary rocks (limestone, sandstone) compose its south catchment area. During

Cretaceous, more chalk (CaCO_3 deposited by the shells of marine invertebrates) was formed than in any other period in the Phanerozoic, including Devonian and Permo-Triassic (conglomerate, sandstone, lutite, andesite, shale). These carbonate rocks, composed mainly by limestone, are very sensitive to weathering, explaining the high DIC in this lake. The basins and/or catchment of the lakes ARA, BAD, PAR, AZU, PEC and ORD are mainly composed by Devonian sedimentary rocks, but granitic rocks are also present in their surroundings. While the second ones are igneous rocks containing mainly quartz and feldspar and hard to dissolve, the first ones contain limestone.

This could explain their reasonably high DIC ($600 - 800 \mu\text{mol kg}^{-1}$) although it is not as high as in SAB. Among these lakes, PEC shows the lowest DIC values probably due to a higher granitic basin percentage. These lakes also present the highest concentrations of silicate, which might be related to the sandstone (quartz and feldspar) highly soluble of the Devonian rocks. The lakes from the Ayous area have a Permo-Triassic volcanic bedrock which also agrees with the lower DIC ($300 \mu\text{mol kg}^{-1}$). DIC values around $400 \mu\text{mol kg}^{-1}$ are observed for lakes PAN and BAC, which are connected to other lakes upstream, either rich in carbonate or not. The DIC values, around $300 \mu\text{mol kg}^{-1}$, measured in lakes ARN and OPA are related to the Devonian rocks located in the surroundings dragging CaCO_3 in their granitic basin. Finally, CAM, PEY, and COA have a granitic basin which agrees with their very low DIC values.

The relative standard deviation (RSD) of the NPOC values is 5 %, and for silicate is 2 %, where both uncertainties were calculated as the square root of the sum of the variances due to repetition and the intrinsic one. In the case of DIC, the uncertainty was calculated in the same way and the RSD values were below 1 %. These are rather high RSD values for this kind of studies, but considering the low DIC values obtained, it is normal to have higher RSD values.

Taking into account the relative high concentrations of NPOC and the low DIC values, the contribution of organic alkalinity can be considered significant. Regarding the determination of TA, the 0.1 mol L^{-1} HCl solution was used to evaluate the usability of Tris for its standardisation. Using the CRM, the HCl concentration obtained was $0.10462 \pm 0.00003 \text{ mol L}^{-1}$ (0.03 % RSD), while using Tris the HCl concentration obtained was $0.1044 \pm 0.0009 \text{ mol L}^{-1}$ (0.9 % RSD). The repeatability obtained using the CRM was considerably better than using Tris. The reason might be that the calculation of the equivalence volume using Gran II equations is very dependent of the amount of titration points used. It could probably be improved by performing more and smaller volume additions of the titrant. However, the relative difference between both values is of 0.2 % and both are statistically comparable at a 99 % of confidence level. Therefore, Tris was used for the standardisation of HCl when its concentration was $< 0.1 \text{ mol L}^{-1}$.

For the determination of TA, first, the curve fitting was performed by refining both E^0 and TA, as it is usually done. As an example, **Figure 4.2** shows both the experimental and calculated curves for the case of AZU, where the black dots correspond to the experimental titration points while the red striped dots correspond to the fitted curve using the refined parameters. This model will be called (1) for now on.

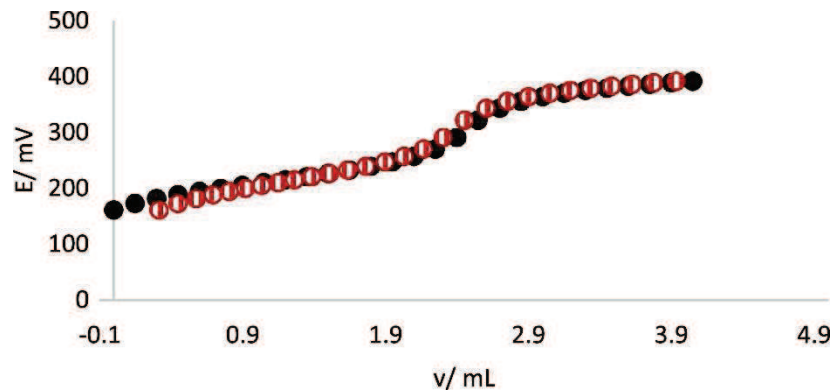


Figure 4.2: Fitting between the experimental curve (black dots) and the calculated curve (red striped dots) for the titration of the lake AZU sample when TA and E^0 are refined

As can be seen, the fitting between both curves is not perfect. This suggests that all the acid-base species present in the water were not considered. Therefore, different refinement approaches were tested and contrasted, as can be seen in Erreur ! Source du renvoi introuvable., again for the case of AZU used as an example.

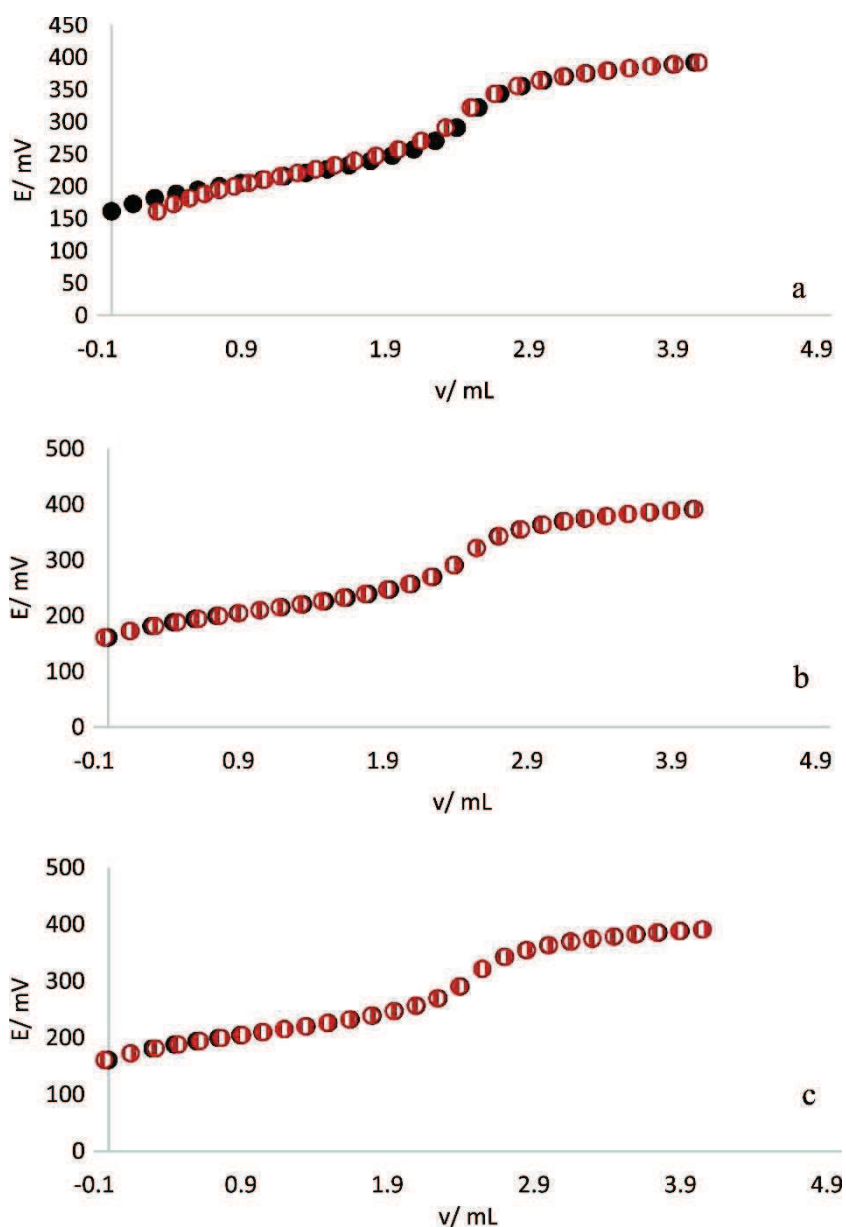


Figure 4.3: Fitting between the experimental curves (black dots) and the calculated curve (red striped dots) for the titration of the lake AZU sample when a) TA, E^0 and the a_0 values in **Equation 4.2** are refined, b) TA, E^0 and both the pK_a and the total concentration of the new acid-base species were refined and c) all the above mentioned parameters were simultaneously refined

In **Figure 4.3.a**, besides the TA and E_0 , the a_0 values in **Equation 4.2** for the calculation of both pK_a values of the carbonate system were also refined. These last two values were refined according to the work published by *Kortazar et al.* [15] for the determination of TA in estuarine waters. This model will be called (2).

As mentioned before, the contribution of organic alkalinity might be significant and therefore it seemed necessary to consider its contribution. Since the nature and concentration of the possible acid-base organic species was unknown, a single species was considered for each lake and both its pK_a and total concentration were refined as shown in **Figure 4.3.b**, which will be called model (3). This “new species alkalinity” would be the sum of all the acid-base species that was not considered in **Equation 4.1**, and

probably, not only the organic alkalinity. Finally, in **Figure 4.3.c**, the previously mentioned 6 parameters were refined and will be called model (4).

Table 4.3 shows the values of the refined parameters as well as the residual sum of squares (RSS) along with their uncertainties, calculated with the help of the Microsoft Excel macro SolverAid (<http://www.bowdoin.edu/~rdelevie/excellaneous/>). The RSS is a measure of the discrepancy between the empirical data and an estimation model.

Table 4.3: Values of the refined parameters as well as the residual sum of squares (RSS), along with their uncertainties, calculated with the help of the Microsoft Excel macro SolverAid when 1) TA and E_0 are refined, 2) TA, E_0 and the a_0 values in **Equation 4.2** were refined, 3) TA, E_0 and both the pK_a and the total concentration of the new acid-base species [New-Spe] were refined and 4) when all the above mentioned parameters were refined

Model	RSS	TA ($\mu\text{mol kg}^{-1}$)	E_0 (mV)	a_0 (pK_1)	a_0 (pK_2)	pK_{new}	[New-Spe] ($\mu\text{mol kg}^{-1}$)
1)	0.5	818 ± 18	586 ± 2	–	–	–	–
2)	0.2	833 ± 24	585 ± 2	14.5 ± 0.2	(21 ± 91)	–	–
3)	0.005	852 ± 2	585.8 ± 0.2	–	–	6.58 ± 0.04	196 ± 7
4)	0.003	850 ± 2	585.8 ± 0.2	15 ± 1	(21 ± 41)	6 ± 2	(189 ± 22)

First, it has to be mentioned that the a_0 parameter for the pK_2 of the carbonate system is negligible in this example due to the sample's pH. This is the reason for having such high uncertainties. Both **Figure 4.2** and **Figure 4.3** and **Table 4.3** show that in models 1) and 2) the experimental and calculated curves do not match fully. The high RSS values obtained indicate that these two models are not appropriate for the determination of TA. The RSS of model 4) is the lowest one. However, the high correlation between the pK_{new} and the concentration of the new acid-base species results in very large uncertainties. This model has too many parameters to be refined for the relatively low amount of data used in the calculation. Therefore, model 3) seems to be the most adequate for the calculation of TA in these lakes. The correlation between the pK_{new} and the concentration of the new acid-base species is also quite high in this case, resulting in a RSD value for [New-Spe] close to 5 %.

As mentioned before, the Matlab script version of CO2SYS was used to calculate pH and $f\text{CO}_2$ from TA and DIC. This script had to be modified to take into account two new important aspects: 1) the set of stability constants for the carbonate system published by *Kortazar et al.* [15] which have been used in this work and 2) the contribution of the new acid-base species to the TA. To fulfil this last requirement, the script was modified to allow the addition of the new acid-base species total concentration and its pK_{new} values as input parameters. Provisions were also made to ensure convergence of the calculations since the low TA and DIC values of some samples sometimes prevented it. To ease the calculations, an Excel template was developed to manually add the input parameters into the script, which was also

used to collect all the output parameters. Both the script and the Excel template are available upon request.

Table 4.4 shows the values of all the parameters used to characterise the CO₂ system (TA, DIC, pH and fCO₂) as well as the predicted new acid-base species concentration and pK_{new} values obtained for the studied lakes.

Table 4.4: Values of all the parameters used to characterise the CO₂ system (TA, DIC, pH and fCO₂) as well as the predicted new acid-base species concentration and pK_{new} values of the studied lakes

	[New-Spe] ($\mu\text{mol kg}^{-1}$)	pK _{new}	DIC ($\mu\text{mol kg}^{-1}$)	TA ($\mu\text{mol kg}^{-1}$)	pH	fCO ₂
ARA	256	7.07	777	815	7.23	1998
BAD	171	6.76	778	825	7.37	1450
CAM	143	6.40	162	154	6.36	1618
PEY	110	6.00	79	85	5.94	1034
OPA	194	6.76	307	291	6.74	1788
PAR	187	6.74	642	618	6.99	2639
GEN	549	7.24	368	378	6.74	2462
ROU	384	7.28	359	374	6.87	1943
BER*	13	7.31	237	222	7.41	446
AZU	196	6.58	803	852	7.27	1803
ARN	158	6.53	309	309	6.79	1737
BAC	258	6.85	358	350	6.75	2194
PEC	765	7.46	444	438	6.79	2489
COA	264	6.46	125	106	6.02	1523
PAN	359	7.00	372	334	6.64	2718
ORD	199	6.75	573	540	6.90	2740
SAB	243	6.57	1691	1839	7.71	1584
ARA	256	7.07	777	815	7.23	1998

*The discrepancies between BER and the rest of the lakes in the Ayous area might indicate an experimental error when measuring this sample and, therefore, it will not be considered for the discussion

As can be seen, pK_{new} ranges between 6.5 and 7.0 in all the lakes except for those of Ayous. This might indicate that whatever it is being considered as acid-base species shows a similar nature for all these lakes. Furthermore, these pK_a values are in agreement with those found by *Yang et al.* [44] for organic acids found coastal waters. It might be hypothesised that in the lakes of the Ayous area a different number and/or type of acid-base species would be present compared to the rest of the lakes, but this aspect clearly deserves further investigation. Furthermore, considering that the concentration of the refined species is sometimes higher than the NPOC, it can be concluded that not only organic matter is being considered but also something else.

Concerning the CO₂ system parameters, the obtained pH values range between 6.0 and 7.7. As expected, SAB showed the highest pH value, which is logical considering the carbonate-based basin. PEY, the highest lake located on granitic bedrocks, shows always the lowest pH values, which corresponds with the lowest TA and DIC values. Moreover, according to *Skjelkvale et al.* [3] low pH values can be caused by organic cations (humic acids) and, as can be seen, PEY shows one of the highest new species concentration and NPOC concentrations. Finally, the fugacity shows, as published before, that these lakes contribute to increase the CO₂ (g) concentration in the atmosphere. The atmospheric pCO₂ is around 415 ppm nowadays and if the fugacity is above that value it means that the equilibrium is displaced to the gas phase, and thus, CO₂ is released to the atmosphere. As can be seen in **Table 4.4** the fugacities of these lakes are well above this atmospheric value and therefore it is crucial to monitor them closely to understand the effects of the excess of atmospheric CO₂.

Regarding the precisions/uncertainties of the measured/derived variables, some observations can be made. Even if **Table 4.4** does not show the uncertainties of the results, general RSD values were calculated for each parameter to discuss them briefly. Most uncertainties were calculated as the square root of the sum of variances due to repetition and the intrinsic one, calculated differently in every case. In the case of the pH and the fugacity, only the standard deviation due to the repetition was considered and, thus, even if the repeatability is supposed to be the main contribution to the total uncertainty, the RSD values could be slightly higher.

The intrinsic uncertainty of TA was the one obtained from the fitting of titration data with the help of the SolverAid Excel macro. In general, RSD values were below 2 %, with very few exceptions. As happened for the DIC values, this RSD is quite high, but it can be explained by the low TA values. The RSD for the concentration of the new acid-base species was generally below 5 %, whereas for the pK_{new} was below 1 %. In the case of pH and fugacity, values were below 1 % and below 3 %, respectively. Considering these RSD values, the methodology can be considered precise, much more than those found in bibliography [27,29]. As previously stated, the low TA and DIC values of some samples imply higher RSD values, but the repeatability is as good as in other works which make use of this equipment [15]. The uncertainties of pH and fugacity derived from the refined parameters need further investigation, although there is a recent published work that study the uncertainty propagation for the marine CO₂ system [43].

4.5. Conclusions

A robust procedure was developed to determine the total alkalinity in high altitude mountain lakes, which allows the determination of the CO₂ system parameters with improved precision and accuracy that can also be useful for any other inland freshwater body with similar characteristics. This approach, derived from that developed for the accurate determination of acidification parameters in estuarine waters, allows the determination of TA in a highly improved way, compared to the currently available methodologies which have reported uncertainties of 100 μmol L⁻¹. Moreover, the methodologies used for the determination of TA in lakes are far from being acceptable for studies of the CO₂ system. The fitting between the experimental and calculated titration curves is very good and the obtained values are in good agreement with the expected ones. The obtained uncertainties are reasonably low, which indicates the high precision of this methodology. Moreover, the modified script for the Matlab version of CO2SYS allows the calculation of the rest of the parameters of the CO₂ system in a precise way. The incorporation of a new acid-base species to explain the deviation between the experimental and calculated curves is a great advantage that could be also used in any other natural water systems where not all acid-base species present in the samples, particularly those of organic nature, are explicitly known or can be adequately quantified. Moreover, most of the obtained results were explained taking into account the characteristics of the bedrock of the lakes' basin. However, further investigation is necessary in some cases, such as to explain the higher pH in the Ayous area. This methodology will help researchers from different areas to share common practices allowing the comparison and use of results from others, which would encourage multidisciplinary and long-term studies in these important ecosystems.

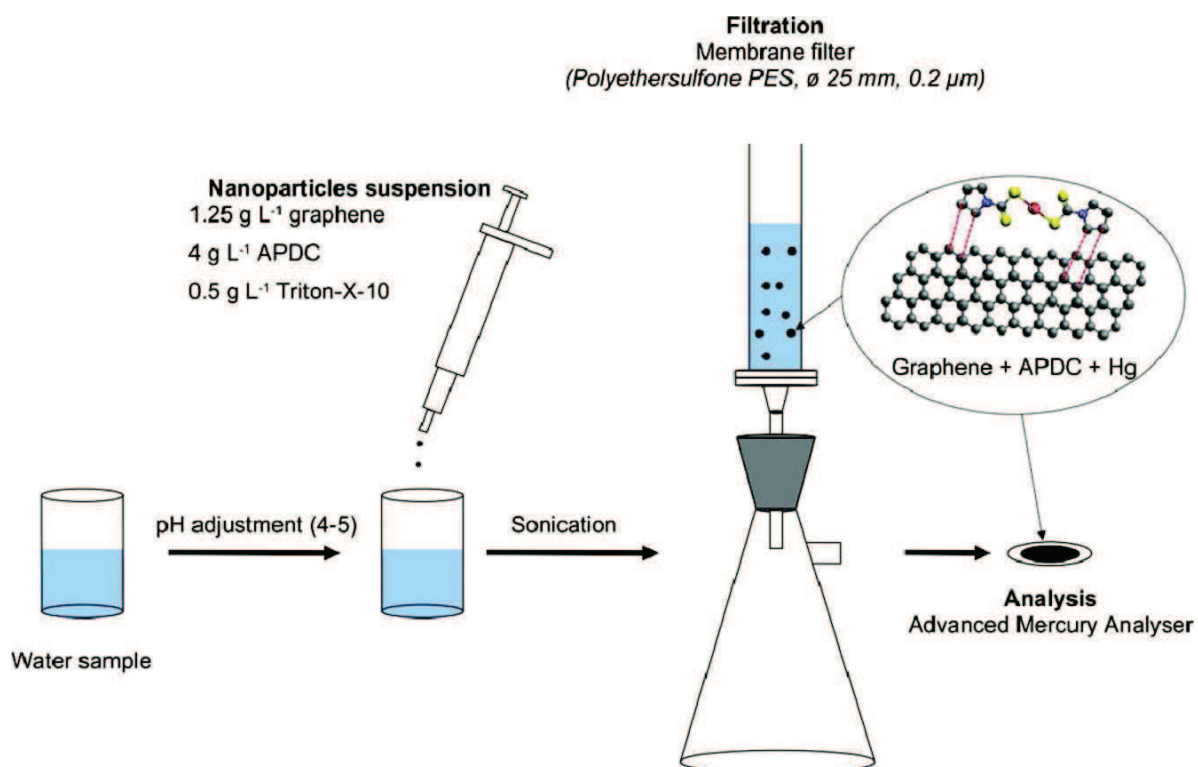
4.6. References

- [1] L. Camarero, J. Catalan, A SIMPLE MODEL OF REGIONAL ACIDIFICATION FOR HIGH MOUNTAIN LAKES: APPLICATION TO THE PYRENEAN LAKES (NORTH-EAST SPAIN), *Water Research*. 32 (1998) 1126–1136. [https://doi.org/10.1016/S0043-1354\(97\)00291-1](https://doi.org/10.1016/S0043-1354(97)00291-1).
- [2] R. Mosello, A. Lami, A. Marchetto, M. Rogora, B. Wathne, L. Lien, J. Catalan, L. Camarero, M. Ventura, R. Psenner, K. Koinig, H. Thies, S. Sommaruga-Wögrath, U. Nickus, D. Tait, B. Thaler, A. Barbieri, R. Harriman, Trends in the Water Chemistry of High Altitude Lakes in Europe, (n.d.) 16.
- [3] B.L. Skjelkvaale, R.F. Wright, Mountain lakes; sensitivity to acid deposition and global climate change, 27 (1998) 280–286.
- [4] R. Mosello, B.M. Wathne, L. Lien, H.J.B. Birks, Al:Pe projects: Water chemistry and critical loads, *Water, Air, & Soil Pollution*. 85 (1995) 493–498. <https://doi.org/10.1007/BF00476877>.
- [5] R. Adrian, C.M. O'Reilly, H. Zagarese, S.B. Baines, D.O. Hessen, W. Keller, D.M. Livingstone, R. Sommaruga, D. Straile, E. Van Donk, G.A. Weyhenmeyer, M. Winder, Lakes as sentinels of climate change, *Limnology and Oceanography*. 54 (2009) 2283–2297. https://doi.org/10.4319/lo.2009.54.6_part_2.2283.
- [6] T.F. Stocker, Intergovernmental Panel on Climate Change, eds., Climate change 2013: the physical science basis ; summary for policymakers, a report of Working Group I of the IPCC, technical summary, a report accepted by Working Group I of the IPCC but not approved in detail and frequently asked questions ; part of the Working Group I contribution to the fifth assessment report of the Intergovernmental Panel on Climate Change, Intergovernmental Panel on Climate Change, New York, 2013.
- [7] C. Le Quéré, R.J. Andres, T. Boden, T. Conway, R.A. Houghton, J.I. House, G. Marland, G.P. Peters, G.R. van der Werf, A. Ahlström, R.M. Andrew, L. Bopp, J.G. Canadell, P. Ciais, S.C. Doney, C. Enright, P. Friedlingstein, C. Huntingford, A.K. Jain, C. Jourdain, E. Kato, R.F. Keeling, K. Klein Goldewijk, S. Levis, P. Levy, M. Lomas, B. Poulter, M.R. Raupach, J. Schwinger, S. Sitch, B.D. Stocker, N. Viovy, S. Zaehle, N. Zeng, The global carbon budget 1959–2011, *Earth System Science Data*. 5 (2013) 165–185. <https://doi.org/10.5194/essd-5-165-2013>.
- [8] C. Le Quéré, R.M. Andrew, J.G. Canadell, S. Sitch, J.I. Korsbakken, G.P. Peters, A.C. Manning, T.A. Boden, P.P. Tans, R.A. Houghton, R.F. Keeling, S. Alin, O.D. Andrews, P. Anthoni, L. Barbero, L. Bopp, F. Chevallier, L.P. Chini, P. Ciais, K. Currie, C. Delire, S.C. Doney, P. Friedlingstein, T. Gkritzalis, I. Harris, J. Hauck, V. Haverd, M. Hoppema, K. Klein Goldewijk, A.K. Jain, E. Kato, A. Körtzinger, P. Landschützer, N. Lefèvre, A. Lenton, S. Lienert, D. Lombardozzi, J.R. Melton, N. Metzl, F. Millero, P.M.S. Monteiro, D.R. Munro, J.E.M.S. Nabel, S. Nakaoka, K. O'Brien, A. Olsen, A.M. Omar, T. Ono, D. Pierrot, B. Poulter, C. Rödenbeck, J. Salisbury, U. Schuster, J. Schwinger, R. Séférian, I. Skjelvan, B.D. Stocker, A.J. Sutton, T. Takahashi, H. Tian, B. Tilbrook, I.T. van der Laan-Luijkx, G.R. van der Werf, N. Viovy, A.P. Walker, A.J. Wiltshire, S. Zaehle, Global Carbon Budget 2016, *Earth System Science Data*. 8 (2016) 605–649. <https://doi.org/10.5194/essd-8-605-2016>.
- [9] J.-P. Gattuso, L. Hansson, eds., Ocean acidification, Oxford University Press, Oxford ; New York, 2011.
- [10] K. Caldeira, M.E. Wickett, Anthropogenic carbon and ocean pH, *Nature*. 425 (2003) 365–365. <https://doi.org/10.1038/425365a>.
- [11] M. Gledhill, E.P. Achterberg, K. Li, K.N. Mohamed, M.J.A. Rijkenberg, Influence of ocean acidification on the complexation of iron and copper by organic ligands in estuarine waters, *Marine Chemistry*. 177 (2015) 421–433. <https://doi.org/10.1016/j.marchem.2015.03.016>.
- [12] J. Newton, R. Feely, E. Jewett, P. Williamson, J. Mathis, Global Ocean Acidification Observing Network: Requirements and Governance Plan, (n.d.) 61.
- [13] E.E. Bockmon, A.G. Dickson, An inter-laboratory comparison assessing the quality of seawater carbon dioxide measurements, *Marine Chemistry*. 171 (2015) 36–43. <https://doi.org/10.1016/j.marchem.2015.02.002>.

- [14] A.G. Dickson, Part 1: Seawater carbonate chemistry, (n.d.) 36.
- [15] L. Kortazar, D. Milea, O. Gómez-Laserna, L.A. Fernández, Accurate determination of total alkalinity in estuarine waters for acidification studies, *TrAC Trends in Analytical Chemistry*. 114 (2019) 69–80. <https://doi.org/10.1016/j.trac.2019.01.010>.
- [16] R.E. Zeebe, D.A. Wolf-Gladrow, *CO₂ in seawater: equilibrium, kinetics, isotopes*, Elsevier, Amsterdam; New York, 2001.
- [17] A.G. Dickson, C.L. Sabine, J.R. Christian, C.P. Barger, North Pacific Marine Science Organization, eds., *Guide to best practices for ocean CO₂ measurements*, North Pacific Marine Science Organization, Sidney, BC, 2007.
- [18] A.G. Dickson, An exact definition of total alkalinity and a procedure for the estimation of alkalinity and total inorganic carbon from titration data, *Deep Sea Research Part A. Oceanographic Research Papers*. 28 (1981) 609–623. [https://doi.org/10.1016/0198-0149\(81\)90121-7](https://doi.org/10.1016/0198-0149(81)90121-7).
- [19] Y.H. Ko, K. Lee, K.H. Eom, I.-S. Han, Organic alkalinity produced by phytoplankton and its effect on the computation of ocean carbon parameters: Organic Alkalinity, *Limnology and Oceanography*. 61 (2016) 1462–1471. <https://doi.org/10.1002/lno.10309>.
- [20] W.-J. Cai, Y. Wang, R.E. Hodson, Acid-Base Properties of Dissolved Organic Matter in the Estuarine Waters of Georgia, USA, *Geochimica et Cosmochimica Acta*. 62 (1998) 473–483. [https://doi.org/10.1016/S0016-7037\(97\)00363-3](https://doi.org/10.1016/S0016-7037(97)00363-3).
- [21] H.-C. Kim, K. Lee, Significant contribution of dissolved organic matter to seawater alkalinity, *Geophysical Research Letters*. 36 (2009). <https://doi.org/10.1029/2009GL040271>.
- [22] C.W. Hunt, J.E. Salisbury, D. Vandemark, Contribution of non-carbonate anions to total alkalinity and overestimation of CO_2 in New England and New Brunswick rivers, *Biogeosciences*. 8 (2011) 3069–3076. <https://doi.org/10.5194/bg-8-3069-2011>.
- [23] F.J. Millero, D. Pierrot, K. Lee, R. Wanninkhof, R. Feely, C.L. Sabine, R.M. Key, T. Takahashi, Dissociation constants for carbonic acid determined from field measurements, *Deep Sea Research Part I: Oceanographic Research Papers*. 49 (2002) 1705–1723. [https://doi.org/10.1016/S0967-0637\(02\)00093-6](https://doi.org/10.1016/S0967-0637(02)00093-6).
- [24] J.J. Cole, Y.T. Prairie, N.F. Caraco, W.H. McDowell, L.J. Tranvik, R.G. Striegl, C.M. Duarte, P. Kortelainen, J.A. Downing, J.J. Middelburg, J. Melack, Plumbing the Global Carbon Cycle: Integrating Inland Waters into the Terrestrial Carbon Budget, *Ecosystems*. 10 (2007) 172–185. <https://doi.org/10.1007/s10021-006-9013-8>.
- [25] B.A. Denfeld, P. Kortelainen, M. Rantakari, S. Sobek, G.A. Weyhenmeyer, Regional Variability and Drivers of Below Ice CO₂ in Boreal and Subarctic Lakes, *Ecosystems*. 19 (2016) 461–476. <https://doi.org/10.1007/s10021-015-9944-z>.
- [26] V. Ducharme-Riel, D. Vachon, P.A. del Giorgio, Y.T. Prairie, The Relative Contribution of Winter Under-Ice and Summer Hypolimnetic CO₂ Accumulation to the Annual CO₂ Emissions from Northern Lakes, *Ecosystems*. 18 (2015) 547–559. <https://doi.org/10.1007/s10021-015-9846-0>.
- [27] K. Finlay, R.J. Vogt, G.L. Simpson, P.R. Leavitt, Seasonality of pCO₂ in a hard-water lake of the northern Great Plains: The legacy effects of climate and limnological conditions over 36 years, *Limnology and Oceanography*. 64 (2019). <https://doi.org/10.1002/lno.11113>.
- [28] Y.T. Prairie, Carbocentric limnology: looking back, looking forward, *Canadian Journal of Fisheries and Aquatic Sciences*. 65 (2008) 543–548. <https://doi.org/10.1139/f08-011>.
- [29] Z. Wen, K. Song, Y. Shang, C. Fang, L. Li, L. Lv, X. Lv, L. Chen, Carbon dioxide emissions from lakes and reservoirs of China: A regional estimate based on the calculated pCO₂, *Atmospheric Environment*. 170 (2017) 71–81. <https://doi.org/10.1016/j.atmosenv.2017.09.032>.
- [30] L.L. Bridgewater, R.B. Baird, A.D. Eaton, E.W. Rice, American Public Health Association, American Water Works Association, Water Environment Federation, eds., *Standard methods for the examination of water and wastewater*, 23rd edition, American Public Health Association, Washington, DC, 2017.
- [31] F.J. Millero, Thermodynamics of the carbon dioxide system in the oceans, (n.d.) 17.

- [32] R.N. Roy, L.N. Roy, K.M. Vogel, C. Porter-Moore, T. Pearson, C.E. Good, F.J. Millero, D.M. Campbell, The dissociation constants of carbonic acid in seawater at salinities 5 to 45 and temperatures 0 to 45°C, *Marine Chemistry*. 44 (1993) 249–267. [https://doi.org/10.1016/0304-4203\(93\)90207-5](https://doi.org/10.1016/0304-4203(93)90207-5).
- [33] D.G. Zaharescu, P.S. Hooda, C.I. Burghilea, A. Palanca-Soler, A Multiscale Framework for Deconstructing the Ecosystem Physical Template of High-Altitudes Lakes, (n.d.) 30.
- [34] E. Serrano-Cañadas, Glacial evolution of the upper Gallego Valley (Panticosa mountains and Ribera de Biescas, Aragonese Pyrenees, Spain), (n.d.) 23.
- [35] Z. Santolaria, T. Arruebo, J.S. Urieta, F.J. Lanaja, A. Pardo, J. Matesanz, C. Rodriguez-Casals, Hydrochemistry dynamics in remote mountain lakes and its relation to catchment and atmospheric features: the case study of Sabocos Tarn, Pyrenees, *Environmental Science and Pollution Research*. 22 (2015) 231–247. <https://doi.org/10.1007/s11356-014-3310-0>.
- [36] J. Ma, R.H. Byrne, Flow injection analysis of nanomolar silicate using long pathlength absorbance spectroscopy, *Talanta*. 88 (2012) 484–489. <https://doi.org/10.1016/j.talanta.2011.11.019>.
- [37] L. Kortazar, S. Alberdi, E. Tynan, L.A. Fernández, An adapted flow injection analysis method of phosphate for estuarine samples avoiding matrix effects, *Microchemical Journal*. 124 (2016) 416–421. <https://doi.org/10.1016/j.microc.2015.09.027>.
- [38] O. Gómez-Laserna, P. Cardiano, M. Diez-García, N. Prieto-Taboada, L. Kortazar, M.Á. Olazabal, J.M. Madariaga, Multi-analytical methodology to diagnose the environmental impact suffered by building materials in coastal areas, *Environmental Science and Pollution Research*. 25 (2018) 4371–4386. <https://doi.org/10.1007/s11356-017-0798-0>.
- [39] G. Gran, Determination of the equivalence point in potentiometric titrations. Part II, *The Analyst*. 77 (1952) 661. <https://doi.org/10.1039/an9527700661>.
- [40] F.J. Millero, Carbonate constants for estuarine waters, *Marine and Freshwater Research*. 61 (2010) 139. <https://doi.org/10.1071/MF09254>.
- [41] E. Lewis, D. Wallace, L.J. Allison, Program developed for CO₂ system calculations, 1998. <https://doi.org/10.2172/639712>.
- [42] D.E. Pierrot, D.W.R. Wallace, E. Lewis, MS Excel Program Developed for CO₂ System Calculations, (2011). https://doi.org/10.3334/CDIAC/otg.CO2SYS_XLS_CDIAC105a.
- [43] J.C. Orr, J.-M. Epitalon, A.G. Dickson, J.-P. Gattuso, Routine uncertainty propagation for the marine carbon dioxide system, *Marine Chemistry*. 207 (2018) 84–107. <https://doi.org/10.1016/j.marchem.2018.10.006>.
- [44] B. Yang, R.H. Byrne, M. Lindemuth, Contributions of organic alkalinity to total alkalinity in coastal waters: A spectrophotometric approach, *Marine Chemistry*. 176 (2015) 199–207. <https://doi.org/10.1016/j.marchem.2015.09.008>.

5. A simple determination of trace mercury concentrations in natural waters using Dispersive Micro-Solid Phase Extraction preconcentration based on functionalized graphene nanosheets



5.1. Abstract

In this work, we developed an innovative analytical method for the trace and ultra-trace determination of total mercury (Hg) concentration in natural water samples (fresh and seawaters). In this method, Dispersive Micro-Solid Phase Extraction (DMSPE) is applied using graphene nanosheets to quantitatively preconcentrate dissolved Hg from natural water samples, before its direct analysis by commercially available pyrolysis gold amalgamation and atomic absorption spectroscopy (AAS). In this new methodology, only two easy steps are necessary, saving time and effort. First, the operator has to add 500 μL of nanoparticles suspension containing graphene, Ammonium Pyrrolidine DithioCarbamate (APDC) and Triton-X-100 in the water sample. This solution is filtered under vacuum and the Hg complex on the functionalized graphene can be simply collected on a membrane filter (Polyethersulfone PES, 0.2 μm). The filter obtained can then be analysed back at the laboratory by direct pyrolysis of the PES filter using a commercial mercury analyser. Different parameters have been tested to optimize this preconcentration procedure, such as the sample volume, the amount of nanoparticles suspension and the extraction time. The stability conditions of the Hg preconcentrated on PES filters during storage and before analysis has also been investigated. The influence of the occurrence of marine salts (sodium chloride), natural organic matter or competing metals (calcium) in the sample has also been evaluated to prevent possible matrix effects. This method is fully operational after application to real water sample matrices and exhibits suitable limit of detection, as low as 0.38 ng L⁻¹ using 200 mL of the water sample, and excellent reproducibility (< 5 % as RSD).

Keywords:

Mercury; Preconcentration; Ultra-trace analysis; Graphene nanosheets; Dispersive Micro-Solid Phase Extraction (DMSPE); Water sample

B. Duval, A. Gredilla, S. Fdez-Ortiz de Vallejuelo, E. Tessier, D. Amouroux, A. de Diego, A simple determination of trace mercury concentrations in natural waters using dispersive Micro-Solid phase extraction preconcentration based on functionalized graphene nanosheets, *Microchemical Journal*. 154 (2020) 104549. <https://doi.org/10.1016/j.microc.2019.104549>.

5.2. Introduction

Among other pollutants, mercury (Hg) is of major concern in aquatic environments. While mercury is present at low concentration in natural waters [1], its specific biogeochemical cycling allows bioaccumulation and biomagnification in the food chain leading to serious consequences for animals and higher predators, including humans [2,3]. Consequences of mercury contamination are not only noticeable in terms of people's health [4,5] but also in the economic sphere [6–9].

Thereby, mercury concentrations in topsoil, atmosphere and oceanic surface waters have increased respectively by a factor of 1.2, 4-6 and 3 since the pre-industrial period [8,10]. Besides, the numerous ecological studies about mercury show that primary anthropogenic mercury emissions are still increasing [9,10]. Therefore, the scenarios for the future are quite pessimistic, predicting a change in mercury emission of -4 % to 96 % [11].

Monitoring natural concentrations of total mercury in aquatic systems remains a difficult challenge since Hg is mainly occurring at ultra-trace levels: 0.3 to 8 ng L⁻¹ in waters free from local sources of mercury, either anthropogenic or natural, and 10 to 40 ng L⁻¹ for waters influenced by mercury mining and/or industrial pollution [12]. Indeed, a wide range of study has highlighted such levels of mercury in natural waters either seawater [1,8] or freshwater [13].

The development of low cost and easy handling analytical methods is then a necessity and it is required to fulfil some of the objectives of the Minamata Convention on Mercury, a global treaty to protect human health and the environment from the adverse effects of mercury. In that sense, Solid Phase Extraction (SPE) procedures to preconcentrate Hg before its analysis have shown a great interest in the scientific community due to its efficiency and simplicity. Most of the studies focus on the preparation of micro-column filled with specific adsorbents for Hg preconcentration. Polymers such as zwitterion-functionalized polymer microspheres (ZPMs) [14] or ion-imprinted polymer (IIP) especially designed for Hg adsorption [15] can be successfully used for rapid enrichment of mercury species. More simple in its preparation yet more expensive, the use of aminated Amberlite XAD-4 resin [16] or silica reversed-phase (RP-C₁₈) [17] respectively followed by FI-CVG-AAS and GC/MS analysis allows determination of Hg species, but its applicability to real samples remains difficult due to high limits of detection.

The investigation of new materials for Hg selective preconcentration made a great step forward in recent years. Indeed, due to their specific properties, nanomaterials have attracted increasing interest in the development of preconcentration methods for contaminants [18], and, more recently, Hg analysis. Then, the micro-column used to preconcentrate Hg can be packed with nanocomposites, previously functionalized for specific adsorption of Hg: magnetite (Fe₃O₄) nanoparticles [19], graphene oxide (GO) [20], multiwalled carbon nanotubes (MWCNTs) [17,21], carbon nanotube sponges (CNT sponges) [22]. Hence, all these methodologies include synthesis of the adsorbent, preparation of the column, elution of the Hg species directly followed by analysis, preventing direct application on the field. Moreover, multiplication of the preparation steps, from collection to analysis, may be problematic considering the potential contaminations or losses of Hg [23].

The use of field techniques reduces travelling and storage times of the samples, and facilitate the acquisition of results in developing countries and/or remote areas. In that sense, *K. Leopold et al.* [24–26] have conducted various studies in the last decade to develop a passive sampler for reagent-free on-site Hg preconcentration: nanogold-coated dipsticks. Thermal desorption of trapped Hg followed by AFS detection allows determination of Hg contents lower than the ppt level (ng L^{-1}), and applicability to real samples, either seawater or freshwater, have been demonstrated. Nevertheless, implementation of this methodology in developing countries remains difficult because of the heavy preparation of the dipsticks (cleaning, coating, and functionalization) and their high cost (reagents and chemicals): sampling campaigns would need numerous of this passive sampler. Also, dipsticks have to be regenerated by thermal annealing at $600\text{ }^{\circ}\text{C}$ for 20 min before each use, which greatly lengthens the preparation time of a sampling campaign. Finally, reproducible production of the nanogold-coated dipsticks remains difficult. As an alternative to expensive gold materials, *Tavares et al.* [27] have produced magnetite nanoparticles using iron oxide nanoparticles coated with silica shells functionalized with dithiocarbamate groups in order to take advantage of the strong affinities between Hg and thiol group (R-SH) [28,29] to preconcentrate Hg prior to its analysis by thermal decomposition AAS with gold amalgamation. Again, synthesis of the nanoparticles includes numerous steps and reagents, and requires important scientific knowledge. Besides, extraction of Hg using these nanoparticles with recovery close to 100% necessitates at least 24 hours. Finally, the limit of detection of 1.8 ng L^{-1} , reached with this procedure prevents its application in pristine areas.

Several studies conducted by *Sitko et al.* have already been made using modified graphene nanomaterials for Dispersive Micro-solid Phase Extraction (DMSPE) such as carbon nanotubes [30], multiwalled carbon nanotubes (MWCNTs) [31], graphene oxide (GO) [32] or graphene nanosheets [33] in order to preconcentrate various elements (Mn, Fe, Co, Ni, Cu, Zn, Se, Pb, Cd). Nevertheless, none of these works deals with Hg, probably because of the high limit of detection of the apparatus (wavelength-dispersive X-ray fluorescence WDXRF, total-reflection X-ray fluorescence spectrometry TXRF, or energy-dispersive X-ray fluorescence spectrometry EDXRF) and the difficulties of working with such element (contaminations or losses).

In this work, we have used the specific properties of graphene nanosheets, a cheap material, to develop an innovative analytical method. Firstly, graphene is flexible so it can be easily attached to a support, which makes it a worthwhile candidate in the use of Micro-solid Phase Extraction (MSPE). It is as well hydrophobic and non-polar with a strong affinity for carbon-based ring compound due to the hexagonal arrays of carbon atoms in its structure. Graphene shows also a huge specific surface ($2630\text{ m}^2\text{ g}^{-1}$) [34], which encourages its use as a sorbent in MSPE. It should be noted that this amazing material could be synthesized easily and affordably in most of the laboratories all around the world, including those of developing countries. Among graphene-based material, graphene nanosheets display great adsorption capacities. Indeed, both surfaces of a planar sheet of graphene are accessible to adsorption of analytes [35]. Also, nanostructured material as graphene nanosheets allows the adsorption of the organic compound via non-covalent interactions [36].

In the proposed method, based on *Kocot et Sitko* [33], dissolved Hg in water samples is first preconcentrated using a nanoparticles suspension consisting of graphene nanosheets as an adsorbent, Ammonium Pyrrolidine DithioCarbamate (APDC) as a chelating agent and Triton-X-100 as a surfactant. To obtain high recovery of the Hg on the nanoparticles, the procedure is optimized for various analytical parameters such as the amount of nanoparticles, sonication time and sample volume. The Hg-rich nanoparticles are then collected in a Polyethersulfone (PES) filter, whose stability at different storage conditions is also checked. The potential existence of matrix effects due to the presence of chloride salts (estuarine or seawater), organic matter (continental water) and metals (calcium) able to compete with mercury for the binding sites of the sorbent is investigated, and the applicability of the whole method is finally verified by the analysis of real samples (seawater and lake water).

Together with the in-field preconcentration of a large volume of water on a small and light membrane filter and the direct analysis of this filter back to the lab greatly enhance the simplicity of all the analytical process for a precise and accurate determination of mercury content in water samples: from the sampling to the result!

5.3. Material and methods

5.3.1. Preparation of nanoparticles suspension

The principle of our method is based on the adsorption of mercury on graphene nanosheets. Nevertheless, metal ions in the form of hydrophilic complexes, including dissolved mercury, cannot be adsorbed directly on the graphene surface with a great efficiency [33]. Therefore, it is necessary to functionalize the graphene nanosheets using a chelating agent that will be adsorbed on the graphene nanosheets via non-covalent interactions (π - π stacking) [35]. Ammonium Pyrrolidine DithioCarbamate (APDC) was chosen as a chelating agent due to some specificity in its structure. Indeed, strong affinities between APDC and mercury, mainly due to the presence of thiol groups (R-SH) in the structure of APDC, lead to the chelation of mercury by APDC (covalent bonds) [33]. -SH groups have already shown one of the strongest binding affinity either for inorganic mercury (sulphur-containing organic matter or polymers with Hg(II)) or organic mercury (sulphur-containing organo-metallic compounds or thiolate-like species with MeHg) [29]. We also need to add some Triton-X-100 in the nanoparticles suspension to increase the viscosity of the solution, hence improving the buoyancy of graphene nanosheets and, in this way, to obtain a real suspension of nanoparticles.

Then, following the recommendations of *Kocot and Sitko* [33], that applied DMSPE for the preconcentration of Co, Ni, Cu and Pb, the graphene/APDC/Triton-X-100 nanoparticles suspension was prepared as follows: 25 mg of graphene nanosheets ($\sim 5 \mu\text{m}$ diameter, 1-5 nm thickness, *Green Stone Swiss Co.*), 80 mg of APDC (*Purum p.a. $\geq 98.0\%$, Sigma-Aldrich*) and 10 mg of Triton-X-100 (*Laboratory-grade, Sigma-Aldrich*) in 20 mL of high purity water (18.2 M Ω cm), sonicated for 60 min, to obtain concentrations of 1.25 g L⁻¹; 4 g L⁻¹ and 0.5 g L⁻¹ for graphene, APDC and Triton-X-100, respectively. To avoid the aggregation of the graphene and to ensure its homogeneity within the nanoparticles suspension, the solution was sonicated 5 min before each use.

5.3.2. Procedure for mercury preconcentration (optimum conditions)

The chelation between APDC and mercury can effectively occur only with a pH between 4 and 5, so initially, the pH of the water sample containing mercury was adjusted by the addition of ultrapure HCl and/or NH₃ solutions (*Optima grade, Fisher Scientific*). In the second step, 0.5 mL of nanoparticles suspension was added to either 20 mL or 200 mL of the aqueous solution to be analysed. Then, the solution containing the complex formed by Hg, APDC and graphene was sonicated for 5 min and collected on a membrane filter (*Polyethersulfone PES, ø 25 mm, 0.2 µm, Pall Corporation*) by filtration (*250 mL Erlenmeyer glass flask*) under vacuum. **Figure 5.1** shows Transmission Electron Microscopy (TEM) images of water samples containing (a) graphene alone, (b) graphene and APDC, and (c) Hg, APDC and graphene. This figure really highlights an increase of the size in the observed particles from graphene alone (67 nm) to the complex Hg/APDC/Graphene (700 nm to 1.89 µm). Consequently, the size of this complex is larger than the membrane filter pores and is quantitatively retained by the filtering PES membrane. We noticed that the size of the complex Hg/APDC/Graphene remains lower than the certified commercial size of graphene nanosheets (*~5 µm diameter, 1-5 nm thickness*). In our study, we assume that both the time in the ultrasonic bath (about 60 min) and the use of Triton-X-100 during the preparation of the nanoparticles suspension would promote the dislocation of aggregates, hence reducing the size in comparison with the raw graphene nanosheets [37].

Finally, the membrane filter obtained is dried for 5 min in a laminar flow hood (*Class 100*) and kept into polycarbonate filters holder (*Petri slides*) at low temperature (-7°C) before its analysis.

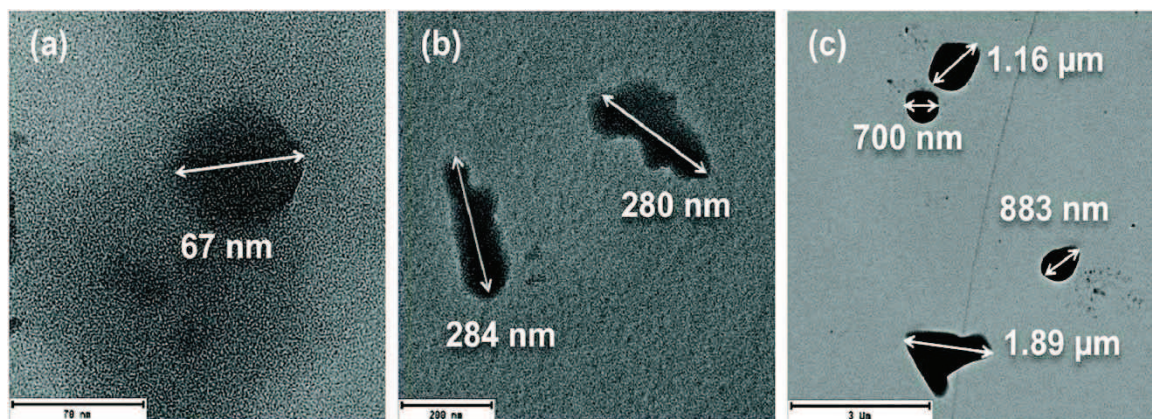


Figure 5.1: Transmission Electron Microscopy TEM of (a) Graphene, (b) Graphene + APDC and (c) Graphene + APDC + Hg(II)

5.3.3. Instrumentation and method for mercury analysis

Direct pyrolysis gold amalgamation and atomic absorption spectroscopy (AAS), using an Advanced Mercury Analyser (*Altec AMA-254, SymaLab*), allows the quantification of Hg in solid samples. The whole membrane filter is dropped on a nickel boat especially designed for this instrument ($1000 \mu\text{L}$, *SymaLab*). To increase analytical performances, nickel boats used for the analysis of the PES filters were previously cleaned by burning at $750 \text{ }^\circ\text{C}$ daily, using the AMA-254. This step has been repeated until a relative standard deviation under 10 % between two successive burnings is obtained. After the introduction of the sample into the analyser using the nickel boat, an increase in temperature up to $750 \text{ }^\circ\text{C}$ under oxygen atmosphere allows first the drying of the matrix, and then the decomposition of the sample and its dry mineralization. Decomposition products and mercury are driven by the oxygen stream through a catalytic tube continuously heated at $550 \text{ }^\circ\text{C}$. This catalytic tube allows decomposition and reduction of methylmercury to gaseous elemental mercury Hg^0 and the removal of halogens. Then, total mercury vapour is trapped in a quartz tube filled with gold-coated sand that allows the preconcentration of mercury, and so improve the sensitivity of the instrument. A few seconds later, the gold amalgamator is heated at about $950 \text{ }^\circ\text{C}$. The quantification of this released mercury is carried out using two absorption cells (1 cm and 10 cm lengths, wavelength = 253.65 nm), both of them thermostatically controlled at $125 \text{ }^\circ\text{C}$, that allows sequential quantification of mercury at two different ranks (Rank 1 < 25 ng Hg, and Rank 2 > 25 ng Hg).

All instrumental parameters have been optimized for analysis of PES filters as follow: drying step of 150 sec, decomposition step of 150 sec and waiting step of 45 sec. Accuracy and reproducibility of the AMA-254 were assessed by using the Certified Reference Material BCR-320R (channel sediment $0.85 \pm 0.09 \text{ mg kg}^{-1}$ of total Hg), analysed regularly all along the measurement process according to the EPA method 7473 (SW-846).

5.3.4. Calibration for mercury quantification

To quantify the accumulated mass of mercury on the PES filter, the AMA-254 was calibrated using an external matrix-matched calibration curve in the absolute mass of mercury (2.3 – 207 ng Hg). Indeed, matrix effects can occur during the analysis of the PES filters and there is no existing certified reference material with a similar matrix. The Hg(II) standard solution (*Strem Chemicals, USA*) was prepared in 1% HCl with a concentration of $400 \mu\text{g Hg L}^{-1}$ and various amounts were directly dropped into a nickel boat containing a PES filter resulting in absolute Hg masses of 2, 4, 10, 21, 31, 42, 53, 85, 144 and 207 ng. Here, we used Hg(II) considering the low fraction of MeHg in natural waters (< 10 % of total mercury) and assuming there would not be any difference in the adsorption process using either Hg(II) and/or MeHg (**5.3.1 Preparation of nanoparticles suspension**). The absorbance (A) resulting from the analysis of unused filters was used for blank correction. The calibration functions obtained provide a reliable way to determine Hg content in the PES filters for both absorption cells, Rank1 ($R^2 = 0.99947$) and Rank2 ($R^2 = 0.99996$), with slopes of respectively (36.4 ± 0.3) and (560 ± 1) ng Hg AbsorbanceUnit

1.

The calibration curves according to the present procedure under the optimized conditions were also set up in the absolute mass of mercury (1.9 – 210 ng). Various samples containing 200 mL of high purity water were spiked with known amounts of Hg(II) standard solution ($[Hg] = 400 \mu\text{g L}^{-1}$) resulting in absolute Hg masses of 2, 4, 8, 13, 19, 22, 43, 85, 148 and 211 ng. These samples were subjected to the preconcentration process previously described (**5.3.2 Procedure for mercury preconcentration (optimum conditions)**). The obtained calibration functions provide a reliable way to determine Hg content in the PES filters for both absorption cells, Rank1 ($R^2 = 0.99974$) and Rank2 ($R^2 = 0.99971$), with slopes of respectively (38.6 ± 0.1) and (576 ± 3) ng Hg Absorbance Unit⁻¹.

Coefficients of determination R^2 of the four different calibration curves are all above 0.99947, suggesting validated good linear relationship. Nevertheless, taking into account the standard deviations, the slopes given by these models are significantly different at a 95 % confidence level. This could be explained by the relative difficulty to weigh correctly the mass of Hg(II) standard solution added directly in the nickel boat in the case of matrix-matched calibration. Indeed, in practice, when the operator drops the solution into the nickel boat, the balance is not stable either due to adsorption on the nickel boat surface and/or evaporation. Therefore, in this work, we decided to use the calibration curves obtained according to the procedure developed in this study under optimized conditions for data treatment.

5.3.5. Sampling of natural waters

To check the suitability of the proposed method to the analysis of natural waters, real samples were collected in April 2017 at two locations of the Pyrénées-Atlantiques (Nouvelle-Aquitaine, France). Freshwater was collected from Lac Des Carolins ($43^{\circ}20'15''$ N, $0^{\circ}24'23''$ W), at a depth of 40 cm using acid cleaned polyethylene bottles (2 L) that were rinsed three times with the sampling water. Important wildlife in the surroundings of the lake has a great influence on its biogeochemical characteristics, especially concerning the relatively high content of organic matter measured in the sample ($[DOC] = 5.6 \text{ mg L}^{-1}$). Coastal seawater was collected in the same way out of the Bay of St Jean de Luz ($43^{\circ}23'37''$ N, $1^{\circ}39'44''$ W, Bay of Biscay, North-East Atlantic Ocean). Time collection of the samples corresponds to high tide, and the seawater is characterized by a lower amount of organic matter ($[DOC] = 0.90 \text{ mg L}^{-1}$) and a high salinity (35.6 PSU). All water samples were filtered through a PES membrane ($0.2 \mu\text{m}$), acidified with ultra-pure hydrochloric acid (1 % v/v) and stored at 4 °C for no longer than two days before further manipulation and analysis.

5.4. Results and discussion

5.4.1. Optimisation of the Hg preconcentration method

1. Amount of nanoparticles

The amount of nanoparticles used in the preconcentration step will have a great influence on the efficiency of the proposed procedure. Enough nanoparticles must be available to chelate all the mercury present in the sample. Furthermore, an extra amount of nanoparticles will i) ensure that the possible presence of other competing metals will not negatively affect the effectiveness of Hg sequestration and ii) allow the use of a larger volume of sample to eventually improve the detection limit of the method. In this work, the influence of the amount of nanoparticles has been studied. High purity water samples of 25 mL (n=4) were spiked with 100 ng of mercury (Hg(II) standard solution), and various amounts of nanoparticles have been added (expressed as volume of nanoparticles suspension added, from 100 μ L to 2000 μ L). Then, all the samples were subjected to the preconcentration procedure with a sonication time of 5 min. Blanks (n=4) were also produced for the various amounts of nanoparticles, following the same procedure with unspiked high purity water. The results are shown in **Figure 5.2.a**, which provides the mercury recovery, obtained as a function of the amount of nanoparticles. No significant change was noticed in the recovery but the best condition selected was for a volume of nanoparticles suspension of 500 μ L, to ensure that all the mercury in the sample would be trapped even in the presence of a high amount of other competing metals. Indeed, a large amount of nanoparticles suspension leads to an increase in the blanks signal. The graphene shows similar properties to activated carbon so it can adsorb the gaseous species of mercury present in the air during the preparation of the nanoparticles suspension [38–40]. This could lead to the contamination in the blanks, making necessary to work under a clean atmosphere and to minimize the amount of nanoparticles suspension.

2. Sonication time

In previous works about preconcentration of metals using graphene nanoparticles as a sorbent, it is shown that the contact time between the nanoparticles suspension and the water sample does not appear as a critical variable as sorption occurs immediately [30,41]. Nevertheless, this parameter has been investigated here (**Figure 5.2.b**) within the time range of 1-15 min in the ultrasonic bath. So, high purity water samples of 25 mL (n=4) were spiked with 100 ng of mercury, and preconcentrated using 500 μ L of nanoparticles suspension with various sonication times (1-15 min). Blanks (n=4) were also performed for each condition, following the same procedure with unspiked high purity water. Results depicted in **Figure 5.2.b** show that sorption of mercury is significantly less effective when the time in the ultrasonic bath is lower than 1 min. Besides, for 2 min of sonication, the procedure shows a lower reproducibility (two replicates with about 87% of recovery and two replicates with about 100% recovery) confirming that the sorption of mercury does not occur immediately. Finally, longer sonication times result in poorer reproducibility. This might be due to the influence of the ultrasonic bath that could degrade the non-covalent interactions (π - π stacking) between graphene nanosheets and APDC. Therefore, sonication time of 5 min allows an effective and reproducible activation of the binding sites.

For in-field direct application, we can imagine that the use of the ultrasonic bath can be easily replaced by a simple shaking, with longer time.

3. Sample volume

The volume of the water sample used during the method of preconcentration is one of the critical steps in the analytical performance. Indeed, the choice of a larger volume of samples leads to an increase in the preconcentration factor and, hence, to a decrease in the detection limits, provided that the nanoparticles present (same amount, lower concentration) can sequester quantitatively all the mercury that can be much more diluted in the medium. Calibration curves were obtained as described in **5.3.4 Calibration for mercury quantification** using two different volumes of ultrapure water, i.e. 20 and 200 mL. **Figure 5.2.c and d** show the absorbance obtained after the analysis of the filters produced according to the procedure described in **5.3.2 Procedure for mercury preconcentration (optimum conditions)** as a function of the theoretical amount of mercury added to the sample. Blanks ($n=3$ for 20 mL and $n=2$ for 200 mL of the sample) have been carried out for the two volumes, following the same procedure with unspiked high purity water. From 1.6 ng to 210 ng of mercury added to the test solution, no significant change can be observed in the efficiency of the preconcentration when working with 20 or 200 mL. A larger volume could have been tested, nevertheless, increasing the volume above 200 mL will be more time consuming for the operator in charge of the procedure because the filtration step will be much longer, especially with samples containing a high content of organic matter and/or suspended material. For future use of this method to quantify mercury in an aquatic environment, it is then important to adapt the sample volume to the specification of the water sample, especially when the concentration of Hg is very low.

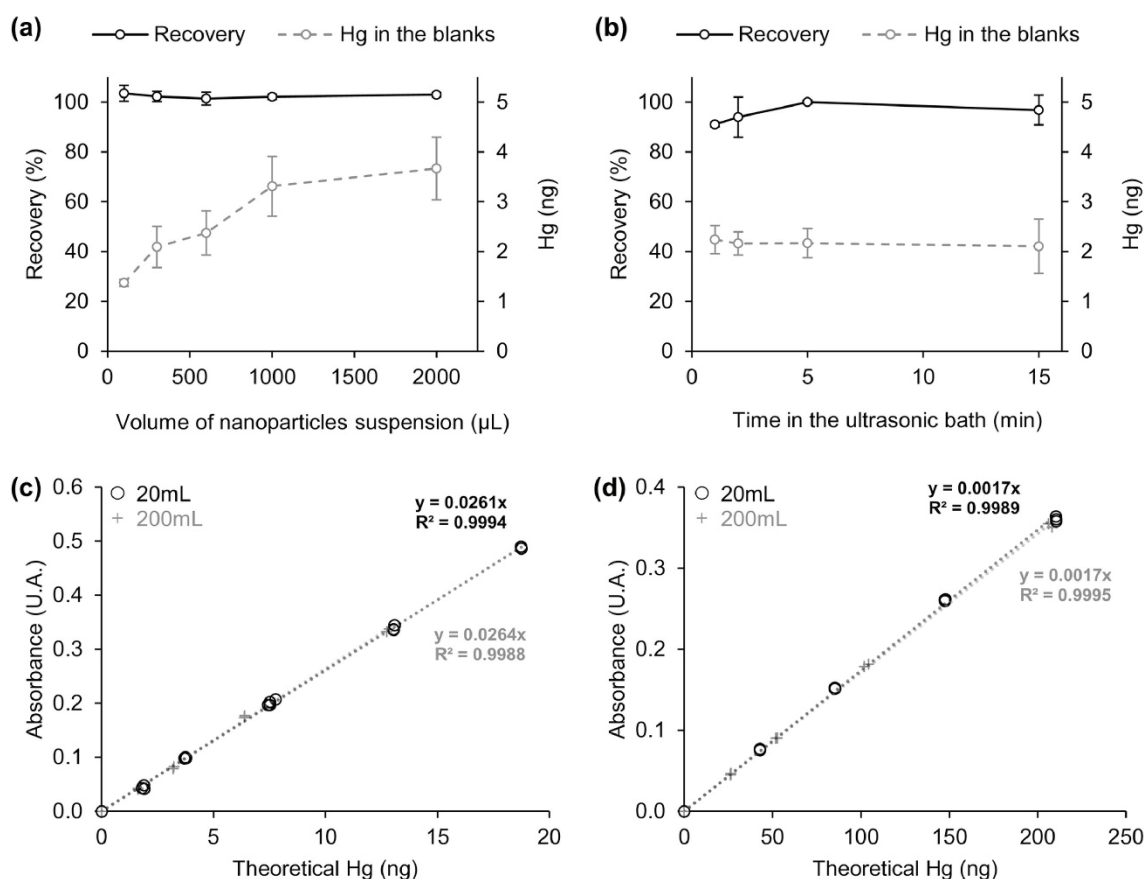


Figure 5.2: Recovery ($n = 4$) of Hg (a) as a function of the volume of nanoparticles suspension and (b) as a function of the time in the ultrasonic bath. Theoretical Hg (ng) as a function of the absorbance given by AMA-254 to (c) Rank 1 and (d) Rank 2 for 20 mL and 200 mL of water sample

5.4.2. Optimization of the storage conditions

The possible application of this preconcentration method directly in the field, in remote areas, implies the transportation of the filters from the sampling site back to the laboratory for their analysis. Thus, storage conditions of the filters is an important factor to take into account to minimize sample contamination as well as potential losses of mercury by evaporation. On the one hand, elemental mercury (Hg^0) is present at trace levels in the ambient air. Typically, Total Gaseous Mercury (TGM) concentrations averages about 1.5 ng m^{-3} in background ambient air throughout the world [42]. In our laboratory, TGM concentrations have been reported by *Lusilao-Makiese et al.* [40] ($6.3 \pm 1.6 \text{ ng m}^{-3}$), and are higher than the background ambient air levels due to the activities that take place in the laboratory (analysis and development of methodologies for metals and metalloids). This concentration, though, remains quite low for a laboratory building located in an urban area. Then, as Hg^0 is subject to adsorption on all solid surfaces, it could eventually be adsorbed on the Hg-enriched filters produced in the preconcentration step and lead to an overestimation of the Hg content. On the other hand, the complex formed by Hg, APDC and graphene may be sensitive to degradation by light, temperature, oxygen, humidity etc... Then the exposure of the filters to various environmental conditions could lead to desorption of the mercury from the filters.

To avoid such problems, the stability of Hg-enriched filters has been evaluated using various storage conditions according to an isochronous design [43–45]. It is based on a storage design of the samples at various temperatures for different time intervals allowing all measurements to be done at the same time i.e. at the end of the study. In classical stability studies, measurements of the samples are achieved throughout the study i.e. at a different time so any drift of the measurement system over time can lead to incorrect conclusions. Thus, isochronous measurements only require repeatability conditions whereas classical stability studies require also long-term reproducibility.



The storage design set up in this study is shown in **Table 5.1**. Hg-enriched filters were obtained according to the present procedure under optimized conditions (500 μL of nanoparticles suspension, 5 min sonication time), using 25 mL of high purity water samples spiked with 100 ng of mercury ($n=3$). Then, the filters were kept into polycarbonate filter holders (Petri slides) and Zip-lock bags at the corresponding temperature for the required time. It has been assumed that mercury is stable on the filters at low temperature ($-7 \text{ }^\circ\text{C}$). Thus, this reference temperature (i.e. $-7 \text{ }^\circ\text{C}$ in a freezer) is the temperature at which the samples were always transported or kept before the analysis and the testing temperatures (i.e. $4 \text{ }^\circ\text{C}$ in a cool room and $21 \text{ }^\circ\text{C}$ in a flow hood at ambient temperature) were the conditions at which test samples were stored for a selected period of time, before returning to the reference temperature. The total amount of Hg in all the filters was measured together at the end of the experiment.

To distinguish the various storage conditions of the filters and their efficiency, a Kruskal-Wallis test (nonparametric test), followed by a Conover and Iman test has been performed. **Figure 5.3** summarizes the data collected in the isochronous measurement experiment along with the results of the Kruskal-Wallis test. On the one hand, after eight weeks of storage, the ratio between the recovery of the testing

temperature T1 (21 °C) and the recovery of the reference temperature decreases significantly down to $84.7 \pm 1.9 \%$. On the other hand, after eight weeks, the decrease of this ratio with the testing temperature T2 (4 °C) is less important ($93.2 \pm 1.4 \%$) but still significant. The only storage condition that does not show a significant difference with the results from the reference temperature is as follows: one week of storage at 4 °C. This allows the in-field application of the mercury preconcentration method as it is usually possible to keep the filters at low temperature (4 °C) in a portable fridge before coming back to the lab where the filters can be stored at low temperature ($< -7 \text{ °C}$). If filters must be stored for a longer time, it is recommended to do it at freezing temperature, and even in that case, possible loss of mercury should be expected.

Table 5.1: Storage design for isochronous measurements to evaluate stability of the filters

Storage t (weeks) \ Temperature (°C)	0	1	2	3	4	5	6	7	8	9	10	11	12	
	T ₁ (21°C)													
T ₂ (4°C)														
T _{ref} (-7°C)														
Analysis														✘

 Storage at temperature T
 Storage at very low temperature (T_{ref})

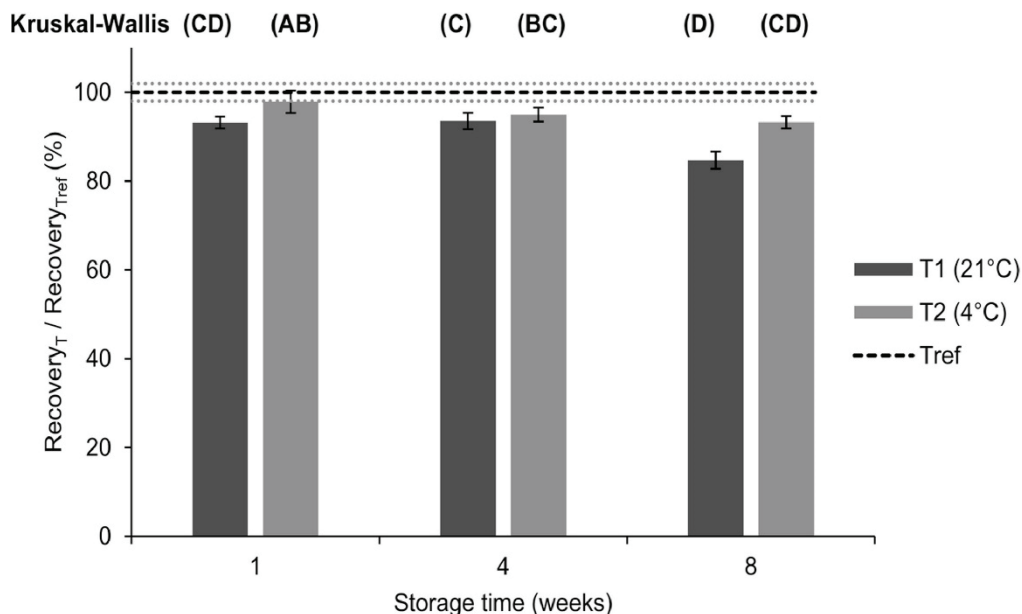


Figure 5.3: Ratio between the recovery of Hg for the testing temperature T (n = 3) and the recovery of Hg for the reference temperature T_{ref}

5.4.3. Potential interferences: matrix effects

The potential occurrence of matrix effects due to the presence of interfering compounds in the sample was also investigated. For the sake of simplicity, the possible effect of salinity, organic matter and competing metals were modelled with NaCl, natural organic matter (NOM) and Ca²⁺, respectively. Then, applicability to real samples with high organic matter content, and high salinity was demonstrated.

1. Organic matter

According to various studies about the adsorption of dissolved mercury and the influence of organic matter on this process, the efficiency of our new methodology could be eventually reduced by the presence of organic matter [46–48]. The reference material Suwanee River natural organic matter (SRNOM), purchased from International Humic Substances Society (IHSS, USA) was used to model organic matter. A solution with NOM = 500 mg L⁻¹ was prepared by dissolving 12.5 mg of NOM in 25 mL of high purity water. Firstly, high purity water samples of 25 mL (n=4) were spiked with 100 ng of mercury, and various amounts of natural organic matter solution were added ([NOM] = 0 – 18.4 mg L⁻¹). Blanks (n=4) were also produced in the same extent and under the same conditions with unspiked high purity water. The whole samples were preconcentrated using 500 µL of nanoparticles suspension and 5 min sonication time. Recoveries in **Figure 5.4.a**, calculated using the theoretical amount of Hg in the water sample and the amount of Hg obtained from the analysis of the Hg-enriched filter, show us

that for NOM < 5 mg L⁻¹ there is no significant influence of the organic matter on the preconcentration of mercury on the nanoparticles (98±2 % < R < 105±1 %). Nevertheless, for NOM > 5 mg L⁻¹, the recovery decreases steadily down to 84±3 % for NOM = 18.4 mg L⁻¹.

The potential influence of organic matter was also tested with real samples from Lac des Carolins ([DOC] = 5.6 mg L⁻¹). 200 mL of water sample from this lake (n=2) spiked with a known amount of mercury (1.6 – 208 ng of mercury), and control solutions (n=2) with the same amount of mercury in 200 mL of high purity water were simultaneously prepared. Then, samples were stored at room temperature, protected from light, in a laminar flow hood at least for 12 hours (equilibrium step). The samples were then treated according to the procedure described in **5.3.2 Procedure for mercury preconcentration (optimum conditions)**. The percentage of controls, calculated as the ratio between mercury found in the real sample and mercury found in the controls for the same amount of spiked mercury (**Figure 5.4.c**) demonstrates that our new methodology for mercury preconcentration can be applied successfully to samples with a relatively high content of organic matter.

Bravo et al. [49] have studied the influence of organic matter on mercury species concentrations within 29 streams across Europe. In this study, total organic carbon (TOC) values range from 0.6 to 22.2 mg L⁻¹ and 76 % of the streams show TOC < 5 mg L⁻¹, suggesting that our method is applicable to many freshwater systems.

2. Salinity

By analogy with organic matter, it has been shown that the presence of chloride salts might reduce the efficiency of the adsorption because of the formation of the resistant complex HgCl₄⁻ leading to an inhibition of the mercury adsorption on other sorbents [50,51]. The presence of chloride salts and their influence on the efficiency of the preconcentration procedure have been studied to determine applicability to seawater samples. Firstly, sodium chloride (*NaCl*, Merck KGaA, Denmark) has been added to high purity water samples of 25 mL (NaCl, 0 – 36 g L⁻¹), also spiked with 100 ng of mercury. Replicates (n=4) of these synthesized solutions allowed us to produce Hg-enriched filters that have been analysed by AMA-254. Recoveries in **Figure 5.4.b**, calculated using the theoretical amount of Hg in the water sample and the amount of Hg obtained from the analysis of the Hg-enriched filter, show us that for NaCl < 22 g L⁻¹ there is no significant influence of sodium chloride on the preconcentration of mercury on nanoparticles (100±1 % < R < 107±1 %). Nevertheless, the recovery decreases slightly until 93±2 % for NaCl = 36 g L⁻¹. For most natural waters, including groundwater, continental and estuarine waters, the presence of moderate amounts of salt should not lead to significant errors derived from the occurrence of matrix effects. Even in the case of high salinity seawaters, the effect should not be very pronounced (about 7 % suppression of the analytical signal).

To validate this hypothesis, we decided to apply the method of preconcentration to real samples with high salinity. 200 mL of water sample (n=2) from St Jean de Luz were spiked with a known amount of mercury (1.9 – 208 ng of mercury). Control solutions (n=2) with the same amount of mercury in 200 mL of high purity water samples were simultaneously prepared. After an equilibration step of 12 hours, Hg-enriched filters were produced according to the preconcentration procedure. The percentage of control,

depicted in **Figure 5.4.d**, demonstrates that our new methodology for mercury preconcentration can be applied successfully to samples with high salinity. Elsewhere, even if seawater contains high amounts of potential sources of exhaustion of the binding sites (sulphate, chloride, sodium, potassium etc...), the successful application of our new methodology to real seawater samples underlines the absence of competition of these ions with Hg for binding to the APDC.

3. Competing metals

With the variety of metal ions that could bind competitively with the chelating agent (APDC), calcium (Ca^{2+}) is usually the major species present in water samples, and so it has been selected to investigate the competition with mercury for the chelation step. High purity water samples of 25 mL containing various amount of calcium ($\text{Ca}^{2+} = 0 - 18.5 \text{ mg L}^{-1}$) were spiked with 100 ng of mercury. The ratio between results obtained for the reference filter (without calcium) and other conditions ($R = 102 - 109 \%$) confirms that mercury is predominately bond to the APDC in all the conditions tested. Considering the strong binding affinity between $-\text{SH}$ groups from APDC and Hg, a high competition or influence from the presence of other ions than Ca^{2+} is not expectable

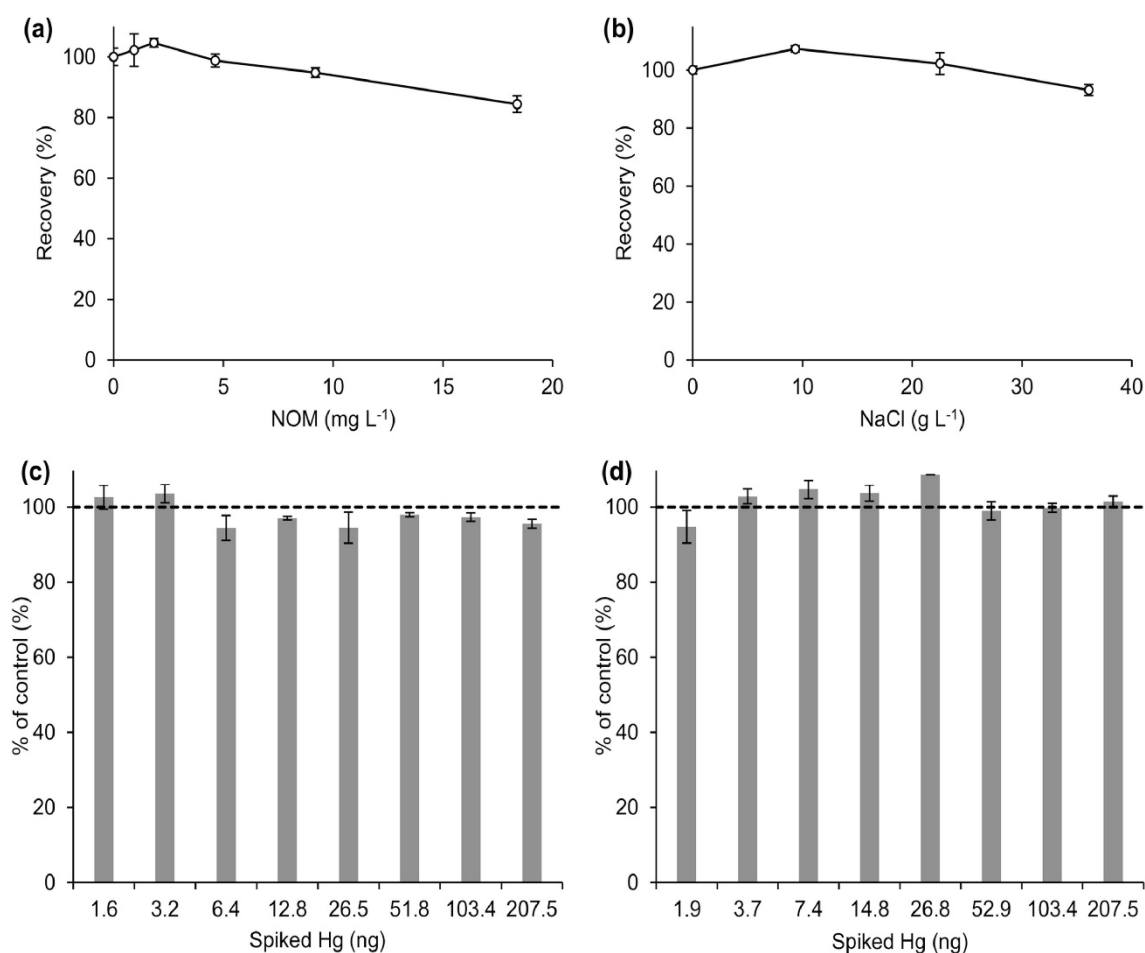


Figure 5.4: Recovery of Hg (a) as a function of the concentration of natural organic matter (NOM) ($n = 4$) and (b) as a function of the concentration of sodium chloride (NaCl) ($n = 5$). Ratio ($n = 2$) between control samples (high purity water) and real samples from (c) Lake Des Carolins (freshwater) and (d) St Jean de Luz (seawater) as a function of the spiked mercury

5.4.4. Method blank levels and optimization

Working under clean conditions is also a crucial consideration for successful analysis at very low concentration levels, in particular with mercury. In that sense, as mentioned in previous sections, for each change in a parameter during the preconcentration procedure (sample volume, nanoparticles suspension, sonication time, and amount of Ca^{2+} , NaCl and organic matter in the sample) replicates of high purity water were submitted to the same protocol. Low levels and good reproducibility for these blank samples lead to a very good limit of detection.

Firstly, to check any contamination before their use, unused PES membrane filters have been analysed using the AMA-254. The absorbance obtained was 0.0025 ± 0.0006 ($n=15$) and this value is not significantly different (t-test, $p < 0.05$) from the value given by the analysis of empty nickel boats, 0.0018 ± 0.0002 ($n=9$), suggesting that no cleaning step is necessary for the PES filters.

Secondly, most of the experiments have been conducted in a trace metals laboratory whereas the last experiments, about real samples, took place in a clean laboratory, dedicated to ultra-trace mercury analysis. In the first cases, plastic flasks of 25 mL, cleaned in a 10% HNO_3 bath, were used as a container and the blanks levels reached 1.9 ± 0.2 ng Hg per filter. In the clean laboratory, special attention was paid to the procedure for cleaning all vessels used for sampling (polyethylene vials) and sample preparation (glass vials, glass filtration system, and filter holders) with successive acid baths (10% HNO_3 , 10% HNO_3 and 10% HCl), reducing the blank levels down to 0.60 ± 0.03 ng Hg per filter.

Finally, it has been shown that graphene on its own can adsorb volatile Hg species, so it is probably responsible for the Hg content in the blank filters. This hypothesis was confirmed by the analysis of graphene directly by AMA-254: 0.82 ± 0.01 mg Hg kg^{-1} . One possibility to reduce such contamination, and therefore to reduce the blank levels, should be to buy new graphene nanosheets that will be managed only in a glove box under argon flux. Another solution could be to find a purification process not affecting graphene nanosheets structure and properties.

5.4.5. Analytical performances

The analytical performances of the method developed in this work are summarized in **Table 5.2** together with other methods for determination of mercury species at trace and ultra-trace levels. Traditional and/or newly developed methods highlight various problems preventing their application in-field and/or in developing countries: heavy sample preparation, high cost due to reagents and/or apparatus, and high limits of detection. Indeed, very sensitive analytical methods commonly used for the determination of Hg species, CV-AFS (LOD < 0.06 ng L^{-1}) [52,53] and GC-ICP-MS (LOD < 0.04 ng L^{-1}) [13], require a strong knowledge in analytical chemistry, and maintenance. Moreover, the use of these techniques implies a significant economic cost, due to either the equipment or the reagents. The use of a commercial mercury analyser for the analysis of the filters produced according to our new procedure greatly simplifies all the analytical process. Most of the newly developed methodologies focus on preconcentration of the Hg species followed by an elution step [15,17,20,54,55], making their application in the field laborious, if not impossible, which is not the case in our new method with the direct analysis

of the filter. Finally, the most interesting published analytical methods for in-field Hg preconcentration need also strong knowledge in analytical chemistry for the preparation of the nanogold-coated passive sampler [26] and the magnetite nanoparticles [27] while the functionalization of the graphene nanosheets in our study appears much simpler. Moreover, in this work, just a few minutes are necessary to recover the whole Hg species on the functionalized graphene nanosheets whereas *Tavares et al.* [27] need 24 hours. Overall, the novelty and the superiority of our work lie mainly on its simplicity all along its process: sampling (easily transportable filter), preconcentration (quickly and effortlessly producible adsorbent) and analysis (direct analysis of the solid without any elution step needed using a cheap equipment).

This new method for quantification of mercury by DMSPE using graphene nanosheets and direct analysis by pyrolysis gold amalgamation and atomic absorption spectroscopy (AAS) resolves many of these limitations and can be still improved. It provides a LOD as low as 0.38 ng L^{-1} for 200 mL of samples, with a large linear range ($0.38 - 1038 \text{ ng L}^{-1}$). As concentration levels of total mercury in water samples (sea, estuarine, fresh) range in the ng L^{-1} , in most of the cases, our method is applicable, only with 600 mL of water sample for triplicate analysis. In the case of water samples presenting smaller mercury content, usually coming from pristine areas, such as ocean and many remote water bodies, the matrix is not complex, making the filtration step easier to manage. Therefore, for these particular cases, increasing the volume up to 1 L should allow a reduction of the LOD to match the Hg concentration in the sample.

Table 5.2: Methods for analysis of mercury species in natural waters

<i>Method</i>	<i>Volume (L)</i>	<i>Water type</i>	<i>Hg species</i>	<i>Quantification</i>	<i>RSD (%)</i>	<i>LOD (ng.L⁻¹)</i>	<i>Note</i>	<i>Reference</i>
Procedure presented in this work	0.2 (5min extraction)	Fresh and seawater	THg	External calibration	4.2 (Blanks) 3.0 (Standard) 3.2 (Fresh water) 4.5 (Seawater)	0.4	APDC/Graphene Nanosheets - DMSPE, filtration, and double gold amalgamation before AAS detection	This work
GC-ICP-MS	0.1	Fresh and seawater	Hg ²⁺ MeHg ⁺	Isotopic Dilution (equilibration time 12h)	2.5 3.4	0.04 0.01	Alkyl derivatization to produce volatile species, extraction in GC organic solvent	[13]
CV-AFS (EPA 245.7)	0.25	Fresh water	THg	External calibration	n.d.	0.04	KBr oxidation, SnCl ₂ reduction, purge of Hg(0), and AFS detection	[53]
CV-AFS (EPA 1631)	0.1	Fresh water	THg	External calibration	~5	0.06	BrCl oxidation, SnCl ₂ reduction, purge of Hg(0), and double gold amalgamation before AFS detection	[52]
IIP-CV-AAS	0.1	Fresh and seawater	Hg ²⁺	External calibration	2.4	0.5	Preparation of the IIP for Hg ²⁺ specific adsorption IIP - SPE column, elution by EDTA, and AAS detection	[15]
MWCNTs-GC-MS	0.025	Fresh and seawater	Hg ²⁺ MeHg ⁺ EtHg ⁺	Internal standard quantification	6.2 6.8 7.2	4 3 3	Complexation of Hg species by NaDDC, MWCNTs - SPE column, elution by ethyl acetate with online alkyl derivatization	[17]
IL-GO-ETAAS	0.005	Fresh water	THg	External calibration	3.9	14	Preparation of the IL-GO hybrid nanomaterial for Hg adsorption IL-GO – SPE column, elution by 20% HNO ₃ and ETAAS detection	[20]
NG-COOH-FI-CV-AAS	0.010	Fresh water	Hg ²⁺ MeHg ⁺ EtHg ⁺	External calibration	<3	9.8	NG-COOH as solid-phase sorbent for US-D-IL-μ-SPE Elution by HNO ₃ and analysis by FI-CV-AAS	[54]
GO-ICP-MS	0.010	Fresh water	Hg ²⁺ MeHg ⁺ EtHg	External calibration	4.5 3.1 3.7	0.005 0.006 0.009	GO as the SPE adsorbent Elution by benzoic acid	[55]
AuNP-AFS	n.d. (10min direct extraction)	Fresh and seawater	THg	External calibration	4.9	0.2	Nanogold-coated dipsticks (AuNP) - SPE Thermal desorption, double gold amalgamation before AFS detection	[26]
NPs-AAS	1	Fresh and seawater	THg	External calibration	<10	1.8	Fe ₃ O ₄ @SiO ₂ SiDTC – DMSPE (24h extraction step), double gold amalgamation before AAS detection	[27]

5.5. References

- [1] B. Gworek, O. Bemowska-Kalabun, M. Kijeńska, J. Wrzosek-Jakubowska, Mercury in Marine and Oceanic Waters—a Review, *Water, Air, & Soil Pollution*. 227 (2016). <https://doi.org/10.1007/s11270-016-3060-3>.
- [2] Z.F. Anual, W. Maher, F. Krikowa, L. Hakim, N.I. Ahmad, S. Foster, Mercury and risk assessment from consumption of crustaceans, cephalopods and fish from West Peninsular Malaysia, *Microchemical Journal*. 140 (2018) 214–221. <https://doi.org/10.1016/j.microc.2018.04.024>.
- [3] M. Arcagni, R. Juncos, A. Rizzo, M. Pavlin, V. Fajon, M.A. Arribére, M. Horvat, S. Ribeiro Guevara, Species- and habitat-specific bioaccumulation of total mercury and methylmercury in the food web of a deep oligotrophic lake, *Science of The Total Environment*. 612 (2018) 1311–1319. <https://doi.org/10.1016/j.scitotenv.2017.08.260>.
- [4] J. Aaseth, B. Hilt, G. Bjørklund, Mercury exposure and health impacts in dental personnel, *Environmental Research*. 164 (2018) 65–69. <https://doi.org/10.1016/j.envres.2018.02.019>.
- [5] F. Khan, S. Momtaz, M. Abdollahi, The relationship between mercury exposure and epigenetic alterations regarding human health, risk assessment and diagnostic strategies, *Journal of Trace Elements in Medicine and Biology*. 52 (2019) 37–47. <https://doi.org/10.1016/j.jtemb.2018.11.006>.
- [6] K. Sundseth, J.M. Pacyna, E.G. Pacyna, J. Munthe, M. Belhaj, S. Astrom, Economic benefits from decreased mercury emissions: Projections for 2020, *Journal of Cleaner Production*. 18 (2010) 386–394. <https://doi.org/10.1016/j.jclepro.2009.10.017>.
- [7] W. Zhang, G. Zhen, L. Chen, H. Wang, Y. Li, X. Ye, Y. Tong, Y. Zhu, X. Wang, Economic evaluation of health benefits of mercury emission controls for China and the neighboring countries in East Asia, *Energy Policy*. 106 (2017) 579–587. <https://doi.org/10.1016/j.enpol.2017.04.010>.
- [8] C.H. Lamborg, C.R. Hammerschmidt, K.L. Bowman, G.J. Swarr, K.M. Munson, D.C. Ohnemus, P.J. Lam, L.-E. Heimbürger, M.J.A. Rijkenberg, M.A. Saito, A global ocean inventory of anthropogenic mercury based on water column measurements, *Nature*. 512 (2014) 65–68. <https://doi.org/10.1038/nature13563>.
- [9] UNEP, 2013, *Global Mercury Assessment 2013: Sources, Emissions, Releases and Environmental Transport*, (n.d.).
- [10] C.T. Driscoll, R.P. Mason, H.M. Chan, D.J. Jacob, N. Pirrone, Mercury as a Global Pollutant: Sources, Pathways, and Effects, *Environmental Science & Technology*. 47 (2013) 4967–4983. <https://doi.org/10.1021/es305071v>.
- [11] D.G. Streets, Q. Zhang, Y. Wu, Projections of Global Mercury Emissions in 2050, *Environmental Science & Technology*. 43 (2009) 2983–2988. <https://doi.org/10.1021/es802474j>.
- [12] J. Wiener, D. Krabbenhoft, G. Heinz, A. Scheuhammer, *Ecotoxicology Of Mercury*, in: D. Hoffman, B. Rattner, G. Allen Burton Jr, J. Cairns Jr (Eds.), *Handbook of Ecotoxicology*, Second Edition, CRC Press, 2002. <https://doi.org/10.1201/9781420032505.ch16>.
- [13] J. Cavalheiro, C. Sola, J. Baldanza, E. Tessier, F. Lestremau, F. Botta, H. Preud'homme, M. Monperrus, D. Amouroux, Assessment of background concentrations of organometallic compounds (methylmercury, ethyllead and butyl- and phenyltin) in French aquatic environments, *Water Research*. 94 (2016) 32–41. <https://doi.org/10.1016/j.watres.2016.02.010>.
- [14] X. Jia, J. Zhao, H. Ren, J. Wang, Z. Hong, X. Zhang, Zwitterion-functionalized polymer microspheres-based solid phase extraction method on-line combined with HPLC–ICP-MS for mercury speciation, *Talanta*. 196 (2019) 592–599. <https://doi.org/10.1016/j.talanta.2019.01.013>.
- [15] M. Soleimani, M.G. Afshar, Highly selective solid phase extraction of mercury ion based on novel ion imprinted polymer and its application to water and fish samples, *J Anal Chem*. 70 (2015) 5–12. <https://doi.org/10.1134/S1061934815010189>.
- [16] O. Çaylak, Ş.G. Elçi, A. Höl, A. Akdoğan, Ü. Divrikli, L. Elçi, Use of an aminated Amberlite XAD-4 column coupled to flow injection cold vapour generation atomic absorption spectrometry for

- mercury speciation in water and fish tissue samples, *Food Chemistry*. 274 (2019) 487–493. <https://doi.org/10.1016/j.foodchem.2018.08.107>.
- [17] J. Muñoz, M. Gallego, M. Valcárcel, Speciation of Organometallic Compounds in Environmental Samples by Gas Chromatography after Flow Preconcentration on Fullerenes and Nanotubes, *Anal. Chem.* 77 (2005) 5389–5395. <https://doi.org/10.1021/ac050600m>.
- [18] A. Kaur, U. Gupta, A review on applications of nanoparticles for the preconcentration of environmental pollutants, *Journal of Materials Chemistry*. 19 (2009) 8279. <https://doi.org/10.1039/b901933b>.
- [19] A. Tadjarodi, A. Abbaszadeh, A magnetic nanocomposite prepared from chelator-modified magnetite (Fe₃O₄) and HKUST-1 (MOF-199) for separation and preconcentration of mercury(II), *Microchim Acta*. 183 (2016) 1391–1399. <https://doi.org/10.1007/s00604-016-1770-2>.
- [20] A.C. Sotolongo, E.M. Martinis, R.G. Wuilloud, An easily prepared graphene oxide–ionic liquid hybrid nanomaterial for micro-solid phase extraction and preconcentration of Hg in water samples, *Anal. Methods*. 10 (2018) 338–346. <https://doi.org/10.1039/C7AY02201H>.
- [21] T.A. Labutin, V.N. Lednev, A.A. Ilyin, A.M. Popov, Femtosecond laser-induced breakdown spectroscopy, *J. Anal. At. Spectrom.* 31 (2016) 90–118. <https://doi.org/10.1039/C5JA00301F>.
- [22] L. Wang, J.-B. Zhou, X. Wang, Z.-H. Wang, R.-S. Zhao, Simultaneous determination of copper, cobalt, and mercury ions in water samples by solid-phase extraction using carbon nanotube sponges as adsorbent after chelating with sodium diethyldithiocarbamate prior to high performance liquid chromatography, *Anal Bioanal Chem.* 408 (2016) 4445–4453. <https://doi.org/10.1007/s00216-016-9542-8>.
- [23] T. Stoichev, D. Amouroux, R.C.R. Martin-Doimeadios, M. Monperrus, O.F.X. Donard, D.L. Tsalev, Speciation Analysis of Mercury in Aquatic Environment, *Applied Spectroscopy Reviews*. 41 (2006) 591–619. <https://doi.org/10.1080/05704920600929415>.
- [24] A. Zierhut, K. Leopold, L. Harwardt, M. Schuster, Analysis of total dissolved mercury in waters after on-line preconcentration on an active gold column, *Talanta*. 81 (2010) 1529–1535. <https://doi.org/10.1016/j.talanta.2010.02.064>.
- [25] J. Huber, L.-E. Heimbürger, J.E. Sonke, S. Ziller, M. Lindén, K. Leopold, Nanogold-Decorated Silica Monoliths as Highly Efficient Solid-Phase Adsorbent for Ultratrace Mercury Analysis in Natural Waters, *Analytical Chemistry*. 87 (2015) 11122–11129. <https://doi.org/10.1021/acs.analchem.5b03303>.
- [26] M. Schlathauer, J. Friedland, M. Lindén, K. Leopold, Sustainable and reagent-free mercury trace determination in natural waters using nanogold dipsticks, *Microchemical Journal*. 147 (2019) 253–262. <https://doi.org/10.1016/j.microc.2019.03.032>.
- [27] D.S. Tavares, C. Vale, C.B. Lopes, T. Trindade, E. Pereira, Reliable quantification of mercury in natural waters using surface modified magnetite nanoparticles, *Chemosphere*. 220 (2019) 565–573. <https://doi.org/10.1016/j.chemosphere.2018.12.149>.
- [28] J. Li, Y. Liu, Y. Ai, A. Alsaedi, T. Hayat, X. Wang, Combined experimental and theoretical investigation on selective removal of mercury ions by metal organic frameworks modified with thiol groups, *Chemical Engineering Journal*. 354 (2018) 790–801. <https://doi.org/10.1016/j.cej.2018.08.041>.
- [29] Y. Huang, Y. Gong, J. Tang, S. Xia, Effective removal of inorganic mercury and methylmercury from aqueous solution using novel thiol-functionalized graphene oxide/Fe-Mn composite, *Journal of Hazardous Materials*. 366 (2019) 130–139. <https://doi.org/10.1016/j.jhazmat.2018.11.074>.
- [30] B. Zawisza, R. Skorek, G. Stankiewicz, R. Sitko, Carbon nanotubes as a solid sorbent for the preconcentration of Cr, Mn, Fe, Co, Ni, Cu, Zn and Pb prior to wavelength-dispersive X-ray fluorescence spectrometry, *Talanta*. 99 (2012) 918–923. <https://doi.org/10.1016/j.talanta.2012.07.059>.
- [31] K. Kocot, B. Zawisza, E. Marguí, I. Queralt, M. Hidalgo, R. Sitko, Dispersive micro solid-phase extraction using multiwalled carbon nanotubes combined with portable total-reflection X-ray fluorescence spectrometry for the determination of trace amounts of Pb and Cd in water samples, *Journal of Analytical Atomic Spectrometry*. 28 (2013) 736. <https://doi.org/10.1039/c3ja50047k>.

- [32] B. Zawisza, R. Sitko, E. Malicka, E. Talik, Graphene oxide as a solid sorbent for the preconcentration of cobalt, nickel, copper, zinc and lead prior to determination by energy-dispersive X-ray fluorescence spectrometry, *Analytical Methods*. 5 (2013) 6425. <https://doi.org/10.1039/c3ay41451e>.
- [33] K. Kocot, R. Sitko, Trace and ultratrace determination of heavy metal ions by energy-dispersive X-ray fluorescence spectrometry using graphene as solid sorbent in dispersive micro solid-phase extraction, *Spectrochimica Acta Part B: Atomic Spectroscopy*. 94–95 (2014) 7–13. <https://doi.org/10.1016/j.sab.2014.02.003>.
- [34] M.D. Stoller, S. Park, Y. Zhu, J. An, R.S. Ruoff, Graphene-Based Ultracapacitors, *Nano Letters*. 8 (2008) 3498–3502. <https://doi.org/10.1021/nl802558y>.
- [35] R. Sitko, B. Zawisza, E. Malicka, Graphene as a new sorbent in analytical chemistry, *TrAC Trends in Analytical Chemistry*. 51 (2013) 33–43. <https://doi.org/10.1016/j.trac.2013.05.011>.
- [36] M. Valcárcel, S. Cárdenas, B.M. Simonet, Y. Moliner-Martínez, R. Lucena, Carbon nanostructures as sorbent materials in analytical processes, *TrAC Trends in Analytical Chemistry*. 27 (2008) 34–43. <https://doi.org/10.1016/j.trac.2007.10.012>.
- [37] J. Gigault, B. Grassl, G. Lespes, A new analytical approach based on asymmetrical flow field-flow fractionation coupled to ultraviolet spectrometry and light scattering detection for SWCNT aqueous dispersion studies, *The Analyst*. 137 (2012) 917–923. <https://doi.org/10.1039/C2AN15449H>.
- [38] D. Amouroux, E. Tessier, C. Pécheyran, O.F.X. Donard, Sampling and probing volatile metal(loid) species in natural waters by in-situ purge and cryogenic trapping followed by gas chromatography and inductively coupled plasma mass spectrometry (P-CT-GC-ICP/MS), *Analytica Chimica Acta*. 377 (1998) 241–254. [https://doi.org/10.1016/S0003-2670\(98\)00425-5](https://doi.org/10.1016/S0003-2670(98)00425-5).
- [39] X.Q. Wang, P. Wang, P. Ning, Y.X. Ma, F. Wang, X.L. Guo, Y. Lan, Adsorption of gaseous elemental mercury with activated carbon impregnated with ferric chloride, *RSC Advances*. 5 (2015) 24899–24907. <https://doi.org/10.1039/C5RA01011J>.
- [40] J. Lusilao-Makiese, E. Tessier, D. Amouroux, E. Cukrowska, Analytical Performances of Nanostructured Gold Supported on Metal Oxide Sorbents for the Determination of Gaseous Mercury, *International Journal of Analytical Chemistry*. 2014 (2014) 1–8. <https://doi.org/10.1155/2014/490291>.
- [41] E.R. Pereira, B.M. Soares, J.V. Maciel, S.S. Caldas, C.F.F. Andrade, E.G. Primel, F.A. Duarte, Development of a dispersive liquid–liquid microextraction method for iron extraction and preconcentration in water samples with different salinities, *Analytical Methods*. 5 (2013) 2273. <https://doi.org/10.1039/c3ay26294d>.
- [42] Europäische Kommission, Ambient Air Pollution by Mercury (Hg) Position Paper: 17 October 2001, 2011. <https://nbn-resolving.org/urn:nbn:de:101:1-2012111733715> (accessed September 30, 2020).
- [43] A. Lamberty, H. Schimmel, J. Pauwels, The study of the stability of reference materials by isochronous measurements, *Fresenius' Journal of Analytical Chemistry*. 360 (1998) 359–361. <https://doi.org/10.1007/s002160050711>.
- [44] T.P.J. Linsinger, A.M.H. van der Veen, B.M. Gawlik, J. Pauwels, A. Lamberty, Planning and combining of isochronous stability studies of CRMs, *Accreditation and Quality Assurance*. 9 (2004) 464–472. <https://doi.org/10.1007/s00769-004-0818-x>.
- [45] B.M. Gawlik, R. Loos, G. Bidoglio, G. Fauler, X. Guo, E. Lankmayr, T. Linsinger, Testing sample stability in short-term isochronous stability studies for EU-wide monitoring surveys of polar organic contaminants in water, *TrAC Trends in Analytical Chemistry*. 36 (2012) 36–46. <https://doi.org/10.1016/j.trac.2012.04.001>.
- [46] Y. Yang, L. Liang, D. Wang, Effect of dissolved organic matter on adsorption and desorption of mercury by soils, *Journal of Environmental Sciences*. 20 (2008) 1097–1102. [https://doi.org/10.1016/S1001-0742\(08\)62155-5](https://doi.org/10.1016/S1001-0742(08)62155-5).
- [47] F. Wu, H. Liu, M. Zhang, W. Ma, X. Huang, S. Liu, J. Dai, Adsorption Characteristics and the Effect of Dissolved Organic Matter on Mercury(II) Adsorption of Various Soils in China, *Soil and Sediment*

- [48] X. Wang, X. Pan, G.M. Gadd, Soil dissolved organic matter affects mercury immobilization by biogenic selenium nanoparticles, *Science of The Total Environment*. 658 (2019) 8–15. <https://doi.org/10.1016/j.scitotenv.2018.12.091>.
- [49] A.G. Bravo, D.N. Kothawala, K. Attermeyer, E. Tessier, P. Bodmer, J.L.J. Ledesma, J. Audet, J.P. Casas-Ruiz, N. Catalán, S. Cauvy-Fraunié, M. Colls, A. Deininger, V.V. Evtimova, J.A. Fonvielle, T. Fuß, P. Gilbert, S. Herrero Ortega, L. Liu, C. Mendoza-Lera, J. Monteiro, J.-R. Mor, M. Nagler, G.H. Niedrist, A.C. Nydahl, A. Pastor, J. Pegg, C. Gutmann Roberts, F. Pilotto, A.P. Portela, C.R. González-Quijano, F. Romero, M. Rulík, D. Amouroux, The interplay between total mercury, methylmercury and dissolved organic matter in fluvial systems: A latitudinal study across Europe, *Water Research*. 144 (2018) 172–182. <https://doi.org/10.1016/j.watres.2018.06.064>.
- [50] C. Green-Ruiz, Effect of salinity and temperature on the adsorption of Hg(II) from aqueous solutions by a Ca-montmorillonite, *Environmental Technology*. 30 (2009) 63–68. <https://doi.org/10.1080/09593330802503859>.
- [51] X. Huang, J. Yang, J. Wang, J. Bi, C. Xie, H. Hao, Design and synthesis of core–shell Fe₃O₄@PTMT composite magnetic microspheres for adsorption of heavy metals from high salinity wastewater, *Chemosphere*. 206 (2018) 513–521. <https://doi.org/10.1016/j.chemosphere.2018.04.184>.
- [52] G.L. Lescord, K.A. Kidd, J.L. Kirk, N.J. O’Driscoll, X. Wang, Derek.C.G. Muir, Factors affecting biotic mercury concentrations and biomagnification through lake food webs in the Canadian high Arctic, *Science of The Total Environment*. 509–510 (2015) 195–205. <https://doi.org/10.1016/j.scitotenv.2014.04.133>.
- [53] K. Eklöf, J. Fölster, L. Sonesten, K. Bishop, Spatial and temporal variation of THg concentrations in run-off water from 19 boreal catchments, 2000–2010, *Environmental Pollution*. 164 (2012) 102–109. <https://doi.org/10.1016/j.envpol.2012.01.024>.
- [54] H. Shirkhanloo, A. Khaligh, H.Z. Mousavi, A. Rashidi, Ultrasound assisted-dispersive-ionic liquid-micro-solid phase extraction based on carboxyl-functionalized nanoporous graphene for speciation and determination of trace inorganic and organic mercury species in water and caprine blood samples, *Microchemical Journal*. 130 (2017) 245–254. <https://doi.org/10.1016/j.microc.2016.09.012>.
- [55] S. Yang, D. Zhang, H. Cheng, Y. Wang, J. Liu, Graphene oxide as an efficient adsorbent of solid-phase extraction for online preconcentration of inorganic and organic mercurials in freshwater followed by HPLC-ICP-MS determination, *Analytica Chimica Acta*. 1074 (2019) 54–61. <https://doi.org/10.1016/j.aca.2019.04.066>.

6. Occurrence, distribution and characteristics concentrations of Potential Harmful Trace Elements (PHTEs) in Pyrenean lakes and their relation to aquatic biogeochemistry

6.1. Abstract

High altitude ecosystems are of primary importance for the preservation of the biodiversity and water resources. They are also essential to help sustain the economic development of touristic regions. These ecosystems are very unstable due to human activity, and are already affected by climate change on both local and global scale. Various studies have demonstrated chemical contamination of anthropogenic origin in Pyrenean lakes and ecosystems. This contamination is due to both local pollution (mining, industry, road traffic) and atmospheric transport from regional or global pollution sources. The use of alpine lakes as proxies of global environmental changes implies a deep understanding of their hydrological functioning and physicochemical dynamics, taking especially into consideration the combined effects of seasonal variations, altitudinal gradient and the own properties of the lake. One of the possibilities to study alpine lakes dynamics is to focus on the presence and the fate of trace elements and metals. Indeed, the dynamic of metals and metalloids is directly related to hydrology and geochemical processes, themselves sensitive to changes in environmental conditions such as temperature, atmospheric deposition or biological productivity. Even if several research projects have highlighted the presence and the impact of contaminants such as toxic metals, metalloids and organometals in Pyrenean ecosystems, the chemical cycle of these elements has been barely investigated in detail. In this study, a seasonal sampling has been conducted in order to investigate the distribution and the fate of Potential Harmful Trace Elements (PHTEs) (As, Sb, Cd, Cr, Cu, Ni, Pb, Zn,...) within the water column of several alpine lakes, and how such contamination can be constrained by climatic, hydrological and local to long range anthropogenic inputs. Water samples were collected in June 2017, October 2017, June 2018 and October 2018 in 20 different lakes of the Central Pyrenees on both French and Spanish slopes to understand the spatial and seasonal variations of PHTEs contamination within the lake ecosystems. During the first two sampling campaigns, spatial variability has been evaluated in each lake by collecting subsurface water samples at upstream, center and downstream. In 2018, a more in-depth study was performed in lakes Gentau, Arratille, Azules and Sabocos, by sampling at different depths along the day. A classification of the lakes according to their water geochemistry was done, highlighting the importance of the trophic status of the lakes, the geological background and the atmospheric inputs. The occurrence, sources and behavior of the PHTEs in the studied lakes was investigated. Finally, the intensive monitoring of the four lakes mentioned above allow to identify some PHTEs sensitive to environmental changes induced either by Climate Change or anthropogenic pressure.

Keywords:

Potential Harmful Trace Elements; Water; Lakes; Pyrenees

6.2. Introduction

High altitude ecosystems are of primary importance for the preservation of the biodiversity. They are also essential to help sustain the economic development of touristic regions. These ecosystems are very unstable due to human activity and are already affected by climate change [1–4] with increasing temperature, decreasing precipitations, glacier recession, and decreasing of the snow cover as main observable phenomena. All these environmental perturbations of high altitude ecosystems may have strong impact on the functioning of sensitive aquatic systems, such as high altitude lake ecosystems. *Sánchez-España et al.* [4], in a recent study conducted in the Lake Enol (1070m asl, North West Spain), also suggested that climate factors (warmer and drier spring and autumn) are reducing oxygen levels in deep waters through a long and increasingly steep thermal stratification.

The use of alpine lakes as proxies of global environmental changes [4–8] implies a deep understanding of their natural processes and physicochemical dynamics [9]. For this purpose, *Camarero et al.* [10] have focused on the main chemical parameters of mountain lake waters and their relation to environmental drivers such as weathering, sea salt inputs, atmospheric deposition of N and S, and biological activity of soils in the catchment that consumes NO_3^- and produces DOC. Various studies have also demonstrated chemical contamination of anthropogenic origin in Pyrenean lakes [11–17]: Potential Harmful Trace Elements (PHTEs), PolyBrominated Diphenyl Ether (PBDE), PolyChlorinated Biphenyl (PCB), pesticides, Polycyclic Aromatic Hydrocarbon (PAH). This contamination is due to both local pollution (mining, industry, road traffic) and atmospheric transport from regional or global pollution sources.

Therefore, it is important to investigate the presence and fate of contaminants in alpine lakes, especially those known as Potential Harmful Trace Elements (PHTEs), which constitute a threat for aquatic ecosystems because of their persistency in the environment and their potential toxicity on biological functions [18–21]. PHTEs dynamics are directly related to hydrological and geochemical processes, themselves sensitive to changes in environmental conditions. Combined, the concentration of PHTEs constitutes less than 0.1 % of the Earth's crust [22], and several studies have shown that the contamination by PHTEs is widespread and that PHTEs can be found in remote areas that are far from contamination sources. For example, lead isotopes analysis in Greenland ice cores highlighted large-scale atmospheric pollution by this toxic metal over a thousand years [23]. An evaluation of various contaminants of anthropogenic origin, among which lead and mercury, over the past few centuries has been possible using ice cores from polar regions and high altitude glaciers [24]. *Cooke et al.* [25] review the use of lake sediment, peat, ice, marine sediment and tree rings as environmental archives of the global biogeochemical mercury cycle. Released by different sources, both natural and anthropic, PHTEs can be dispersed in the environment through various physical processes and accumulated in plants and, ultimately, in human body, causing serious health problems such as intoxication, neurological disturbance and cancer [26]. Some elements are essential to human health (Fe, Cu, Zn) whereas some others are toxic (As, Hg, Pb), responsible for serious human diseases with frequent lethal

consequences. They can reach high altitude lakes through direct atmospheric deposition and/or release from sediments and soils from the catchment [27].

Worldwide, the occurrence of PHTEs in surface waters of alpine lakes have been scarcely studied. In the Alps, human activities in the lowlands (industries and intensive agriculture) resulted in the transport and deposition of pollutants in alpine areas [28]. The ICP Waters Programme supported investigations to assess the effects of cross-border air pollution on aquatic ecosystems, especially on PHTEs such as As, Cu, V, Ni, Cr, Cd, Se and Zn [29]. *Hofer et al.* [30] also reported Pb, Cd, Ni, Cu and Zn concentrations in surface waters from 17 alpine lakes in the Alps. In the Himalaya, PHTEs biogeochemical cycle in the aquatic compartment has been studied in only two alpine lakes, regarding seasonal variations with the influence of the monsoon [31], and in relation to elevation particularly with higher enrichment of Cd and Pb in high altitude lakes [32].

The presence and potential impact of such contaminants have been successfully highlighted studying sediment cores from Pyrenean lakes [12,27,33,34]. Nevertheless, their biogeochemical cycle, especially in the aquatic compartment, has been barely investigated in this mountain range [35,36]. Indeed, *Zaharescu et al.* [36] investigated the sources of some trace elements (As, Cd, Co, Cu, Mn, Ni, Pb and Zn) in the Lake Respomuso (2200 m asl., Central Pyrenees) by analyses of surface waters and sediments from the lake and its catchment. In this lake, the main source of these trace elements appears to be the bedrock, rich in metal-bearing minerals. The other study dealing with trace elements in Pyrenean lake waters has been conducted by *Bacardit and Camarero* [35] on three different alpine lakes from the Central Pyrenees (Lakes Légunabens, Plan and Vidal d'Amunt). In this work, only three trace elements, Pb, Zn and As, have been quantified in atmospheric depositions, sediments and surface waters from the lakes and their catchment. Terrestrial inputs from the catchment to the lakes dominate for the three trace elements, with distinct sources for Pb (anthropogenic origin) and As (weathering of As-rich rocks).

Overall, even if alpine lakes are sensitive to changes in atmospheric pollution and climate, offering strong research opportunities, there is a lack of knowledge about the aquatic biogeochemical cycle of PHTEs in such remote areas. This is probably due to the difficult accessibility to these remote environments with all required material and to the extremely low concentrations of the PHTEs, usually below the $\mu\text{g L}^{-1}$, avoiding their quantification without ultra-trace sampling protocols, clean lab methodologies and high sensitivity instruments (**3. Sampling and analytical strategy**).

This work presents an integrated investigation conducted in twenty high altitude pristine lakes from the Central Pyrenees. These small lakes show similar physical properties (i.e. size, depth) but differ mainly from their catchment characteristics and geological background (i.e. granitic vs sedimentary rocks). They also span a wide range of altitude, from 1620 to 2600 m asl. To study the water hydrological and geochemical characteristics (temperature, dissolved oxygen, conductivity, redox potential, chlorophyll-a, silicates, TOC, DIC, Total Alkalinity, pH, anions, major and trace elements), subsurface (~0.5 m depth) water samples from all the lakes were collected in June-July/October 2017/2018, and a more in-depth study was performed in three of these lakes by sampling at different depths along the same day in June-

July/October 2018. All the procedures used to collect and analyse the samples have been fully described in **3 Sampling and analytical strategy**.

The more specific objectives of this study were to i) evaluate the effectiveness of the sampling strategy in terms of intra-lake variability and truly dissolved vs total concentration of PHTEs, ii) establish a categorisation of the lakes according to their water chemical composition iii) contribute to the knowledge on PHTEs biogeochemical cycle by an evaluation of the main sources and processes controlling their fate in alpine lake waters. This study is also the first one to report 15 PHTEs detected and quantified in all the water samples collected in alpine lakes.

6.3. Subsurface lake water geochemistry

6.3.1. Physico-chemical characteristics and PHTEs concentrations

Statistical descriptors of the main physico-chemical parameters of the 74 subsurface water samples collected during the four sampling campaigns are summarized in **Table 6.1**, and those of the concentrations of major, trace and ultra-trace cations are shown in **Figure 6.1**.

The 24 major/minor and trace/ultra-trace cations detected in all the samples can be separated in two categories according to their concentration. On the one hand, major/minor and trace elements, with concentrations mainly above the ppb level ($\mu\text{g L}^{-1}$), occurred in the following order of abundance: Ca > Na > Mg > K > Al > Sr > Fe > Mn > Ba. On the other hand, ultra-trace elements, mainly PHTEs, occurred in the following order of abundance: As > U > Cu > Ti > Mo > V > Ni > Cr > Pb > Sb > Co > Cd > Tl > Se > Hg.

Temperatures of the lake water vary strongly among and within the studied lakes, ranging from 2 to 19 °C. Altitude is a key factor explaining these variations with an opposite correlation with temperature ($r = -0.48$). The highest temperature was found in Replim1 (spring 2017) in ORD (2100 m asl), a low altitude, shallow and well exposed to sunlight lake, while the lowest one was recorded in Replim3 in CAM (2344 m asl) while ice was still covering a part of the lake. Over the four sampling campaigns, the temperature has been always measured in 6 lakes (ARA, CAM, AZU, ARN, COA and PAN) and the lowest values were recorded in Replim3 (spring 2018). As previously highlighted, this can be explained by the fact that a few days before Replim3 sampling many of the studied lakes were still partially frozen (high snow accumulation during winter 2017-2018).

Regarding the dissolved oxygen, most of the subsurface lake waters were oversaturated. The fluorescence signal of the chlorophyll-a in the samples, as Relative Fluorescence Units (RFU), was always below the limit of detection. Indeed, there was no significant difference between the signal measured by the probe out of the water and the signal measured at 0.5m depth. These two parameters will be discussed later using the depth profiles obtained in some specific lakes.

Conductivity (5 to 130 $\mu\text{S cm}^{-1}$), pH (4.87 to 7.91), Total Alkalinity (TA) (14 to 1839 $\mu\text{mol kg}^{-1}$) and Dissolved Inorganic Carbon (DIC) (33 to 1727 $\mu\text{mol kg}^{-1}$) are all together significantly correlated ($r = 0.74$, 0.74 and 0.75 respectively between pH and conductivity, pH and TA, and pH and DIC; $p\text{-value} < 0.05$) with the lowest values for the granitic lake PEY and the highest values for the limestone and dolomite enriched lake SAB. This variability is a direct consequence of weathering of Calcium (Ca) mainly as calcite (180 to 22229 $\mu\text{g L}^{-1}$) and, to a less extent, dolomite also with an important Magnesium (Mg) content (51 to 6129 $\mu\text{g L}^{-1}$): a strong correlation ($r = 0.78$; $p\text{-value} < 0.05$) can be observed between pH and the sum of Ca and Mg concentrations.

Strontium (Sr) (0.3 to 73.8 $\mu\text{g L}^{-1}$) is strongly associated with Ca ($r = 0.93$; $p\text{-value} < 0.05$). The presence of Barium (Ba) (0.1 to 5.4 $\mu\text{g L}^{-1}$) in surface waters is strongly controlled by the abundance of Ba in the bedrock. Along with the four sampling campaigns, the highest Ba concentrations were found in AZU ($4.7 \pm 0.4 \mu\text{g L}^{-1}$) and SAB ($4.3 \pm 0.1 \mu\text{g L}^{-1}$). Therefore, both Sr and Ba are also indicative of calcareous rocks, in association with Ca, Mg and Sr.

The presence of Aluminium (Al) (6 to 96 $\mu\text{g L}^{-1}$) might be related to atmospheric transport of dust. Its distribution in the lake waters is strongly dependent on pH: Al is characterised by a low solubility that increases sharply with decreasing pH, therefore directly influencing its toxicity. This is well supported by the negative correlation between Al and Ca ($r = -0.40$; $p\text{-value} < 0.05$): lower Ca induces high sensitivity to acidification hence increases of Al concentrations. Al is also well correlated ($r = 0.91$; $p\text{-value} < 0.05$) with Ti (22 to 1882 ng L^{-1}).

The most significant sources of Chloride (Cl⁻) in freshwaters are rainfall and marine aerosols. Chloride in the high altitude lakes of this study (69 to 684 $\mu\text{g L}^{-1}$) is significantly correlated with Sodium (Na) (35 to 1084 $\mu\text{g L}^{-1}$) ($r = 0.83$; $p\text{-value} < 0.05$) and to Potassium (K) (20 to 202 $\mu\text{g L}^{-1}$) ($r = 0.61$; $p\text{-value} < 0.05$). The sulphate (SO₄²⁻) concentrations ranged between $< 0.21 \text{ mg L}^{-1}$ and 7.56 mg L^{-1} . The highest SO₄²⁻ concentrations, of geological origin, are found in ARA ($3.0 \pm 0.4 \text{ mg L}^{-1}$), BAD ($3.9 \pm 1.1 \text{ mg L}^{-1}$) and AZU ($6.1 \pm 1.2 \text{ mg L}^{-1}$).

Dissolved Organic Matter (DOC) (0.6 to 4.6 mg L^{-1}) and Nitrate (NO₃⁻) (< 0.065 to 1.132 mg L^{-1}) were low and vary strongly among lakes and sampling campaigns. Together with Silicate (0.1 to 7.0 mg L^{-1}), DOC and NO₃⁻ can be indicators of possible biological activity, especially the production of phytoplankton (including diatoms for silicates), in the studied lakes [10]. The highest concentrations of Silicate over the four sampling campaigns were found in Lakes ARA (4.7 ± 0.2), BAD (4.6 ± 0.7) and PAR (6.5 ± 0.3), in relation to the sandstone (quartz and feldspar) highly soluble of the Devonian rocks.

Fe and Mn concentrations ranged respectively from 3 to 68 $\mu\text{g L}^{-1}$ and from 0.2 to 10.9 $\mu\text{g L}^{-1}$. The fate of Fe and Mn dissolved in lake waters is complex as they are relatively immobile under most environmental conditions due to limited solubility. These two elements, mainly from lithogenic origin, can be rapidly adsorbed onto particles depending on the physico-chemical characteristics of the water, in particular pH, redox potential and dissolved oxygen. Strong variations of dissolved oxygen occur in stratified lakes, with hypoxic to anoxic zone at the bottom part of these lakes. Therefore, the study of depth profile in such lakes, that will be discussed later, will provide new insights on the biogeochemical

cycle of these two particular elements. It is also important to underline that various PHTEs can be either trapped or released together with Fe and Mn [37].

PHTEs (As, U, Cu, Mo, V, Ni, Cr, Pb, Se, Sb, Co, Cd, Tl and Hg) were found at very low concentrations in the lake waters, below the maximum allowable concentrations (MAC) set by the Council Directive 98/83/EC for human consumption. Arsenic (As) concentrations varied strongly (31 to 8910 ng L⁻¹) with the highest values over the four sampling campaigns in lakes AZU (4980 ± 920 ng L⁻¹) and PEC (8410 ± 600 ng L⁻¹) close to the MAC (10 µg L⁻¹). Such enrichment in As has already been attributed to local geological sources. Indeed, the sediments of Pyrenean lakes present a remarkably higher As content compared to other alpine lakes [12]. Arsenic can be released from hydrothermal and magmatic ore deposits in granites or metamorphic rocks, which are naturally rich in As as sulphide minerals in the Pyrenees [35].

Other PHTEs have shown much higher concentrations in some particular lakes, also probably linked to the characteristics of the bedrock of the affected lakes and their associated catchment. Indeed, Uranium (U) (5 to 2402 ng L⁻¹) is a non-essential element and is chemotoxic, radiotoxic and carcinogen. The highest concentrations were found in PAR (2313 ± 79 ng L⁻¹). Vanadium (V) (23 to 397 ng L⁻¹) also presented its higher concentrations in PAR (392.0 ± 4.0 ng L⁻¹) probably due to the presence of carnotite minerals present in sandstone (K₂(UO₂)₂(VO₄)₂·3H₂O) also supported by the important content of K in this lake (187 ± 15 µg L⁻¹). Nevertheless, PAR is the only lake with concentrations of V at least 3 times higher than the rest of the studied lakes. The particular status of this lake can also be responsible for this anomaly in V concentration. Indeed, it is a very shallow lake, partly occupied by a peatland, with the highest organic matter content (NPOC = 2.6 ± 0.4 mg L⁻¹), and reactivity at the water-sediment interface is important. V buried in the anoxic sediments of Lake PAR might be remobilized, and released into the water column [38].

U veins can also appear in granitic rocks. That is the case of Lake OPA where important U (1430 ± 350 ng L⁻¹) and K (133 ± 11 µg L⁻¹) were measured, while V (100.0 ± 8.0 ng L⁻¹) was not significantly different from the results obtained in all the other lakes except PAR (Kruskal-Wallis test, p-value = 0.292). Toxicity of V highly depends on its speciation and oxidation state. Airborne anthropogenic V might be an important source, especially for high altitude lakes without V geological inputs.

Molybdenum (Mo) (6 to 618 ng L⁻¹) and Selenium (Se) (12 to 89 ng L⁻¹) are both essential elements, and both deficiencies and excesses can cause health problems. Mo species are strongly adsorbed by clay particles, oxyhydroxides (Fe, Al and Mn) and can coprecipitate with organic matter and/or other cations. Nevertheless, all these reactions depend on the pH and redox potential; therefore, the occurrence and mobility of Mo in lake water are difficult to predict. Highest concentrations of Mo were also found in PAR (570 ± 38 ng L⁻¹), probably also as a result of the remobilization of Mo at the water-sediment interface. Se is widely present as a micronutrient, replacing sulphur in many sulphide minerals such as pyrite, chalcopyrite, pyrrhotite and sphalerite. Therefore, we have found a significant correlation between Se and SO₄²⁻ in our results (r = 0.83; p-value < 0.05) and the highest concentrations of Se were

found in the lakes with the highest concentration of SO_4^{2-} , ARA ($60.0 \pm 2.0 \text{ ng L}^{-1}$), BAD ($69 \pm 15 \text{ ng L}^{-1}$) and AZU ($60 \pm 10 \text{ ng L}^{-1}$) (Romero *et al.*, manuscript in preparation).

Although possible local soils and bedrocks sources should not be discarded, Lead (Pb) (13 to 503 ng L^{-1}) was found associated to Al ($r = 0.81$) and Ti ($r = 0.87$) suggesting an important input of Pb from dust depositions. Precipitation might be an important source of Nickel (Ni) (23 to 797 ng L^{-1}) and Copper (Cu) (94 to 434 ng L^{-1}) in the lakes under study, as suggested for other lakes [3].

Atmospheric transport and both dry and wet deposition are the main sources of Mercury (Hg) in high altitude lakes. In our study, the concentration of Hg in subsurface waters ranged from 0.1 to 2.9 ng L^{-1} . Even if Hg occurs at very low concentrations in marine systems and remote lakes, it is very important because of its biomagnification capacity, also depending on its speciation.

This study is one of the first providing results in surface water samples from various alpine lakes for some important potential toxic elements: Chromium (Cr) (23 to 279 ng L^{-1}), Antimony (Sb) (5 to 85 ng L^{-1}), Cobalt (Co) (5 to 80 ng L^{-1}), Cadmium (Cd) (1 to 12 ng L^{-1}) and Thallium (Tl) (0.2 to 2.5 ng L^{-1}). In our study, the highest Cr concentrations were found in ARA ($146 \pm 59 \text{ ng L}^{-1}$), BAD ($178 \pm 52 \text{ ng L}^{-1}$) and PAR ($161 \pm 14 \text{ ng L}^{-1}$). Sb has no known function in living organisms, and, because of its low natural abundance, it is a useful indicator of anthropogenic contamination. The highest concentrations were found in GEN ($71 \pm 12 \text{ ng L}^{-1}$), ROU ($70.0 \pm 5.0 \text{ ng L}^{-1}$) and AZU ($69 \pm 7 \text{ ng L}^{-1}$). The concentration of Cd did not present strong variations within the sampled lakes ($3 \pm 2 \text{ ng L}^{-1}$). The studied lakes differ mainly from their geological substrate, and the small variations in Cd observed suggests that the weathering of rocks and the catchment should not influence significantly Cd distribution. The constant concentrations of Cd measured in the studied lakes are rather due to a common source, maybe atmospheric, rather than local and specific processes occurring in the lakes. Cobalt, as well as Mo and Se, is an essential micronutrient but excess doses or deficiencies are toxic. Small variations were also detected in Co concentrations along with the whole data set ($15 \pm 11 \text{ ng L}^{-1}$), with some punctual high concentrations. Finally, the toxicity of Tl is similar to that of Cd, Hg and Pb, but the fate of this element in lake water has been poorly studied as it occurs at extremely low concentrations. Together with Hg, this element, mainly below the ppt level (ng L^{-1}), was the less abundant and detected for the first time in the high altitude lakes of our study, with small variations among lakes ($0.70 \pm 0.40 \text{ ng L}^{-1}$).

Overall, it is worth noting that the samples collected in PAR presented significantly higher values for many of the measured parameters (DOC, trace and ultra-trace elements, Silicate). This lake is completely different from the other ones, mainly because of i) its very small size (close to a pond) and the very low depth that enhances resuspension of sediments and organic material, ii) the remobilization of trace elements from organic sediment diagenesis and peat leachates, iii) its gradual transformation into a wetland/peatland, and iv) its low altitude together with the dense forest vegetation surrounding the lake.

The studied lakes span a wide range of chemical characteristics in particular related to their sensitivity to acidification, a consequence of the widely different lithological characteristics of the lake catchments (i.e. easily erodible sedimentary rocks vs granite).

Table 6.1: Main chemical parameters of the studied lakes measured by the multiparametric probe (temperature, conductivity, redox potential), the TOC analyser (TOC as NPOC), Flow Injection Analysis (Silicate), the VINDTA 3C Instrument (DIC, Total Alkalinity) and the ionic chromatograph (Cl⁻, NO₃⁻ and SO₄²⁻). pH was calculated according to Kortazar et al. (2020) [39]. Chlorophyll-a is not mentioned as it was always below LOD. Dissolved oxygen, as mentioned in Chapter X, was calibrated only once before each sampling campaign and the sensor is sensitive to elevation: the whole lakes were oversaturated in subsurface but the values measured differ among lakes because of elevation. All the methodological details can be found **3.Sampling and analytical strategy**.

Sampling	Lakes		Elevation (m asl)	Temperature (°C)	pH	Conductivity ($\mu\text{S cm}^{-1}$)	Redox Potential (mV)	TOC (mg L^{-1})	Silicate (mg L^{-1})	DIC ($\mu\text{mol kg}^{-1}$)	Total Alkalinity ($\mu\text{mol kg}^{-1}$)	Cl ⁻ (mg L^{-1})	NO ₃ ⁻ (mg L^{-1})	SO ₄ ²⁻ (mg L^{-1})	
Replim1	16	Min	1620	4.63	6.01	7.2	97	0.63	1.20	92	80	0.15	0.12	0.28	
		Max	2600	18.3	7.47	61	270	2.90	6.20	800	830	0.49	0.90	6.50	
		Median			8.84	6.93	23	160	1.10	2.20	310	310	0.19	0.65	1.60
		Mean			9.29	6.89	28	160	1.40	2.70	390	400	0.21	0.57	1.70
		SD			3.30	0.44	19	51	0.70	1.50	260	270	0.10	0.24	1.60
Replim2	11	Min	1620	7.22	6.00	7.0	46	1.30	0.54	87	84	0.15	< 0.14	0.35	
		Max	2493	11.1	7.91	72	150	3.10	7.00	880	910	0.48	0.75	7.60	
		Median			9.85	7.07	36	110	1.90	2.40	410	400	0.19	0.37	2.30
		Mean			9.80	7.07	39	110	2.10	2.60	480	490	0.22	0.39	2.40
		SD			1.10	0.53	23	32	0.69	1.90	290	310	0.10	0.24	2.10
Replim3	16	Min	1620	2.43	4.87	5.4	36	0.62	0.10	33	14	0.10	0.10	< 0.21	
		Max	2493	18.7	7.65	130	320	2.40	6.40	1700	1800	0.50	1.13	5.40	
		Median			6.87	6.88	28	170	0.86	2.40	350	360	0.20	0.47	1.70
		Mean			8.49	6.77	39	160	1.10	2.70	570	570	0.22	0.49	1.80
		SD			4.80	0.64	35	79	0.51	1.50	480	510	0.10	0.28	1.50
Replim4	16	Min	1620	5.33	5.94	4.5	36	0.94	0.81	79	85	0.14	< 0.10	< 0.29	
		Max	2493	13.4	7.71	100	260	4.60	6.40	1700	1800	0.68	0.82	6.80	
		Median			9.32	6.79	25	170	1.60	1.50	370	380	0.22	0.17	1.70
		Mean			9.30	6.92	38	170	1.80	2.20	590	610	0.27	0.31	1.70
		SD			2.56	0.49	29	63	0.87	1.40	500	550	0.15	0.30	1.60

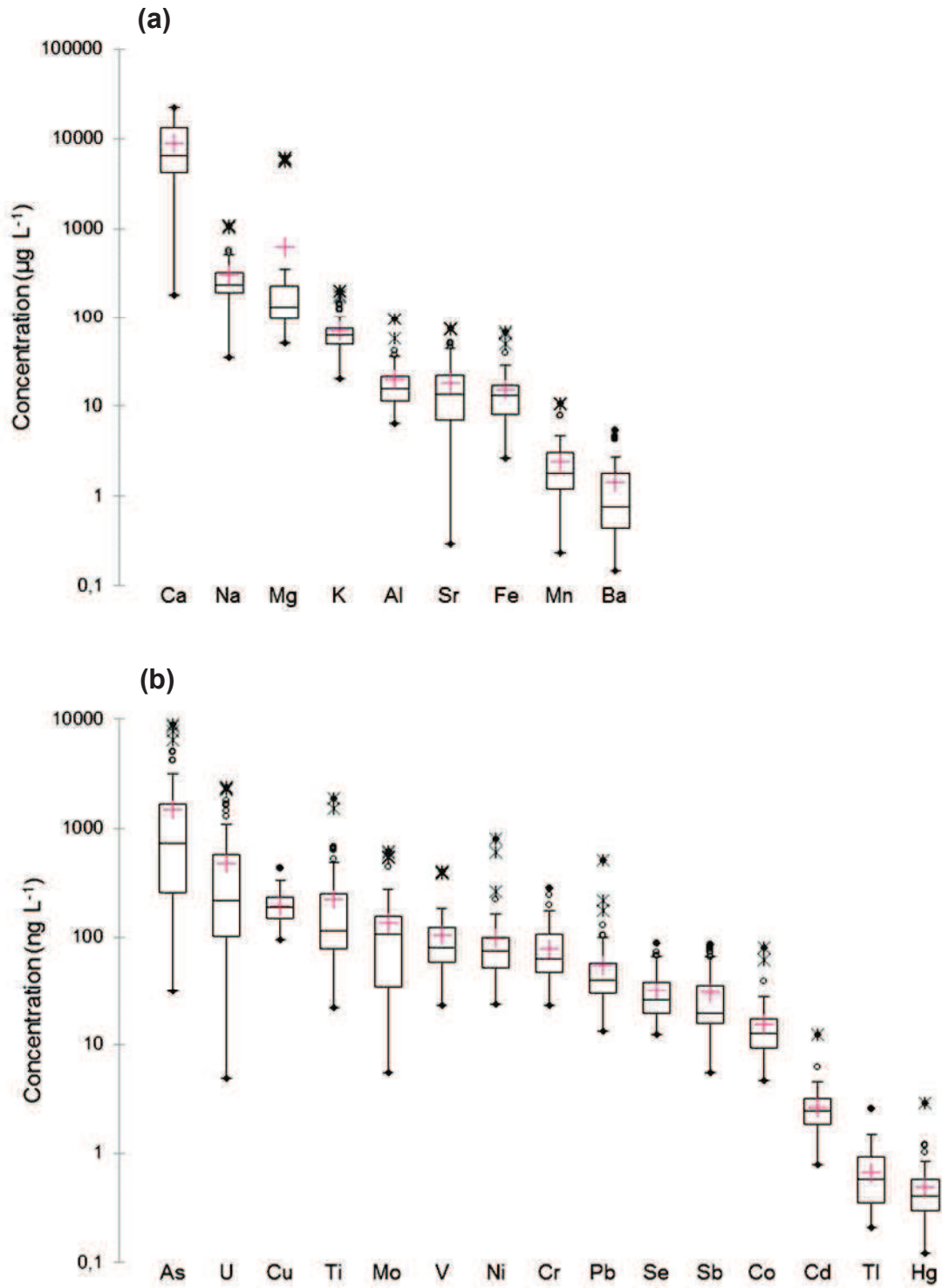


Figure 6.1: (a) Major and trace elements (median concentrations above $1 \mu\text{g L}^{-1}$) and (b) ultra-trace elements (median concentrations below $1 \mu\text{g L}^{-1}$) concentrations in unfiltered subsurface water samples of the 20 studied lakes over the four sampling campaigns. Dots are minimum and maximum, white circles and black crosses are extreme values, bars indicate 10th and 90th percentile, boxes indicate 25th and 75th, marks within each box are medians and red crosses are mean.

6.3.2. Intra-lake variability

In most of the publications related to the geochemistry of lake waters, the spatial variation in the sampling process has not been evaluated, that means the potential variations observed in the chemical parameters linked to the sampling location in each lake and sampling campaign. Indeed, water samples were collected either at the outflow or at the central part of each lake (usually the deepest part of the lake), assuming that the inter-lake variability in the chemistry variables is larger than the intra-lake variability [29,30,40,41], regardless of the lake size. In another way, *Pertsemli and Voutsas* [42] collected three water samples at different locations and mixed them to ensure that the sample is well representative of the site. In *Markert et al.* [43], considering the large size of the studied lakes (> 1640 ha), the sampling points were chosen carefully according to the local status, i.e. low direct anthropogenic influence: in this publication, results are rather representative of a specific area of the lake rather than representative of its global status.

In this work, a triplicate sampling in each studied lake was carried out during the first two sampling campaigns (Replim1 and Replim2) to assess the intra-lake variability in water geochemistry. The uncertainty associated to the analytical measurement has been evaluated in **3.Sampling and analytical strategy**, and only Al (9 %), Cu (10 %), and Ni (9 %) have shown values above 3 %, mainly due to random contamination and/or possible interferences (i.e. double Carbon interferes with Aluminium). **Figure 6.2** depicts the Relative Standard Deviation (RSD) calculated for each major and trace element considered using the results obtained after the analysis of the three samples collected at different parts of each lake. The red dashed lines associated with each element correspond to the uncertainty associated to the analytical measurement.

Overall, the median value for each element is below 15 % (except Ni (21 %)), which is very low assuming that the uncertainty related to the sampling process is more important than the analytical one. Moreover, in this figure, elements range from the most abundant (Ca) to the less one (Hg), and no clear trend is observed regarding this classification. Usually, higher uncertainty is expected at lower concentrations due to the drop in the precision of the instrument, a lower recovery or potential sample contamination. Therefore, in our study, the uncertainty is not related to the analysis processes.

In addition, only a few elements have shown median RSD above 10 %: Al (12 %), Cu (15 %), Ti (10 %), Ni (21 %), Pb (15 %), Cd (12 %) and Hg (14 %). Apart from local sources (rich ores), Hg, Pb and Cd contributions from atmospheric compartment is also important in high altitude lakes [12]. Al and Ti, terrigenous elements (weathering of rocks) are also atmospherically transported to the lake with the dust [3]. Climatic conditions (precipitation, wind, and temperature) may strongly vary between a short distance and timescale in high altitude environments and might be partly responsible for the variation of Hg, Pb, Cd, Al and Ti concentrations among the selected sampling points. Indeed, it has been shown that periods of high deposition of crustal elements occurs during both spring/early summer and late summer/autumn, which correspond to the biannual sampling periods of our study [3]. On the one hand, during spring and early summer, extreme events, more important, are responsible for strong

atmospheric depositions. On the other hand, air masses from the South (North Africa and the Iberian Peninsula) are more important during late summer and autumn [11].

Apart from these phenomena, Ni and Cu have shown in our study one of the most important analytical uncertainties due to random contaminations and consequently we can assume that the sampling process has probably increased the global uncertainty related to these two elements for the same reason.

At the light of these results, we decided to sample just a single point of the lake (the deepest one) in the two last campaigns (Replim3 and Replim4) of the study.

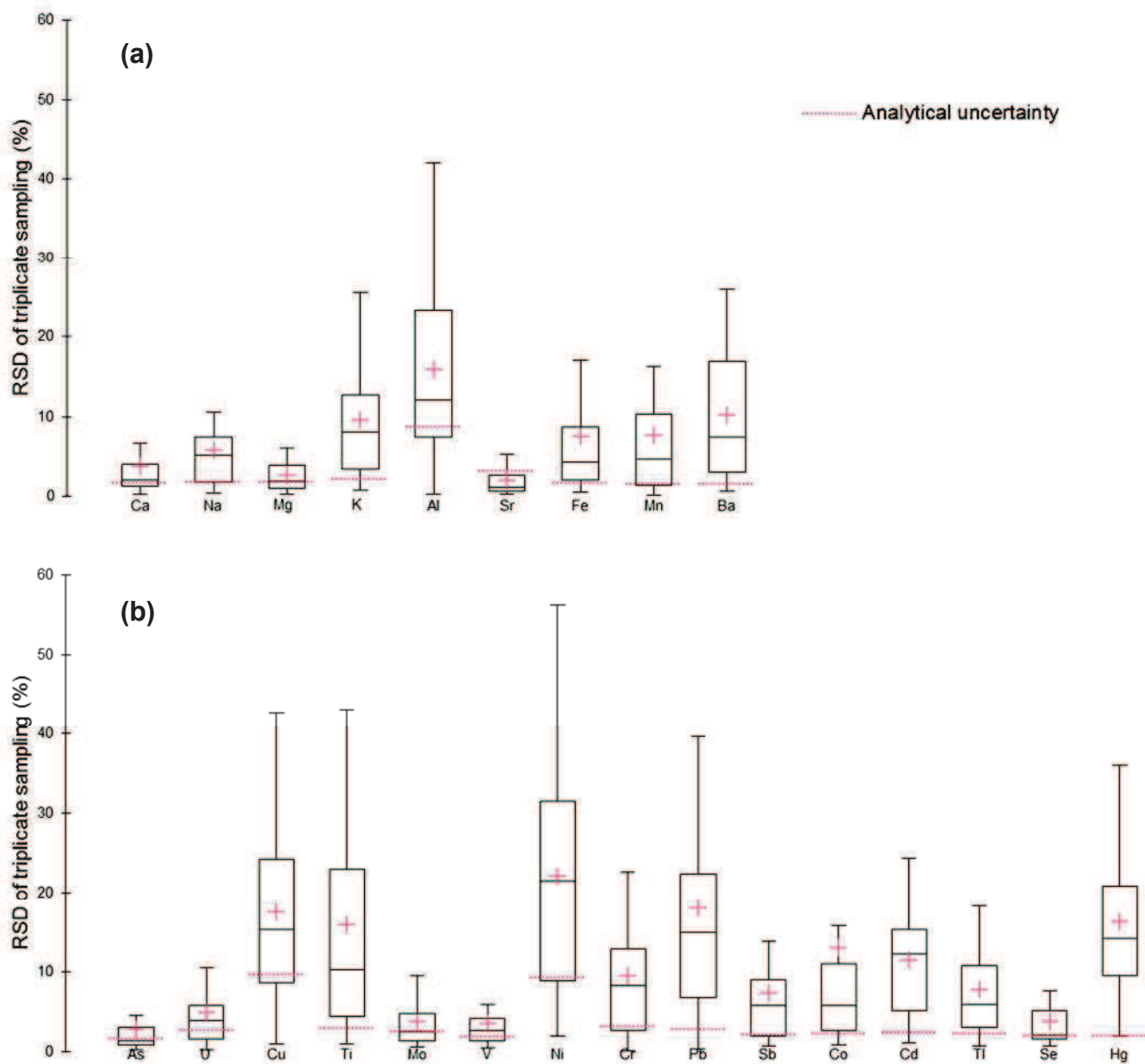


Figure 6.2: Relative Standard Deviation (RSD) calculated for each (a) major and trace element and (b) ultra-trace element considered using the results obtained after the analysis of the three samples collected at different parts of each lake. Bars indicate 10th and 90th percentile, boxes indicate 25th and 75th, marks within each box are medians and red crosses are mean.

6.3.3. Daily variations

In Replim3 and Replim4, water samples were collected in four selected lakes (GEN, ARA, AZU and SAB) at different times of the day at the same point of the lake in order to investigate the reactivity of some of the trace and ultra-trace elements in high altitude lakes.

Over the 24 elements investigated, only nine of them have shown a clear diurnal variation: Al, Fe, Mn, Cu, Ti, Ni, Pb, Cd and Hg (**Table 6.2**). As mentioned previously, variation for some of these elements may be due to an increase or decrease in the magnitude of the deposition processes including snow melting much higher during the day, but reactivity might also be partially responsible. Indeed, these trace elements are reactive and can precipitate rapidly as (oxy)hydroxide species, poorly soluble in the water. The precipitation reaction, as well as dissolution, depend on some variables such as pH, temperature and organic matter [44]. Considering the oligotrophic status of the studied lakes and the small content of organic matter ($\text{TOC} < 4.6 \text{ mg L}^{-1}$), organic matter itself and/or biological productivity should not be the most important driving force responsible of the precipitation reactions.

For Al, Fe, Mn, Ti and Pb, pH seems to have a great influence with an opposite relation: increasing concentrations of the trace elements as pH decreases, even by less than one pH unit. Indeed, significant correlations have been found between pH and Fe ($r = -0.69$; $p\text{-value} < 0.05$), Mn ($r = -0.68$; $p\text{-value} < 0.05$), Ti ($r = -0.60$; $p\text{-value} < 0.05$) and Pb ($r = -0.53$; $p\text{-value} < 0.05$). In the case of Al ($r = -0.44$; $p\text{-value} = 0.06$), the larger analytical uncertainty associated to Al (9 %) might prevent a significant correlation. These oxyanions have the particularity to express high variations in their pH-dependent diagrams [45] in the range of 4 to 8 pH values, which corresponds to the values registered during the four sampling campaign in our study.

Cd presents significant correlations with both pH ($r = -0.47$; $p\text{-value} < 0.05$) and temperature ($r = -0.78$; $p\text{-value} < 0.05$).

Hg displays a biogeochemical cycle much more complex in aquatic ecosystems, especially regarding its speciation with inter-species conversions (reduction, demethylation, methylation etc ...) and important reemissions of gaseous Hg (ie $\text{Hg}(0)$) from the surface water directly to the atmospheric compartment [46]. Mercury species dynamic and cycling will be further presented and discussed in detail in **Part XX**.

Ni and Cu results do not express any clear trend regarding pH and temperature. As for Hg, this might be related to the complexity of their biogeochemical cycle.

Overall, even if some elements are showing significant daily variations in their water concentrations, for further discussions we can assume that seasonal and spatial inter-lake variability will be more important than daily variations.

Table 6.2: Temperature, pH and concentrations of several elements measured in water samples collected in four selected lakes at different times of the day

Lake	Time	T° (°C)	pH	Al (µg L ⁻¹)	Fe (µg L ⁻¹)	Mn (µg L ⁻¹)	Cu (ng L ⁻¹)	Ti (ng L ⁻¹)	Ni (ng L ⁻¹)	Pb (ng L ⁻¹)	Cd (ng L ⁻¹)	Hg (ng L ⁻¹)
ARA	08:30	5.86	7.09	9.50	13.7	3.23	161	99	120	42	3.0	0.12
(Replim3)	11:05	5.70	6.99	9.82	15.4	3.30	145	90	103	20	2.3	0.21
	13:25	5.72	6.94	9.00	14.8	3.06	141	87	102	39	2.5	0.18
	16:00	6.64	6.88	13.1	13.0	2.96	204	89	109	48	2.5	0.21
GEN	06:30	6.89	6.70	17.8	11.8	3.28	202	382	164	58	1.9	0.85
(Replim3)	10:50	6.87	6.72	20.8	11.4	3.05	256	356	260	93	3.7	0.39
	15:50	6.87	6.90	15.9	11.8	3.27	196	317	150	40	1.7	0.69
	21:10	7.21	6.64	17.6	22.9	10.9	434	329	797	174	2.6	0.40
AZU	09:35	4.87	7.17	13.9	11.0	2.97	158	131	98	44	3.0	0.31
(Replim3)	12:00	5.03	7.58	11.6	10.3	2.61	132	101	91	35	2.8	0.39
SAB	09:45	16.6	7.65	10.0	7.84	2.40	231	31	114	21	1.2	0.72
(Replim3)	12:35	17.2	7.53	12.2	9.84	2.70	285	39	85	42	0.9	0.66
	15:35	18.7	7.47	10.9	8.09	1.67	263	92	86	18	0.9	0.75
GEN	07:50	12.6	6.74	7.15	15.3	7.77	192	43	36	38	1.4	0.26
(Replim4)	12:50	12.8	6.75	6.62	17.6	10.4	137	45	25	35	1.1	0.34
	17:45	12.8	6.71	13.9	24.9	7.88	242	485	50	34	1.4	0.19
SAB	09:30	10.4	7.71	11.0	10.7	1.80	197	125	61	17	0.9	0.61
(Replim4)	14:05	10.7	7.64	6.30	10.4	1.24	171	22	64	13	0.8	0.61
	16:10	10.8	7.67	8.65	10.9	1.26	208	36	64	36	0.8	0.56

6.3.4. Filtered vs unfiltered trace element concentrations

As mentioned in **3.Sampling and analytical strategy**, the HR-ICPMS was only used to analyse unfiltered samples. Consequently, the results obtained after the analysis of the samples by ICP-MS were used to evaluate the tendency of metals to get adsorbed onto suspended particles by comparison of the concentrations found in filtered ($< 0.22 \mu\text{m}$ for Se and Hg; $< 0.45 \mu\text{m}$ for others) and unfiltered samples. For most of the ultra-trace elements, the results obtained after the ICP-MS analysis are close or below the LOD. **Figure 6.3**, consequently, does not display results for Ni, Cd, Pb, Tl and Co. In addition, the amount of data is smaller for many trace elements.

Dissolved Fraction (DF) is defined as the ratio between the concentrations of the element considered in the sample after ($[X]_{\text{Filtered}}$) and before ($[X]_{\text{Unfiltered}}$) filtration:

Equation 6.1

$$DF = \frac{[X]_{\text{Filtered}}}{[X]_{\text{Unfiltered}}}$$

The **Figure 6.3** displays the DF in subsurface water samples calculated for each major, trace and ultra-trace element considered using the results obtained by ICP-MS (only unfiltered samples were analysed by HR-ICP-MS).

The solubility of an element in wet deposition (precipitation and snow) may be related to the origin and the mechanism of aerosol formation, both of which affect the size and the chemical properties of the particles. Thus resuspension of terrigenous substrates produces coarse particles with a high content of insoluble species, whereas soluble species are often gaseous species in origin that have been adsorbed onto particles [47].

Most of the elements exhibit Dissolved Fraction close to one, so mainly present in dissolved form, with median Dissolved Fraction of 0.99, 1.03, 0.98, 1.02, 0.98, 0.95, 0.95, 0.90, 1.01, 0.92, 0.90, 0.80 and 0.97 respectively for Ca, Na, Mg, K, Sr, Ba, As, Cu, Mo, V, Cr, Se and Sb. Only Al (median DF = 0.56), Fe (median DF = 0.41), Mn (median DF = 0.58), Ti (median DF = 0.59) and Hg (median DF = 0.72) show DF well below one. Consequently, it can be concluded that an important fraction of these elements can be found associated with particles (organic matter and/or suspended inorganic solids). Variability of the DF is particularly high for these elements supporting the hypothesis of important reactivity: regular precipitation and dissolution reactions that can occur either during atmospheric transport or in the water column itself. The analysis of the snowpack of the Maladeta valley (Central Pyrenees) made by Bacardit et Camarero (2010) [47] highlighted the association of Al, Ti and Fe to particles by comparison of the dissolved and particulate fractions. In waters from Lakes Légunabens, Plan and Vidal d'Amunt, Pb was bound mostly to particles while As and Zn were detected mostly as dissolved forms [35].

The case of Cu differs well as we observed important variability regarding the sampling point and the daytime of sampling but according to the results of the ICP-MS analysis of 22 samples, the DF for Cu is close to one (median DF = 0.90). It confirms the hypothesis that the variations observed previously for Cu (intra-lake variability and daily variation) can be due to either contamination or differences in the deposition process rather than to an important reactivity regarding this element.

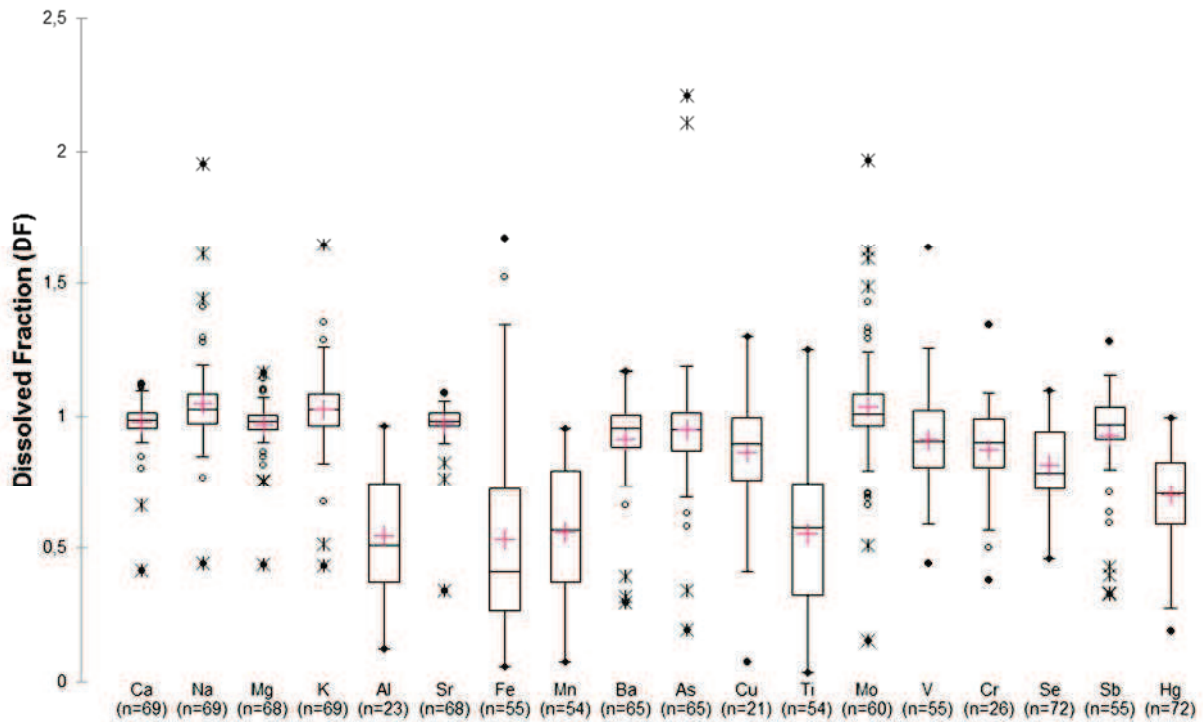


Figure 6.3: Dissolved Fraction (DF) in subsurface water samples calculated for each major, trace and ultra-trace element considered using the results obtained by ICP-MS. Dots are minimum and maximum, white circles and black crosses are extreme values, bars indicate 10th and 90th percentile, boxes indicate 25th and 75th, marks within each box are medians and red crosses are mean. For each element, the number n of samples above the LOD for both filtered and unfiltered samples are indicated.

6.4. Lake classification

6.4.1. Trophic status and water quality

The Trophic State Index (TSI) was first proposed in 1977 by Carlson [48] and is defined as the total weight of biomass in a given water body at the time of measurement. This index, from 0 to 100, can be calculated using several parameters such as total phosphorus (TP), total nitrogen (TN), chlorophyll and Secchi disk transparency (SD). Each major division (10, 20, 30 etc.) represents a doubling in algal biomass. In our study, TP, TN and SD were not evaluated and chlorophyll-a was only measured at subsurface in all the lakes, with values below the limit of detection. Thus, it was not possible to calculate the chlorophyll-a concentration over all the water body. The only parameters that could probably estimate the trophic status of 20 studied lakes are Nitrate (NO_3^-), TOC and to a lesser extent Silicate. Indeed, the presence of phytoplankton communities is highly dependent on the quality and ratio of macro- and micronutrients (nitrogen N and phosphorous P) [11]. Diatoms are a major group of microalgae found in all aquatic systems, and represent a major component at the base of the marine food web, responsible for up to 50 % of total lake and oceanic primary production and 25 % of all oxygen produced on the planet [49]. Thus, these microorganisms intake NO_3^- (and to a lesser extent Silicate for diatoms) to develop themselves, subsequently increasing the TOC values in the lakes, especially during the spring-summer time.

Therefore, in order to evaluate the trophic status and classify the 19 studied lakes (PAR excluded), the TSI was calculated using TOC values according to Dunalska (2011) [50] and using the following formula:

Equation 6.2

$$\text{TSI (TOC)} = 20.59 + 15.71 \ln\text{TOC}$$

The TSI estimated for the lakes under study over the four sampling campaigns vary from 13 to 45 with a median value of 24 (**Figure 6.4**). A TSI below 30 to 40 is typical from oligotrophic lakes, where waterbodies have the lowest level of biological productivity, while TSI from 40 to 50 is characteristic of a mesotrophic lake with a moderate level of biological productivity. Lake ORD presents the highest TSI in the three sampling campaigns this lake was sampled and it is the only one showing TSI above 40 (TSI = 45 in Replim4). Apart from this lake, all the samples analysed showed a TSI value typical from oligotrophic lakes. In the Central Pyrenees, the trophic status of high altitude lakes range between ultraoligotrophic to mesotrophic [10,11,51]. Pasture is the most important source of eutrophication, but is restricted to small and very shallow lakes. Therefore, our data about TOC and TSI are in accordance with previous studies that use TP to define the trophic status of high altitude lakes in the Pyrenees.

There are strong variations of TSI between sampling campaigns, and a significant increase (Kruskal-Wallis test, p-value < 0.05) occurs during the algal summer bloom. Indeed, an increase in TSI of 7 ± 3 between Replim1 and Replim2 for the ten lakes sampled in these two sampling campaigns (ARA, BAD, CAM, PEY, OPA, AZU, ARN, BAC, COA and PAN), and of 8 ± 3 between Replim3 and Replim4 (ARA,

BAD, CAM, PEY, OPA, GEN, ROU, BER, BAC, PEC, COA, PAN, ORD and SAB) were observed. This increase in the TSI is probably due to the more important primary productivity during summer: decreasing NO_3^- associated to increasing TOC (significant negative correlation between NO_3^- and TOC; $r = 0.59$; $p\text{-value} < 0.05$; **Figure 6.5**).

NO_3^- appears to be a limiting nutrient in the primary production as it was below the limit of detection in autumn samples for lakes PEY (both Replim2 and Replim4), GEN, BER and ROU (Replim4). Diminution of NO_3^- during summer was the most important in Lakes ARA, BAD and COA. Lakes GEN, BER and ROU are impacted by agropastoralism, probably leading gradually to their eutrophication. COA such as ORD is a shallow lake. ARA and BAD are also impacted by agropastoralism but to a lesser extent than the three lakes from the Ayous location (GEN, ROU and BER).

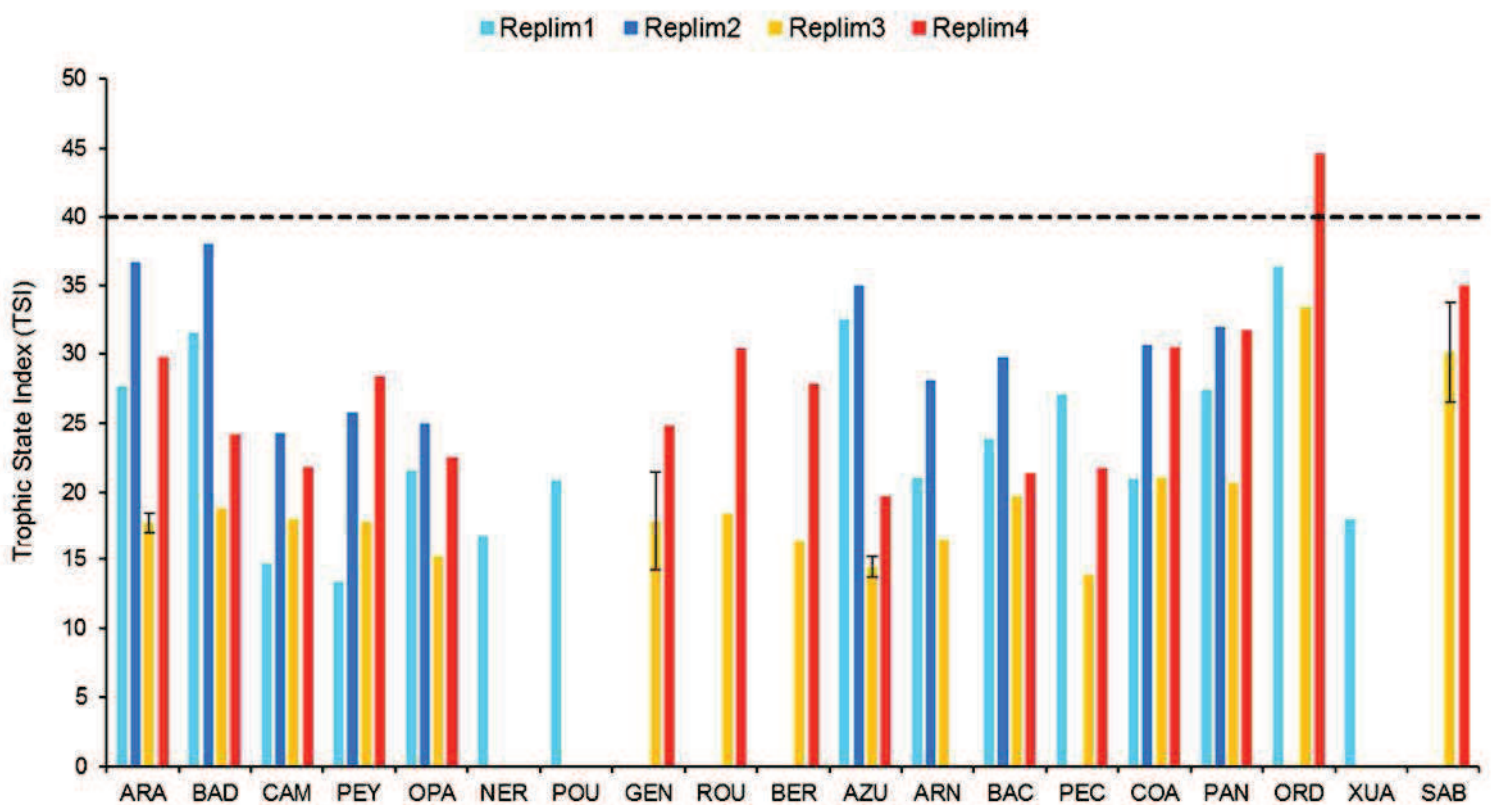


Figure 6.4: Trophic State Index (TSI) calculated for all the sampled lakes according to the sampling campaign. TSI below the dashed line (TSI = 40) indicate oligotrophic lakes. Error bars for Lakes ARA, GEN, AZU and SAB are associated to the samples from different times of the day

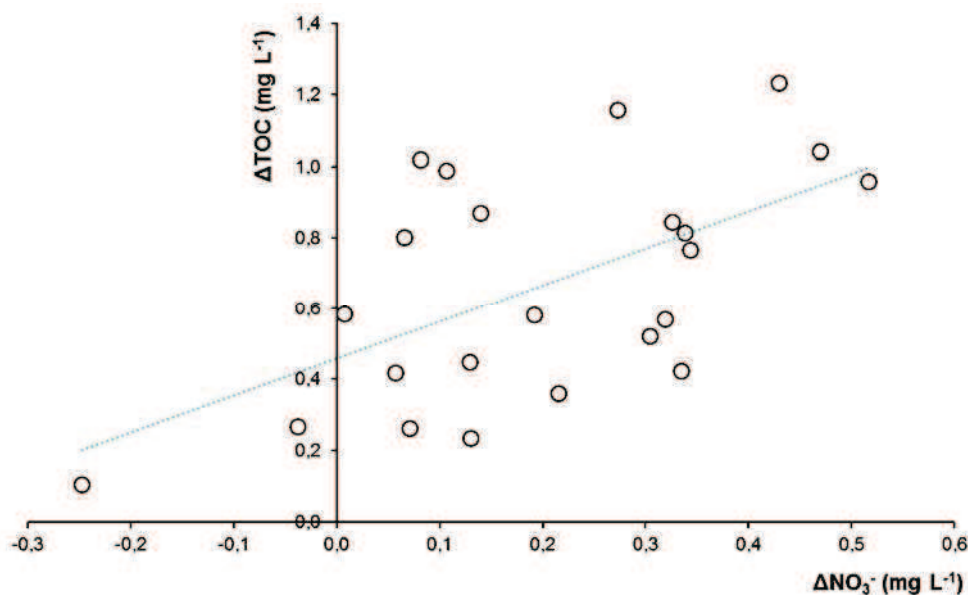


Figure 6.5: Relation between TOC and NO_3^- with ΔTOC corresponding to the increase of TOC between spring value and autumn values, and ΔNO_3^- corresponding to the decrease of NO_3^- between spring value and autumn values

6.4.2. Classification of the lakes according to the water geochemistry

Water chemistry varies widely within and among the studied lakes. Principal Component Analysis (PCA) was carried out to investigate the main sources of variation in data. PCA is an ordination method that allows analysis and a visualisation of a dataset described by various quantitative variables. This statistical method uses an orthogonal transformation to convert a set of observations of possibly correlated variables into a set of values of linearly uncorrelated variables called principal components. The variables in the first principal component (PC1) explain most of the total variance of the system under study, and their loadings help identifying what contributes most to the differences among the individual sites. Similarly, the projection of the sites on the first principal components (scores) helps identifying groups of samples with similar characteristics. As a resume, PCA reduces the dimensions of a multivariate data to two or three principal components, that allows us visualizing the main sources of variance in the data matrix by means of the scores and loadings plots.

PCA of the data matrix made up of the main physicochemical parameters analysed in unfiltered subsurface water samples (Altitude, Ca, Na, Mg, K, Al, Sr, Fe, Mn, Ba, Cl⁻, NO_3^- , SO_4^{2-} , TOC, DIC, Silicate and Alkalinity) as variables and the water samples collected at the different studied lakes during the four sampling campaigns as objects was carried out in order to i) identify the major sources of variability, and ii) to look for groups of lakes with similar characteristics. Lake PAR was not considered because it differs too much from all the other studied lakes and would behave as a statistical outlier.

The data set were previously centred and scaled to rend normalized variables (mean value = 0; standard deviation = 1).

The main results of the PCA analysis are displayed in **Table 6.3**, **Figure 6.6**, **Table 6.4** and **Figure 6.7**. Three principal components were extracted explaining approximately 66 % of the total variance. PC1 explained 36 % of variance, and was positively correlated with Ca (loading = 0.97), Mg (0.80), Sr (0.96), DIC (0.98) and TA (0.97). This PC indicates mainly the weathering of rocks supplying alkalinity. PC2 explained 18 % of variance, and was positively correlated with Na (0.84) and Cl⁻ (0.83), and negatively with Elevation (-0.83). The important weight of both Na and Cl⁻ on this PC suggests a strong influence of atmospheric depositions through sea-salt inputs. Finally, PC3 explained 13 % of the variance and is positively correlated with Silicate (0.76) and NO₃⁻ (0.59). It might indicate a mixture of lithogenic inputs (weathering of siliceous rocks) and primary productivity (consumption of Si and NO₃⁻).

Using the scores of the observations on each of the three PCs (**Table 6.4** and **Figure 6.7**), a classification of the lakes according to the chemical characteristics of their unfiltered subsurface waters can be proposed. Depending on these scores together with data previously published by *Camarero et al.* [10], different classes have been created for each PC. The cut off for each class have also been chosen to minimize the overlapping of the data for the main variables of a PC.

Table 6.3: Loadings of the variables on PC1, PC2 and PC3 after Principal Component Analysis of the dataset. Bold value are significant at 95 % confidence interval

Principal Component (% of total variance)	PC1 36	PC2 18	PC3 13
Elevation	-0.32	-0.83	-0.02
Ca	0.97	-0.08	0.11
Na	-0.21	0.84	0.37
Mg	0.80	0.07	-0.49
K	0.20	0.17	0.20
Al	-0.47	-0.19	-0.51
Sr	0.96	-0.03	-0.08
Fe	-0.28	0.13	-0.38
Mn	-0.04	0.62	0.01
Ba	0.66	0.12	-0.29
Cl ⁻	-0.01	0.83	0.28
NO ₃ ⁻	0.13	-0.53	0.59
SO ₄ ²⁻	0.64	-0.35	0.45
TOC	0.49	0.28	-0.09
DIC	0.98	0.00	-0.14
Silicate	0.26	-0.12	0.76
Total Alkalinity	0.97	0.00	-0.15

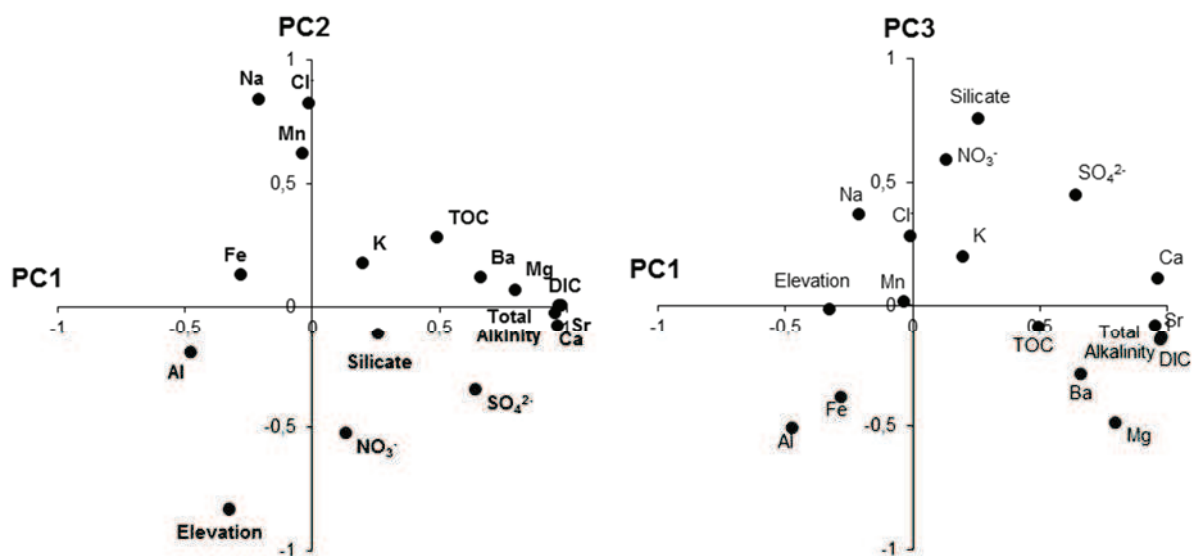


Figure 6.6: Loading plots on the PC1-PC2 and PC1-PC3 planes obtained after Principal Component Analysis of the dataset

Table 6.4: Scores of the observations on PC1, PC2 and PC3 after Principal Component Analysis of the dataset, together with the proposed classification of these lakes: for PC1, Class 1 (Score < 0) / Class 2 (0 < Score < 3) and Class 3 (Score > 3); for PC2, Class 1 (Score < 0) / Class 2 (Score > 0); for PC3, Class 1 (Score < 0.5) / Class 2 (Score > 0.5)

Lake	PC1 Score	PC1 Class	PC2 Score	PC2 Class	PC3 Score	PC3 Class
ARA	0.8 ± 0.5	Class 2	-0.8 ± 0.4	Class 1	1.4 ± 0.6	Class 2
BAD	1.8 ± 0.6	Class 2	-1.5 ± 1.0	Class 1	1.7 ± 0.7	Class 2
CAM	-2.1 ± 0.2	Class 1	-0.6 ± 0.7	Class 1	-0.2 ± 0.2	Class 1
PEY	-3.4 ± 0.7	Class 1	-1.4 ± 0.6	Class 1	-3.1 ± 1.9	Class 1

The PC1, explaining most of the variance, relates to the influence of the weathering of rocks supplying alkalinity, mainly dependent on the composition of the geological basin of the lakes. Indeed, dissolution of calcium carbonate CaCO_3 , and to a lesser extent magnesium carbonate MgCO_3 , contributes significantly to the alkalinity of lake water as indicated by the strong and significant correlation between Ca and TA ($r = 0.93$; $p\text{-value} < 0.05$). From this PC, three different classes have been extracted (**Table 6.4**): low weathering (Class 1) ($n=14$), medium weathering (Class 2) ($n=4$) and high weathering (Class 3) ($n=1$). The highest values of Ca (median = $21358 \mu\text{g L}^{-1}$) and TA (median = $1810 \mu\text{mol kg}^{-1}$) were found in SAB whose basin lies on Devonian (limestone, sandstone, shale) and Cretaceous (limestone, sandstone) sedimentary rocks, rich in limestone (mainly CaCO_3) and dolomite (mainly $\text{CaMg}(\text{CO}_3)_2$). It is worth noting that during Cretaceous, more chalk (CaCO_3 deposited by the shells of marine invertebrates) was formed than in any other period in the Phanerozoic, including Devonian and Permian-Triassic (conglomerate, sandstone, lutite, andesite, shale). These carbonate rocks are very soluble and sensitive to weathering, explaining the high values for Ca and TA. The contribution of Mg (concentrations up to 100 times higher in SAB), through dolomite dissolution, to the TA is also much more important than in any other lake [52]. The second class, medium weathering, includes the four lakes whose basin lies exclusively on Devonian sedimentary rocks (ARA, BAD, AZU and ORD; $13559 \mu\text{g L}^{-1}$ and $733 \mu\text{mol kg}^{-1}$ median values of Ca and TA). Finally, the last fourteen lakes make up the third class ($5427 \mu\text{g L}^{-1}$ and $302 \mu\text{mol kg}^{-1}$ median values of Ca and TA), low weathering, with the lowest values of Ca and TA observed for the lakes lying on non-erodible granites. Overall, this PC1 expresses well a weathering rate gradient related to soil and bedrock mineralogy from non-erodible granite to high soluble sedimentary rocks (**Figure 6.8**).

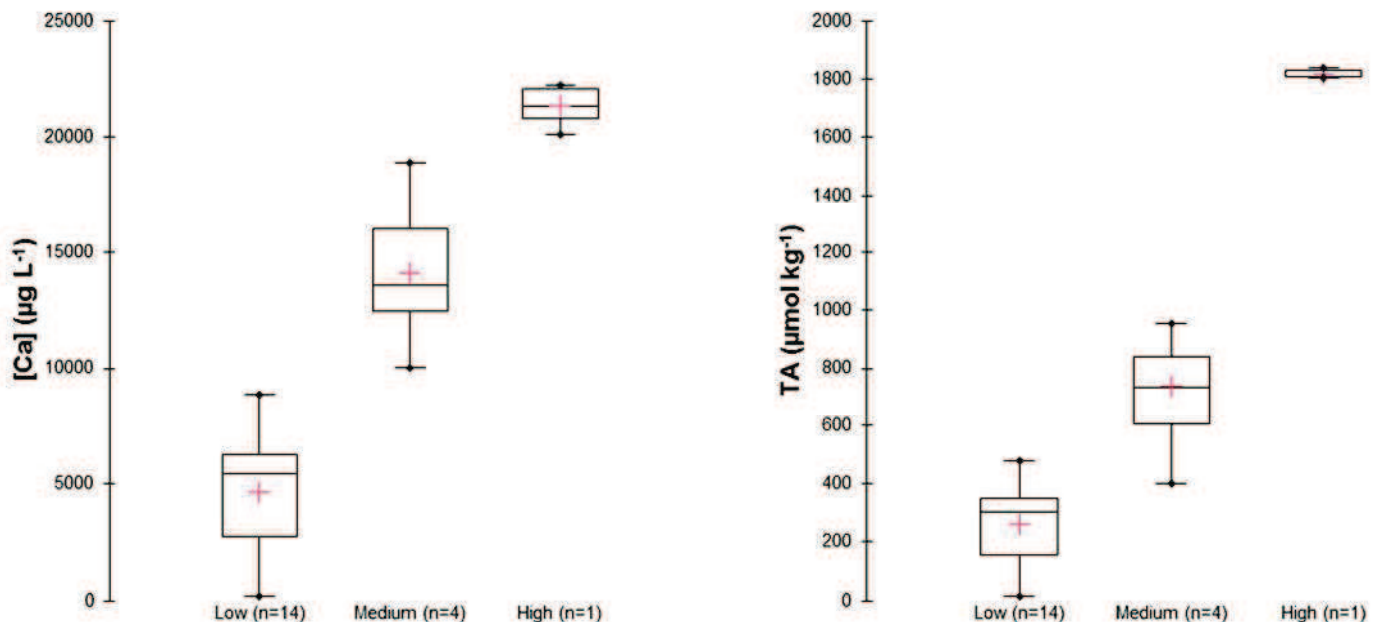


Figure 6.8: Ca concentrations and TA values according to the classification extracted from the PC1, importance of the weathering supplying alkalinity: Low (Lakes CAM, PEY, OPA, NER, POU, GEN, ROU, BER, ARN, BAC, PEC, COA, PAN and XUA), Medium (Lakes ARA, BAD, AZU and ORD) and High (Lake SAB)

The PC2 is also related to typical parameters of lake water geochemistry and highlights the marine influence with atmospheric deposition of airborne sea-salt. Concentrations of Na and Cl⁻, the two chemical variables with the highest loadings on PC2, allow classifying the lakes in two classes: very weak (Class 1) (n=14) and weak (Class 2) (n=5) marine influence (**Table 6.4** and **Figure 6.9**). Na and Cl⁻ have also an opposite relation with elevation as shown on **Figure 6.10**: decreasing concentrations as elevation increases ($r = 0.67$ for Na and $r = 0.66$ for Cl⁻ without SAB; p-values < 0.05). Due to orographic effect, heavy rain usually deposits at the mountain foothills, not at the summits: lakes located at higher altitude may be less influenced by sea-salt depositions. In addition to this process influencing directly the wet and dry depositions, at very high altitude, vegetation is scarce and influence of the leaching from the catchment on the lake water might be less important than at lower altitude so dry depositions of sea-salt are expected to be lower. One lake, SAB, does not follow the same trend as it is in the very weak marine influence class. This is probably due to the location of this lake, the southernmost lake.

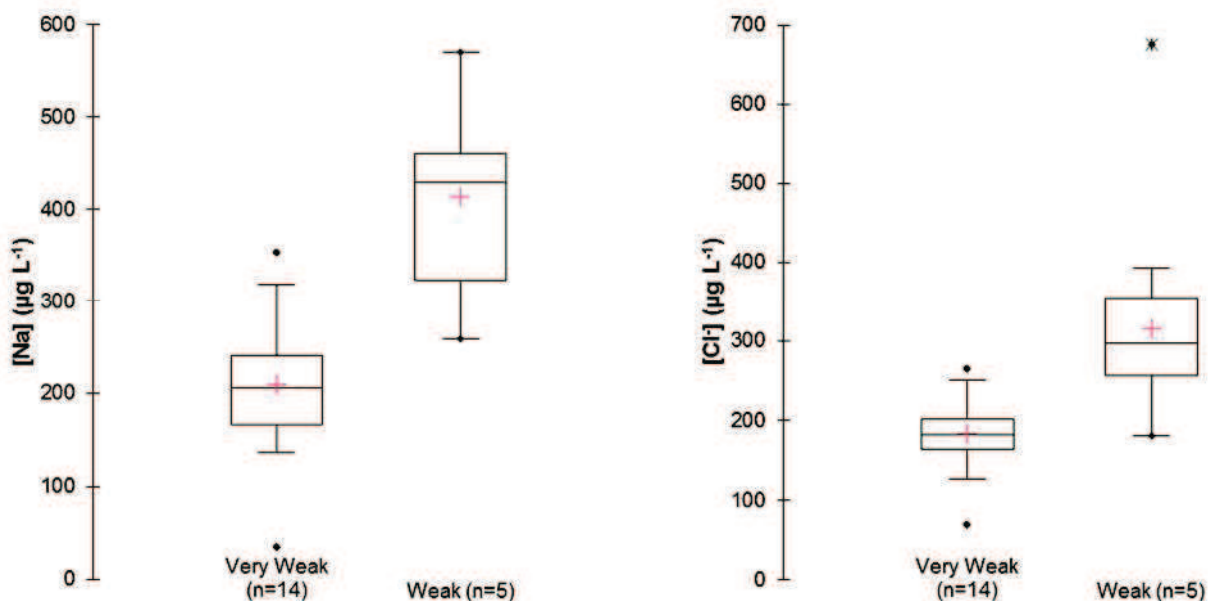


Figure 6.9: Na and Cl⁻ concentrations according to the classification extracted from the PC2, importance of the marine influence: Very weak (Lakes ARA, BAD, CAM, PEY, OPA, NER, POU, AZU, ARN, BAC, PEC, COA, XUA and SAB) and Weak (Lakes GEN, ROU, BER, PAN and ORD)

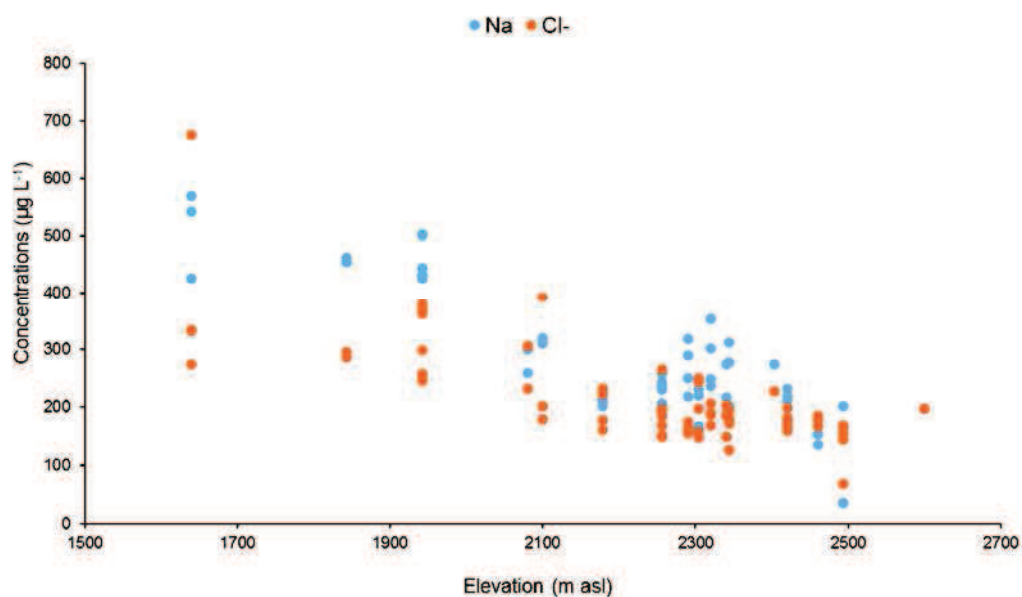


Figure 6.10: Negative correlation between elevation and i) Na and ii) Cl⁻ concentrations (SAB not considered)

Finally, the PC3 is mainly characterized by positive loadings of Silicate and NO₃⁻ and might be related to a mixture of lithogenic inputs and primary productivity. Silicate may reach lake waters through weathering of siliceous rocks, but also from atmospheric mineral depositions. Moreover, Silicate (Si) is an essential macronutrient, especially in the development of diatoms microorganisms that consume both Silicate and NO₃⁻. Silicate is also important for the carbon cycle (calculation of alkalinity) [39]. Only two classes are defined with this PC: low (Class 1) (n=13) and high (Class2) (n=6).

Among the main parameters, SO₄²⁻ is of particular interest. Indeed, sulphate occurs as the principal anion in lake waters. It provides sulphur S to the lake water, an essential plant nutrient just as nitrate or phosphate. The PC1 and PC3, related to the weathering processes, explains most of the variability of SO₄²⁻ (respectively 0.64 and 0.45): weathering of soil mineral, through mineral-bearing S and Mg²⁺, might be the main sources of S in high altitude lakes. Nevertheless, even if the contribution is less important, especially with reducing emissions of S, it is important to make the difference between the geological and atmospheric supply of sulphur. *Camarero et al.* [10] proposed a threshold of SO₄²⁻ concentrations: below 50 µeq L⁻¹ (2.40 mg L⁻¹) in lake water, atmospheric deposition of S is the main controlling factor, whereas above this threshold geological supply of S is dominant. Nevertheless, this study uses data obtained in a sampling campaign carried out in 2000, and S emissions have declined by about 80 % in Spain and in France between 2000 and 2016 (<http://www.emep.int/Emerge>). Therefore, considering this recent and significant decrease in the S emissions, we proposed here lowering this threshold to 15 µeq L⁻¹ (0.72 mg L⁻¹). **Figure 6.11** displays the concentrations of SO₄²⁻ against the concentrations of Mg²⁺, and allows classifying lakes as a function of S deposition processes. With this new limit, half of the lakes display SO₄²⁻ values below the established limit, in relation to their

geological background. On the one hand, CAM, PEY, OPA, NER, POU, COA and XUA are mainly lying on non-soluble granites, explaining well the atmospheric inputs. On the other hand, GEN, ROU and BER, lying on Cretaceous sedimentary rocks, expressed higher Mg^{2+} concentrations but low SO_4^{2-} . It might be rather due to production of sulphide under more anoxic conditions and its precipitation in those two lakes.

The other lakes, lying on well soluble sedimentary rocks, have shown a strong relation between SO_4^{2-} and Mg^{2+} (**Figure 6.11**) highlighting their geological supply of S ($r = 0.98$ for AZU and ARN; $r^2 = 0.77$ for ARA, BAD, BAC, PEC, PAN and ORD; p -value < 0.05 ; Mg^{2+} 100 fold higher in SAB because of dolomites and high SO_4^{2-} content).

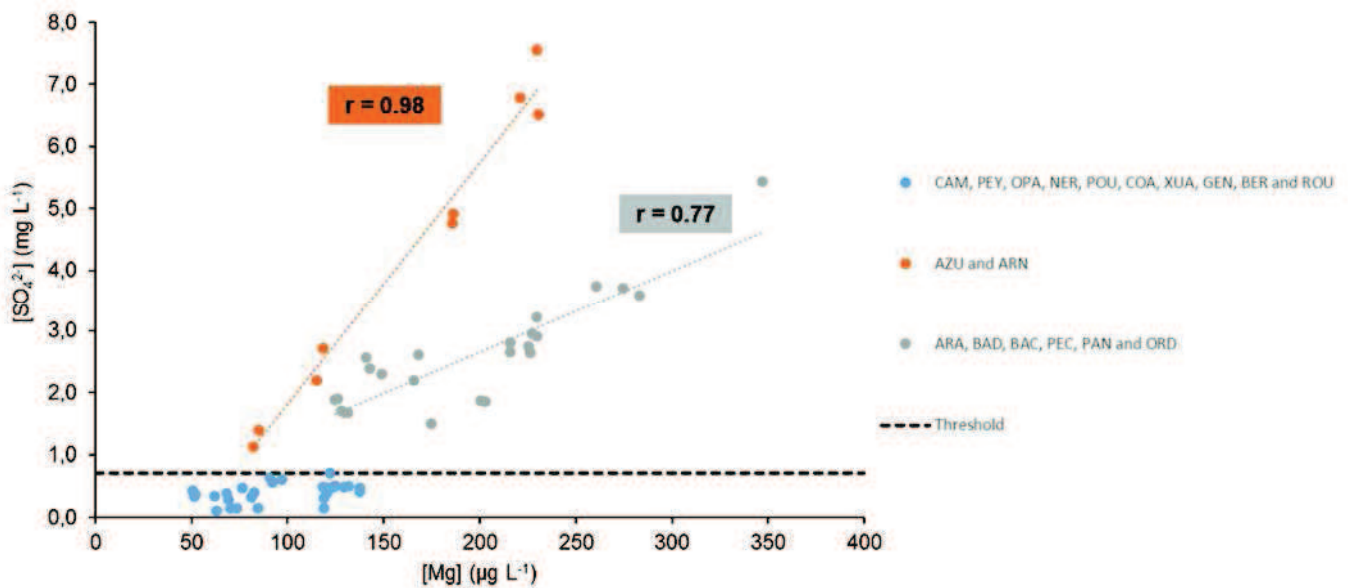


Figure 6.11: Concentrations of SO_4^{2-} as a function of Mg concentrations. Black dashed line is the threshold set up at 0.7 mg L^{-1} to distinguish between atmospheric and geological supply of SO_4^{2-} : below this limit SO_4^{2-} is mainly originated from atmospheric depositions. Significant correlations between SO_4^{2-} from geological supply and Mg have been found ($r = 0.98$ for Lakes AZU and ARN; $r = 0.77$ for Lakes ARA, BAD, BAC, PEC, PAN and ORD)

6.4.3. Characteristic concentrations and major sources of Potential Harmful Trace Elements (PHTEs)

Discussion about the main parameters in the paragraphs above brings insights about the typology of the studied high-altitude lakes. The main outcome from this statistical analysis was the predominant importance of the geological background on the water chemistry of these lakes with the evidence for a gradient from non-soluble granite, where atmospheric inputs are more relevant than weathering inputs, to easily erodible sedimentary rocks. Therefore, to a better understanding and interpretation of PHTEs distribution among these lakes, it is necessary to split the lakes in three main categories depending on the influence of weathering of rocks supplying alkalinity (cf PC1):

- Category 1 with low weathering and more acidic lakes: 14 lakes (ARN, BAC, BER, CAM, COA, GEN, NER, OPA, PAN, PEC, PEY, POU, ROU and XUA)
- Category 2 with medium weathering: 4 lakes (ARA, BAD, ORD and AZU)
- Category 3 with high weathering and more alkaline lake: 1 lake (SAB)

Note that PAR has been removed from this discussion because, as mentioned previously, it is an outlier in many ways.

In order to investigate the occurrence and origin of PHTEs in the studied lakes, three complementary different tools were used: i) estimation of the characteristic concentrations (minimum, maximum, median and threshold) of each lake category, ii) calculation of enrichment factors (EF), and iii) Multiple Linear Regression (MLR) of data. The results obtained will be discussed all together in this section

Table 6.5 presents a summary of the results (minimum, maximum, median and threshold) obtained for PHTEs in unfiltered subsurface water samples. Three different groups of lakes have been defined according to the classification proposed in **6.4.2 Classification of the lakes according to the water geochemistry**. Bibliographic data extracted from remote and/or alpine lakes is also presented in **Table 6.5** for comparison purposes.

The threshold values have been calculated according to the guidelines from the Idaho Geological Survey [53] for non-normal distributed data, which do not meet the steady state condition and for which possible seasonal effects were not corrected:

Equation 6.3

$$\text{Threshold} = \text{Median} + 1.65 \times (\text{interquartile range})$$

Figure 6.12 displays the Crustal Enrichment Factors (EF_{UCC}) calculated for each PHTEs of interest in the unfiltered subsurface water samples. EF_{UCC} is defined as the concentration ratio of a given element to that of one element which originates mainly from rock and soil dust (usually Al or Ti),

normalized to the same reference concentration ratio characteristic of the upper continental crust (UCC) given by *Wedepohl* (1995) [54].

Equation 6.4

$$EF_{UCC} = \frac{\frac{[X]_{Sample}}{[Al\ or\ Ti]_{Sample}}}{\frac{[X]_{UCC}}{[Al\ or\ Ti]_{UCC}}}$$

where X is the element of interest. Crustal enrichment factors (EF_{UCC}) have been already used in previous studies to estimate the relative contribution of elements from natural versus anthropogenic sources, either in sediments [12] or atmospheric depositions [47] in the Pyrenees.

Enrichment factors below 10 times the mean crustal composition are unlikely to indicate contributions other than crustal sources while values between 10 and 100 suggest moderate enrichment and values above 100 a high enrichment. Enrichment factors interpretation has to be done carefully, especially because of the variable composition of the Earth's crust. Therefore, we also calculated the EF_{MDT} in a similar way than the EF_{UCC} , but using the Maladeta bedrock (Central Pyrenees) [55] as a reference.

The non parametric test Kruskal-Wallis was used to check if there was significant differences between EF according to the geological category.

Multiple Linear Regression (MLR) of data was carried out (XLSTAT software) in an attempt to explain the variations in PHTEs concentrations within lakes (dependent variables) using a combination of explanatory factors (independent variables).

The independent variables considered in the calculation were either physical parameters (elevation, catchment size to lake size ratio, maximum depth of the lake, temperature) or chemical parameters (pH, Ca, Na, Mg, K, Al, Sr, Fe, Mn, Ba, Cl⁻, SO₄²⁻, NO₃⁻, DOC, Si, TA). The significance of each parameter was evaluated using the stepwise procedure. With this procedure, the selection process starts by adding the variable with the largest contribution to the model (the criterion used is Student's t statistic). If a second variable is such that the probability associated with its t statistic (the ratio between the corresponding standard deviation of the parameter and the parameter itself) is less than the "probability for entry", it is added to the model. The same for a third variable. After the third variable is added, the impact of removing each variable present in the model after it has been added is evaluated (still using the t statistic). If the probability is greater than the "Probability of removal", the variable is removed. The procedure continues until no more variables can be added or removed.

In order to increase the power of this multivariate regression technique, Cat2 and Cat3 have been grouped together as the five lakes with more important weathering.

A summary of the results is shown in **Table 6.6**.

In the next paragraphs, an element-by-element discussion of the results shown in **Table 6.5** (characteristic concentrations), **Figure 6.12** (EFs) and **Table 6.6**. (MLR) follows to i) compare the occurrence of PHTEs in the studied lakes with that in other similar environments, ii) characterize the different groups of lakes concerning the PHTEs in their unfiltered sub-surface waters, iii) investigate the magnitude of anthropogenic sources of PHTEs to the lakes, and iv) identify the physico-chemical variables more directly implicated in the variability of the data.

Arsenic has shown a wide range of concentrations with significant differences within and among each category of lakes: from 31 to 8910 ng L⁻¹ in more acidic lakes (Cat1), from 445 to 6462 ng L⁻¹ in medium alkaline lakes (Cat2) and from 124 to 172 ng L⁻¹ in the alkaline lake SAB (Cat3). The thresholds set up for Cat1 and Cat2, respectively 2949 and 4525 ng L⁻¹, are higher than most of the median As concentrations measured in water of many lakes worldwide, either from remote locations or not [29,40,41,43,56–58]. This may present a risk to arsenic sensitive biota to the concerned lakes and these strong variations in the As content may be related to local geological sources. Such strong variations in As concentrations have been already documented in the catchment of Lake Respomuso (Central Pyrenees, 2130 m asl) [36] and in the three lakes studied by Bacardit and Camarero [35] in a close area. Arsenic presents an important enrichment (>100) in more than 90% of the samples, and it was significantly higher in medium and high alkaline lakes (Kruskall-Wallis test, p-value < 0.05). The EF were lower when using the MDT reference rather than the UCC, supporting the hypothesis of local sources of As. The best MLR models obtained for medium and high alkaline lakes (Categories 2&3) highlight the significant influence of Sulphate on the As distribution. This is well supported by the strong positive correlation (r = 0.69) between As and Sulphate in these lakes. Dissolution of sulphide and sulpharsenide minerals, notably arsenopyrite FeAsS, in the easily erodible bedrock lakes might be responsible of the presence of As in those lakes. Moreover, desorption of As from soils and/or at the sediment-water interface might be enhanced by the presence of sulphate as mentioned in a recent study [59].

U concentrations were found to be higher in the less alkaline lakes (Category1) with a threshold set up at 1395 ng L⁻¹ while it was at 425 and 191 ng L⁻¹ respectively in medium (Category2) and high alkaline lakes (Category3). None publications related to high altitude lakes document the concentrations of U in such environment but lower concentrations, a few ng L⁻¹, were found in remote lakes such as in Antarctica [56] or in Lake Kawagama (Canada) [57]. When looking at the EF, no differences (Kruskall-Wallis test, p-value = 0.75) were found between lake categories, and most of the samples were highly enriched (>100), suggesting a common source of U in all the lakes. This assumption is well supported by the results of the MLR. Indeed, in the non-easily erodible lakes of Category1, the main significant variable explaining the distribution of U is the concentration of potassium. Transport of U-bearing minerals (i.e. carnotite) by Iberian and north African dust might be responsible of most of the U in low alkaline lakes where lower pH can promote the dissolution of these minerals [60]. Another possibility would be local sources from bearing rocks but mining of U ores was very small in the Pyrenees.

Cu, which is known to be atmospherically transported and deposited through precipitations [3] over long distances, is present in the high altitude lakes independently of the geological background. Indeed, the distribution is not significantly different among categories with thresholds at 292 ng L⁻¹ in low alkaline lakes (Category1), 325 ng L⁻¹ in medium alkaline lakes (Category2), and 310 ng L⁻¹ in high alkaline lakes (Category3). Nevertheless, when looking at the EF, Cu was mainly moderately enriched (10 < EF < 100). There were also significantly higher EF in medium and high alkaline lakes (Kruskall-Wallis, p < 0.05) suggesting small local inputs from weathering of Cu-bearing minerals in those lakes. The MLR technique does not provide us with relevant information due to the small coefficient of multiple determination associated to the model (0.32 for Category1 and 0.41 for Categories2&3).

Mo concentrations were in the same range than in the remote lakes from Antarctica [56]: from 6 to 544 ng L⁻¹ (threshold = 192 ng L⁻¹) in less alkaline lakes (Category1), from 104 to 247 ng L⁻¹ (threshold = 249 ng L⁻¹) in medium alkaline lakes (Category2) and from 38 to 55 ng L⁻¹ in the high alkaline lake SAB (threshold = 46 ng L⁻¹). As mentioned previously, Mo mobility is hardly predictable because it depends on many parameters. EF indicated moderately enrichment (between 10 and 100) for most of the samples with significantly higher EF (Kruskall-Wallis, p-value < 0.05) observed for the medium to high alkaline lakes suggesting that weathering processes are influencing the concentrations of Mo. The results from the MLR suggest a strong influence of sulphate on the distribution of Mo, especially for low alkaline lakes with a positive correlation between Mo and sulphate (r = 0.60) where sulphate is mainly atmospherically originated.

V concentrations were extremely low in comparison with data from other remote lakes. Indeed, concentrations range from 30 to 174 ng L⁻¹ in low alkaline lakes (Category1), from 42 to 186 ng L⁻¹ in medium alkaline lakes (Category2) and from 23 to 35 ng L⁻¹ in the high alkaline lake SAB (Category 3), while the minimum value documented for V in the Alps was 300 ng L⁻¹ [29]. Usually of anthropogenic origin (combustion of coal/oil and road traffic), V is a good indicator for the remoteness of a studied area. This element shows also extremely low EF values, independently from the geological substrate of the lake (Kruskall-Wallis, p-values = 0.20). Nevertheless, the best MLR models obtained for V highlight strong differences according to the geological background. Indeed, while Na, probably from geological origin, is triggering the distribution of V in erodible lakes (Categories 2&3), V is associated to SO₄²⁻ in non-erodible lakes (Category1) where sulphate is mainly atmospherically deposited. Therefore, these types of lakes could eventually be used to follow the atmospheric deposition of V.

Ni is showing a comparable behaviour to that of Cu with no clear dependence of concentrations on the geological substrate, therefore suggesting atmospheric depositions as the main source of Ni. Indeed, the thresholds calculated for the low alkaline lakes (148 ng L⁻¹), for the medium alkaline lakes (120 ng L⁻¹), and for the lake SAB (110 ng L⁻¹) were comparable. Concentrations are also globally lower than all the bibliographic data for remote lakes. According to the EF, Ni was non enriched to moderately enriched in the studied lakes with higher EF in medium to high alkaline lakes (Kruskall-Wallis, p-value < 0.05). The MLR technique was not able to explain the distribution of Ni

neither for low alkaline (Category1) or medium to high alkaline lakes (Categories2&3), with coefficient of multiple determination of, respectively, 0.20 and 0.36.

Cr is present at very low concentrations in the studied lakes ranging from 23 to 129 ng L⁻¹ in low alkaline lakes, from 59 to 279 ng L⁻¹ in medium alkaline lakes and from 29 to 47 ng L⁻¹ in Lake SAB. For the low alkaline lakes, the range is comparable with the measurement made in the Alps [29] while the more erodible lakes are showing higher concentrations. EF are showing non enrichment for the whole samples when using the Maladeta reference while Cr is moderately enriched in medium alkaline lakes using the UCC reference, then suggesting some local and geological sources.

Pb concentrations were in the range of the studies already made in the Pyrenees by Zaharescu et al (2009) [36] and Bacardit and Camarero (2010) [35] and highest concentrations were found in the low alkaline lakes suggesting an influence of pH on the distribution of Pb. When taking Maladeta as a reference, Pb was always lower than 10 suggesting non enrichment. Using the UCC reference, EF were significantly higher suggesting possible local geological sources of Pb. Nevertheless, for low alkaline lakes, this potential source of Pb does not influence its distribution as well demonstrated by the best MLR models. Indeed, Ti is the main significant parameter influencing the concentrations of Pb in those low alkaline lakes suggesting a common source, probably Iberian and North Africa dust. This is also well supported by the positive correlation between Ti and Pb for low alkaline lakes ($r = 0.79$).

Se concentrations were extremely low in comparison with other studies in remote lakes, with thresholds of 40 ng L⁻¹ for low alkaline lakes (Category1), 81 ng L⁻¹ for medium alkaline lakes (Category2) and 23 ng L⁻¹ for Lake SAB. Se was constant and did not significantly change over sampling campaign, suggesting local geological sources. These sources might be significant as the EF calculated were the second highest (after As), and dependant on the geological substrate (Kruskall-Wallis, p -value < 0.05). The MLR analysis on the low alkaline lakes highlight well the importance of Sulphate, with positive correlation observed ($r = 0.72$) between sulphate and Se concentration. Se in lake waters behave the same as Sulphate as it replaces sulphur in sulphide minerals such as pyrite, chalcopyrite, pyrrhotite and sphalerite.

Sb is present at very low concentrations in the studied lakes, ranging from 5 to 85 ng L⁻¹ in low alkaline lakes (Category1), from 10 to 80 ng L⁻¹ in medium alkaline lakes (Category2) and from 33 to 36 ng L⁻¹ in Lake SAB. It displays moderate to intense EF values both in low or medium to high alkaline lakes. Sb in low alkaline lakes was the highest in lakes GEN and PEC where Ca was also the highest, explaining the results obtained for the MLR statistical method. In addition, Sb in medium to high alkaline lakes was the highest in Lake AZU.

The concentration of Co in the lakes investigated in this work was lower than the values reported by Zaharescu et al (2009) [36] for the catchment of Lake Respomuso. Calculated thresholds were 20, 28 and 14 ng L⁻¹ from low alkaline to high alkaline lakes. Co EF were among the lowest calculated ones, indicating no anthropogenic enrichment of Co. Only for low alkaline lakes, Fe is the main

variable explaining the distribution of Co, and both parameters are significantly correlated in these lakes ($r = 0.86$; $p\text{-value} < 0.05$). Therefore, once in the lake, Co probably behaves closely together with other oxide-hydroxide elements.

Cd is present at very low concentrations but the moderate values of EF obtained may suggest an anthropogenic origin. Nevertheless, the MLR model was not able to further explain the distribution and origin of Cd.

TI concentration was much lower than in some remote lakes from Antarctica [56], the only pristine lakes in which the TI concentration has been measured so far. This element shows a clear dependence with geology: highest concentrations in low alkaline lakes (0.2 to 2.5 ng L^{-1}) and lowest ones in medium (0.2 to 0.8 ng L^{-1}) and high alkaline lakes (0.3 to 0.3 ng L^{-1}). EF were very low, suggesting no anthropogenic inputs. The MLR models calculated for TI suggest a common source or behaviour for Al and TI in low alkaline lakes, and for Na and TI in high alkaline lakes.

Hg, supposed to reach the lake water mainly through wet and dry deposition, exhibits very low concentrated, similar level found in open seawater and independently of the geological substrate. This supports the hypothesis of atmospheric deposition as the main processes responsible of Hg in the high altitude lakes. EF is also from moderate to intense suggesting long-range transport of both natural and anthropogenic Hg to the lakes. Finally, in the MLR model, TOC is the main parameter influencing the Hg distribution supported the role of organic matter to control Hg level in the aqueous phase as already observed in previous studies [61,62]. The role of Hg and its cycle in lake environments is discussed in the next chapters of this manuscript: **6. And 7.**

Table 6.5: Characteristic concentrations for unfiltered subsurface water samples as minimum, median and maximum concentration as well as the calculated threshold for each PHTEs for our study together with data extracted from bibliography (remote and alpine lakes)

Reference	Location	Lakes	Elevation (masl)	Data	As	U	Cu	Mo	V	Ni	Cr	Pb	Se	Sb	Co	Cd	Tl	Hg
					ng L ⁻¹													
This Work	Central Pyrenees (France/Spain)	14 (Cat1)	1620 - 2600	Min - Max	31 - 8910	5 - 1796	94 - 434	6 - 544	30 - 174	23 - 797	23 - 129	15 - 503	12 - 46	5 - 85	5 - 61	1 - 12	0.2 - 2.5	0.1 - 2.9
				Median	396	328	176	52	82	64	59	42	21	21	10	2	0,6	0,4
				Threshold	2949	1395	292	192	165	148	102	99	40	62	20	5	1,4	0,7
		4 (Cat2)	2100 - 2420	Min - Max	445 - 6462	69 - 434	110 - 334	104 - 247	42 - 186	37 - 124	59 - 279	17 - 105	25 - 89	10 - 80	8 - 80	1 - 4	0.2 - 0.8	0.1 - 1.2
				Median	1112	195	188	143	96	96	121	42	59	18	17	3	0,4	0,3
				Threshold	4525	425	325	249	188	120	194	81	81	61	28	4	0,8	0,7
		1 (Cat3)	1900	Min - Max	124 - 172	98 - 146	171 - 285	38 - 55	23 - 35	61 - 114	29 - 47	13 - 42	18 - 24	33 - 36	12 - 13	1 - 1	0.3 - 0.3	0.6 - 0.8
				Median	142	111	219	40	26	74	41	20	20	34	13	1	0,3	0,6
				Threshold	191	123	310	46	32	110	58	44	23	36	14	1	0,3	0,8
Skjelkvåle et al. (2001)	Finland	464	Min - Max	<30 - 4060		70 - 13000			10 - 8340	20 - 47600	7 - 2830	14 - 2780			1 - 20300	1 - 230		
			Median	290		420		290	370	290	170			58	11			
	Norway	985	Min - Max	<50 - 12700		30 - 37700			3 - 5920	10 - 7050	1 - 6140	4 - 15000			1 - 3200	0 - 1070		
			Median	<50		330		100	240	70	140			45	12			
	Sweden	1036	Min - Max	<30 - 126000		20 - 8200			7 - 3680	10 - 11100	3 - 27700	3 - 12900			1 - 5500	1 - 540		
			Median	280		360		150	350	130	160			55	10			
	Denmark	19	Min - Max	<30 - 4000		<100 - 3200			<1000 - 3300	<500 - 5300	<500 - 500	50 - 8120			<50 - 790	<5 - 266		
			Median	1200		600		1000	1000	<500	380			70	50			
	Russian Kola	460	Min - Max			100 - 20000				100 - 450000								
			Median			730		330										
	Chen et al. (2000)	USA	20	Min - Max	0 - 587								0 - 1040				1 - 114	
				Median	587									20			73	
Markert et al. (1997)	Argentina	4	Lake Mascardi (Tronador)			1400				<800	<1500	<700			<200	<200		
			Lake Mascardi (Catedral)	<300		2600			8700	<2000	<2200			<200	<200			
			Lake Gutierrez	<1200		<1200			<800	<2000				<200	<200			
			Lake Nahuel Huapi	<400		<1100			<500	<1200	<600			<200	<200			
Green et al. (2004)	Antarctica	1		Lake Vanda			254			200					12			
Kakareka et al. (2019)	Antarctica	4	Min - Max	52 - 989	<1 - 12	<22 - 2173	10 - 1602	155 - 3907	46 - 687	44 - 12063	<5 - 1865	32 - 4295	1 - 5406	0 - 286	1 - 551	<1 - 31		
			Median	422	5	644	264	670	376	1666	178	1240	553	22	40	3		
Shotyk and Krachler (2009)	Canada	1	356	Lake Kawagama	137	4	470	8	62	289	75	57		30	12	8		
Yang et al. (2002)	Scotland	1	785	Lake Lochnagar			750			200		820				150		
Rosseland et al. (2013)	Himalaya (Nepal)	1	782	Lake Phewa	800		500			400	900	1000						
Sharma et al. (2015)	Himalaya (Nepal)	2	782	Lake Phewa			1760		260	760	210	650			110	20		
			4300	Lake Gosainkunda			300		130	280	710	160			1440	3		
Deka et al. (2016)	Himalaya (India)	1	3962	P.T. Tso (pre-monsoon)			4200				3100	7000				6000		
				P.T. Tso (post-monsoon)			<LOD				<LOD	2000				1000		
Hofer et al. (2010)	Alps (Italy/Austria)	17	1092 - 2387	Min - Max			50 - 19400			90 - 2100		20 - 5300				3 - 100		
			Median			690		730		220						30		
Tornimbeni and Rogora (2011)	Alps (Italy)	32	1895 - 2672	Min - Max	500 - 2200		200 - 2400		300 - 5400	100 - 1200	50 - 100		1000 - 5700			50 - 80		
			Median	1100		400		800	350	100		2600			80			
ICP Water Annual Report (2016)	Alps (Switzerland)	21	1692 - 2580	Min - Max			100 - 400			100 - 6100		100 - 100						
			Median			200		100		100								
Zaharescu et al. (2009)	Central Pyrenees (Spain)	5	2130	Min - Max	60 - 9650		980 - 46800			540 - 38610	140 - 1030	50 - 3390			20 - 260	30 - 990		
			Median	2630		3130		2165	280	250			70	60				
Bacardit and Camarero (2010)	Central Pyrenees (France/Spain)	3	1655	Légunabens	2110							260						
			2188	Plan	310							50						
			2684	Vidal d'Amunt	140							40						

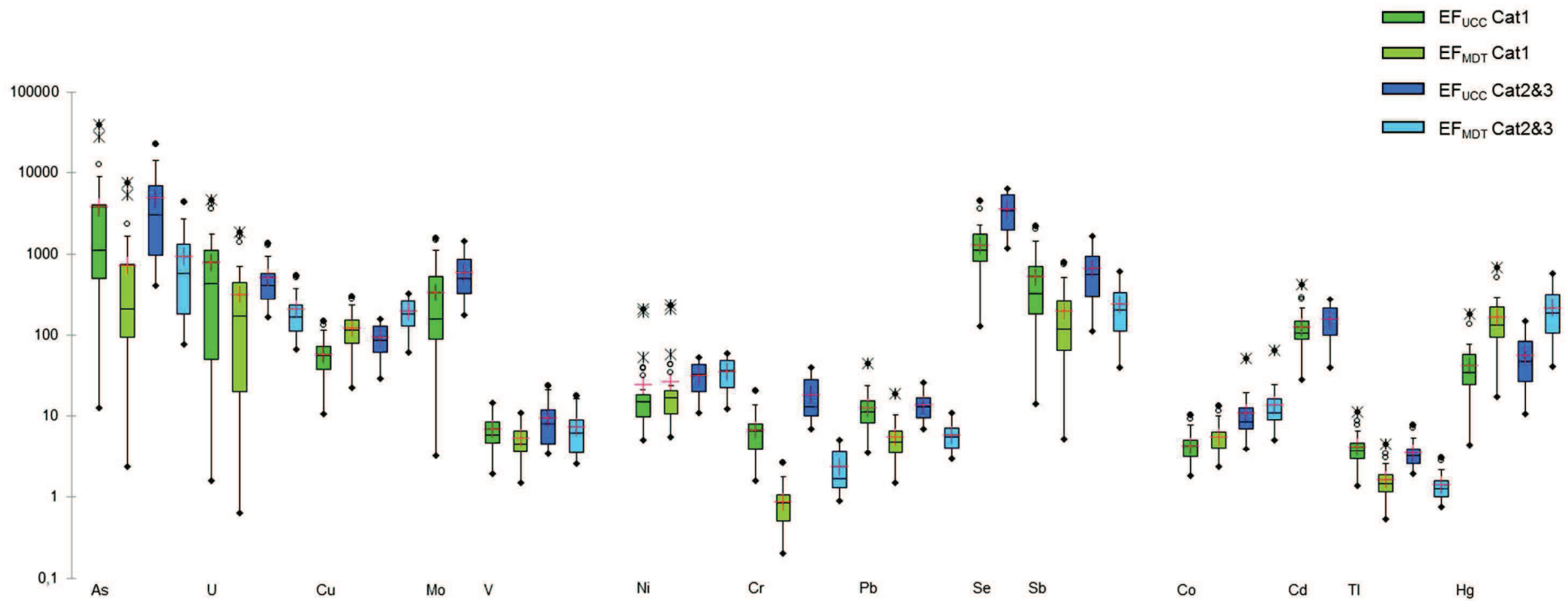


Figure 6.12: Enrichment factors (EF) for unfiltered subsurface water samples using concentration ratios in the upper continental crust (UCC) and in the Maladeta (MDT) bedrock. Green boxes have been generated using data from low alkaline lakes (Category 1) and blue boxes have been generated using data from medium and high alkaline lakes (Categories 2 and 3). Dots are minimum and maximum, bars indicate 10th and 90th percentile, boxes indicate 25th and 75th, marks within each box are medians and red crosses are mean.

Table 6.6: Summary of the results obtained after multiple linear regression of data conducted on each PHTEs using 21 various variables (Catchment influence, Elevation, Maximum depth, Temperature, pH, Ca, Na, Mg, K, Al, Sr, Fe, Mn, Ba, Ti, Cl⁻, NO₃⁻, SO₄²⁻, TOC, Silicate and Total Alkalinity) according to the geological classification of the studied lakes (Low Alkaline vs Medium and High Alkaline Lakes). Significant variables with its normalized coefficient associated are shown in this table, together with the equation of the model.

Low Alkaline Lake (Category1): Lakes ARN, BAC, BER, CAM, COA, GEN, NER, OPA, PAN, PEC, PEY, POU, ROU and XUA				
Element	Samples	Coefficient of multiple determination (adjusted r ²)	Significant variables and associated normalized coefficient (bold is the most influencing variable)	Equation of the model
As	40	0.86	Sr (0.77) Na (-0.66) Ba (-0.34) Cl ⁻ (0.25) SO ₄ ²⁻ (0.29)	As = 1002 + 348.Sr – 12.Na – 1163.Ba + 5557.Cl ⁻ + 790.SO ₄ ²⁻
U	40	0.74	K (0.94) Ba (-0.54) Mg (-0.38) NO ₃ ⁻ (-0.37) pH (0.30)	U = -1422 + 16.K – 423.Ba – 6.0.Mg – 680.NO ₃ ⁻ + 341.pH
Cu	40	0.32	Cl⁻ (0.59) pH (-0.46)	Cu = 562 + 416.Cl ⁻ - 72.pH
Mo	40	0.79	SO₄²⁻ (1.22) Na (0.69) Sr (-0.58) Cl ⁻ (-0.30) Catchment (-0.24)	Mo = 154. SO ₄ ²⁻ + 0.56.Na -12.Sr – 309.Cl ⁻ - 0.13.Catchment
V	40	0.72	SO₄²⁻ (0.93) Al (0.57) Ca (-0.58) Na (0.31) K (0.28)	V = 23 + 41.SO ₄ ²⁻ + 1.1.Al – 0.009.Ca + 0.09.Na + 0.32.K
Ni	40	0.20	Ba (0.47)	Ni = 3.5 + 105.Ba
Cr	40	0.80	SO₄²⁻ (0.73) Fe (0.60) Ba (0.46) Max.Depth (-0.32) Temperature (-0.25)	Cr = 40 + 22.SO ₄ ²⁻ + 1.06.Fe + 17.Ba – 1.4.MaxDepth – 2.3.Temperature
Pb	40	0.78	Ti (0.89)	Pb = 11 + 194.Ti
Se	40	0.94	SO₄²⁻ (0.53) Mg (0.47) TOC (0.40) Na (-0.32) Fe (-0.18) Elevation (0.18) Temperature (- 0.13)	Se = -4 + 5.SO ₄ ²⁻ + 0.1.Mg + 8.0.TOC – 0.02.Na – 0.1.Fe + 0.005.Elevation – 0.3.Temperature
Sb	40	0.91	NO₃⁻ (-0.45) Ca (0.89) Catchment (-0.40) Cl ⁻ (0.31) TOC (-0.24) pH (-0.22)	Sb = 83 – 35.NO ₃ ⁻ + 0.009.Ca – 0.05.Catchment + 67.Cl ⁻ - 14.TOC – 11.pH
Co	40	0.91	Fe (0.92) Mn (-0.16) pH (-0.13)	Co = 23 + 0.68.Fe – 0.61.Mn – 2.8.pH
Cd	40	0.34	Sr (-0.53) TOC (0.45)	Cd = 1.9 – 0.19.Sr + 2.1.TOC
TI	40	0.77	Al (0.69) TOC (0.45) Sr (-0.43) Silicate (0.24)	TI = -0.09 + 0.014.Al + 0.47.TOC – 0.035.Sr + 0.14.Silicate
Hg	40	0.23	TOC (0.49) pH (-0.36)	Hg = 2.2 + 0.56.TOC – 0.35.pH

Medium and High Alkaline Lakes (Categories 2&3): Lakes ARA, BAD, ORD, AZU and SAB

Element	Samples	Coefficient of multiple determination (adjusted r ²)	Significant variables and associated normalized coefficient (bold is the most influencing variable)	Equation of the model
As	24	0.98	SO₄²⁻ (0.65) Mg (-0.68) Silicate (-0.66) Catchment (0.18) Ti (-0.09)	As = 2077 + 726.SO ₄ ²⁻ - 0.51.Mg - 881.Silicate + 25.Catchment - 1521.Ti
U	24	0.94	Ba (-0.69) Na (0.52) pH (0.33) Temperature (0.20) Cl ⁻ (-0.19)	U = -775 - 35.Ba + 1.02.Na + 118.pH + 4.6.Temperature - 401.Cl ⁻
Cu	24	0.41	Temperature (0.66)	Cu = 120 + 8.2.Temperature
Mo	24	0.91	Mg (-2.54) TA (1.60) Al (-0.41) NO ₃ ⁻ (-0.16)	Mo = 109 - 0.063.Mg + 0.20.TA - 5.0.Al - 32.NO ₃ ⁻
V	24	0.95	Na (0.66) Ba (-0.46) Catchment (-0.25) Cl ⁻ (-0.20)	V = 30 + 0.62.Na - 11.Ba - 0.9.Catchment - 199.Cl ⁻
Ni	24	0.36	Mn (0.41) K (-0.41)	Ni = 100 + 9.2.Mn - 0.5.K
Cr	24	0.98	Al (0.23) Ba (-0.70) Silicate (0.30) NO ₃ ⁻ (0.21) Ca (0.16) Catchment (-0.14) SO ₄ ²⁻ (0.13)	Cr = 24 + 2.4.Al - 18.Ba + 11.Silicate + 37.NO ₃ ⁻ + 0.002.Ca - 0.5.Catchment + 4.0.SO ₄ ²⁻
Pb	24	0.74	Al (0.70) Mn (0.49) K (0.32)	Pb = -51 + 3.0.Al + 11.Mn + 0.39.K
Se	24	0.96	Silicate (0.79) SO ₄ ²⁻ (0.61) Fe (-0.12)	Se = -14 + 12.Silicate + 7.7.SO ₄ ²⁻ - 0.30.Fe
Sb	24	1.00	Ba (1.12) Mg (-0.53) SO ₄ ²⁻ (0.14) NO ₃ ⁻ (-0.10) Catchment (0.06)	Sb = 6 + 12.Ba - 0.005.Mg + 1.8.SO ₄ ²⁻ - 7.0.NO ₃ ⁻ + 0.09.Catchment
Co	24	0.13	Na (0.41)	Co = -5 + 0.11.Na
Cd	24	0.94	Ba (0.62) Mg (-1.59) MaxDepth (0.76) Na (0.50)	Cd = -0.3 + 0.26.Ba - 0,001.Mg + 0.09.MaxDepth
TI	24	0.85	Na (0.77) Catchment (-0.36) TOC (0.32)	TI = -0.076 + 0.003.Na - 0.004.Catchment + 0,055.TOC
Hg	24	0.77	TOC (0.54) Silicate (-0.51) pH (-0.39) Temperature (0.26)	Hg = 2.9 + 0.14.TOC - 0.09.Silicate - 0.35.pH + 0.01 Temperature

6.4.4. Water column dynamic and trace elements distribution in selected alpine lakes

The studied lakes have been successfully classified according to their water geochemistry using the unfiltered subsurface water samples, highlighting the importance of geological background. This paragraph focus on the dynamic of some particular lakes, and how different processes affect the chemistry involved in their water column.

The concerned lakes are AZU, ARA, SAB and GEN and they have been chosen according to their importance in the REPLIM Network. They are also relatively easily accessible. They mainly all lied on sedimentary rocks: Devonian rocks for AZU and ARA, Cretaceous rocks for SAB and Permo-Triassic rocks for GEN. These lakes are located at various altitudes (1900 m asl. for SAB, 1942 m asl. for GEN, 2256 m asl. for ARA and 2420 m asl. for AZU) and span a wide range of maximum depth (8 m for AZU, 12 m for ARA, 20 m for GEN and 25 m for SAB). Lake GEN is well impacted by agropastoralism and has shown one of the lowest value of nitrate, either in spring or in autumn, suggesting an important primary productivity in this lake. Lake ARA, which displays one of the most important variation in nitrate content during summer, is also impacted by agropastoralism but to a lesser extent. Lake SAB stood out from the other lakes mainly because of its high alkalinity, and lake AZU is the most pristine.

Analytical results for the water column of those four lakes are displayed in **Figure 6.13** (AZU), **Figure 6.14** (ARA), **Figure 6.15** (SAB) and **Figure 6.16** (GEN).

The physical parameters provided by the multiparametric probe (temperature, dissolved oxygen and chlorophyll) are giving insights on the lakes and allow us to discriminate them more efficiently.

The shallower and more elevated lake AZU expresses constant temperature and dissolved oxygen from surface to bottom of the lake, either in spring or in autumn, respectively of 4.8 ± 0.1 °C and 76 ± 1 % in spring and 5.1 ± 0.2 °C and 71 ± 2 % in autumn. The chlorophyll measured by the probe all along the water column was also not significantly different from zero. This lake is a very pristine and well-mixed lake all over the year.

The less shallow lake ARA behaves differently depending on the time of the year. In spring, temperature was relatively higher at the surface but did not vary significantly along the water column while in autumn a thermocline was observed around 10m with constant temperature above this limit (8.4 ± 0.1 °C) and much lower temperature at the bottom part of the lake (from 8.0 to 5.6 °C). In both spring and autumn, a chemocline at around 10m is observed and dissolved oxygen started to decrease at this depth in Lake ARA. Chlorophyll in spring was not significantly different from zero while a very small increase was observed in the signal at the last centimetres of the water column in autumn, probably due to algae material that are growing or accumulating at the lake bottom.

In the deepest and lowest elevated Lake Sabocos, both temperatures and dissolved oxygen vary strongly depending on the depth with lower values at the bottom and anoxic zone of the lake. The maximum signal of Chlorophyll (2.3) was detected at 18.62 m depth in spring corresponding to the algae accumulation and oxygen consumption, while in autumn the production was over and the maximum

chlorophyll was identified at the bottom part of the lake, below 23 m depth (33.1 ± 9.9). Primary production in this lake is relatively important during summer time [52], thus our observation suggest that a large part of the algae material accumulates at the lake where it decomposes in the post-productive period (fall).

Lake Gentau differs clearly from the other three lakes. This lake was chemically stratified in spring and autumn suggesting a quasi-permanent stratification (holomixis normally occurs in late fall) probably due to intense agropastoralism and touristic activities that promote the primary production through the release of nutrients in the lake. In this lake three different zone can be set up according to the physical parameters. Epilimnion (from 0 to 6.5 m depth in spring; from 0 to 9 m depth in autumn) is the top layer of the lake, well mixed and where oxygen was at its maximum. Metalimnion (or chemocline) (from 6.5 to 13.5 m depth in spring; from 9 to 16 m depth in autumn) is the middle zone of the lake where primary production is the most important (maximum chlorophyll) and the oxygen is also decreasing. Finally, Hypolimnion (below 13.5 m depth in spring; below 16 m depth in autumn) is characterised by the quasi absence of oxygen. Overall, this lake, where primary production is probably the most important, is well stratified in various layers leading to strong variations of the geochemical parameters along the water column depth.

These differences of dynamics are also well highlighted by the results of the chemical parameters. Indeed, while chemical parameters, either TOC, Silicate, anions or cations, did not significantly vary significantly in the well-mixed Lake AZU, chemistry in Lake GEN varies strongly, especially due to the presence of the anoxic zone. Around the chemocline, in autumn, SO_4^{2-} decreases with the depth, likely due to anaerobic conditions and microbial activity in the hypolimnion layer, as sulphur-reducing bacteria cause the transformation of sulphates to hydrogen sulphide. In autumn, higher concentration of NO_3^- at the bottom part of the lake is probably due to nitrification.

However, the most important phenomena is again linked to the reactivity of Fe and Mn, for which the concentrations increase sharply in the hypolimnion: both elements are released into bottom water by reductive dissolution of Mn and Fe oxides at the water-sediment interface. The Fe and Mn particles are able to remove other dissolved trace elements which is clearly the case here with increasing concentrations of As, Cu (only spring), Mo, Co and Cd. The same tendency is observed in Lake SAB with increasing concentrations of Fe, Mn, As, Mo, Ni (only spring) and Co when dissolved oxygen is decreasing, and to a lesser extent in Lake ARA with increasing concentrations of Fe, Mn and Co. Fe, Mn and Co have been commonly used as tracers to describe redox conditions along the sediment cores [13].

Environmental changes in lake ecosystems, induced by either Climate Change (temperature gradient) or anthropogenic pressure (lake productivity), are likely to produce unexpected cascading impacts between PHTEs biogeochemical cycles and such mountainous ecosystems. In a near future, increasing redox changes and amplitude due to anthropogenic inputs of nutrients and organic matter will induce a potential increase of primary productivity and microbial activity. In addition, higher temperature maximum and amplitude will possibly increase thermocline duration/extent and biological turnover.

Overall, these processes will likely modify the availability of some specific PHTEs such as As, Cu, Ni, Mo, Co and Cd.

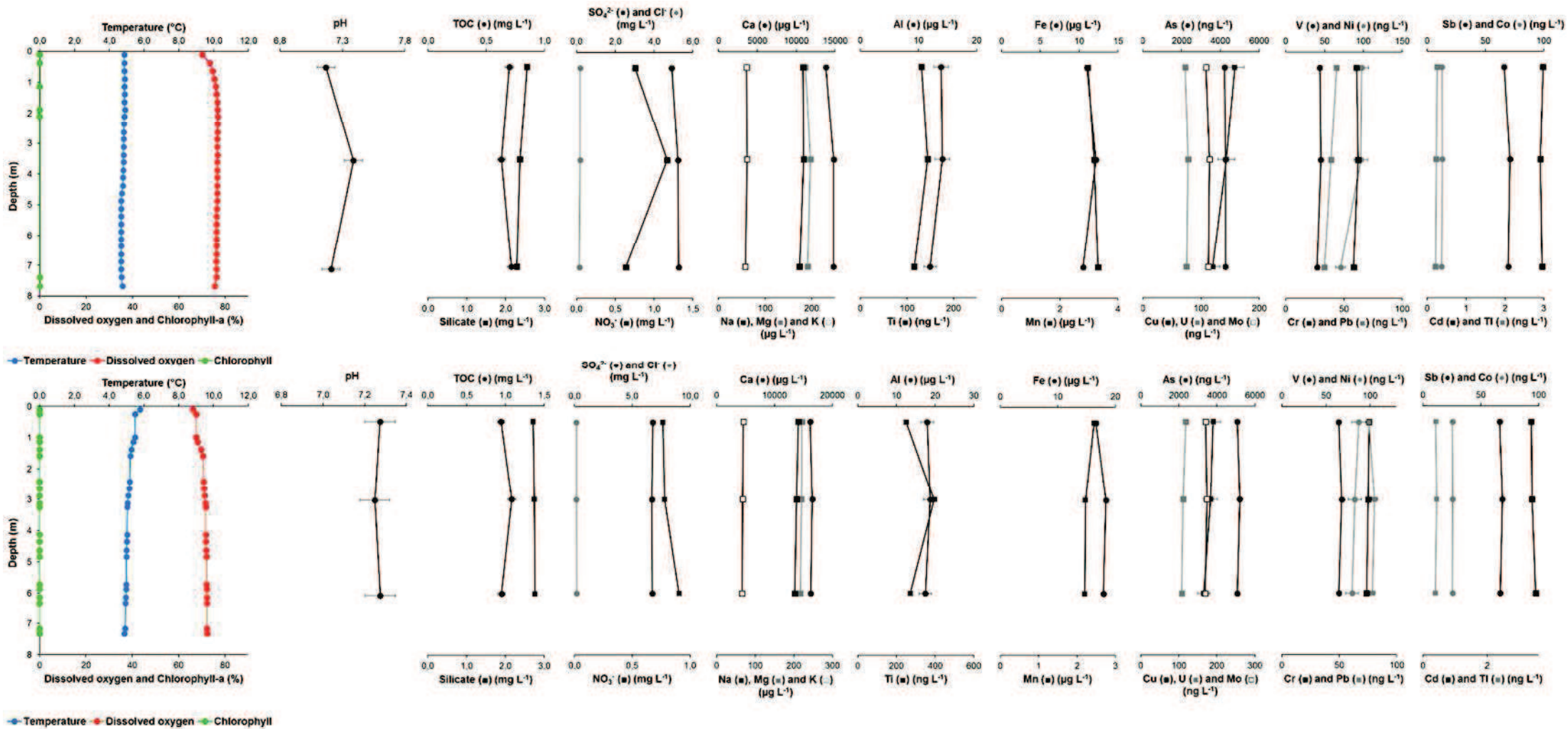


Figure 6.13: Depth profiles of temperature, percentage of dissolved oxygen saturation, chlorophyll-a (RFU) and the chemical parameters obtained during (a) the third sampling campaign (Spring 2018) and (b) the fourth sampling campaign (Autumn 2018) in Lake Azules

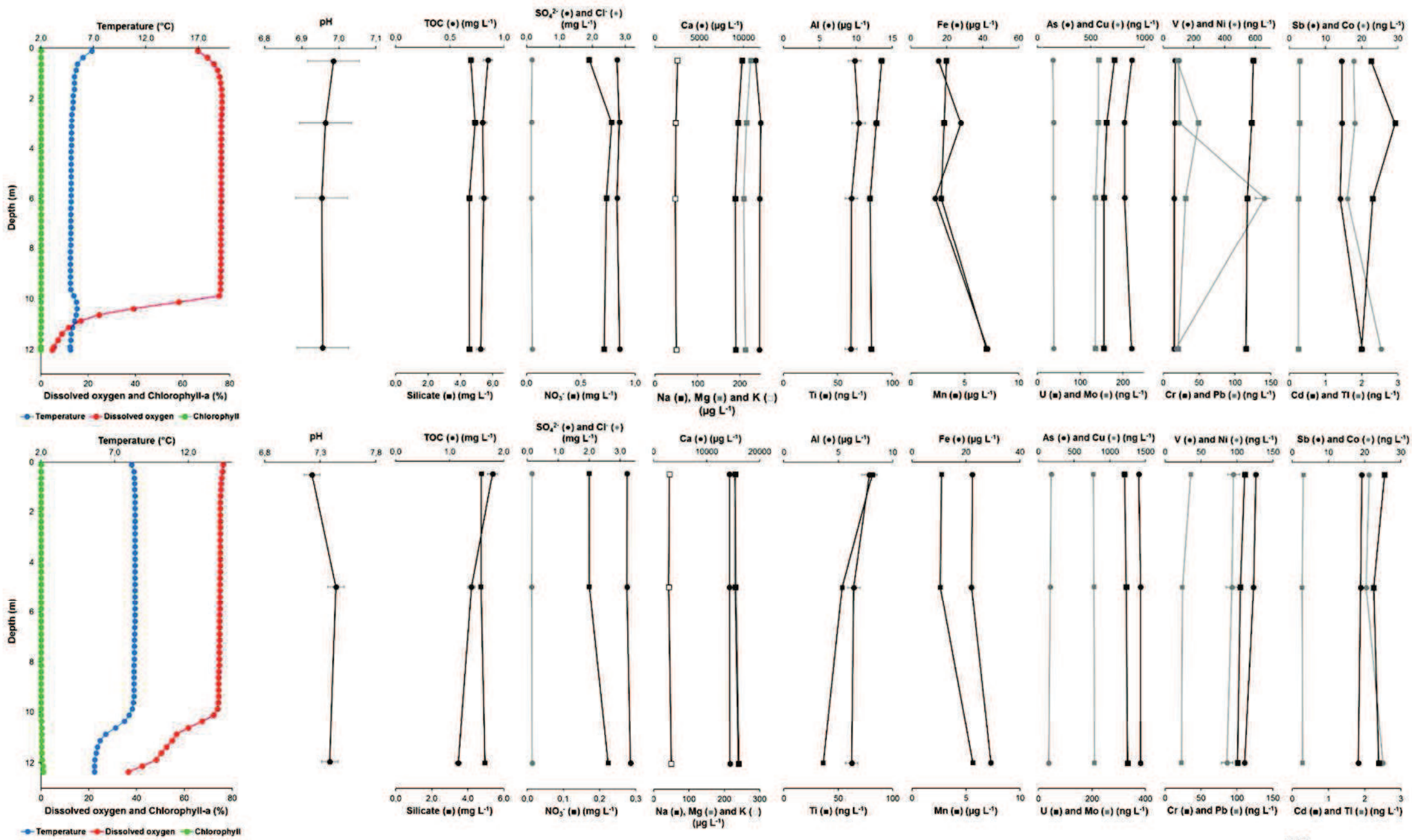


Figure 6.14: Depth profiles of temperature, percentage of dissolved oxygen saturation, chlorophyll-a (RFU) and the chemical parameters obtained during (a) the third sampling campaign(Spring 2018) and (b) the fourth sampling campaign (Autumn 2018) in Lake Arratille

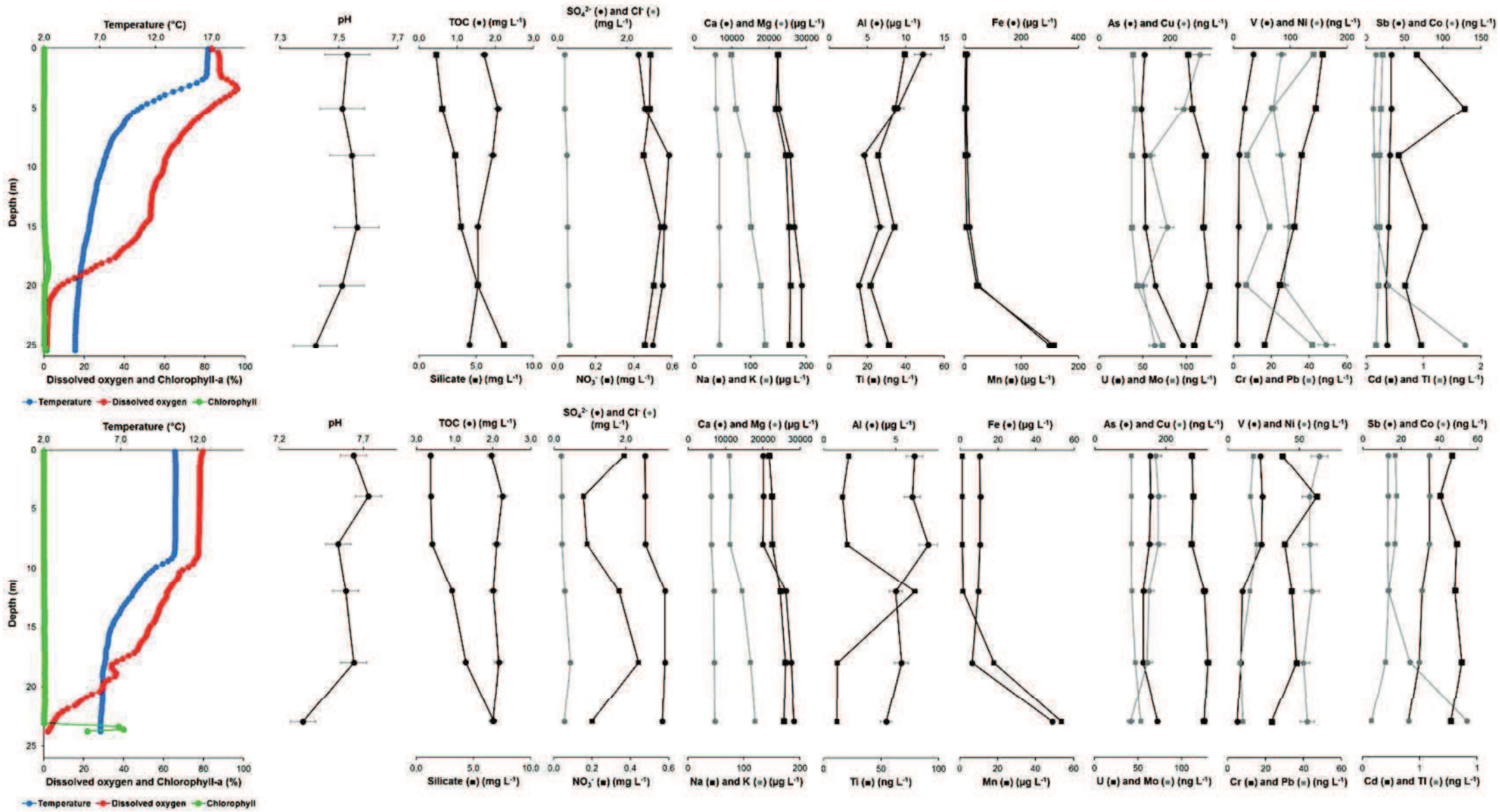


Figure 6.15: Depth profiles of temperature, percentage of dissolved oxygen saturation, chlorophyll-a (RFU) and the chemical parameters obtained during (a) the third sampling campaign (Spring 2018) and (b) the fourth sampling campaign (Autumn 2018) in Lake Sabocos

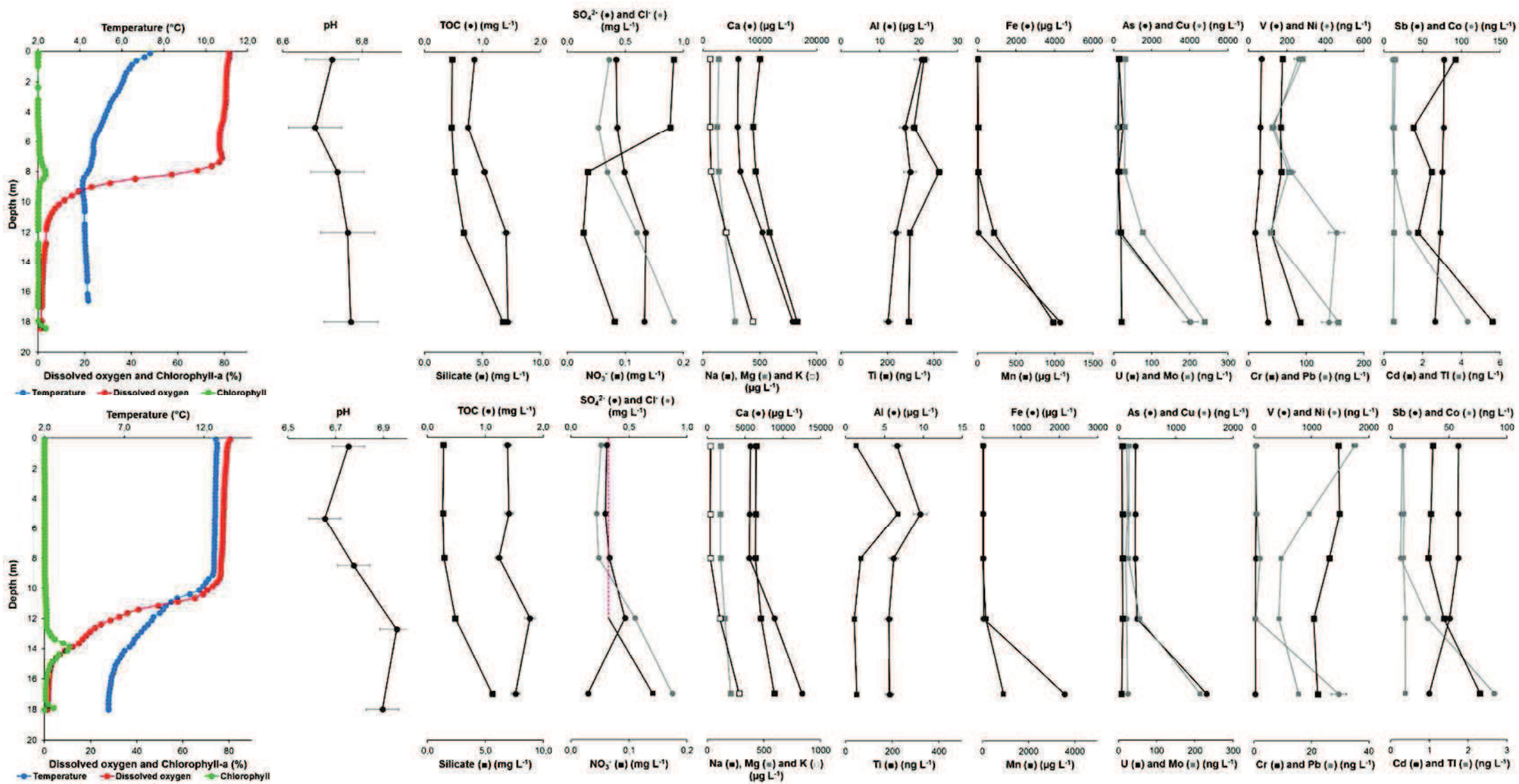


Figure 6.16: Depth profiles of temperature, percentage of dissolved oxygen saturation, chlorophyll-a (RFU) and the chemical parameters obtained during (a) the third sampling campaign (Spring 2018) and (b) the fourth sampling campaign (Autumn 2018) in Lake Gentau

6.5. References

- [1] J.S. Baron, T.M. Schmidt, M.D. Hartman, Climate-induced changes in high elevation stream nitrate dynamics, *Global Change Biology*. 15 (2009) 1777–1789. <https://doi.org/10.1111/j.1365-2486.2009.01847.x>.
- [2] A. Martı́nez-Cortizas, Mercury in a Spanish Peat Bog: Archive of Climate Change and Atmospheric Metal Deposition, *Science*. 284 (1999) 939–942. <https://doi.org/10.1126/science.284.5416.939>.
- [3] L. Camarero, M. Bacardit, A. de Diego, G. Arana, Decadal trends in atmospheric deposition in a high elevation station: Effects of climate and pollution on the long-range flux of metals and trace elements over SW Europe, *Atmospheric Environment*. 167 (2017) 542–552. <https://doi.org/10.1016/j.atmosenv.2017.08.049>.
- [4] J. Sánchez-España, M.P. Mata, J. Vegas, M. Morellón, J.A. Rodríguez, Á. Salazar, I. Yusta, A. Chaos, C. Pérez-Martínez, A. Navas, Anthropogenic and climatic factors enhancing hypolimnetic anoxia in a temperate mountain lake, *Journal of Hydrology*. 555 (2017) 832–850. <https://doi.org/10.1016/j.jhydrol.2017.10.049>.
- [5] J. Catalan, L. Camarero, M. Felip, S. Pla, M. Ventura, T. Buchaca, F. Bartumeus, G. de Mendoza, A. Miró, E.O. Casamayor, J.M. Medina-Sánchez, M. Bacardit, M. Altuna, M. Bartrons, D.D. de Quijano, High mountain lakes: extreme habitats and witnesses of environmental changes, (n.d.) 35.
- [6] P. González-Sampériz, J. Aranbarri, A. Pérez-Sanz, G. Gil-Romera, A. Moreno, M. Leunda, M. Sevilla-Callejo, J.P. Corella, M. Morellón, B. Oliva, B. Valero-Garcés, Environmental and climate change in the southern Central Pyrenees since the Last Glacial Maximum: A view from the lake records, *CATENA*. 149 (2017) 668–688. <https://doi.org/10.1016/j.catena.2016.07.041>.
- [7] M. Morellón, B. Valero-Garcés, P. González-Sampériz, T. Vegas-Vilarrúbia, E. Rubio, M. Rieradevall, A. Delgado-Huertas, P. Mata, Ó. Romero, D.R. Engstrom, M. López-Vicente, A. Navas, J. Soto, Climate changes and human activities recorded in the sediments of Lake Estanya (NE Spain) during the Medieval Warm Period and Little Ice Age, *J Paleolimnol*. 46 (2011) 423–452. <https://doi.org/10.1007/s10933-009-9346-3>.
- [8] M. Rogora, R. Mosello, S. Arisci, The Effect of Climate Warming on the Hydrochemistry of Alpine Lakes, (n.d.) 15.
- [9] D.G. Zaharescu, P.S. Hooda, C.I. Burghilea, A. Palanca-Soler, A Multiscale Framework for Deconstructing the Ecosystem Physical Template of High-Altitudes Lakes, (n.d.) 30.
- [10] L. Camarero, M. Rogora, R. Mosello, N.J. Anderson, A. Barbieri, I. Botev, M. Kernan, J. Kopáček, A. Korhola, A.F. Lotter, G. Muri, C. Postolache, E. Stuchlík, H. Thies, R.F. Wright, Regionalisation of chemical variability in European mountain lakes: *Regionalisation of mountain lakes chemistry*, *Freshwater Biology*. 54 (2009) 2452–2469. <https://doi.org/10.1111/j.1365-2427.2009.02296.x>.
- [11] L. Camarero, J. Catalan, Atmospheric phosphorus deposition may cause lakes to revert from phosphorus limitation back to nitrogen limitation, *Nature Communications*. 3 (2012) 1118. <https://doi.org/10.1038/ncomms2125>.
- [12] L. Camarero, Spreading of trace metals and metalloids pollution in lake sediments over the Pyrénées, *Journal de Physique IV (Proceedings)*. 107 (2003) 249–253. <https://doi.org/10.1051/jp4:20030289>.
- [13] I. Lavilla, A.V. Filgueiras, F. Valverde, J. Millos, A. Palanca, C. Bendicho, Depth Profile Of Trace Elements In a Sediment Core Of a High-Altitude Lake Deposit At The Pyrenees, Spain, *Water, Air, and Soil Pollution*. 172 (2006) 273–293. <https://doi.org/10.1007/s11270-006-9079-0>.
- [14] Variation historique Pb dans des sédiments Pyrénées (Camarero et al. 1998).pdf, (1998).
- [15] J.M. Blais, S. Charpentíe, F. Pick, L.E. Kimpe, A.St. Amand, C. Regnault-Roger, Mercury, polybrominated diphenyl ether, organochlorine pesticide, and polychlorinated biphenyl concentrations in fish from lakes along an elevation transect in the French Pyrénées,

- [16] E. Escartín, C. Porte, Biomonitoring of PAH Pollution in High-Altitude Mountain Lakes through the Analysis of Fish Bile, *Environmental Science & Technology*. 33 (1999) 406–409. <https://doi.org/10.1021/es980798a>.
- [17] R.M. Vilanova, P. Fernandez, J.O. Grimalt, Polychlorinated biphenyl partitioning in the waters of a remote mountain lake, *Science of the Total Environment*. 279 (2001) 51–62.
- [18] C.G. Fraga, Relevance, essentiality and toxicity of trace elements in human health, *Molecular Aspects of Medicine*. 26 (2005) 235–244. <https://doi.org/10.1016/j.mam.2005.07.013>.
- [19] A. Mehri, R.F. Marjan, Review article Trace Elements in Human Nutrition: A Review, (2013) 15.
- [20] M. Mikulewicz, K. Chojnacka, B. Kawala, T. Gredes, Trace Elements in Living Systems: From Beneficial to Toxic Effects, *BioMed Research International*. 2017 (2017) 1–2. <https://doi.org/10.1155/2017/8297814>.
- [21] V. Antoniadis, S.M. Shaheen, E. Levizou, M. Shahid, N.K. Niazi, M. Vithanage, Y.S. Ok, N. Bolan, J. Rinklebe, A critical prospective analysis of the potential toxicity of trace element regulation limits in soils worldwide: Are they protective concerning health risk assessment? - A review, *Environment International*. 127 (2019) 819–847. <https://doi.org/10.1016/j.envint.2019.03.039>.
- [22] H.B. Bradl, Chapter 1 Sources and origins of heavy metals, in: *Interface Science and Technology*, Elsevier, 2005: pp. 1–27. [https://doi.org/10.1016/S1573-4285\(05\)80020-1](https://doi.org/10.1016/S1573-4285(05)80020-1).
- [23] K.J.R. Rosman, W. Chisholm, S. Hong, J.-P. Candelone, C.F. Boutron, Lead from Carthaginian and Roman Spanish Mines Isotopically Identified in Greenland Ice Dated from 600 B.C. to 300 A.D. †, *Environmental Science & Technology*. 31 (1997) 3413–3416. <https://doi.org/10.1021/es970038k>.
- [24] P. Gabrielli, P. Vallenga, Contaminant Records in Ice Cores, in: J.M. Blais, M.R. Rosen, J.P. Smol (Eds.), *Environmental Contaminants*, Springer Netherlands, Dordrecht, 2015: pp. 393–430. https://doi.org/10.1007/978-94-017-9541-8_14.
- [25] C.A. Cooke, A. Martínez-Cortizas, R. Bindler, M. Sexauer Gustin, Environmental archives of atmospheric Hg deposition – A review, *Science of The Total Environment*. 709 (2020) 134800. <https://doi.org/10.1016/j.scitotenv.2019.134800>.
- [26] C. Bini, M. Wahsha, Potentially Harmful Elements and Human Health, in: C. Bini, J. Bech (Eds.), *PHEs, Environment and Human Health*, Springer Netherlands, Dordrecht, 2014: pp. 401–463. https://doi.org/10.1007/978-94-017-8965-3_11.
- [27] M. Bacardit, M. Krachler, L. Camarero, Whole-catchment inventories of trace metals in soils and sediments in mountain lake catchments in the Central Pyrenees: Apportioning the anthropogenic and natural contributions, *Geochimica et Cosmochimica Acta*. 82 (2012) 52–67. <https://doi.org/10.1016/j.gca.2010.10.030>.
- [28] M. Rogora, R. Mosello, S. Arisci, M.C. Brizzio, A. Barbieri, R. Balestrini, P. Waldner, M. Schmitt, M. Stähli, A. Thimonier, M. Kalina, H. Puxbaum, U. Nickus, E. Ulrich, A. Probst, An Overview of Atmospheric Deposition Chemistry over the Alps: Present Status and Long-term Trends, *Hydrobiologia*. 562 (2006) 17–40. <https://doi.org/10.1007/s10750-005-1803-z>.
- [29] O. Tornimbeni, M. Rogora, An Evaluation of Trace Metals in High-Altitude Lakes of the Central Alps: Present Levels, Origins and Possible Speciation in Relation to pH Values, *Water, Air, & Soil Pollution*. 223 (2012) 1895–1909. <https://doi.org/10.1007/s11270-011-0993-4>.
- [30] R. Hofer, R. Lackner, J. Kargl, D. Tait, L. Bonetti, R. Vistocco, G. Flaim, Organochlorine and Metal Accumulation in Fish (*Phoxinus phoxinus*) Along a North-South Transect in the Alps, (n.d.) 12.
- [31] J.P. Deka, S. Singh, P.K. Jha, U.K. Singh, M. Kumar, Imprints of long-range-transported pollution on high-altitude Eastern Himalayan lake water chemistry, *Environmental Earth Sciences*. 75 (2016). <https://doi.org/10.1007/s12665-015-4813-9>.
- [32] C.M. Sharma, S. Kang, M. Sillanpää, Q. Li, Q. Zhang, J. Huang, L. Tripathee, S. Sharma, R. Paudyal, Mercury and Selected Trace Elements from a Remote (Gosainkunda) and an Urban

- (Phewa) Lake Waters of Nepal, *Water, Air, & Soil Pollution*. 226 (2015). <https://doi.org/10.1007/s11270-014-2276-3>.
- [33] J.P. Corella, A. Saiz-Lopez, M.J. Sierra, M.P. Mata, R. Millán, M. Morellón, C.A. Cuevas, A. Moreno, B.L. Valero-Garcés, Trace metal enrichment during the Industrial Period recorded across an altitudinal transect in the Southern Central Pyrenees, *Science of The Total Environment*. 645 (2018) 761–772. <https://doi.org/10.1016/j.scitotenv.2018.07.160>.
- [34] J.P. Corella, B.L. Valero-Garcés, F. Wang, A. Martínez-Cortizas, C.A. Cuevas, A. Saiz-Lopez, 700 years reconstruction of mercury and lead atmospheric deposition in the Pyrenees (NE Spain), *Atmospheric Environment*. 155 (2017) 97–107. <https://doi.org/10.1016/j.atmosenv.2017.02.018>.
- [35] M. Bacardit, L. Camarero, Modelling Pb, Zn and As transfer from terrestrial to aquatic ecosystems during the ice-free season in three Pyrenean catchments, *Science of The Total Environment*. 408 (2010) 5854–5861. <https://doi.org/10.1016/j.scitotenv.2010.07.088>.
- [36] D.G. Zaharescu, P.S. Hooda, A.P. Soler, J. Fernandez, C.I. Burghilea, Trace metals and their source in the catchment of the high altitude Lake Respomuso, Central Pyrenees, *Science of The Total Environment*. 407 (2009) 3546–3553. <https://doi.org/10.1016/j.scitotenv.2009.02.026>.
- [37] R. Salminen, Forum of the European Geological Surveys Directors, eds., Background information, methodology and maps, Geological Survey of Finland, Espoo, 2005.
- [38] A. Chappaz, Chromium, tungsten and vanadium diagenesis in lake sediments, (n.d.) 2.
- [39] L. Kortazar, B. Duval, O. Liñero, O. Olamendi, A. Angulo, D. Amouroux, A. de Diego, L.A. Fernandez, Accurate determination of the total alkalinity and the CO₂ system parameters in high-altitude lakes from the Western Pyrenees (France – Spain), *Microchemical Journal*. 152 (2020) 104345. <https://doi.org/10.1016/j.microc.2019.104345>.
- [40] C.Y. Chen, R.S. Stemberger, B. Klaue, J.D. Blum, P.C. Pickhardt, C.L. Folt, Accumulation of heavy metals in food web components across a gradient of lakes, *Limnology and Oceanography*. 45 (2000) 1525–1536. <https://doi.org/10.4319/lo.2000.45.7.1525>.
- [41] B.L. Skjelkvåle, T. Andersen, E. Fjeld, J. Mannio, A. Wilander, K. Johansson, J.P. Jensen, T. Moiseenko, Heavy Metal Surveys in Nordic Lakes; Concentrations, Geographic Patterns and Relation to Critical Limits, *AMBIO: A Journal of the Human Environment*. 30 (2001) 2–10. <https://doi.org/10.1579/0044-7447-30.1.2>.
- [42] E. Pertsemli, D. Voutsas, Distribution of heavy metals in Lakes Doirani and Kerkini, Northern Greece, *Journal of Hazardous Materials*. 148 (2007) 529–537. <https://doi.org/10.1016/j.jhazmat.2007.03.019>.
- [43] B. Markert, F. Pedrozo, W. Geller, K. Friese, S. Korhammer, G. Baffico, M. Díaz, S. Wöfl, A contribution to the study of the heavy-metal and nutritional element status of some lakes in the southern Andes of Patagonia (Argentina), *Science of The Total Environment*. 206 (1997) 1–15. [https://doi.org/10.1016/S0048-9697\(97\)00218-0](https://doi.org/10.1016/S0048-9697(97)00218-0).
- [44] O.S. Pokrovsky, L.S. Shirokova, Diurnal variations of dissolved and colloidal organic carbon and trace metals in a boreal lake during summer bloom, *Water Research*. 47 (2013) 922–932. <https://doi.org/10.1016/j.watres.2012.11.017>.
- [45] V. Hatje, T.E. Payne, D.M. Hill, G. McOrist, G.F. Birch, R. Szymczak, Kinetics of trace element uptake and release by particles in estuarine waters: effects of pH, salinity, and particle loading, *Environment International*. 29 (2003) 619–629. [https://doi.org/10.1016/S0160-4120\(03\)00049-7](https://doi.org/10.1016/S0160-4120(03)00049-7).
- [46] D. Obrist, J.L. Kirk, L. Zhang, E.M. Sunderland, M. Jiskra, N.E. Selin, A review of global environmental mercury processes in response to human and natural perturbations: Changes of emissions, climate, and land use, *Ambio*. 47 (2018) 116–140. <https://doi.org/10.1007/s13280-017-1004-9>.
- [47] M. Bacardit, L. Camarero, Atmospherically deposited major and trace elements in the winter snowpack along a gradient of altitude in the Central Pyrenees: The seasonal record of long-range fluxes over SW Europe, *Atmospheric Environment*. 44 (2010) 582–595. <https://doi.org/10.1016/j.atmosenv.2009.06.022>.
- [48] R.E. Carlson, A trophic state index for lakes1: Trophic state index, *Limnology and Oceanography*. 22 (1977) 361–369. <https://doi.org/10.4319/lo.1977.22.2.0361>.

- [49] M.T. Kiran, M.V. Bhaskar, A. Tiwari, Phycoremediation of Eutrophic Lakes Using Diatom Algae, in: M.N. Rashed (Ed.), *Lake Sciences and Climate Change*, InTech, 2016. <https://doi.org/10.5772/64111>.
- [50] J. Dunalska, Total organic carbon as a new index for monitoring trophic states in lakes, *Oceanological and Hydrobiological Studies*. 40 (2011). <https://doi.org/10.2478/s13545-011-0022-7>.
- [51] J. Catalan, E. Ballesteros, E. Gacia, A. Palau, L. Camarero, Chemical composition of disturbed and undisturbed high-mountain lakes in the Pyrenees: A reference for acidified sites, *Water Research*. 27 (1993) 133–141. [https://doi.org/10.1016/0043-1354\(93\)90203-T](https://doi.org/10.1016/0043-1354(93)90203-T).
- [52] Z. Santolaria, T. Arruebo, J.S. Urieta, F.J. Lanaja, A. Pardo, J. Matesanz, C. Rodriguez-Casals, Hydrochemistry dynamics in remote mountain lakes and its relation to catchment and atmospheric features: the case study of Sabocos Tarn, Pyrenees, *Environmental Science and Pollution Research*. 22 (2015) 231–247. <https://doi.org/10.1007/s11356-014-3310-0>.
- [53] X. Dai, J. Welhan, Statistical Guidance for Determining Background Ground Water Quality and Degradation, in: 2014.
- [54] K.H. Wedepohl, The composition of the continental crust, (n.d.) 16.
- [55] E. Arranz Yagüe, *Petrología del macizo granítico de La Maladeta (Huesca-Lérida)*, 1997.
- [56] S. Kakareka, T. Kukharchyk, P. Kurman, Major and trace elements content in freshwater lakes of Vecherny Oasis, Enderby Land, East Antarctica, *Environmental Pollution*. 255 (2019) 113126. <https://doi.org/10.1016/j.envpol.2019.113126>.
- [57] W. Shotyk, M. Krachler, Determination of trace element concentrations in natural freshwaters: How low is “low”, and how low do we need to go?, *Journal of Environmental Monitoring*. 11 (2009) 1747. <https://doi.org/10.1039/b917090c>.
- [58] B.O. Rosseland, H.-C. Teien, S. Basnet, R. Borgstrøm, C.M. Sharma, Trace elements and organochlorine pollutants in selected fish species from Lake Phewa, Nepal, *Toxicological & Environmental Chemistry*. 99 (2017) 390–401. <https://doi.org/10.1080/02772248.2016.1189915>.
- [59] S. Li, C. Yang, C. Peng, H. Li, B. Liu, C. Chen, B. Chen, J. Bai, C. Lin, Effects of elevated sulfate concentration on the mobility of arsenic in the sediment–water interface, *Ecotoxicology and Environmental Safety*. 154 (2018) 311–320. <https://doi.org/10.1016/j.ecoenv.2018.02.046>.
- [60] T. Moreno, X. Querol, S. Castillo, A. Alastuey, E. Cuevas, L. Herrmann, M. Mounkaila, J. Elvira, W. Gibbons, Geochemical variations in aeolian mineral particles from the Sahara–Sahel Dust Corridor, *Chemosphere*. 65 (2006) 261–270. <https://doi.org/10.1016/j.chemosphere.2006.02.052>.
- [61] A.G. Bravo, D.N. Kothawala, K. Attermeyer, E. Tessier, P. Bodmer, J.L.J. Ledesma, J. Audet, J.P. Casas-Ruiz, N. Catalán, S. Cauvy-Fraunié, M. Colls, A. Deininger, V.V. Evtimova, J.A. Fonvielle, T. Fuß, P. Gilbert, S. Herrero Ortega, L. Liu, C. Mendoza-Lera, J. Monteiro, J.-R. Mor, M. Nagler, G.H. Niedrist, A.C. Nydahl, A. Pastor, J. Pegg, C. Gutmann Roberts, F. Pilotto, A.P. Portela, C.R. González-Quijano, F. Romero, M. Rulík, D. Amouroux, The interplay between total mercury, methylmercury and dissolved organic matter in fluvial systems: A latitudinal study across Europe, *Water Research*. 144 (2018) 172–182. <https://doi.org/10.1016/j.watres.2018.06.064>.
- [62] C.T. Driscoll, R.P. Mason, H.M. Chan, D.J. Jacob, N. Pirrone, Mercury as a Global Pollutant: Sources, Pathways, and Effects, *Environmental Science & Technology*. 47 (2013) 4967–4983. <https://doi.org/10.1021/es305071v>.

7. Biogeochemistry of mercury species in the water column of high altitude lakes of the Western Pyrenees (France-Spain)

7.1. Abstract

While Hg is a major concern in all aquatic environments where methylation and biomagnification take place, very few studies consider Hg cycling in remote alpine lakes and their use as proxies of global environmental changes. This work presents an integrated investigation conducted in nineteen high altitude pristine lakes from Western Pyrenees. Subsurface water samples were collected in June/October 2017/2018 for Hg speciation analysis (iHg, MMHg, DGM) to investigate spatial and seasonal variations. DGM provided information on biotic and photoreduction of Hg as well as atmospheric re-emission extents. In June/October 2018, a more in-depth study was performed in lakes Gentau, Arratille and Sabocos, by sampling at different depths along the day. Besides, in situ incubation experiments using isotopically enriched Hg species (^{199}iHg , $^{201}\text{MMHg}$) were conducted to investigate Hg transformation mechanisms in the water column (methylation, demethylation, reduction). While iHg did not show seasonal variations in the subsurface water samples, MMHg was significantly higher in autumn 2017, as a consequence of in-situ methylation probably induced by spring algal bloom. DGM vary strongly among and within lakes, and exhibit higher levels in comparison with other pristine areas: significant photoreduction occurs in high altitude lakes from the Pyrenees. Depth sampling highlighted the importance of in-situ biotic methylation triggered by anoxic conditions. Results from the incubation experiments confirm these hypotheses with significant methylation, demethylation and photoreduction observed. Overall, drastic environmental changes occurring daily and seasonally in alpine lakes are providing conditions that can both promote Hg methylation (stratified anoxic waters) and MMHg demethylation (intense UV light). Both climate change (warming) and human impact (through eutrophication) may have important implications on those pathways and the fate of Hg in these remote lakes.

Keywords:

Mercury; Biogeochemistry; Pristine lakes; Methylation; Demethylation ; Photoreduction

7.2. Introduction

Mercury is a persistent pollutant with unique physicochemical properties, making this trace element one of the most intensively studied of all times. Owing to its high volatility, natural sources of Hg (volcanic degassing, evasion from oceans and continental water bodies) and increasing anthropogenic sources of Hg (mainly fossil fuel combustion) contribute to the global pool of Hg in the atmosphere, and lead to long-range dispersion and deposition away from point sources [1–3]. Combined with Hg's tendency to be converted into organometallic compounds of elevated neurotoxicity and persistence, namely monomethylmercury (MMHg), Hg has created a scenario of global health concerns.

Mercury is an “exceptional” contaminant because its most harmful organometallic species (MMHg) is naturally produced in aquatic systems thanks to a complex, but poorly known interplay between microbiological and chemical processes. MMHg is a persistent contaminant because it bioaccumulates from one trophic level to another, leading its concentration to increase naturally along food chains. Since MMHg is a very potent neurotoxin [4–6], maximum tolerable Hg levels have been defined in food products, in particular for pregnant women to avoid neurological damage to their offspring [7]. The U.S. Environmental Protection Agency lists Hg and its compounds in 3rd place on the “Priority List of hazardous Substances”. The European Water Framework Directive (WFD-2000/60/EG) classifies Hg as one of the 30th most “precarious dangerous pollutants”. Human exposure to MMHg is actually well defined, and mainly associated with fish consumption [8]. Yet, most risk assessment studies lack fundamental information as to what exactly controls Hg levels in fish. Without detailed knowledge of the Hg biogeochemical cycle, and in particular the fundamental processes at the origin of MMHg production [9–11], it is difficult to estimate precisely Hg's health impacts and socio-economical costs [12].

Complexity and specificity of the global Hg cycle, especially in its organic species such as MMHg and dimethylmercury (DMHg), is known to be a highly toxic element and its presence in all compartments of the environment is due to multiple transformations in a complex biogeochemical cycle [13]. Methylmercury is the most hazardous compound among mercury (Hg) species due to its ability to bioaccumulate in aquatic biota, reaching higher levels than recommended values in top predators of aquatic environments. The net production of MMHg in aquatic ecosystems is closely dependent on the environmental conditions, such as presence of methylating microorganisms, temperature, pH, organic matter, redox conditions, or salinity, which influence the equilibrium between methylation and demethylation pathways [14]. Managing bioaccumulation of MMHg in aquatic food chains requires differentiation between biotic and abiotic pathways that lead to its production and degradation. Microorganisms such as sulphate-reducing or iron-reducing bacteria are known to be widely involved both in the methylation of inorganic Hg (iHg) and demethylation of MMHg [15,16] in aquatic ecosystems.

While alpine lakes, through sediment cores analysis, have been successfully used to reconstruct temporal trends in atmospheric Hg deposition [2,3,17], Hg behavior in the aquatic compartment of those pristine areas has been barely investigated. *Guédron et al.* [18] and *Alanoca et al.* [19] have been studied Hg cycle in high altitude Bolivian lakes, but these ecosystems are directly influenced by human activities (urban and mining activities). Regarding pristine high altitude lakes, Hg species distribution has been

investigated only in one recent study on four lakes from the Alps [20]. Thus, while Hg transformations in the aquatic compartment are well known in easy accessible areas [19,21–26], there is a need for studying pristine areas, that are more sensitive to global changes.

In this work, we report for the first time a complete inventory of Hg levels and speciation (iHg, MMHg, DGM) in water column from high altitude pristine lakes from the Western Pyrenees. The objectives of this study were i) to assess the Hg species levels the aquatic compartment of these ecosystems, ii) to evaluate the importance of redox and methylation pathways for Hg in mountain lakes, iii) to highlight the climatic and biogeochemical processes controlling these pathways.

7.3. Material and methods

All the sampling sites and their characteristics have been described in **3 Sampling and analytical strategy** and the analytical methods for the determination of mercury species are gathered in **3.3.4 Organometals (Hg and Sn species), 3.3.5 Dissolved Gaseous Mercury (DGM) and 3.3.6 Mercury species incubations**.

The methodology described in **3.3.4 Organometals (Hg and Sn species)** allows the measurement of divalent inorganic mercury iHg, and methylated Hg species MeHg i.e. the sum monomethylmercury MMHg + dimethylmercury DMHg. Indeed, after acidification, both MMHg and DMHg are in the form of MMHg.

The methodology described in **3.3.5 Dissolved Gaseous Mercury (DGM)** allows the measurement of dissolved gaseous mercury species, i.e. the sum elemental mercury Hg(0) + volatile dimethylmercury DMHg.

7.4. Results and discussion

7.4.1. Major biogeochemical characteristics and « total » Hg in the aqueous phase

Major biogeochemical characteristics of the studied lakes have been discussed previously (**6 Occurrence, distribution and characteristics concentrations of Potential Harmful Trace Elements (PHTEs) in Pyrenean lakes and their relation to aquatic biogeochemistry**). The oligotrophic status of the studied lakes, the importance of the geological background and the importance of atmospheric processes have been identified to be essential to define the chemical characteristics of the studied lakes.

In this study, Lake Paradis was also not considered because it differs too much from all other studied lakes and would behave as a statistical outlier.

7.4.2. Mercury speciation in subsurface water samples

Inorganic mercury (iHg) in water

Filtered and unfiltered iHg levels (iHg_F and iHg_{UF}) in subsurface water from the 19 sampled lakes over the five sampling campaigns were low in comparison with other worldwide lakes [18–20,27–31], open oceans [32] and freshwaters from the same area [25,33] (**Table 7.1**). iHg_F ranges from 0.08 to 2.68 ng L⁻¹ with a median value of 0.39 ng L⁻¹ and iHg_{UF} ranges from 0.11 to 3.12 ng L⁻¹ with a median value of 0.39 ng L⁻¹, similar to concentration levels found in open oceans [32] and typical from a pristine environment. The filtered fraction of mercury (iHg_F) represents about 68 ± 19 % of the unfiltered fraction (iHg_{UF}), suggesting that most of the mercury in the Pyreneans lakes is found in the dissolved fraction: particulate Hg might be negligible.

iHg is quite homogenous along the five sampling campaigns (**Figure 7.1**) with only one outlier observed in Lake Coanga on October 2018 at 8:50 a.m. (Grubbs's test, p-value < 0.05; $iHg_F = 2.68$ ng L⁻¹; $iHg_{UF} = 2.88$ ng L⁻¹). In this sample, filtered and unfiltered MMHg and DGM does not differ strongly from the other samples suggesting that this high iHg, either filtered or unfiltered, might be due to punctual inorganic mercury deposition or to contamination during the sample collection.

The homogeneity observed in the iHg concentrations, either filtered or unfiltered, along the five various seasons is surprising. Indeed, in *Alanoca et al.* [19], on one hand total iHg in Lake Uru Uru (3686 m asl) was significantly higher during the dry season over the wet season because of the enhanced evaporation occurring at the end of the dry season. On the other hand, no significant seasonal trends were observed in the dissolved mercury fraction in this lake. In the present study (Pyrenean lakes), the concentration of Hg in autumn (Replim 2 and 4), where the lake levels is the lowest, is not higher than in early spring (Replim 1, 3 and 5) (Kruskal-Wallis test, p-value = 0.79 and 0.54 respectively for iHg_{UF} and iHg_F). Thus, the evaporation effect is probably compensate by the transformation of iHg into Hg(0) induced by important solar radiation occurring during the summer period. Organic matter may play a key role in the importance of Hg photoreduction, and it is worth noting that DOC concentrations exhibit very low values in the Pyrenean lakes (from 0.62 to 4.63 mg L⁻¹). In that sense, higher Hg photoreduction to elemental Hg in open water where DOC content is low has been observed in open waters of Lago Mayor and Menor [18]. Nevertheless, the role of dissolved organic matter in the Hg(0) production is subject to debate. Indeed, some studies have shown inverse correlation between DOC and photoreduction of iHg [34,35], while in other studies the photoreduction rate of iHg increases with DOC levels [36]. Thus, air-water exchange of Hg(0) is critical to understand the biogeochemical cycle of Hg and the various parameters triggering the production of Hg(0) are not yet fully understood. Finally, the homogeneity in the iHg concentration in the Pyrenean lakes suggests that local sources through geogenic inputs are not significant, and does not play a key role in the biogeochemistry of Hg. This also confirms the fact that Hg in the Pyrenees is mainly coming from wet and dry atmospheric deposition. Unfiltered Non Gaseous Mercury vary from 2 to 14 ng L⁻¹ in the precipitation from the Pyrenees (880 m asl) in 2014 [37] and from 2 to 170 ng L⁻¹ in the surface snow from the Alps (2448 m asl) in 2008 – 2009. These reported concentrations in atmospheric depositions are much higher than the levels observed in

the surface water from the high altitude lakes, suggesting a diluting effect and/or a capture by the catchment of the mercury atmospherically deposited.

Methylated mercury in water

The purge experiment described in **3.3.4 Organometals (Hg and Sn species)**, together with data from literature [19] allow us to affirm that DMHg species are negligible in comparison with MMHg, thus methylated species in the lake waters are mainly MMHg.

Filtered and unfiltered MMHg levels (MMHg_F and MMHg_{UF}) in subsurface water from the 19 sampled lakes over the five sampling campaigns vary respectively from <0.003 to 0.035 ng L^{-1} and from <0.003 to 0.062 ng L^{-1} . The median values, 0.008 for MMHg_F and 0.011 for MMHg_{UF} , are typical from pristine environment, in the range of what have been found in Lake Superior ($\text{MMHg}_F = 0.005 \pm 0.001 \text{ ng L}^{-1}$ in April 2000; $\text{MMHg}_F = 0.008 \pm 0.002 \text{ ng L}^{-1}$ in August 2000) [29] and in some high altitude lakes in the Alps ($0.002 - 0.005 \text{ ng L}^{-1}$).

Studying the surface snow from the French Alps (2448 m asl) *Maruszczak et al.* [38] concluded that biotic production of MMHg in the snowpack is unlikely, considering the constant ratio MMHg/THg measured throughout the season in this study. Considering that the main contributor to Hg in the high altitude lakes is the atmospheric deposition, the higher proportion of MMHg observed in the surface water from the high altitude lakes ($3 \pm 2 \%$ for MMHg_F and $4 \pm 3 \%$ for MMHg_{UF}) in comparison with the surface snow (MMHg vary from non-determined to 1.21% of the total Hg) might be due to in-situ methylation. Among the different pathways involved in Hg methylation, MMHg can be produced by bacterial activity [16,22,39]. Thus, the methylated Hg produced can be distributed in the water column by the presence of phytoplankton (diatoms) that act as a carrier for Hg.

Regarding the MMHg levels in the surface waters of the Pyrenean lakes, Replim 4 (autumn 2017) stands out from the other sampling campaigns. Indeed, the median values for MMHg_{UF} for Replim1, 2, 3 and 5 were respectively 0.011 , 0.006 , 0.011 and 0.013 ng L^{-1} while the median value for Replim4 was 0.025 ng L^{-1} . If we compare Replim3 (spring 2017) and Replim4 (autumn 2017), MMHg_{UF} increased significantly in the lakes Arratilles (from 0.007 to 0.017 ng L^{-1}), Gentau (from 0.008 to 0.029 ng L^{-1}), Roumassot (from 0.014 to 0.034 ng L^{-1}), Bachimaña (from 0.012 to 0.026 ng L^{-1}), Coanga (from 0.011 to 0.025 ng L^{-1}), Panticosa (from 0.011 to 0.062 ng L^{-1}) and Sabocos (from 0.012 to 0.027 ng L^{-1}) and moderately in most of the other studied lakes. Spring algal bloom can be responsible of an increase in the methylation processes in the sediments [28,40]. Arratilles, Gentau, Roumassot, Coanga and Sabocos also express among the lowest Nitrate (NO_3^-) values (from below LOD to 0.171 mg L^{-1}) in Replim4, which can be an indicator of the biological productivity (**6.4.1 Trophic status and water quality**). Indeed, the presence of Si-consuming organisms in the lakes biota (e.g., diatoms) that intake NO_3^- (and Si) to produce DOC is a good indicator of the biological productivity. In-situ methylation rates in lakes have already been linked to the trophic status, with a more eutrophication leading to more methylation [18].

Dissolved Gaseous Mercury (DGM)

As a reminder, the methodology described in **3.3.5 Dissolved Gaseous Mercury (DGM)** allow measurement of the sum of Hg(0) + DMHg. Nevertheless, regarding the very small levels of methylated species (MMHg + DMHg) in comparison with DGM, we can assume that DGM is mainly elemental mercury Hg(0).

Dissolved Gaseous Mercury (DGM) vary strongly, from 0.02 to 10.79 ng L⁻¹, and, overall, was higher than the measured DGM in other pristine areas (**Table 7.1**). Indeed, DGM in Bolivian lakes vary from 0.001 to 0.017 ng L⁻¹ in Lake Titicaca [18] and from 0.003 to 0.125 ng L⁻¹ in Lake Uru Uru [19]. In the Lake Superior, in Canada, DGM measured un august 2000 was 0.020 ± 0.003 ng L⁻¹ [29]. Even in the Adour Estuary, downstream to the Pyrenees, DGM content was lower than in the Pyrenean Lakes with values ranging from 0.024 to 0.056 ng L⁻¹ [25]. Finally, the DGM measured in the present study, with a median value of 0.12 ng L⁻¹, was in the range of the open ocean waters [32]. This is well in accordance with the hypothesis noted above: photo-reduction is probably important in high altitude lakes from the Pyrenees. This photo-reduction might be triggered by important solar radiation, and the general ultra-oligotrophic state of the Pyrenean lakes, in comparison with Bolivian or Canadian lakes, might play a key role in this process. DGM accounted for 29 ± 18 % of the total Hg (Non Gaseous Mercury + Gaseous Mercury) and may represent up to 97% of the total Hg. Indeed, during Replim 3 (spring 2017), Lakes Gentau and Sabocos expressed important DGM with highest values around midday (respectively 10.79 and 4.65 ng L⁻¹), when the light incidence is the highest (**Figure 7.2**). These two lakes stand out from the other lakes sampled in spring 2017 because the highest value of DGM, Gentau and Sabocos excluded, was measured in Peyregnets (0.39 ng L⁻¹). The explanation is not clear but this important DGM might be due to i) Accumulation of DGM under the ice cover during the winter and sudden release of this accumulated DGM during the snowmelt, or ii) Important iHg provided by the snow and transformed into Hg(0). In both cases, it implies that the sampling has been done right after the winter period, where the lakes are frozen and the catchment is covered by snow, which is the case in Replim 3. Indeed, a few days before the sampling, more than 90 % of the studied lakes were completely frozen. However, a question remained, why this incredibly levels of DGM have been measured only in two lakes? Further studies, with intensive monitoring and sampling during several days at the snowmelt period are needed in order to fully understand the mechanisms occurring in the Pyrenean Lakes.

Table 7.1: Comparison of filtered and unfiltered inorganic mercury (iHg), monomethylmercury (MMHg) and Dissolved Gaseous Mercury (DGM) concentrations in the subsurface water samples of the 20 studied lakes with literature data for worldwide pristine areas (oceans, boreal lakes, high altitude lakes) and local areas (freshwaters and estuary). %MMHg is calculated as the ratio between MMHg and Mercury Dissolved Ionic Compound (MDIC = MMHg + iHg). %DGM is calculated as ratio between DGM and Total Mercury (THg = MMHg + iHg + DGM). *THg, **Reactive Hg and ***Surface and Depth samples

Reference	Location	Elevation (m asl)	Sampling period	iHg _F ng L ⁻¹	iHg _{UF} ng L ⁻¹	MMHg _F (% MMHg _F) ng L ⁻¹	MMHg _{UF} (% MMHg _{UF}) ng L ⁻¹	DGM (% DGM) ng L ⁻¹
This Work	Central Pyrenees (France/Spain)	1640 - 2600	2017-2019	0.08 - 2.68 median = 0.23	0.11 - 3.12 median = 0.39	<0.003 - 0.035 (3 ± 2%) median = 0.008	<0.003 - 0.062 (4 ± 3%) median = 0.011	0.02 - 10.79 (29 ± 18%) median = 0.12
Fitzgerald et al. (and references therein) [32]	Equatorial Pacific Ocean North Pacific Ocean North Atlantic Ocean South Atlantic Ocean			0.03 - 0.39* 0.48 ± 0.32*	0.08 - 1.38** 0.58 ± 0.34*	0.209 ± 0.217 <0.010 - 0.030	<0.010 - 0.116	0.003 - 0.138 0.096 ± 0.062 0.241 ± 0.160
Cavalheiro et al. [33]	Freshwaters (France)		2012	<0.14 - 2.10		<0.04 - 0.14		
Sharif et al. [25]	Adour Estuary (France)		2007 & 2010	0.28 - 0.59	0.40 - 2.66	0.014 - 0.054	0.018 - 0.124	0.024 - 0.056
Emmertson et al. [27]	Boreal Lakes (Canada, n=50)		2012 - 2016		0.36 - 5.33*		<0.01 - 0.344	
Bravo et al. [28]	Boreal Lakes (Sweden, n=10)***	3 - 229	2012 & 2013		0.9 - 7.3		0.2 - 2.9	
Rolfhus et al. [29]	Lake Superior (Canada/USA)	183	April 2000 August 2000		0.57 ± 0.07* 0.47 ± 0.03*		0.005 ± 0.001 0.008 ± 0.002	0.020 ± 0.003
Meuleman et al. [30]	Lake Baïkal (Russia)***	456	1992 & 1993	0.14 - 0.77*		0.002 - 0.038		
Malczyk and Branfireun [31]	Lake Zapotlán (Mexico)	1497	2007 & 2008	0.5 - 2.4*	0.9 - 10.7*	0.006 - 0.119		
Maruszczak et al. [20]	Lake (Alps, n=4)	1648 - 2448	2008		<0.1 - 3.12*		0.002 - 0.005	
Alanoca et al. [19]	Uru Uru Lake (Bolivia)	3686	2010 & 2011	0.7 - 6.3	0.2 - 2.5	0.2 - 3.8	0.2 - 4.5	0.003 - 0.125
Guédron et al. [18]	Lake Titicaca	3809	2013 & 2015	0.10 - 0.82*	0.08 - 1.81*	0.003 - 0.243	0.013 - 0.306	0.001 - 0.017

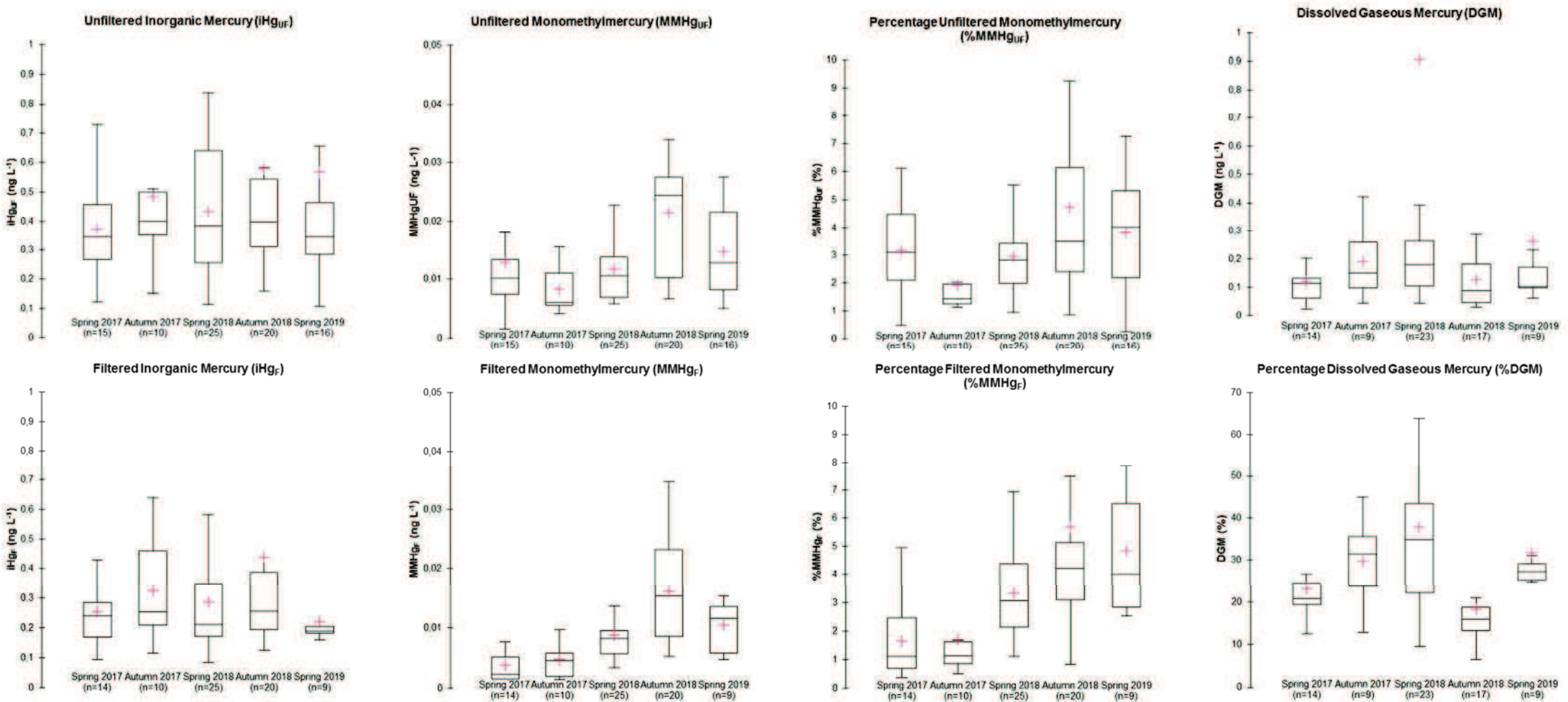


Figure 7.1: Boxplot representations of unfiltered and filtered iHg, MMHg and percentage of MMHg (calculated as ratio between MMHg and Mercury Dissolved Ionic Compound (MDIC = MMHg + iHg), and DGM and percentage of DGM (calculated as ratio between DGM and Total Mercury (THg = MMHg + iHg + DGM)) in subsurface water samples of the 19 studied lakes. Bars indicate 10th and 90th percentile, boxes indicate 25th and 75th, marks within each box are medians, and red crosses are mean

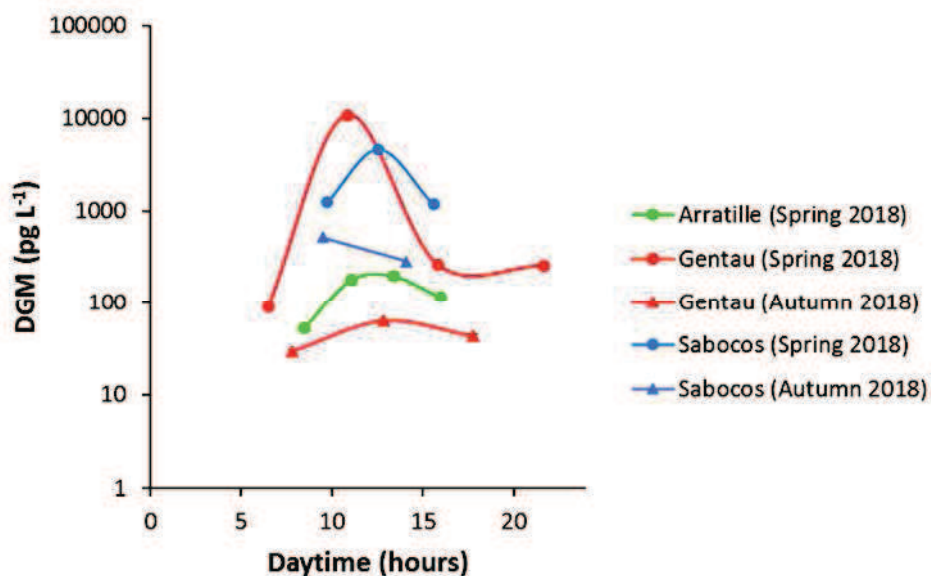


Figure 7.2: Daily variation of DGM in Lakes Arratille, Gentau and Sabocos

7.4.3. Mercury species distribution in the water column in selected alpine lakes

The **Figure 7.3** (Lake Gentau), **Figure 7.4** (Lake Sabocos), **Figure 7.5** (Lake Arratille) and **Figure 7.6** (Lake Azules) display some physical (temperature, dissolved oxygen saturation and chlorophyll-a) and selected chemical parameters (TOC, Silicate, SO_4^{2-} , Cl^- and NO_3^-) that could be linked to the mercury species (iHg, MMHg and DGM) distribution in the water column of four various lakes intensively monitored during Replim3 (spring 2017), Replim4 (autumn 2017) and Replim5 (spring 2018).

Features and specificities of these four lakes have been already discussed in **6 Occurrence, distribution and characteristics concentrations of Potential Harmful Trace Elements (PHTEs) in Pyrenean lakes and their relation to aquatic biogeochemistry**. Globally, even if their catchment is mainly composed of easily erodible sedimentary rocks (Devonian, Cretaceous and Permo-Triassic rocks) Gentau, Sabocos, Arratille and Azules span a wide range of physical characteristics with maximum depth from 8 to 25m, altitude from 1900 m to 2420 m.

Lake Gentau is chemically stratified in the three sampling campaigns (Spring 2018, Autumn 2018 and Spring 2019). Indeed, all along the year, this lake can be divided in three various sections: Epilimnion (top layer of the lake, well mixed with maximum of oxygen), Metalimnion (middle zone of the lake characterized by a decrease in oxygen, and the maximum of chlorophyll), and Hypolimnion (deepest and quasi-anoxic part of the lake). Additionally to the oxygen chemocline, Gentau presents also a thermocline in the Spring 2018 sampling campaign in the metalimnion part of the lake.

Lake Gentau

The highest iHg concentrations, either unfiltered or filtered, were detected at the deepest sampling point of the lakes in Spring (0.75 and 0.66 ng L⁻¹ in unfiltered and filtered samples respectively) and Autumn 2018 (0.39 and 0.36 ng L⁻¹ in unfiltered and filtered samples respectively). In Spring 2019, the surface water samples were characterized by the highest iHg concentrations (0.27 and 0.18 ng L⁻¹ in unfiltered and filtered samples respectively). Bravo et al. [41] have shown that the highest total mercury concentrations in river stream systems were associated with important terrestrial DOM (Dissolved Organic Matter) and low nutrient content. In our study, TOC was slightly constant all along the water column during the three sampling campaigns (1.1 ± 0.3 mg L⁻¹ in Spring 2018, 1.5 ± 0.2 mg L⁻¹ in Autumn 2018, and 1.2 ± 0.1 mg L⁻¹ in Spring 2019). NO₃⁻, a good indicator of biological productivity and an important nutrient, decreases with depth in Spring 2018, increases with depth in Autumn 2018, and varies strongly along the water column in Spring 2019. Therefore, the important increase observed for iHg in the deepest point of the lake in Spring and Autumn 2018 is due to some exchanges of iHg at the water-sediment interface rather than to discharge from the catchment.

MMHg concentrations were significantly higher at the deepest point of the lake in comparison with the other four sampled points. Indeed while unfiltered and filtered MMHg in the water column in Spring 2018 vary from 0.008 to 0.057 ng L⁻¹ and 0.006 to 0.023 ng L⁻¹ respectively, MMHg unfiltered and filtered levels were respectively 0.426 and 0.318 ng L⁻¹ at 18 m depth. In Autumn 2019, the same trend is observed for MMHg: unfiltered and filtered MMHg vary from 0.027 to 0.055 ng L⁻¹ and 0.011 to 0.026 ng L⁻¹ respectively while the deepest sampled point (17m depth) exhibit MMHg levels as high as 0.388 and 0.341 ng L⁻¹ for the unfiltered and filtered samples. In Spring 2019, unfiltered and filtered MMHg concentrations vary from 0.007 to 0.059 ng L⁻¹ and <0.004 to 0.019 ng L⁻¹ respectively, while 0.236 and 0.157 ng L⁻¹ were the unfiltered and filtered MMHg concentrations measured at the deepest sampled point (17.5m depth). Anoxic conditions observed in the deepest point of Lake Gentau may promote the development of biological activity, thus in-situ biotic methylation in both water and surface sediments. Indeed, Sulphate Reducing Bacteria that should occur in this lake (median value of SO₄²⁻ levels equal 0.49 mg L⁻¹) are known to be responsible of Hg methylation in anoxic aquatic environment.

Finally, vertical distribution of DGM in Gentau is quite simple with a constant and progressive decrease from surface waters (10.79 ng L⁻¹ in Spring 2018; 0.06 ng L⁻¹ in Autumn 2018; 0.10 ng L⁻¹ in Spring 2019) to the deepest sampled point (0.14 ng L⁻¹ in Spring 2018 at 18m depth; 0.03 ng L⁻¹ in Autumn 2018 at 17m depth; 0.01 ng L⁻¹ in Spring 2019 at 17.5m depth). This support the previous assumption regarding the importance of photo-reduction processes in those high altitude lakes, which is induced by the important solar radiation occurring at the surface waters. In addition, the Autumn 2018 DGM levels are lower than the Spring 2018 and 2019 DGM levels all along the water column, highlighting the more important photo-reduction occurring in early spring.

Lake Sabocos

Lake Sabocos is not perfectly stratified as Lake Gentau, but oxygen and temperature vary strongly along the water column with depletion of both physical parameters with depth, leading to almost anoxic conditions in the bottom part of this alkaline lake.

iHg, either unfiltered or filtered, vary strongly all along the water column in the three sampling campaigns (respectively from 0.39 to 1.29 ng L⁻¹ and from 0.29 to 0.53 ng L⁻¹ in Spring 2018; from 0.53 to 0.90 ng L⁻¹ and from 0.17 to 0.68 ng L⁻¹ in Autumn 2018; from 0.08 to 0.34 ng L⁻¹ and from 0.02 to 0.21 ng L⁻¹ in Spring 2019). There is no evidence for a specific trend in the iHg distribution in the Lake Sabocos but the strong variations suggest that important Hg species transformations occur (photoreduction, resuspension, and demethylation).

MMHg depth profiles in Lake Sabocos highlight the probable presence of in-situ methylation promoted by microbial bacteria. This transformation is well observed in both Spring 2018 and 2019 with the highest MMHg unfiltered and filtered levels measured in the deepest part of the lake where the oxygen level is the lowest (respectively 0.060 and 0.025 ng L⁻¹ in Spring 2018; 0.052 and 0.021 ng L⁻¹ in Spring 2019). Increase of MMHg levels is not observed in Autumn 2018. Indeed, in this sampling campaign, the maximum of chlorophyll was identified at the bottom part of the lake, indicating the post-productive period (fall) with very low bacterial activity.

Regarding the DGM concentrations, the high levels measured in surface waters in comparison with deepest samples in both Spring 2018 and 2019 (4.65 and 1.34 ng L⁻¹ respectively) is consistent with the important photoreduction occurring in early Spring.

Lake Arratille and Azules

In the shallow Arratille lake, hydrobiological parameters measured with the multiparameter probe (temperature, oxygen and chlorophyll) do not vary strongly within the water column. Nevertheless it is worth noting that a short decrease in both temperature and oxygen is observed in the last 2 meters of the lake in both Spring and Autumn 2018. Concerning the mercury species distribution, no significant differences can be observed for iHg, MMHg or DGM along the water column, suggesting a well-mixed lake with clear water.

In the shallower and more elevated lake, Azules, oxygen and temperature do not vary at all along the water column in both Spring and Autumn 2018. However, regarding Hg species, while no specific trend is observed in Spring 2018, unfiltered and filtered iHg, unfiltered and filtered MMHg and DGM are significantly increasing with the depth. It may be linked to a punctual source of Hg in-depth of this lake, most probably from reducing conditions in bottom sediments.

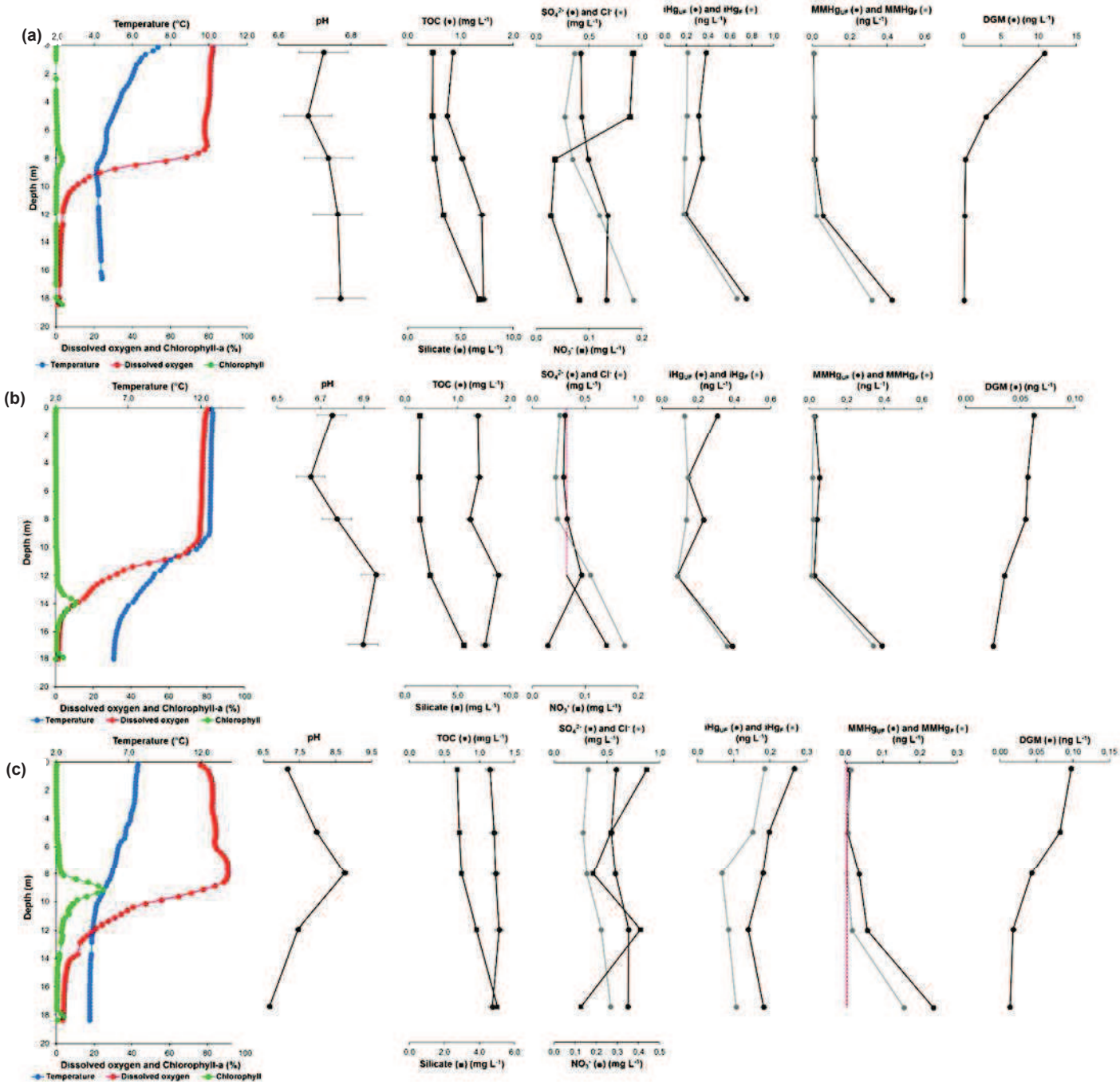


Figure 7.3: Depth profiles of temperature, percentage of dissolved oxygen saturation, chlorophyll-a (RFU) and some chemical parameters including mercury speciation obtained during (a) the third sampling campaign (Spring 2018), (b) the fourth sampling campaign (Autumn 2018) and (c) the fifth sampling campaign (Spring 2019) in Lake Gentau

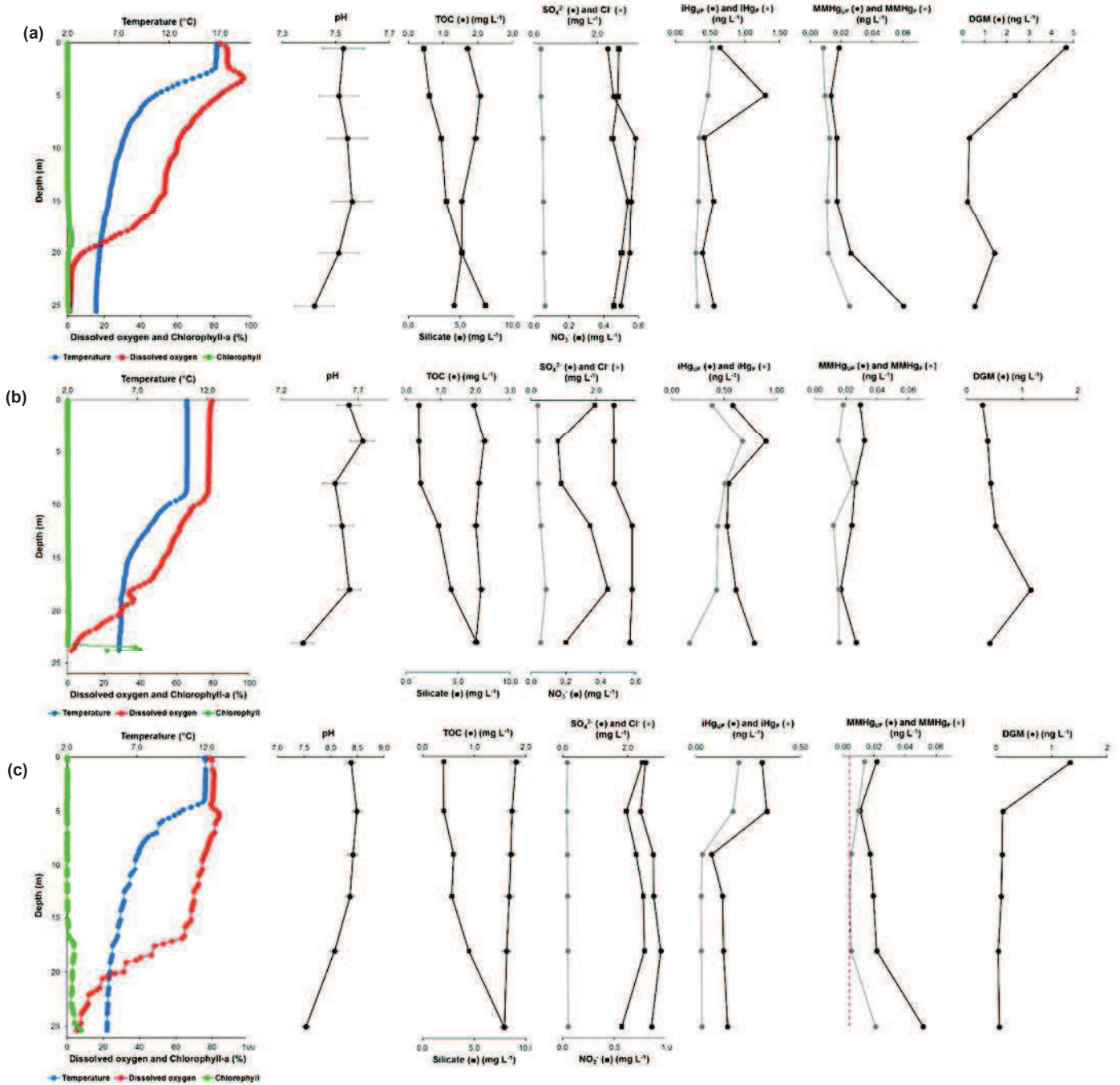


Figure 7.4: Depth profiles of temperature, percentage of dissolved oxygen saturation, chlorophyll-a (RFU) and some chemical parameters including mercury speciation obtained during (a) the third sampling campaign(Spring 2018), (b) the fourth sampling campaign (Autumn 2018) and (c) the fifth sampling campaign (Spring 2019) in Lake Sabocos

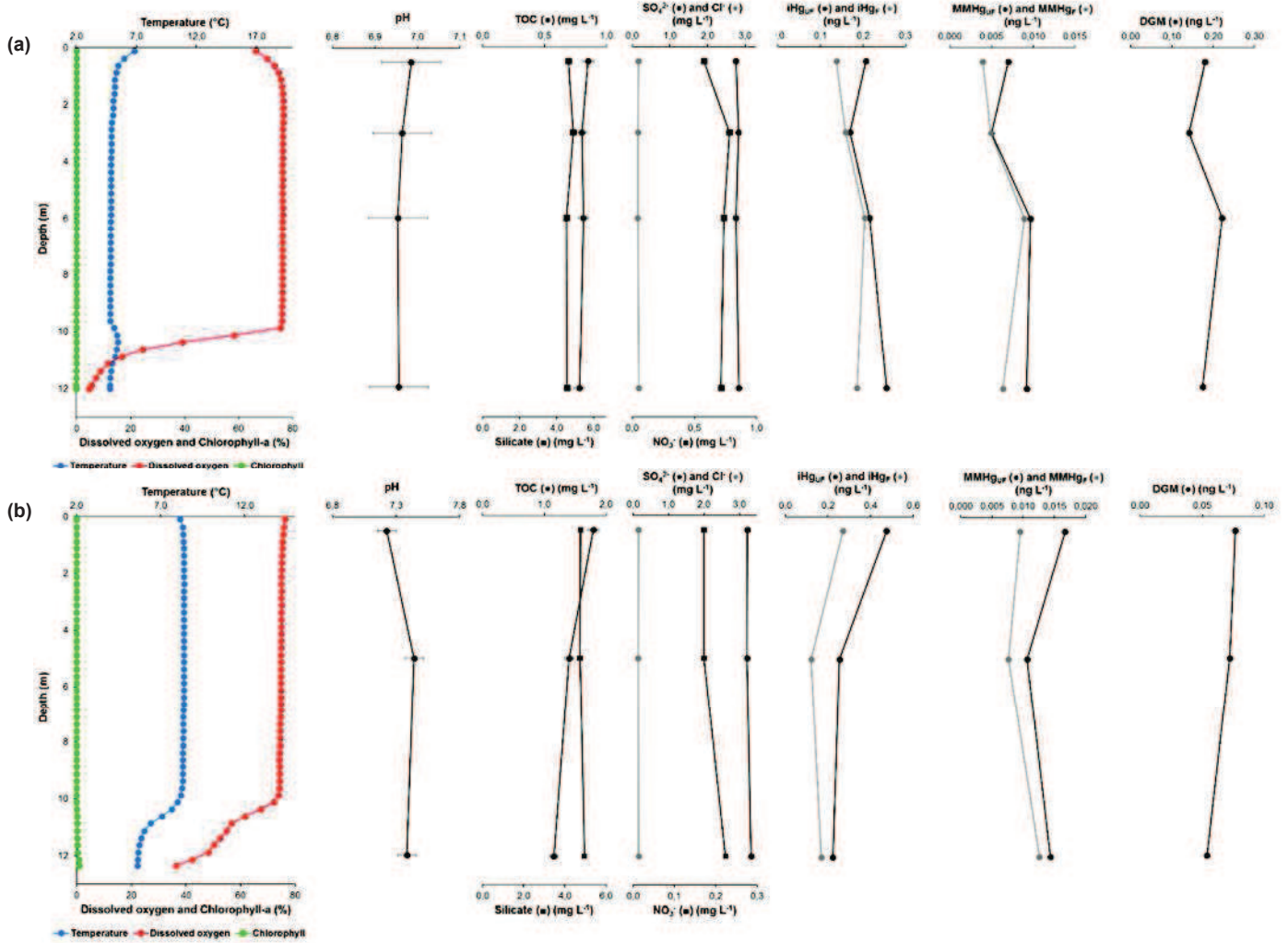


Figure 7.5: Depth profiles of temperature, percentage of dissolved oxygen saturation, chlorophyll-a (RFU) and some chemical parameters including mercury speciation obtained during (a) the third sampling campaign (Spring 2018) and (b) the fourth sampling campaign (Autumn 2018) in Lake Arratilles

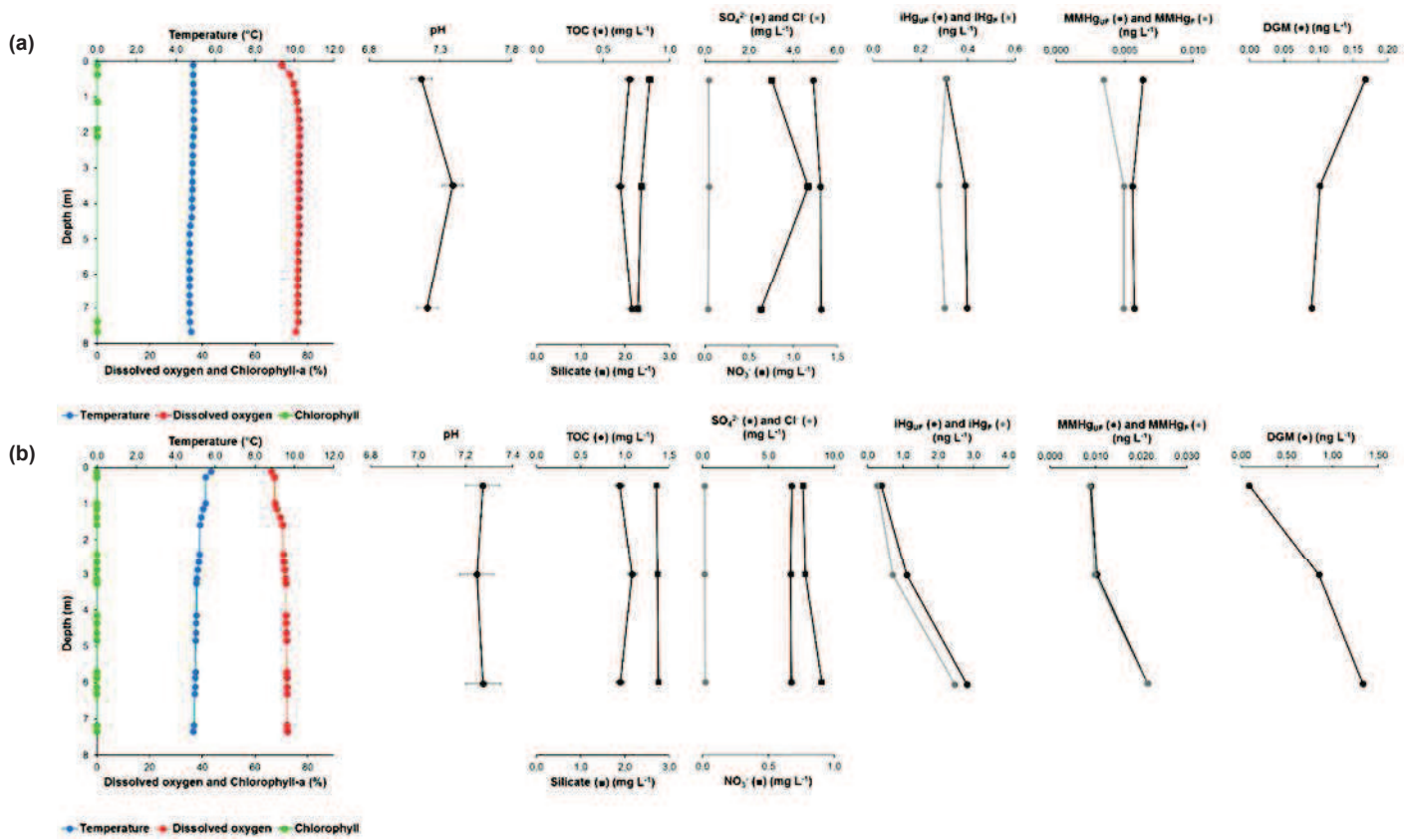


Figure 7.6: Depth profiles of temperature, percentage of dissolved oxygen saturation, chlorophyll-a (RFU) and some chemical parameters including mercury speciation obtained during (a) the third sampling campaign (Spring 2018) and (b) the fourth sampling campaign (Autumn 2018) in Lake Azules

7.4.4. Mercury species transformations in the water column in selected alpine lakes

In order to quantify the importance of the suggested Hg species transformations occurring in the high altitude lakes, Hg species incubations conducted in Lakes Gentau, Sabocos and Arratille are relevant. The obtained results are summarized in **Table 7.2**, together with some bibliographic data.

Methylation

Methylation potentials obtained in unfiltered water samples ranged between <0.03 and 6.8 \% day^{-1} in Lake Gentau, between <0.03 and 1.0 \% day^{-1} in Lake Sabocos, and between <0.03 and 0.4 \% day^{-1} in Lake Sabocos. These methylation potentials are in accordance with data obtained for surface waters in high altitude Bolivian lakes [18,19] and for marine and coastal waters [22,25]. The highest methylation potentials have been measured in the bottom anoxic zone for Lake Gentau ($4.3 \pm 0.4 \text{ \% day}^{-1}$ in Spring 2018; $6.8 \pm 0.6 \text{ \% day}^{-1}$ in Autumn 2018 and $1.6 \pm 0.1 \text{ \% day}^{-1}$ in Spring 2019) as well as for Lake Sabocos ($0.8 \pm 0.3 \text{ \% day}^{-1}$ in Spring 2018; $1.0 \pm 0.4 \text{ \% day}^{-1}$ in Autumn 2018 and $0.6 \pm 0.3 \text{ \% day}^{-1}$ in Spring 2019). For all the performed incubation, no significant differences can be observed for methylation potentials according to the light exposure, confirming that abiotic methylation is not significant in those high altitude pristine lakes. Reductive conditions (stratified anoxic waters) can promote Hg methylation by occurrence of anaerobic bacteria.

Some significant methylation also occurs in the oxic subsurface waters of Lakes Gentau, Lake Sabocos and Lake Arratille. The formation of MMHg in the oxic water column is not fully understood. A recent work conducted in Lake Geneva highlights that particles sinking through oxygenated water column can produced MMHg [26]. In our work, even if the methylation rate measured is small, oxic layer of the lake correspond to the larger part of the volume of the lake.

Demethylation

Significant demethylation potentials were measured in the subsurface waters of Lake Gentau ($23.8 \pm 4.4 \text{ \% day}^{-1}$ in Spring 2018; $23.9 \pm 2.9 \text{ \% day}^{-1}$ in Autumn 2018 and $35.6 \pm 2.2 \text{ \% day}^{-1}$ in Spring 2019) and Lake Sabocos ($35.2 \pm 9.7 \text{ \% day}^{-1}$ in Spring 2018; $9.0 \pm 0.5 \text{ \% day}^{-1}$ in Autumn 2018 and $12.4 \pm 4.2 \text{ \% day}^{-1}$ in Spring 2019) only at daylight conditions. These important demethylation potentials have been observed in previous studies and was associated to both abiotic and biotic processes [24,25,25]. Clearly, our study suggest that in high altitude pristine lakes, direct light-induced photochemical demethylation is a significant pathway that contribute to reduce MMHg extent in the water column.

Demethylation vs MMHg loss in Lake Gentau

As mentioned previously demethylation, especially in subsurface waters, is important in Lake Gentau. As a reminder, demethylation potentials calculated here correspond to the transformation of MMHg into iHg. In **Table 7.3**, additionally to the demethylation potentials, loss of MMHg potentials for Lake Gentau are displayed. Loss of MMHg correspond to the decrease of MMHg during the incubation and could be

connected to both the transformation of MMHg into iHg, and the transformation of MMHg into Hg(0). As shown in **Table 7.3**, both potentials calculated (demethylation and loss of MMHg) are well in accordance, supporting the robustness and accuracy of the incubation experiments

Reduction

Reduction potentials measured in subsurface waters of Lake Gentau ($60.8 \pm 1.8 \text{ \% day}^{-1}$ in Spring 2018; $74.1 \pm 3.0 \text{ \% day}^{-1}$ in Autumn 2018 and $63.5 \pm 4.9 \text{ \% day}^{-1}$ in Spring 2019) and Lake Sabocos ($81.6 \pm 6.3 \text{ \% day}^{-1}$ in Spring 2019) are extremely important, and less significant in subsurface waters of Lake Arratille ($3.0 \pm 0.4 \text{ \% day}^{-1}$ in Spring 2018; $1.8 \pm 0.8 \text{ \% day}^{-1}$ in Autumn 2018), but still remained high in comparison to other previous studies [19,22,25]. These important reduction potentials are consistent with the high DGM concentrations measured, especially in Lakes Gentau and Sabocos. Intensive UV light occurring in high altitude lakes can promote reduction. However, specific conditions of Lakes Gentau and Sabocos promote this reduction in a higher way than for Lake Arratille.

Table 7.2: Methylation (M), Demethylation (D) and Reduction (R) potentials (mean \pm SD, n=3 for M and D, n=2 for R) in unfiltered waters performed under light and dark conditions at different depths for Lakes Gentau, Sabocos and Arratilles and for sampling campaigns Spring and Autumn 2018 and Spring 2019, together with data from literature. Detection limits are 0.03, 4 and 0.3 % day⁻¹ for Methylation, Demethylation and Reduction yields, respectively. n.d. is not determined.

Reference	Location	Sampling period	Sampling Type	Incubation time (h)	iHg Methylation (%day ⁻¹)		MMHg Demethylation (%day ⁻¹)		Hg Reduction (%day ⁻¹)	
					Diurnal	Dark	Diurnal	Dark	Diurnal	Dark
This Work	Lake Gentau (Central Pyrenees)	Spring 2018	Subsurface (0.5m)	7,4	0.4 \pm 0.1	0.4 \pm 0.2	23.8 \pm 4.4	<LOD	60.8 \pm 1.8	2.4 \pm 4.1
			Middle Depth (8m)	8,5	<LOD	<LOD	13.6 \pm 1.2	<LOD	15.3 \pm 2.1	1.6 \pm 0.7
			Bottom (17m)	8,7	n.d.	4.3 \pm 0.4	n.d.	<LOD	n.d.	<LOD
	Autumn 2018	Subsurface (0.5m)	7,2	<LOD	<LOD	23.9 \pm 2.9	<LOD	74.1 \pm 3.0	5.5 \pm 1.5	
		Middle Depth (8m)	6,0	0.4 \pm 0.2	0.5 \pm 0.2	<LOD	<LOD	<LOD	<LOD	
		Bottom (17m)	7,2	n.d.	6.8 \pm 0.6	n.d.	<LOD	n.d.	<LOD	
	Spring 2019	Subsurface (0.5m)	8,7	0.2 \pm 0.2	<LOD	35.6 \pm 2.2	<LOD	63.5 \pm 4.9	0.8 \pm 0.7	
		Middle Depth (8m)	8,5	<LOD	<LOD	13.6 \pm 0.4	<LOD	12.9 \pm 4.7	0.7 \pm 1.5	
		Bottom (17m)	8,5	n.d.	1.6 \pm 0.1	n.d.	<LOD	n.d.	<LOD	
Lake Sabocos (Central Pyrenees)	Spring 2018	Subsurface (0.5m)	6,3	0.1 \pm 0.0	0.3 \pm 0.0	35.2 \pm 9.7	<LOD	n.d.	n.d.	
		Bottom (27m)	6,3	n.d.	0.8 \pm 0.3	n.d.	<LOD	n.d.	n.d.	
	Autumn 2018	Subsurface (0.5m)	6,3	0.3 \pm 0.2	0.2 \pm 0.1	9.0 \pm 0.5	<LOD	n.d.	n.d.	
		Bottom (23m)	6,3	n.d.	1.0 \pm 0.4	n.d.	<LOD	n.d.	n.d.	
	Spring 2019	Subsurface (0.5m)	6,8	<LOD	<LOD	12.4 \pm 4.2	<LOD	81.6 \pm 6.3	1.0 \pm 0.9	
		Middle Depth (9m)	6,8	0.3 \pm 0.3	0.2 \pm 0.0	7.4 \pm 3.9	<LOD	16.1 \pm 5.9	0.9 \pm 1.9	
Lake Arratilles (Central Pyrenees)	Spring 2018	Subsurface (0.5m)	6,0	0.4 \pm 0.1	n.d.	<LOD	n.d.	3.0 \pm 0.4	n.d.	
		Middle Depth (6m)	5,3	0.4 \pm 0.2	<LOD	<LOD	<LOD	2.9 \pm 1.0	3.1 \pm 0.5	
	Autumn 2018	Subsurface (0.5m)	5,3	<LOD	<LOD	<LOD	<LOD	1.8 \pm 0.8	0.2 \pm 0.6	
			Bottom (12m)	6,7	n.d.	<LOD	n.d.	<LOD	<LOD	
Eckley et Hintelmann (2006)	Lake (Canada)	2002	Oxycline, Water column	24		0.6 - 14.8		<12		
Monperrus et al (2007)	Mediterranean Sea	2003 & 2004	Surface Water	24	<0.02 - 6.3	<0.02 - 3.8	3.3 - 24.5	<1.5 - 10.9	1.1 - 16.9	1.0 - 12.3
Ribeiro Guevara et al. (2008)	Lake Moreno (Argentina)	April 2007	Upper limit of metalimnion (30m depth)	72	27.3 - 50.8	15.4 - 23.5				
Bouchet et al. (2013)	Arcachon Bay (France)	2006 & 2007	Water column	24	<0.02 - 0.8	<0.02 - 1.1	1.8 - 11.9	1.3 - 9.0		
Sharif et al. (2014)	Adour river estuary (France)	2007 & 2010	Surface Water	24	<0.01 - 0.4	<0.01 - 0.1	6.6 - 55.3	<2.0 - 22.1	4.3 - 43.5	0.3 - 14.7
Alanoca et al. (2016)	Lake Uru Uru (Bolivia)	2010 & 2011	Surface Water	24	<0.02 - 4.9	<0.02 - 7.7	<0.02 - 21.0	<0.02 - 20.5	0.1 - 1.0	

Table 7.3: Methylation (M), Demethylation (D), Mercury Loss (ML) and Reduction (R) potentials (mean \pm SD, n=3 for M, D and ML, n=2 for R) in unfiltered waters performed under light and dark conditions at different depths for Lake Gentau for sampling campaigns Spring and Autumn 2018 and Spring 2019. Detection limits are 0.03, 4 and 0.3 % day⁻¹ for Methylation, Demethylation and Reduction yields, respectively. n.d. is not determined.

Reference	Location	Sampling period	Sampling Type	Incubation time (h)	iHg Methylation (%day ⁻¹)		MMHg Demethylation (%day ⁻¹)		MMHg Loss (%day ⁻¹)		Hg Reduction (%day ⁻¹)	
					Diurnal	Dark	Diurnal	Dark	Diurnal	Dark	Diurnal	Dark
This Work	Lake Gentau (Central Pyrenees)	Spring 2018	Subsurface (0.5m)	7,4	0.4 \pm 0.1	0.4 \pm 0.2	23.8 \pm 4.4	<LOD	44.5 \pm 4.4	7.8 \pm 1.9	60.8 \pm 1.8	2.4 \pm 4.1
			Middle Depth (8m)	8,5	<LOD	<LOD	13.6 \pm 1.2	<LOD	23.3 \pm 0.3	8.7 \pm 3.6	15.3 \pm 2.1	1.6 \pm 0.7
			Bottom (17m)	8,7	n.d.	4.3 \pm 0.4	n.d.	<LOD	n.d.	7.0 \pm 3.3	n.d.	<LOD
		Autumn 2018	Subsurface (0.5m)	7,2	<LOD	<LOD	23.9 \pm 2.9	<LOD	41.7 \pm 7.8	15.7 \pm 13.1	74.1 \pm 3.0	5.5 \pm 1.5
			Middle Depth (8m)	6,0	0.4 \pm 0.2	0.5 \pm 0.2	<LOD	<LOD	9.1 \pm 7.4	1.6 \pm 1.5	<LOD	<LOD
			Bottom (17m)	7,2	n.d.	6.8 \pm 0.6	n.d.	<LOD	n.d.	42.9 \pm 32.4	n.d.	<LOD
		Spring 2019	Subsurface (0.5m)	8,7	0.2 \pm 0.2	<LOD	35.6 \pm 2.2	<LOD	61.5 \pm 7.0	<LOD	63.5 \pm 4.9	0.8 \pm 0.7
			Middle Depth (8m)	8,5	<LOD	<LOD	13.6 \pm 0.4	<LOD	31.5 \pm 8.3	<LOD	12.9 \pm 4.7	0.7 \pm 1.5
			Bottom (17m)	8,5	n.d.	1.6 \pm 0.1	n.d.	<LOD	n.d.	<LOD	n.d.	<LOD

7.5. References

- [1] C.T. Driscoll, R.P. Mason, H.M. Chan, D.J. Jacob, N. Pirrone, Mercury as a Global Pollutant: Sources, Pathways, and Effects, *Environmental Science & Technology*. 47 (2013) 4967–4983. <https://doi.org/10.1021/es305071v>.
- [2] C.A. Cooke, A. Martínez-Cortizas, R. Bindler, M. Sexauer Gustin, Environmental archives of atmospheric Hg deposition – A review, *Science of The Total Environment*. 709 (2020) 134800. <https://doi.org/10.1016/j.scitotenv.2019.134800>.
- [3] J.P. Corella, M.J. Sierra, A. Garralón, R. Millán, J. Rodríguez-Alonso, M.P. Mata, A.V. de Vera, A. Moreno, P. González-Sampériz, B. Duval, D. Amouroux, P. Vivez, C.A. Cuevas, J.A. Adame, B. Wilhelm, A. Saiz-Lopez, B.L. Valero-Garcés, Recent and historical pollution legacy in high altitude Lake Marboré (Central Pyrenees): A record of mining and smelting since pre-Roman times in the Iberian Peninsula, *Science of The Total Environment*. 751 (2021) 141557. <https://doi.org/10.1016/j.scitotenv.2020.141557>.
- [4] J. Wiener, D. Krabbenhoft, G. Heinz, A. Scheuhammer, Ecotoxicology Of Mercury, in: D. Hoffman, B. Rattner, G. Allen Burton Jr, J. Cairns Jr (Eds.), *Handbook of Ecotoxicology*, Second Edition, CRC Press, 2002. <https://doi.org/10.1201/9781420032505.ch16>.
- [5] J. Aaseth, B. Hilt, G. Bjørklund, Mercury exposure and health impacts in dental personnel, *Environmental Research*. 164 (2018) 65–69. <https://doi.org/10.1016/j.envres.2018.02.019>.
- [6] F. Khan, S. Momtaz, M. Abdollahi, The relationship between mercury exposure and epigenetic alterations regarding human health, risk assessment and diagnostic strategies, *Journal of Trace Elements in Medicine and Biology*. 52 (2019) 37–47. <https://doi.org/10.1016/j.jtemb.2018.11.006>.
- [7] UNEP, 2013, *Global Mercury Assessment 2013: Sources, Emissions, Releases and Environmental Transport*, (n.d.).
- [8] E.M. Sunderland, Mercury Exposure from Domestic and Imported Estuarine and Marine Fish in the U.S. Seafood Market, *Environmental Health Perspectives*. 115 (2007) 235–242. <https://doi.org/10.1289/ehp.9377>.
- [9] H. Hintelmann, K. Keppel-Jones, R.D. Evans, Constants of mercury methylation and demethylation rates in sediments and comparison of tracer and ambient mercury availability, *Environmental Toxicology and Chemistry*. 19 (2000) 2204–2211. <https://doi.org/10.1002/etc.5620190909>.
- [10] N.E. Selin, Global Biogeochemical Cycling of Mercury: A Review, *Annual Review of Environment and Resources*. 34 (2009) 43–63. <https://doi.org/10.1146/annurev.enviro.051308.084314>.
- [11] A.J. Poulain, T. Barkay, Cracking the Mercury Methylation Code, *Science*. 339 (2013) 1280–1281. <https://doi.org/10.1126/science.1235591>.
- [12] K. Sundseth, J.M. Pacyna, E.G. Pacyna, J. Munthe, M. Belhaj, S. Astrom, Economic benefits from decreased mercury emissions: Projections for 2020, *Journal of Cleaner Production*. 18 (2010) 386–394. <https://doi.org/10.1016/j.jclepro.2009.10.017>.
- [13] F.M.M. Morel, A.M.L. Kraepiel, M. Amyot, THE CHEMICAL CYCLE AND BIOACCUMULATION OF MERCURY, *Annual Review of Ecology and Systematics*. 29 (1998) 543–566. <https://doi.org/10.1146/annurev.ecolsys.29.1.543>.
- [14] S.M. Ullrich, T.W. Tanton, S.A. Abdrashitova, Mercury in the Aquatic Environment: A Review of Factors Affecting Methylation, *Critical Reviews in Environmental Science and Technology*. 31 (2001) 241–293. <https://doi.org/10.1080/20016491089226>.
- [15] G.C. Compeau, R. Bartha, Sulfate-Reducing Bacteria: Principal Methylators of Mercury in Anoxic Estuarine Sedimentt, *APPL. ENVIRON. MICROBIOL.* (n.d.) 5.
- [16] R. Bridou, M. Monperrus, P.R. Gonzalez, R. Guyoneaud, D. Amouroux, Simultaneous determination of mercury methylation and demethylation capacities of various sulfate-reducing bacteria using species-specific isotopic tracers, *Environmental Toxicology and Chemistry*. 30 (2011) 337–344. <https://doi.org/10.1002/etc.395>.

- [17] J.P. Corella, A. Saiz-Lopez, M.J. Sierra, M.P. Mata, R. Millán, M. Morellón, C.A. Cuevas, A. Moreno, B.L. Valero-Garcés, Trace metal enrichment during the Industrial Period recorded across an altitudinal transect in the Southern Central Pyrenees, *Science of The Total Environment*. 645 (2018) 761–772. <https://doi.org/10.1016/j.scitotenv.2018.07.160>.
- [18] S. Guédron, D. Point, D. Acha, S. Bouchet, P.A. Baya, E. Tessier, M. Monperrus, C.I. Molina, A. Groleau, L. Chauvaud, J. Thebault, E. Amice, L. Alanoca, C. Duwig, G. Uzu, X. Lazzaro, A. Bertrand, S. Bertrand, C. Barbraud, K. Delord, F.M. Gibon, C. Ibanez, M. Flores, P. Fernandez Saavedra, M.E. Ezpinoza, C. Heredia, F. Rocha, C. Zepita, D. Amouroux, Mercury contamination level and speciation inventory in Lakes Titicaca & Uru-Uru (Bolivia): Current status and future trends, *Environmental Pollution*. 231 (2017) 262–270. <https://doi.org/10.1016/j.envpol.2017.08.009>.
- [19] L. Alanoca, D. Amouroux, M. Monperrus, E. Tessier, M. Goni, R. Guyoneaud, D. Acha, C. Gassie, S. Audry, M.E. Garcia, J. Quintanilla, D. Point, Diurnal variability and biogeochemical reactivity of mercury species in an extreme high-altitude lake ecosystem of the Bolivian Altiplano, *Environmental Science and Pollution Research*. 23 (2016) 6919–6933. <https://doi.org/10.1007/s11356-015-5917-1>.
- [20] N. Maruszczak, C. Larose, A. Dommergue, S. Paquet, J.-S. Beaulne, R. Maury-Brachet, M. Lucotte, R. Nedjai, C.P. Ferrari, Mercury and methylmercury concentrations in high altitude lakes and fish (Arctic charr) from the French Alps related to watershed characteristics, *Science of The Total Environment*. 409 (2011) 1909–1915. <https://doi.org/10.1016/j.scitotenv.2011.02.015>.
- [21] C.S. Eckley, H. Hintelmann, Determination of mercury methylation potentials in the water column of lakes across Canada, *Science of The Total Environment*. 368 (2006) 111–125. <https://doi.org/10.1016/j.scitotenv.2005.09.042>.
- [22] M. Monperrus, E. Tessier, D. Amouroux, A. Leynaert, P. Huonnic, O.F.X. Donard, Mercury methylation, demethylation and reduction rates in coastal and marine surface waters of the Mediterranean Sea, *Marine Chemistry*. 107 (2007) 49–63. <https://doi.org/10.1016/j.marchem.2007.01.018>.
- [23] S. Ribeiro Guevara, C.P. Queimaliños, M. del C. Diéguez, M. Arribére, Methylmercury production in the water column of an ultraoligotrophic lake of Northern Patagonia, Argentina, *Chemosphere*. 72 (2008) 578–585. <https://doi.org/10.1016/j.chemosphere.2008.03.011>.
- [24] S. Bouchet, D. Amouroux, P. Rodriguez-Gonzalez, E. Tessier, M. Monperrus, G. Thouzeau, J. Clavier, E. Amice, J. Deborde, S. Bujan, J. Grall, P. Anschutz, MMHg production and export from intertidal sediments to the water column of a tidal lagoon (Arcachon Bay, France), *Biogeochemistry*. 114 (2013) 341–358. <https://doi.org/10.1007/s10533-012-9815-z>.
- [25] A. Sharif, M. Monperrus, E. Tessier, S. Bouchet, H. Pinaly, P. Rodriguez-Gonzalez, P. Maron, D. Amouroux, Fate of mercury species in the coastal plume of the Adour River estuary (Bay of Biscay, SW France), *Science of The Total Environment*. 496 (2014) 701–713. <https://doi.org/10.1016/j.scitotenv.2014.06.116>.
- [26] E. Gascón Díez, J.-L. Loizeau, C. Cosio, S. Bouchet, T. Adatte, D. Amouroux, A.G. Bravo, Role of Settling Particles on Mercury Methylation in the Oxic Water Column of Freshwater Systems, *Environmental Science & Technology*. 50 (2016) 11672–11679. <https://doi.org/10.1021/acs.est.6b03260>.
- [27] C.A. Emmerton, C.A. Cooke, G.R. Wentworth, J.A. Graydon, A. Ryjkov, A. Dastoor, Total Mercury and Methylmercury in Lake Water of Canada's Oil Sands Region, *Environmental Science & Technology*. 52 (2018) 10946–10955. <https://doi.org/10.1021/acs.est.8b01680>.
- [28] A.G. Bravo, S. Bouchet, J. Tolu, E. Björn, A. Mateos-Rivera, S. Bertilsson, Molecular composition of organic matter controls methylmercury formation in boreal lakes, *Nature Communications*. 8 (2017). <https://doi.org/10.1038/ncomms14255>.
- [29] K.R. Rolfhus, H.E. Sakamoto, L.B. Cleckner, R.W. Stoor, C.L. Babiarz, R.C. Back, H. Manolopoulos, J.P. Hurley, Distribution and Fluxes of Total and Methylmercury in Lake Superior, *Environmental Science & Technology*. 37 (2003) 865–872. <https://doi.org/10.1021/es026065e>.
- [30] C. Meuleman, M. Leermakers, W. Baeyens, Mercury speciation in Lake Baikal, *Water, Air, & Soil Pollution*. 80 (1995) 539–551. <https://doi.org/10.1007/BF01189704>.

- [31] E.A. Malczyk, B.A. Branfireun, Mercury in sediment, water, and fish in a managed tropical wetland-lake ecosystem, *Science of The Total Environment*. 524–525 (2015) 260–268. <https://doi.org/10.1016/j.scitotenv.2015.04.015>.
- [32] W.F. Fitzgerald, C.H. Lamborg, C.R. Hammerschmidt, Marine Biogeochemical Cycling of Mercury, *Chemical Reviews*. 107 (2007) 641–662. <https://doi.org/10.1021/cr050353m>.
- [33] J. Cavalheiro, C. Sola, J. Baldanza, E. Tessier, F. Lestremau, F. Botta, H. Preud'homme, M. Monperrus, D. Amouroux, Assessment of background concentrations of organometallic compounds (methylmercury, ethyllead and butyl- and phenyltin) in French aquatic environments, *Water Research*. 94 (2016) 32–41. <https://doi.org/10.1016/j.watres.2016.02.010>.
- [34] M. Amyot, G. Mierle, D. Lean, D.J. Mc Queen, Effect of solar radiation on the formation of dissolved gaseous mercury in temperate lakes, *Geochimica et Cosmochimica Acta*. 61 (1997) 975–987. [https://doi.org/10.1016/S0016-7037\(96\)00390-0](https://doi.org/10.1016/S0016-7037(96)00390-0).
- [35] K.R. Rolfhus, W.F. Fitzgerald, The evasion and spatial/temporal distribution of mercury species in Long Island Sound, CT-NY, *Geochimica et Cosmochimica Acta*. 65 (2001) 407–418. [https://doi.org/10.1016/S0016-7037\(00\)00519-6](https://doi.org/10.1016/S0016-7037(00)00519-6).
- [36] N.J. O'Driscoll, D.R.S. Lean, L.L. Loseto, R. Carignan, S.D. Siciliano, Effect of Dissolved Organic Carbon on the Photoproduction of Dissolved Gaseous Mercury in Lakes: Potential Impacts of Forestry, *Environmental Science & Technology*. 38 (2004) 2664–2672. <https://doi.org/10.1021/es034702a>.
- [37] M. Enrico, G.L. Roux, N. Maruszczak, L.-E. Heimbürger, A. Claustres, X. Fu, R. Sun, J.E. Sonke, Atmospheric Mercury Transfer to Peat Bogs Dominated by Gaseous Elemental Mercury Dry Deposition, *Environmental Science & Technology*. 50 (2016) 2405–2412. <https://doi.org/10.1021/acs.est.5b06058>.
- [38] N. Maruszczak, C. Larose, A. Dommergue, E. Yumvihoze, D. Lean, R. Nedjai, C. Ferrari, Total mercury and methylmercury in high altitude surface snow from the French Alps, *Science of The Total Environment*. 409 (2011) 3949–3954. <https://doi.org/10.1016/j.scitotenv.2011.06.040>.
- [39] M. Monperrus, E. Tessier, D. Point, K. Vidimova, D. Amouroux, R. Guyoneaud, A. Leynaert, J. Grall, L. Chauvaud, G. Thouzeau, O.F.X. Donard, The biogeochemistry of mercury at the sediment–water interface in the Thau Lagoon. 2. Evaluation of mercury methylation potential in both surface sediment and the water column, *Estuarine, Coastal and Shelf Science*. 72 (2007) 485–496. <https://doi.org/10.1016/j.ecss.2006.11.014>.
- [40] P. Lei, L.M. Nunes, Y.-R. Liu, H. Zhong, K. Pan, Mechanisms of algal biomass input enhanced microbial Hg methylation in lake sediments, *Environment International*. 126 (2019) 279–288. <https://doi.org/10.1016/j.envint.2019.02.043>.
- [41] A.G. Bravo, D.N. Kothawala, K. Attermeyer, E. Tessier, P. Bodmer, J.L.J. Ledesma, J. Audet, J.P. Casas-Ruiz, N. Catalán, S. Cauvy-Fraunié, M. Colls, A. Deininger, V.V. Evtimova, J.A. Fonvielle, T. Fuß, P. Gilbert, S. Herrero Ortega, L. Liu, C. Mendoza-Lera, J. Monteiro, J.-R. Mor, M. Nagler, G.H. Niedrist, A.C. Nydahl, A. Pastor, J. Pegg, C. Gutmann Roberts, F. Pilotto, A.P. Portela, C.R. González-Quijano, F. Romero, M. Rulík, D. Amouroux, The interplay between total mercury, methylmercury and dissolved organic matter in fluvial systems: A latitudinal study across Europe, *Water Research*. 144 (2018) 172–182. <https://doi.org/10.1016/j.watres.2018.06.064>.

8. Mercury stable isotopes in lacustrine archives to tracking human pollution and climate variability during the last 2000 years in the southern central Pyrenees (Aragon, Spain)

8.1. Abstract

Mercury (Hg) isotopic composition variability in lake sediment sequences reflects Hg cycling processes at different levels of the global Hg cycle, including atmospheric trends and more local characteristics controlling watershed-lake interactions. The impact of climate change and anthropogenic emissions on Hg cycling in these ecosystems is preserved in sediment sequences, yet some uncertainties persist on the long-term Human impact on pristine oligotrophic lakes. In this work, two sediment cores from Southern Central Pyrenean lakes have been investigated: Estanya (karstic lake, 670 m asl., core dated last 4 ka) and Marboré (alpine lake, 2612 m asl., core dated last 3 ka). The two study sites show similarities, including small surface lake areas, moderate depths and middle-sized watersheds made up mostly of carbonated bedrock. Nevertheless, bioclimatic conditions are substantially different with lower temperature and higher precipitations in the alpine Lake Marboré. In addition, catchment influences on the biogeochemical characteristics of Lake Estanya are much more important because of the denser vegetation cover surrounding the lake (Mediterranean forest and agricultural fields), the long history of human activities in the watershed and the strong control of groundwater input in the hydrological balance. Determination of total Hg content by pyrolysis gold amalgamation-AAS provide a historical record of the Hg inputs. Besides, Hg stable isotope signatures (MC-ICP-MS) are used as tracers of Hg cycling (MDF- $\delta^{202}\text{Hg}$ and odd MIF- $\Delta^{199}\text{Hg}$), and Hg deposition pathway (even MIF- $\delta^{200}\text{Hg}$ wet vs dry Hg deposition). Temporal trends in Hg accumulation rates (HgARs) show a consistent evolution with low background values ($4.8 \pm 1.0 \mu\text{g m}^{-2} \text{y}^{-1}$ and $14.4 \pm 1.7 \mu\text{g m}^{-2} \text{y}^{-1}$ until the 16th century for Estanya and Marbore lakes, respectively) and a progressive increase since the 16th Century mirroring the mercury production in Almadén Hg mines (Southern Spain). Corresponding shifts in Hg isotope results also highlights this trend, with an Industrial Period characterized by higher odd MIF- $\Delta^{199}\text{Hg}$ values ($0.21 \pm 0.09 \text{‰}$ and $0.26 \pm 0.09 \text{‰}$ at Estanya and Marbore, respectively) compared to pre-16th Century ($0.04 \pm 0.07 \text{‰}$ and $-0.09 \pm 0.05 \text{‰}$ at Estanya and Marbore, respectively). Overall, the records presented here parallel the results derived from previous investigation of Hg deposition using Estibere peat record (2100 m asl., Southern Central Pyrenees). The distinct watershed characteristics of the two investigated lakes are reflected in Hg isotope fingerprints (MIF- $\Delta^{200}\text{Hg}$) as well, with Estanya being more influenced by dry deposition (low $\Delta^{200}\text{Hg}$) than Marboré predomindaly influenced by wet depositions (higher $\Delta^{200}\text{Hg}$, rain and snow).

Keywords:

Mercury; Isotopes; Lake Sediments; Oligotrophic; Pyrenees

8.2. Introduction

Mercury (Hg) is a global pollutant present in all compartments of the Earth that affects human and ecosystem health [1–3]. Primary anthropogenic Hg emissions greatly exceed natural sources by a factor of 2–15 [4,5], and caused increases in Hg reservoirs during the last millennia. The global annual mean lifetime of Hg(0) against the net photochemical oxidation is estimated to be about 1 year [6], and recent findings on the rapid photochemistry of oxidized mercury have postulated that global atmospheric Hg lifetime could increase by a factor 2 [7,8]. While natural primary emission of Hg from geogenic sources consisting in the release of Hg from the continental crust through natural weathering, hydrothermal activities, natural fires and volcanic degassing, anthropogenic emissions include the use of fossil fuels (mainly coal burning), artisanal and small-scale gold mining, iron and non-ferrous metals production, cement production, oil refining and wastes from consumer products [9].

Mercury concentration records derived from natural archives such as lake sediments [10], peat [11] and ice cores [12,13] have already highlighted the influence of anthropogenic activities on the atmospheric Hg deposition with a clear increase since Roman times. *Martínez-Cortizas et al.* [14] proposed the use of the thermal lability of the accumulated mercury in a peat bog as a tool for quantitative paleotemperature reconstruction: to our knowledge, this is the only relevant study relating such conclusion, and none exists for lakes.

The various environmental archives display different enrichment factor depending on their nature or location [4,15]. This is a reflexion of the complex biogeochemical cycle of Hg where deposition of Hg is controlled not only by overall emissions but also by local to regional processes related to emission, transport, redox chemistry, deposition and re-emission [5,16].

On one hand, ombrotrophic mires record the atmospheric mercury pollution [14,17]. Unfortunately, they may suffer from aerial exposure and diagenetic processes altering mercury levels [11,18]. Mercury evasion has also been reported recently in boreal peatland [19], mainly as a result of emission of gaseous elemental Hg and through THg stream discharge: both phenomena may have implications for the estimation of historical Hg accumulation rates from peat profiles. On the other hand, lacustrine sedimentary sequences do not suffer from apparent losses of total mercury concentration in the sediment [20]. However, they often show a mixed-signal between run-off and atmospheric Hg inputs. Furthermore, metal remobilization and redox changes in the water column may affect mercury concentrations [11]. Among lacustrine archives, high-altitude lakes have well demonstrated their use as a proxy of past global atmospheric mercury pollution since i) they have small watersheds and they are scarcely affected by local anthropogenic activities so they can be considered conservative ecosystems overtime; ii) they are emplaced in regional convergence regions of atmospheric pollutants and iii) their oligotrophic status reduces in-situ transformations [16].

Mercury isotopic composition offers new insights to Hg cycling processes in the environment. Mercury has seven stable isotopes that undergo Mass Dependent Fractionation (MDF, $\delta^{202}\text{Hg}$) during both kinetic and equilibrium reactions as a result of many physical, chemical or biological processes such as

evaporation, microbial reduction of Hg(II) and demethylation of MeHg, photochemical reactions, trophic and metabolic processes [21]. Mass Independent Fractionation (MIF) also occurs for Hg isotopes, especially during light induced reactions. While important odd-MIF ($\Delta^{199}\text{Hg}$, $\Delta^{201}\text{Hg}$) is primarily related to photochemical reactions such as photoreduction of both Hg(II) and MeHg [22], the mechanism responsible of positive even-MIF ($\Delta^{200}\text{Hg}$, $\Delta^{204}\text{Hg}$) in rainfall and snow is not well understood [23,24]. A recent study suggested that this fractionation is probably triggered by photo-initiated oxidation occurring on aerosol or solid surfaces in the tropopause [23].

Numerous studies have recorded historical variations of Hg isotopic fingerprints in lake sediments [24–31], ice core [32] and peat cores [18,33]. *Enrico et al.* [18,33] used the distinct, conservative even-MIF signatures of rainfall and atmospheric gaseous Hg(0) to discriminate the main deposition pathways in two remote peatlands and reconstructed past atmospheric Hg levels. Dry deposition, characterized by slightly negative $\Delta^{200}\text{Hg}$ [18,34], involves foliar uptake of Hg(0) [35], whereas wet deposition, with positive $\Delta^{200}\text{Hg}$ [18,23], involves the scavenging of gas-phase and aerosol-phase Hg(II) by cloud droplets. For MDF and odd-MIF, a widely observed significant change in the Hg isotopic signatures occurs in sedimentary archives for periods corresponding to the beginning of anthropogenic activities and exhibits increasing $\delta^{202}\text{Hg}$ and $\Delta^{199}\text{Hg}$ values either due to local or regional industrial development [24,26,30–33].

In the Central Pyrenees, trace metals, Pb and Hg pollution has been linked with the intensive exploitation of Almadén mines and local smelting [16,36,37]. Data from an altitudinal transect of lakes in the central southern Pyrenees suggests that limnological parameters explain the differences between enrichment factors for some trace metals [16].

Several recent studies have described changes in Hg deposition in Pyrenean lakes and peatlands during the last millennia [18,33,37]. In this study, we have selected two of the best dated lacustrine sedimentary sequences from Southern Central Pyrenees along an altitudinal gradient to test climate, anthropogenic and site-specific forcing in Hg deposition during the last 4 ka. Mercury concentration and isotopic analyses in these lacustrine records are used to determine the main Hg deposition pathways, Hg pollution sources and evaluate the use of Hg isotopes as a paleohydrological and paleoclimate proxy and indicator of variable human impact.

8.3. Material and Methods

8.3.1. Study Site

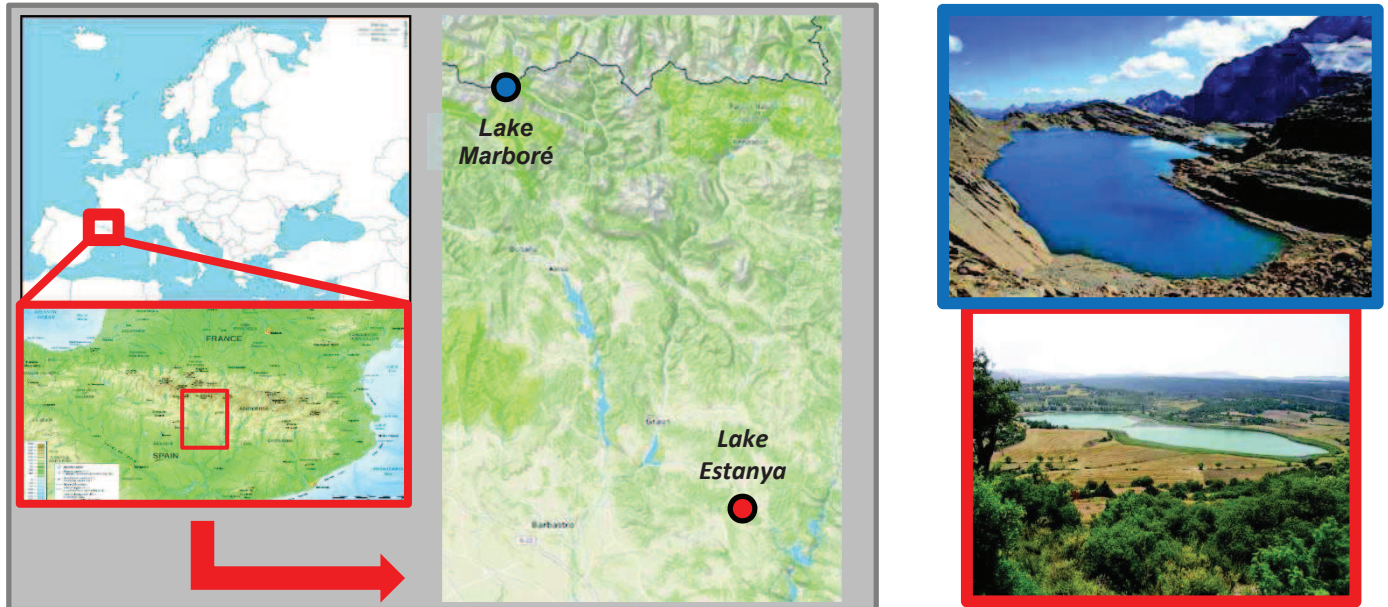


Figure 8.1: Study Sites: Lakes Marboré (42°41'N; 0°2'E, 2612 m asl) and Estanya (42°02'N; 0°32'E, 670 m asl)

The two studied lacustrine ecosystems (**Figure 8.1**), Lake Marboré (42°41'N; 0°2'E, 2612 m asl) and Lake Estanya (42°02'N; 0°32'E, 670 m asl), are located in the Southern Central Pyrenees. They show similarities with small surface lake areas of 14.3 and 18.8 ha, small-sized watersheds of 137 and 106 ha and maximum depths of 30 and 24 m in Lakes Marboré and Estanya respectively [38,39]. The watersheds of both lakes are emplaced in carbonate bedrocks [16]. On the other hand, bioclimatic conditions in both lakes greatly differ with lower temperatures and higher precipitation in Lake Marboré (mean temperatures and precipitation of 5°C and 2000 mm) compared to Lake Estanya (mean temperatures and precipitation of 14°C and 470 mm) [39].

Lake Marboré is a high-alpine lake located above the tree line. Therefore, the vegetation cover around the lake is very scarce with only a few remains of alpine rocky grass species [40]. The lake has a maximum depth of 30 m. The lake's hydrology is controlled by precipitation/evaporation balance, meltwater input along a small NW inlet and outputs through a surface outlet located in the southern area and some groundwater fluxes [39,41]. It is a cold dimictic and ultra-oligotrophic lake with alkaline waters. Ice and snow cover Lake Marboré surface from December to July [42].

Lake Estanya is a karstic lake emplaced in Triassic carbonate, marls and claystones [43,44]. It is a monomictic lake with brackish and oligotrophic waters, and a maximum lake's water depth of 24 m [44]. Mean annual temperature is 14 °C, ranging from 4 °C to 24 °C [38]. Vegetation in the watershed consists of scrublands and oak forest in the high-elevated areas while the lowlands are mostly dedicated to barley cultivation [44].

8.3.2. Sediment sequence and age-depth models

Both lake sequences have been intensively studied from sedimentological, geochemical and palynological points of view [45] and have robust ^{14}C and ^{210}Pb and ^{137}Cs – based age models. Sediment cores were retrieved from the deepest area of the studied lakes using a UWITEC (MAR11-1U sediment core, 27 m depth, 2011) [46] and Kulleberg (LEG04-1K sediment core, 24 m depth, 2004) [44] floating platforms for Lake Marboré and Lake Estanya respectively. UWITEC gravity cores were additionally collected to preserve the uppermost sediments and the water-sediment interphase in both lakes (MAR11-1G-1U, LEG1A-1M sediment cores) [38,46].

The age-depth models in the two lakes are based on ^{137}Cs , ^{210}Pb and Accelerator Mass Spectrometry (AMS) ^{14}C radiometric dating techniques. The Holocene chronology for the Lake Marboré and Estanya sediment sequences was developed using 10 and 11 AMS ^{14}C dates respectively. ^{210}Pb and ^{137}Cs radiometric dating was applied for the recent sediment in both lakes. Mean annual sedimentation rate (SR) in Lake Marboré was constant during the Late Holocene (SR $\approx 0.6 \text{ mm yr}^{-1}$) while SR in Lake Estanya ranged from 0.2 to 2.1 mm yr^{-1} [38,40,44,46].

The selected section for Marboré Lake spans the last 3 ka and it is composed of laminated to banded fine silts composed of silicate minerals and very low organic and carbonate content [46]. The Estanya section spans the last 4 ka and include carbonate-rich silts of mainly detrital origin deposited under relatively high lake level conditions and increased runoff and organic-rich facies with gypsum formed under shallower conditions [38,44]. The reconstructed depositional evolution reflects the impact of climate variability in both lakes and a strong impact of human activities (deforestation, agriculture) in Estanya at least since the 10th century.

8.3.3. Mercury concentrations and fluxes

Mercury analyses were carried out in discrete samples retrieved downcore in the studied cores (27 samples selected for Marboré and 14 samples selected for Estanya). Total Hg concentration measurements were carried out by Cold Vapor Atomic Absorption Spectrophotometry (CV-AAS) using an advance Mercury Analyzer (AMA 254, LECO Company). Certified reference materials (CRM) were used to determine the accuracy and precision of the Hg measurements. These reference materials were ZC73027 (rice, $4.8 \pm 0.8 \mu\text{g kg}^{-1}$) and CRM051–050 (Clay soil, $4.08 \pm 0.09 \text{ mg kg}^{-1}$). The repeatability was $S_r \leq 15\%$ and the relative uncertainty associated with the method ($k = 2$) was $\pm 20\%$. All analyses were run at least in triplicate. Total metal concentrations are expressed in $\mu\text{g g}^{-1}$ of dry weight sediment.

Mass accumulation rates for mercury depositional fluxes estimation (HgAR) were calculated as the product of their concentration in the sediment, the dry bulk density of the sediment, and sedimentation rates according to *Givelet et al.* [47].

8.3.4. Mercury stable isotopes composition

The analytical protocol for the determination of mercury isotopes in sediments is derived from various studies previously conducted [26,48]. Before Hg isotopic analysis, sediment samples (0.5 - 1 g) were first pre-digested overnight at room temperature in a Teflon tube using 3 mL of nitric acid (65 %, INSTRA quality). After addition of 1 mL of hydrochloric acid (37 %, INSTRA quality), extraction of Hg was carried out using a Hotblock at 85 °C (6 h plus 3 h after the addition of about 1.3 mL of hydrogen peroxide (30 %, ULTREX quality). Then, an aliquot of about 1.5 mL was recovered in an Eppendorf Safe-Lock tube and centrifuged at 14 500 rpm for 90 seconds. The supernatant was collected and diluted for isotopic measurements (10 % HNO₃, 2 % HCl, either 0.5 or 1 ppb of Hg depending on the analytical session). Hg isotopic composition was determined using a cold-vapour generator (CVG) with SnCl₂ reduction coupled with MC-ICPMS (Nu Instruments). NIST SRM-997 thallium standard solution was used for mass-bias correction. Sample standard bracketing with NIST SRM-3133 was conducted to report Hg isotopic values as delta notation to allow inter-laboratory comparisons [49]:

Equation 8.1

$$\delta^{xxx}Hg (\text{‰}) = \left[\left(\frac{\left(\frac{^{xxx}Hg}{^{198}Hg} \right)_{sample}}{\left(\frac{^{xxx}Hg}{^{198}Hg} \right)_{NIST\ 3133}} \right) - 1 \right] \times 1000$$

where xxx is the mass of each Hg isotope between 199 and 204, ¹⁹⁸Hg is used as a reference because it is one of the lighters mercury isotopes (¹⁹⁶Hg has a too-small abundance).

Mass Independent Fractionation (MIF) anomalies are expressed with the Δ notation, quantifying the difference between the measured isotope ratio δ^{xxx}Hg and the theoretical value δ^{xxx}Hg_{theo}, calculated based on the Mass Dependent Fractionation (MDF) fractionation laws. As for the δ notation, we report Hg MIF anomalies as proposed by Blum and Bergquist [49] to ensure data comparison:

Equation 8.2

$$\Delta^{199}Hg = \delta^{199}Hg_{exp} - \delta^{202}Hg_{theo} \times 0.2520$$

$$\Delta^{200}Hg = \delta^{200}Hg_{exp} - \delta^{202}Hg_{theo} \times 0.5024$$

$$\Delta^{201}Hg = \delta^{201}Hg_{exp} - \delta^{202}Hg_{theo} \times 0.7520$$

$$\Delta^{204}Hg = \delta^{204}Hg_{exp} - \delta^{202}Hg_{theo} \times 1.4930$$

To validate each analytical session, reference material NIST-8610 (UM-Almadén) was analyzed regularly (n=32). The uncertainty on Hg isotope ratios is evaluated using multiple analyses of a procedural CRM (IAEA-405, estuarine sediment) prepared using a procedure similar to samples. Results obtained for these two CRM are shown in **Table 8.1**. In this manuscript, all reported analytical uncertainties for Hg isotopic values are presented as 2SD of IAEA-405.

Sample standard bracketing with NIST SRM-3133 also allowed us to calculate a Hg recovery related to the extraction of Hg from the sediment samples. For Lake Marboré, recovery was 100 ± 9 % (n=27,

range from 77 to 122 %) whereas, for Lake Estanya, recovery was $87 \pm 9 \%$ (n=14, range from 70 to 100 %). Even if there is an apparent lower recovery for lake Estanya samples, probably due to a more complex matrix (higher organic matter), the recoveries are within the uncertainty of total Hg analysis by CV-AAS and precision of the MC-ICPMS.

Table 8.1: Mean values (\pm 2SD) of Hg isotopic composition obtained for reference materials: NIST-8610 (UM-Almadén) and IAEA-405 (estuarine sediment)

Sample	Reference	n	$\delta^{204}\text{Hg}$ ‰	$\delta^{202}\text{Hg}$ ‰	$\delta^{201}\text{Hg}$ ‰	$\delta^{200}\text{Hg}$ ‰	$\delta^{199}\text{Hg}$ ‰	$\Delta^{204}\text{Hg}$ ‰	$\Delta^{201}\text{Hg}$ ‰	$\Delta^{200}\text{Hg}$ ‰	$\Delta^{199}\text{Hg}$ ‰
NIST RM 8610	This study	32	-0.78 ± 0.18	-0.52 ± 0.12	-0.42 ± 0.12	-0.26 ± 0.10	-0.12 ± 0.14	0.00 ± 0.14	-0.03 ± 0.07	0.00 ± 0.06	-0.01 ± 0.12
	Reference values		-0.82 ± 0.07	-0.56 ± 0.03	-0.46 ± 0.02	-0.27 ± 0.01	-0.17 ± 0.01	-	-0.04 ± 0.01	0.00 ± 0.01	-0.03 ± 0.02
IAEA 405	This study	7	-0.57 ± 0.15	-0.39 ± 0.09	-0.30 ± 0.13	-0.20 ± 0.08	-0.11 ± 0.06	0.02 ± 0.08	0.00 ± 0.08	0.00 ± 0.05	-0.01 ± 0.06
	Moreno et al., [48]	14	-0.62 ± 0.21	-0.41 ± 0.16	-0.31 ± 0.19	-0.19 ± 0.12	-0.12 ± 0.11	-	-0.01 ± 0.09	0.01 ± 0.06	-0.02 ± 0.08
	Guédron et al. [26]	14	-0.50 ± 0.17	-0.30 ± 0.11	-0.29 ± 0.07	-0.22 ± 0.11	-0.17 ± 0.15	-	-0.06 ± 0.06	-0.07 ± 0.13	-0.10 ± 0.15
NIST 1944	IPREM (2011-2015)	15	-0.68 ± 0.17	-0.44 ± 0.14	-0.32 ± 0.18	-0.23 ± 0.13	-0.11 ± 0.12	-	0.01 ± 0.12	-0.01 ± 0.10	-0.00 ± 0.11
	Sherman and Blum [50]	9	-	-0.44 ± 0.12	-0.34 ± 0.08	-0.22 ± 0.05	-0.10 ± 0.04	-	-0.01 ± 0.05	-	0.01 ± 0.04
	Sonke et al., [51]	3	-	-0.48 ± 0.29	-	-	-	-	-	-	0.02 ± 0.05
	Ma et al., [52]	5	-	-0.45 ± 0.06	-	-	-	-	-	-	-0.03 ± 0.02
	Biswas et al., [53]	10	-	-0.42 ± 0.07	-	-	-	-	-0.02 ± 0.01	-	-0.02 ± 0.01

8.4. Results and Discussion

8.4.1. Variability of mercury accumulation rates

In both lakes, Marboré and Estanya, three distinct periods can be distinguished according to the changes in Hg deposition (**Figure 8.2.a**).

In Lake Marboré, background values of Hg fluxes (i.e. until 1500 CE) average $14.4 \pm 1.7 \mu\text{g m}^{-2} \text{y}^{-1}$ (n=12) whereas in Lake Estanya (i.e. until 1500 CE) a lower flux of about $4.8 \pm 1.0 \mu\text{g m}^{-2} \text{y}^{-1}$ (n=5) was found. It is worth noting that these are not natural background values since Hg production has occurred intermittently since the Roman Period [54]. Lake Estanya record is consistent with other pre-anthropogenic Hg fluxes recorded in North America lakes [10,24,30] and peatland from Central Pyrenees [33]. An important natural HgAR, such as in Lake Marboré, has also been noticed in Lake Montcortés with around $30 \mu\text{g m}^{-2} \text{y}^{-1}$ [36] and in Lake August with around $13.2 \mu\text{g m}^{-2} \text{y}^{-1}$ [10] for the pre-anthropogenic period. High HgAR in some Pyrenean Lakes (Marboré, Montcortés) could be related to specific characteristics of the catchments and geographical factors favouring Hg deposition. The Marboré consists of bare rock and very scarce vegetation while Lake Estanya is surrounded by forest and agricultural fields **Figure 8.1**. Moreover, Lake Marboré is ice-covered about 8 months per year [42], and snow is known to be a large reservoir that accumulates Hg until its melting [55]. Inputs from accumulated snow from the catchment and the lake surface could lead to an important HgAR during the sudden annual snowmelt in summer [56]. This may also promote efficient Hg transport to the lake bottom with very little Hg recycling and re-emission from water column processes. Another possible explanation for the difference between HgAR can simply be the nature of the bedrock, and the weathering of the soluble bedrocks, more enriched in Hg in Lake Marboré catchment. Moreover, enrichment factors of both lake Marboré and Lake Estanya [16] are comparable with other records from the remote area cited above, supporting the fact that this difference in HgAR is related with lake and catchment specific features rather than sources or deposition processes.

Then, Modern Period (MP) displays a progressive increase in HgAR for both Lake Marboré (i.e. 1500-1890 CE) and Lake Estanya (i.e. 1500-1780 CE), with HgAR respectively of $24.6 \pm 10.4 \mu\text{g m}^{-2} \text{y}^{-1}$ (n=8) and $22.6 \pm 2.3 \mu\text{g m}^{-2} \text{y}^{-1}$ (n=2). This trend corresponds to the increase in mercury production worldwide and especially in Almadén mines. It is worth noting that the increase in HgAR in North America lakes started later (the 1850s) [24,30] coinciding with the onset of mercury production in North America [57]. This difference between environmental archives from both continents suggests that mercury deposited in remote lakes is coming from local to regional sources rather than global ones [15].

The last period corresponds to the Industrial Period (IP) and is well observed in Lake Marboré (1890-2000 CE) with HgAR of $49.2 \pm 11.7 \mu\text{g m}^{-2} \text{y}^{-1}$ (n=6) and in Lake Estanya (1780-1980 CE) with HgAR of $46.0 \pm 7.3 \mu\text{g m}^{-2} \text{y}^{-1}$ (n=5). It is noticeable that although the background levels are different in both lakes, the modern and industrial HgAR values are quite similar. These remarkable increases parallel the Hg production in Almadén [16,36] and are followed by decreases in recent years in both lakes (since 1970 and 1940 CE for Marboré and Estanya, respectively). This earlier late-industrial decline in HgAR is also

observed in recent lake sediment [24,26,30] and peat cores [33] and corresponds with the local to regional decline in Hg emissions due to the deindustrialization of metal industries and mine closure in Europe, as well as improved technologies to avoid Hg emissions from coal power plants, chlor-alkali plants and waste incinerators [9], thanks to policy stringer requirement (Clean Water Act in North America, recent European laws enforcements). Depending on its location and on local anthropogenic activities, the studied natural archives show this decrease at slightly different times. Then, in order to obtain regional rather than local information, it is important to choose remote areas such as Lake Marboré. Indeed, we observed parallel main trends in both lakes Marboré and Estanya, but low amplitude changes in Marboré reflect regional-scale changes while Estanya is more influenced by local human activities such as farming, deforestation etc ...

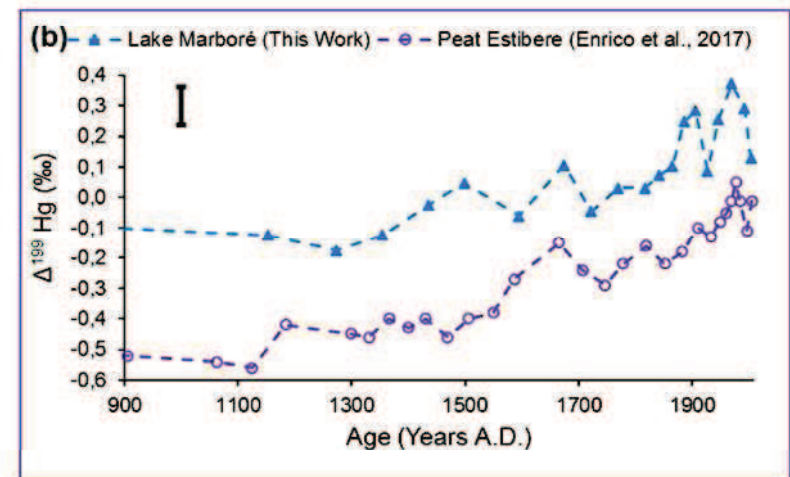
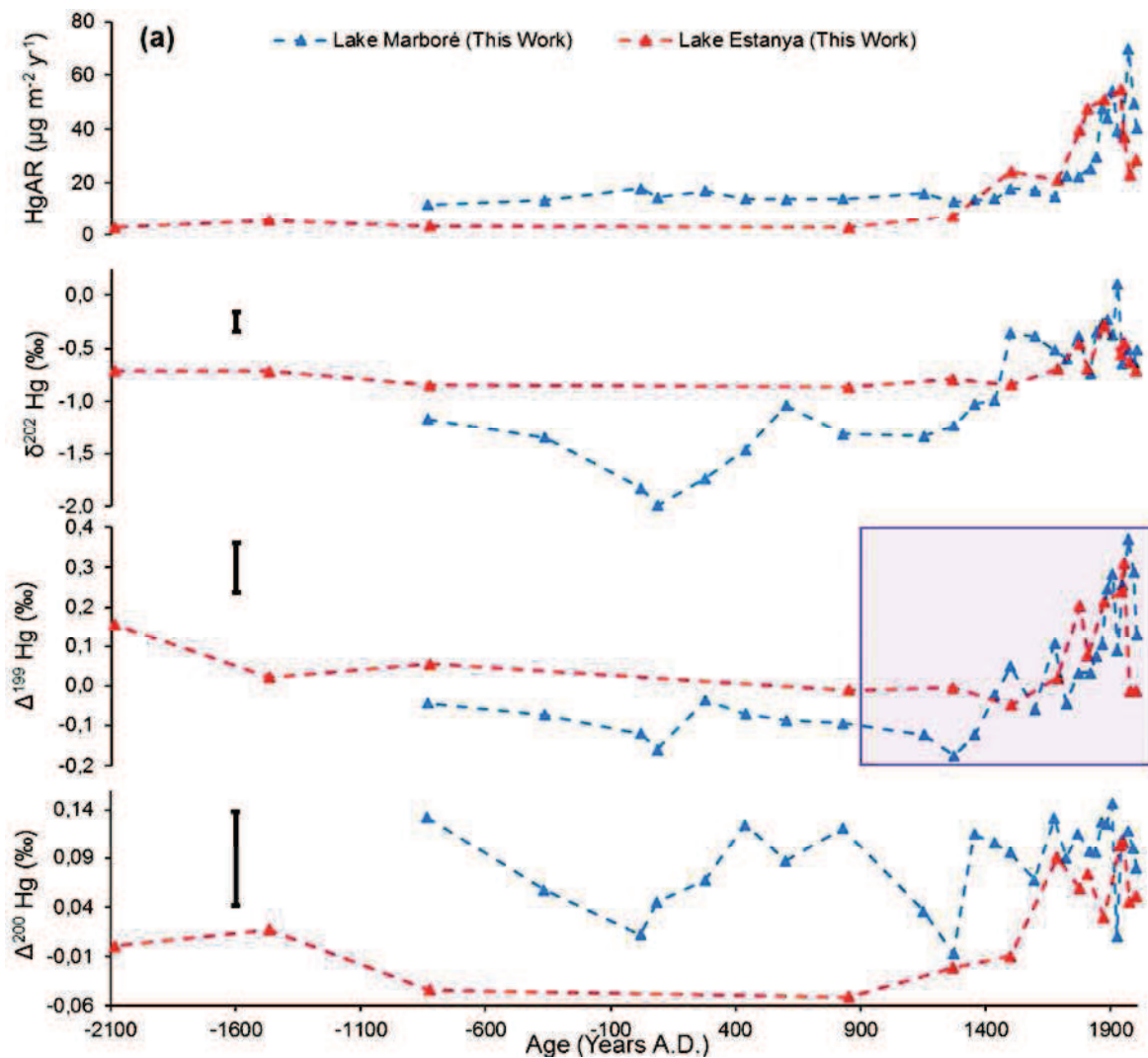


Figure 8.2: (a) From bottom to top, variation overtime (same axis x) of $\Delta^{200}\text{Hg}$, $\Delta^{199}\text{Hg}$, $\delta^{202}\text{Hg}$ and Hg Accumulation Rates (HgAR) in Lakes Marboré and Estanya; (b) $\Delta^{199}\text{Hg}$ comparison, starting from 905 CE, between Lake Marboré (This work) and Estibere Peat (Enrico et al., 2017) [33]

8.4.2. Stable isotopes to refine mercury atmospheric sources and historical pollution in the Pyrenees

Stable isotopes provide new insights on the biogeochemical cycle of Hg in the Geosphere. Our isotopic results show a clear relation between MDF, odd-MIF and even-MIF and the HgAR recorded in the studied sediment cores are well complementary to the HgAR.

Sediments $\delta^{202}\text{Hg}$ range from -1.99 (90 CE) to 0.11‰ (1930 CE) in lake Marboré while we observe narrower range from -0.87 (850 CE) to -0.28‰ (187' CE) in lake Estanya. The same pattern is observed for odd-MIF results with $\Delta^{199}\text{Hg}$ values in Lake Marboré and Lake Estanya ranging from -0.18 (1270 CE) to 0.37‰ (1970 CE) and -0.05 (1500 CE) to 0.31‰ (1950 CE) respectively. The profiles reveal increases in both $\delta^{202}\text{Hg}$ and $\Delta^{199}\text{Hg}$ in the upper part of the core sediments corresponding to the last centuries. On the other hand, the even-MIF $\Delta^{200}\text{Hg}$ display very small variations among the samples with values ranging from -0.01 (1270 CE) to 0.15 ‰ (1910 CE) for Lake Marboré and from -0.05 (850 CE) to 0.11‰ (1950 CE) for Lake Estanya. Nevertheless, for Lake Estanya, a clear shift to a more positive even-MIF is observed starting the 16th century while the signal for Lake Marboré vary more regularly either to more negative or positive values along the sediment core.

The smaller variations for stable isotopes in Lake Estanya (except $\Delta^{200}\text{Hg}$) for most of the record up to the last centuries is a unique feature and suggest a strong control of local factors on the Hg cycle till recent times. Two possible in-lake factors on MDF variability reducing the range of the source signature could be: i) a strong influence of the catchment via vegetation uptake and ii) limnological processes (biological activity). While HgAR has shown an important increase at the beginning of the 16th century, results from both $\delta^{202}\text{Hg}$ and $\Delta^{199}\text{Hg}$ do not display a significant difference between background (respectively -0.79 ± 0.07 ‰ and 0.04 ± 0.07 ‰) and pre-industrial (respectively -0.77 ± 0.11 ‰ and -0.01 ± 0.05 ‰) values (t-test, $p > 0.05$). Most of the archives, either lakes or peatlands, have shown a positive shift in the $\delta^{202}\text{Hg}$ and $\Delta^{199}\text{Hg}$ values along with the beginning of anthropogenic activities [24,26,30,33,58] (**Figure 8.3**), suggesting that this constant MDF and MIF in Lake Estanya is rather due the control exerted by the lake-watershed system properties to the external Hg input. The relatively constant $\delta^{202}\text{Hg}$ and $\Delta^{199}\text{Hg}$ close to background values at the beginning of the 16th century when HgAR increased due to global mercury deposition increase could be explained by change in the vegetation of the catchment that occurred during the 16th century caused by deforestation and land-use for agricultural activities [44]. In fact, the period between 1650 and 1750 CE has recorded the highest runoff and soil erosion rates in the lake Estanya catchment during the last millennium and also coincides with the maximum expansion of cultivars at the expenses of natural vegetation in the area according to pollen data [45] and a relative maximum in lake levels [44]. These environmental conditions occurred in the context of relatively colder and more humid period recorded during the Little Ice Age (14th to 19th centuries CA) in most of the Iberian Peninsula. From a climatic point of view, lakes located in the lowlands (i.e. Estanya) were probably more affected by hydrological changes, whereas sedimentation in high mountain lakes (i.e. Marboré) was likely more affected by decreasing temperatures and associated effects (ice cover phenology, glacier readvances etc ...). These abrupt climatic transitions

(from Medieval Climate Anomaly to Little Ice Age) are one of the most abrupt recorded during the last 4 ka in the region and might have influenced in different ways Hg records of lakes Marboré and Estanya.

In contrast with the 16th century phase, during the Industrial Period (1780-1980 CE) characterized by higher HgAR values, both $\delta^{202}\text{Hg}$ and $\Delta^{199}\text{Hg}$ increased (respectively $-0.49 \pm 0.15 \text{ ‰}$ and $0.21 \pm 0.09 \text{ ‰}$). The $+0.3 \text{ ‰}$ shift in the $\delta^{202}\text{Hg}$ agrees well with the change in bulk atmospheric Hg emissions observed between 1850 and 2010, from mining to the energy sector [59]. The observed decrease in runoff and soil erosion in the lake Estanya catchment after 1850 CE as a result of lower human pressure in the region and natural vegetation recovery [44] might have also influenced this change. A similar increase for both $\delta^{202}\text{Hg}$ and $\Delta^{199}\text{Hg}$ has been observed in remote North American lakes over a geographically widespread area since industrialization ($0.22 \pm 0.07 \text{ ‰}$ and $0.2 \pm 0.03 \text{ ‰}$, respectively) [58]. Then samples dated 1980 and 2000 display $\delta^{202}\text{Hg}$ of -0.62 and -0.70 ‰ and $\Delta^{199}\text{Hg}$ of -0.01 ‰ in both samples, similar to pre-industrial and background values. This change has been already observed for EF and HgAR [16] and might be linked to a decrease of Hg uses because of policy implications.

The sediment core from Lake Marboré displays Hg isotopic signal with five distinct historical periods, following the HgAR and EF variations already documented in a previous publication [37] (**Figure 8.3**): i) Iberian Period (-840 to 20 CE) ii) Roman Period (20 to 440 CE), iii) Middle Ages Period (440 to 1500 CE), iv) Modern Period (1400 to 1890 CE), and v) Industrial Period (1890 to 2000 CE). The Iberian and Middle Ages Periods show values indicative of lower Hg pollution ($\delta^{202}\text{Hg} = -1.21 \pm 0.17 \text{ ‰}$ and $\Delta^{199}\text{Hg} = -0.09 \pm 0.05 \text{ ‰}$), interrupted by the Roman Period with higher Hg deposition ($\delta^{202}\text{Hg} = -1.85 \pm 0.13 \text{ ‰}$ and $\Delta^{199}\text{Hg} = -0.11 \pm 0.06 \text{ ‰}$). No significant difference is observed for $\Delta^{199}\text{Hg}$ (t-test, $p > 0.05$) but a negative shift of about 0.6 ‰ of the $\delta^{202}\text{Hg}$ occurred during the Roman period. Romans were already extracting mercury in the Almadén mines to produce pigment, vermilion, as evidenced by the great number of coins, medals, vessels and other historical objects found in the Almadenejos and Valdeazogues areas [54,60,61]. The negative variation in the MDF can be related to the extraction process of Hg. Indeed, Romans were obtaining vermilion by grinding cinnabar in iron mortars and drying them in furnaces. They collected Hg after evaporation and called it hydrargyrum. Arabs brought to Iberia new processes for obtaining Hg, including the use of pots where they melted the ore and cinnabar and Hg was sublimated. Some of the changes observed around the 7th – 9th century could have been caused by this new technology. Nevertheless, the shift in $\delta^{202}\text{Hg}$ values can simply be due to the vein exploited by Romans. Indeed depending on the minerals associated to the cinnabar, either quartzite, breccia, goethite or pyrite, and depending on the location of the vein, either Almadén, El Entredicho, Nuevo Entredicho, Las Cuevas or Nueva Concepcion, $\delta^{202}\text{Hg}$ in the cinnabar range from -1.73 to 0.15 ‰ [62]. More Hg isotopic analysis depending together on the extraction process and the variety of cinnabar are needed to better understand this negative shift during the Roman Period. As mentioned above for others archives, the Modern and Industrial Periods are characterized by a less negative MDF with $\delta^{202}\text{Hg}$ values of respectively $-0.45 \pm 0.16 \text{ ‰}$ and $-0.38 \pm 0.29 \text{ ‰}$ (t-test, $p < 0.05$). However, for Lake Marboré, the main Hg isotopic feature regarding Hg contamination concerns the odd-MIF signal. Indeed, from Iberian and Middle Ages Periods ($\Delta^{199}\text{Hg} = -0.09 \pm 0.05 \text{ ‰}$), through Modern Period ($\Delta^{199}\text{Hg} = 0.04 \pm 0.06 \text{ ‰}$), to Industrial Period ($\Delta^{199}\text{Hg} = 0.26 \pm 0.09 \text{ ‰}$) and recent sample from 2004 ($\Delta^{199}\text{Hg} = 0.13 \text{ ‰}$)

$\Delta^{199}\text{Hg}$ follow the same trend that HgAR (**Figure 8.5.a**), itself related to the Hg Almadén production. A strong linear relationship between both $1/\text{HgAR}$ and $\Delta^{199}\text{Hg}$ (coefficient of determination $r^2 = 0.72$) is well displayed by the whole Lake Marboré core, providing evidence for the mixing of two distinct sources, one related to the natural background (non-Anthropogenic) and another to the Industrial inputs through atmospheric depositions (wet and dry). As the $\Delta^{199}\text{Hg}/\Delta^{201}\text{Hg}$ slopes (0.89 ± 0.07 for Lake Marboré and 0.97 ± 0.19 for Lake Estanya) are close to the aqueous photoreduction slope (**Figure 8.5**) defined by Bergquist and Blum [22], we could infer that the change in $\Delta^{199}\text{Hg}$ is related to Hg(II) photoreduction in the atmosphere [24]. It is worth noting that starting the 16th century with the increase of HgAR related to the Hg Almadén production, the $\Delta^{199}\text{Hg}$ signal of Lake Estanya versus $1/\text{HgAR}$ follow the same trend that the linear relationship for Lake Marboré above-mentioned.

The linear relationship between $1/\text{Hg}$ and $\Delta^{199}\text{Hg}$ has already been observed for the whole core of Lake Luitel ($r^2 = 0.79$) [26] and Lost Lake ($r^2 = 0.85$) [24], as well as for Estibere Peat ($r^2 = 0.56$) and Pinet Peat ($r^2 = 0.50$) [33] excluding recent samples (>1997 CE). The slopes related to these regressions depends strongly on different parameters such as main sources, deposition pathways (wet vs dry), and internal lake processes (photoreduction within the lake). Globally lakes from remote areas strongly influenced by wet deposition such as Lake Marboré or Lost Lake will be more sensitive to Hg inputs (higher Hg and $\Delta^{199}\text{Hg}$ variations) than lakes more influenced by dry deposition such as Lake Estanya.

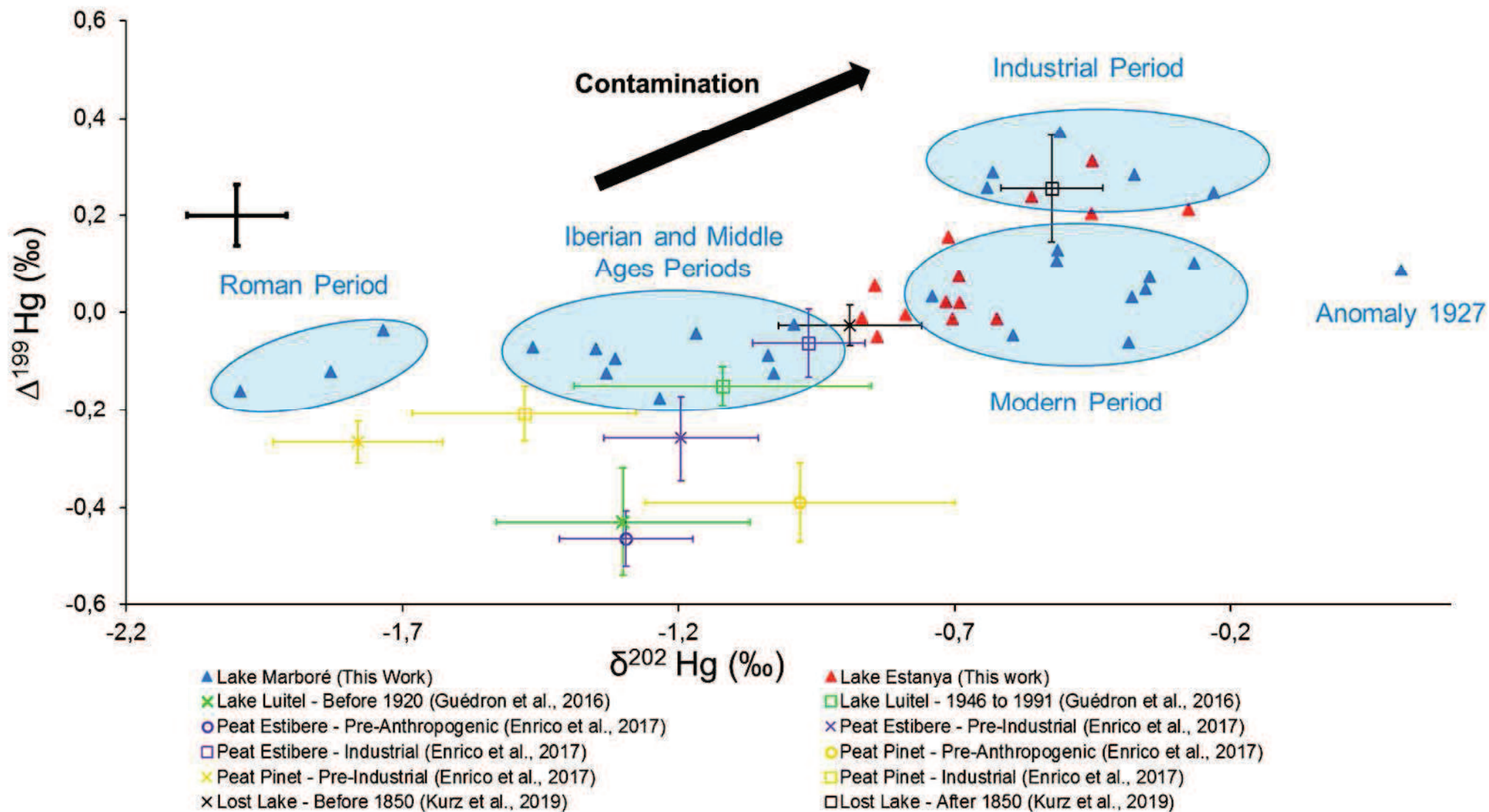


Figure 8.3: $\delta^{202}\text{Hg}$ vs $\Delta^{199}\text{Hg}$ plot for both Lakes Marboré and Lake Estanya together with literature data: both MDF and odd-MIF increase along with contamination

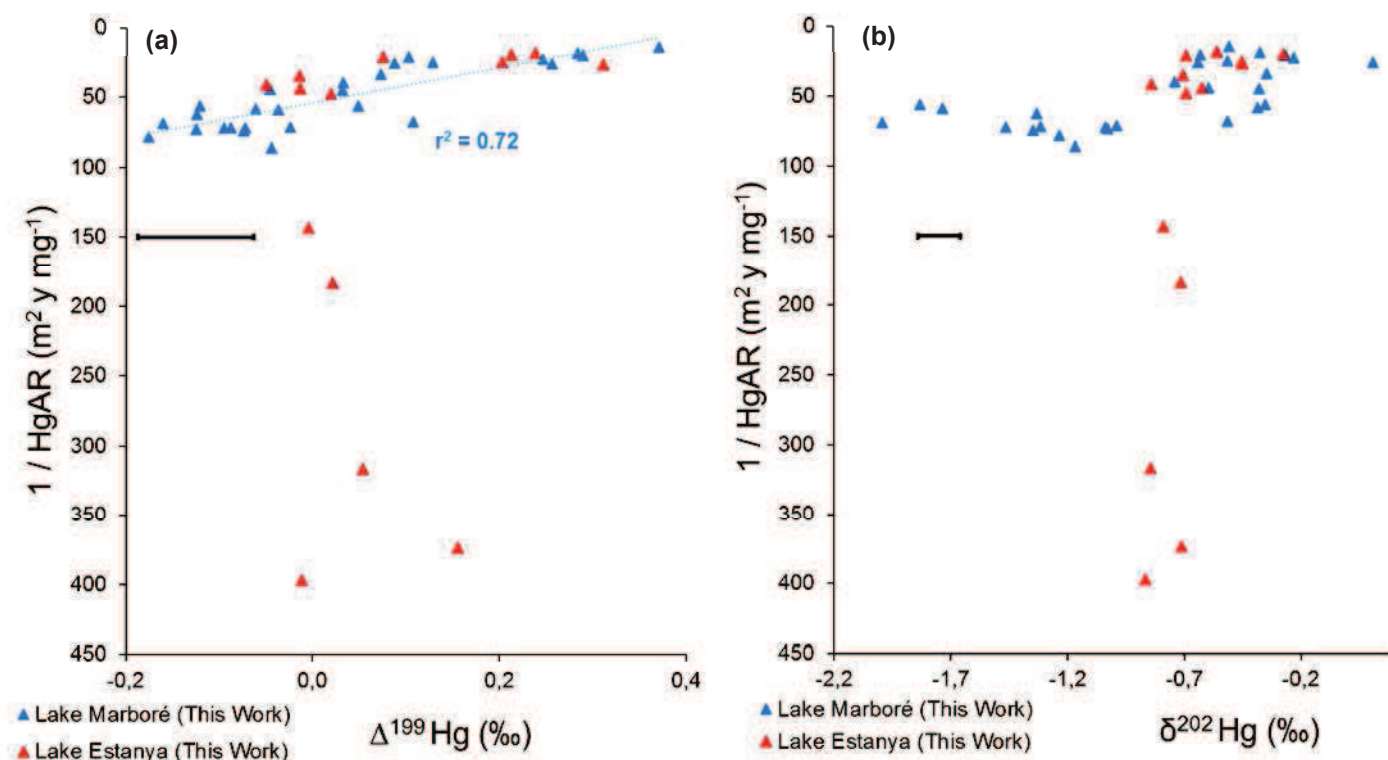


Figure 8.4: (a) $\Delta^{199}\text{Hg}$ vs $1/\text{HgAR}$ plot for both Lakes Marboré and Lake Estanya with strong linear relationship for lake Marboré; (b) $\delta^{202}\text{Hg}$ vs $1/\text{HgAR}$ plot for both Lakes Marboré and Lake Estanya

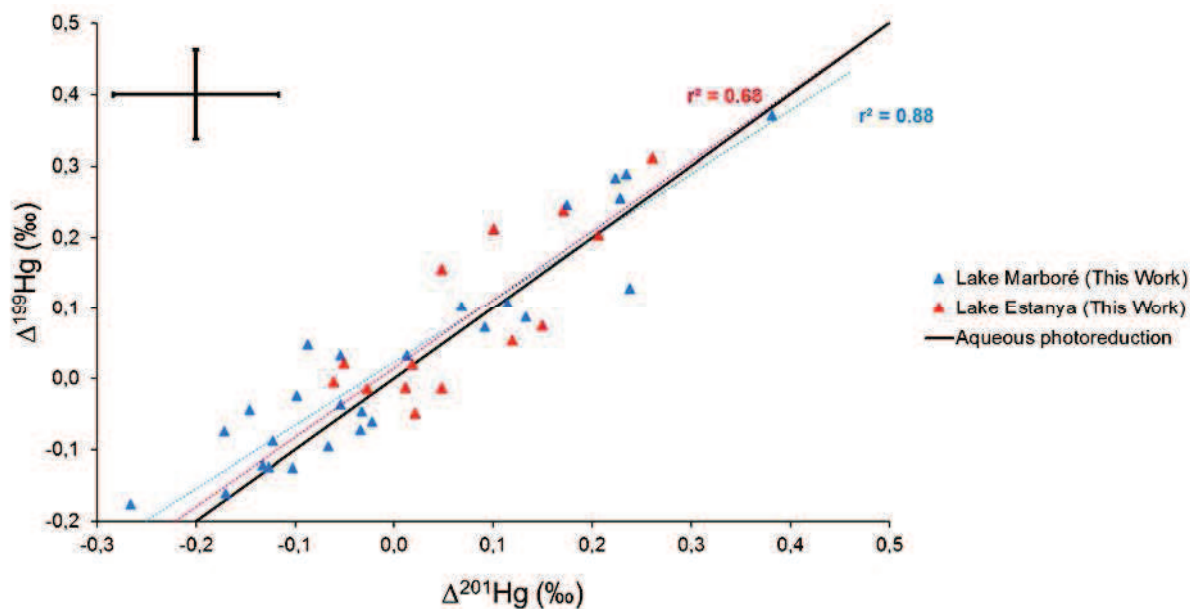


Figure 8.5: $\Delta^{201}\text{Hg}$ vs $\Delta^{199}\text{Hg}$ plot for both Lakes Marboré and Lake Estanya together with the theoretical slope for aqueous photoreduction (Bergquist and Blum, 2007) [22]

8.4.3. Even-MIF isotope reflects Hg deposition pathways and climatic effects in the Pyrenees

Mixing models have been recently used to estimate either Hg pollution sources through MDF [30,48,63] and odd-MIF isotopes [26], or deposition pathways through even-MIF isotope [18,24,31,33,64].

According to previous studies on Hg deposition in lakes, main inputs come from the atmospheric compartment either by direct deposition or indirectly as a consequence of run-off phenomena [5,11,26,64–72].

Wet deposition involves the scavenging of gas-phase and aerosol-phase Hg(II) before their deposition with rainfall and/or snowfall in the lake, whereas GEM dry deposition (Hg(0)) involves surface uptake of Hg(0) directly to the lake by dust transport or through leaching after vegetation uptake. Wet deposition worldwide is characterized by significant positive even-MIF $\Delta^{200}\text{Hg}$ [18,24,33,64,73] whereas GEM dry deposition (Hg(0)) show slight negative $\Delta^{200}\text{Hg}$ values [18,24,34,64].

Downcore sediment from Lake Marboré (**Figure 8.2.a**) displays positive $\Delta^{200}\text{Hg}$ values of 0.09 ± 0.04 ‰ (1σ , $n = 27$) suggesting a significant contribution of wet deposition over GEM dry deposition consistent with the absence of vegetation in its catchment and the important precipitation (2000 mm per year [16]). In this lake, covered by the snow 9-10 months per year, dry deposition likely occurs mainly through Gaseous Elemental Mercury (GEM) adsorption on snow. Indeed, even if Gaseous Oxidized Mercury (GOM), which has a $\Delta^{200}\text{Hg}$ signature similar to wet deposition, is more prone to dry deposition, its very low abundance in the atmospheric boundary layer makes it less important than GEM dry deposition.

In contrast, even-MIF $\Delta^{200}\text{Hg}$ is lower (0.03 ± 0.05 ‰ (1σ , $n = 14$)) in Lake Estanya and exhibits important variability, with a decrease in the fraction of Hg coming from GEM dry deposition since the 16th Century (higher $\Delta^{200}\text{Hg}$, t-test, $p < 0.05$). The relatively constant values in Estanya record before the 16th century suggest that Hg transport to this site seems to have been dominated by GEM dry deposition through foliar uptake followed by run-off from soil catchment. At the onset of 16th Century, dry and wet depositions increase with increasing of atmospheric Hg. Nevertheless, the difference in the lifetime of Hg in the soil and in the atmosphere might explain the observed shift in the $\Delta^{200}\text{Hg}$ signal towards relatively more wet deposition. Another possible explanation for this positive shift is the large changes in the lake catchment occurring since the 16th century in due to human activities, with one of the large scale development of agricultural activities as well as the reduction of the forest cover [45]; these changes in vegetation cover might induce a decrease in the fraction of Hg coming from GEM dry deposition. Finally, changes in local precipitation could also play a role as the 16th – 17th centuries included several wetter phases within the Little Ice Age [44,46].

In Central Pyrenees, $\Delta^{200}\text{Hg}_{\text{Wet}}$ end-member derived from precipitation (0.21 ± 0.04 ‰ (1σ) [18]) and $\Delta^{200}\text{Hg}_{\text{Dry}}$ end-member derived from atmospheric GEM (-0.05 ± 0.04 ‰, 1σ [18]) allow us to calculate a mass balance between wet and dry (GEM) deposition in lakes Marboré and Estanya (**Figure 8.6** and **Figure 8.7**) using the following formula:

Equation 8.3

$$\Delta^{200}\text{Hg} = F_{\text{Wet}} \times \Delta^{200}\text{Hg}_{\text{Wet}} + F_{\text{Dry}} \times \Delta^{200}\text{Hg}_{\text{Dry}}$$
$$F_{\text{Wet}} + F_{\text{Dry}} = 1$$

The applicability of this formula along the whole sediment core relies on the hypothesis that the $\Delta^{200}\text{Hg}$ signature in wet and dry deposition did not change with time [33]. Fractions of Hg from wet depositions vary from 16 to 76 % in Lake Marboré with a median value of 57 % whereas fractions of Hg from wet deposition in Lake Estanya ranges from 0 to 60 % with a median value of 33 %. This is consistent with the difference in precipitations observed between both lakes, higher in Lake Marboré.

As mentioned previously, $\Delta^{200}\text{Hg}$ in Lake Estanya can be affected not only by climate variability but also by the changes of vegetation surrounding the lake, caused by human activities. Lake Marboré watershed, however, has not experienced large changes in vegetation during the last millennia [40], and even-MIF $\Delta^{200}\text{Hg}$ values could be successfully used as a climate proxy. Even if the exact mechanisms involved are not fully understood, the seasonal (temperature) variation of $\Delta^{200}\text{Hg}$, with significant positive $\Delta^{200}\text{Hg}$, in precipitation samples observed by *Chen et al.* [23] a few years ago bring to light the possible use of $\Delta^{200}\text{Hg}$ as a tool to help monitor related climate changes. It is worth noting that the use of Hg as a tool for quantitative paleotemperature reconstruction have been reported in *Martínez-Cortizas et al.* [14]. This assumption is supported by the comparison of the reconstructed wet/dry deposition in this lake using $\Delta^{200}\text{Hg}$ with past climate phases identified in the Pyrenees (**Figure 8.6**). Samples corresponding to warmer periods (MCA and Roman Period) show distinctively lower $\Delta^{200}\text{Hg}$ values than other samples from the sediment core. The two samples dated in the 12th – 13th centuries (1150 and 1270 CE) show lower $\Delta^{200}\text{Hg}$ of respectively 0.04 and -0.01‰ (t-test, $p < 0.05$) and they correspond to the most arid and warm phase of the last millennium, the Medieval Climate Anomaly (MCA, ca. 900-1300 AD) [74]. The Roman Period (-250-450 AD), temperatures were also relatively higher [75] and also, the Marboré samples including in that period – dated -370, 20, 90 and 280 CE – have even-MIF $\Delta^{200}\text{Hg}$ values significantly lower (0.01 to 0.07‰, t-test, $p < 0.05$). Only one more sample, dated 1930 displays a similar anomaly with lower $\Delta^{200}\text{Hg}$ (0.01‰), and also higher MDF and lower odd-MIF in comparison with closest dated samples. No clear explanation can be related to this outlier except a local anthropogenic influence. Recent values also show a decreasing trend, although wet deposition remains higher than 50%. Interestingly, values during colder and more humid periods as the Late Antiquity Little Ice Age and the Little Ice Age show the high even-MIF $\Delta^{200}\text{Hg}$ values and corresponding wet deposition. Overall, although a better understanding of the relationship between $\Delta^{200}\text{Hg}$ and climate is needed, the occurrence of a coherent even-MIF $\Delta^{200}\text{Hg}$ signal in remote areas is a promising result and it could be successfully used as a new paleoclimatic proxy for remote and pristine areas.

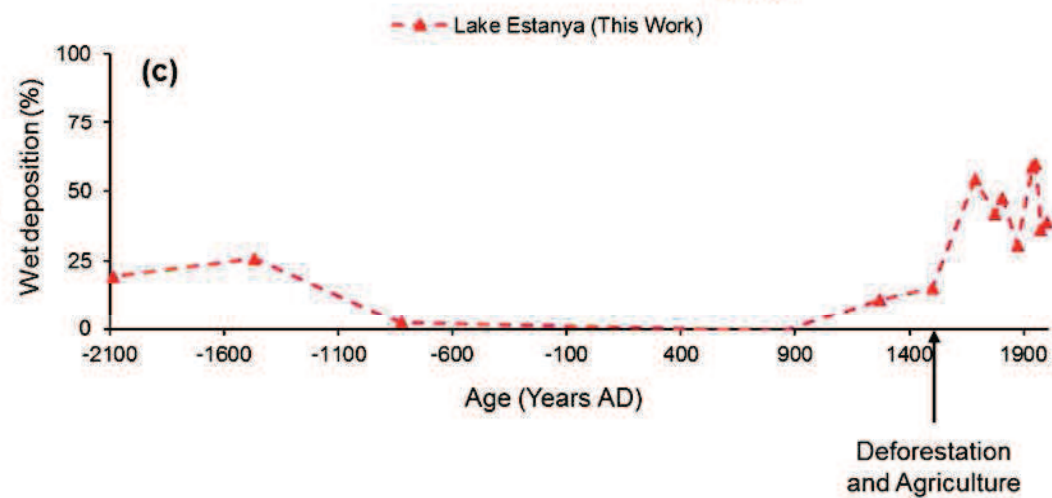
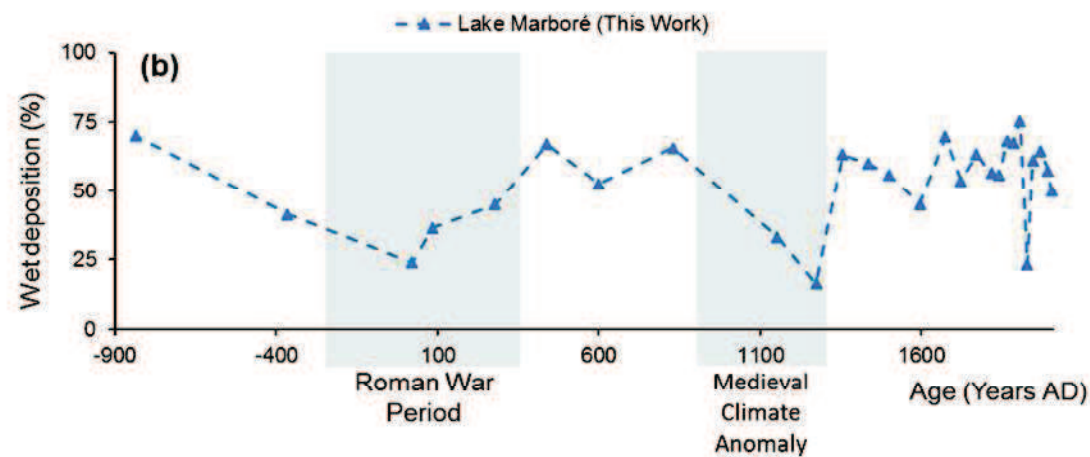
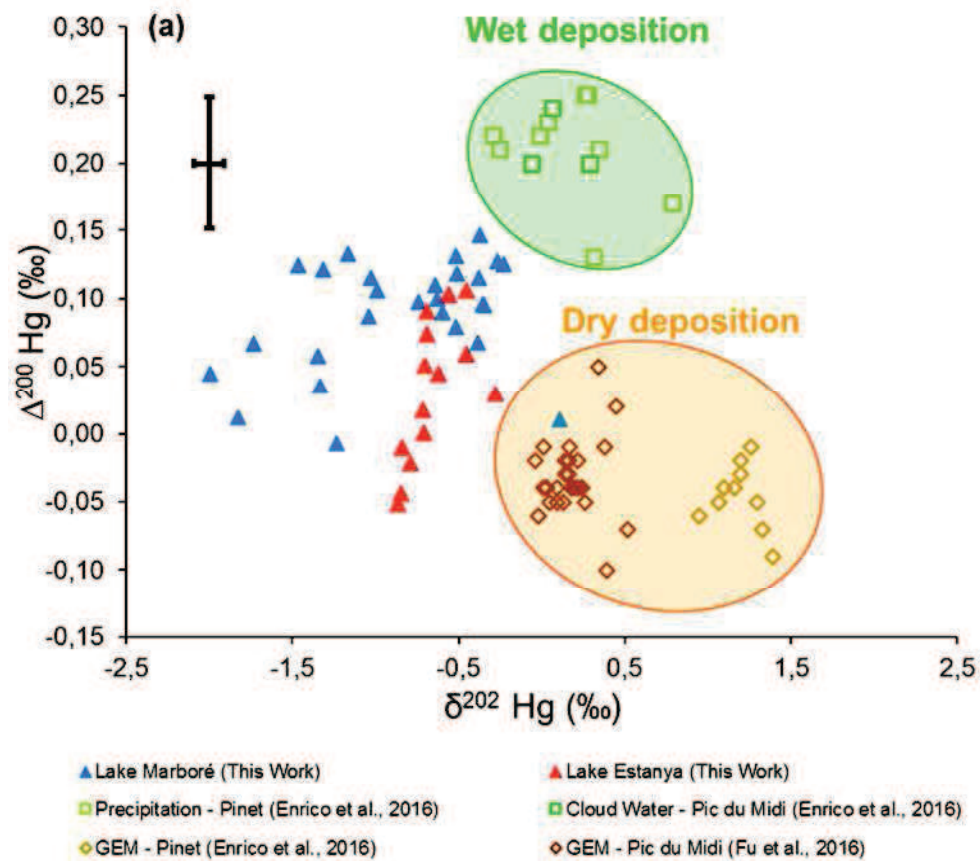


Figure 8.6: (a) $\delta^{202}\text{Hg}$ vs $\Delta^{200}\text{Hg}$ plot for both Lakes Marboré and Lake Estanya together with typical wet (cloud waters and precipitations) and dry (GEM) deposition Hg isotope signatures in the Central Pyrenees (Enrico et al., 2016 [18]; Fu et al., 2016 [34]); (b) Chronology of Hg wet deposition in Lake Marboré and Estanya; (c) Chronology of Hg wet deposition in Lake Estanya

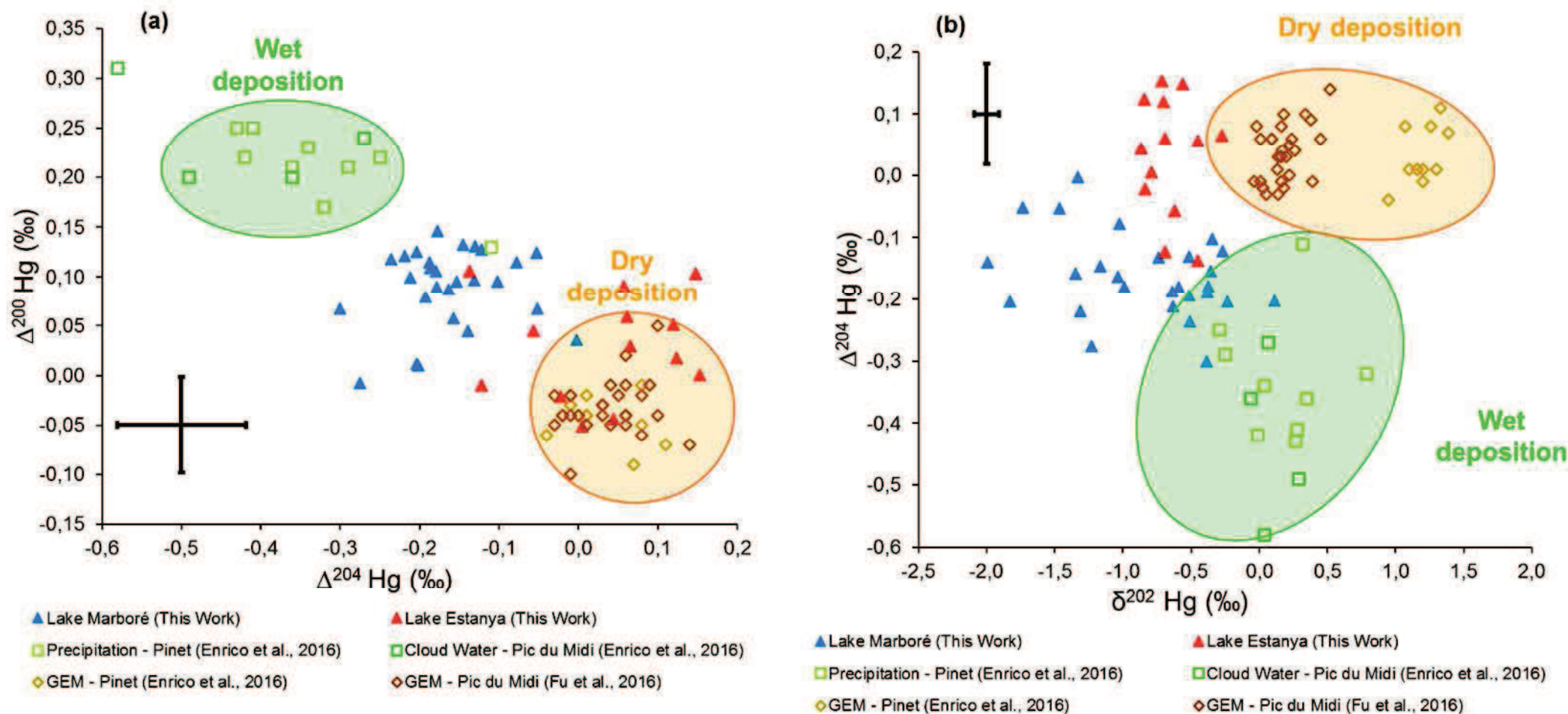


Figure 8.7: (a) $\Delta^{204}\text{Hg}$ vs $\Delta^{200}\text{Hg}$ plot for both Lakes Marboré and Lake Estanya together with typical wet and dry deposition Hg isotope signatures in the Central Pyrenees (Enrico et al. 2016 [18]; Fu et al., 2016 [34]): evidence for derived end-member; b) $\delta^{202}\text{Hg}$ vs $\Delta^{204}\text{Hg}$ plot for both Lakes Marboré and Lake Estanya together with typical wet and dry deposition Hg isotope signatures in the Central Pyrenees (Enrico et al., 2016 [18]; Fu et al., 2016 [34])

8.4.4. Comparing Hg stable isotope records in Lake sediment (Marboré) and Peat (Estibere) cores

The new Marboré site allows a comparison with another well-studied nearby system in the Pyrenees: Estibere peatland, located at 2120m asl, in the French Central Pyrenees at about 18km north-east from Lake Marboré. The peatland receives less annual rainfall than Marboré (1400 mm vs 2000 mm). In addition, isotope signatures of living sphagnum moss and accumulated peat are characteristic of GEM [18], emphasizing the strong influence of dry deposition in peat environment. This difference in the Hg deposition pathways for both, lake and peatland, is well supported by the even-MIF $\Delta^{200}\text{Hg}$ values (0.06 ± 0.03 ‰ for Peat Estibere, 0.09 ± 0.04 ‰ for Lake Marboré).

Except for recent samples (2004 CE for Lake Marboré and 2005 CE for Peat Estibere), the $\Delta^{199}\text{Hg}$ displays a constant shift of 0.33 ± 0.08 ‰ between both archives (**Figure 8.2.b**). Considering the proximity of both ecosystems and their common atmospheric Hg sources, this shift can be either related to i) Deposition pathway or ii) Internal processes. Modern wet deposition displays higher $\Delta^{199}\text{Hg}$ than dry deposition: 0.71 ± 0.14 ‰ in precipitation against -0.18 ± 0.07 ‰ in atmospheric GEM [18]. Then, the difference in annual precipitation between the lake and the peat could be responsible for this shift in $\Delta^{199}\text{Hg}$. Nevertheless, if we compare the $\Delta^{199}\text{Hg}$ between Peat Estibere and Peat Pinet (precipitation of 1161 mm per year) for the Pre-Industrial Period there is no significant difference (t-test, $p > 0.05$) and there is a shift of about 0.15 ‰ for the Industrial Period. Therefore, the constant shift all along the cores of Lake Marboré and Peat Estibere is likely due more to internal processes than to climatic phenomena. One possible process to account for these differences is in-situ fractionation occurring in Lake Marboré during photoreduction of Hg(II) either when the snow covers the lake or within the water column after melting events [76]. In addition, Hg photoreduction from foliage might affect Hg isotope composition in peatland [77].

While the HgAR in both archives decreases in the recent samples, the $\Delta^{199}\text{Hg}$ does not follow this tendency in the peat. It has been noticed that during peat diagenesis, non-quantitative retention and loss of Hg occur [19]. *Enrico et al.* (2016) have studied the potential influence of photoreduction during peat diagenesis but no effect on sphagnum Hg concentration or Hg isotope composition have been observed. Further in-situ experiments should be conducted to better understand Hg cycle and transformations during peat diagenesis.

8.5. References

- [1] Z.F. Anual, W. Maher, F. Krikowa, L. Hakim, N.I. Ahmad, S. Foster, Mercury and risk assessment from consumption of crustaceans, cephalopods and fish from West Peninsular Malaysia, *Microchemical Journal*. 140 (2018) 214–221. <https://doi.org/10.1016/j.microc.2018.04.024>.
- [2] M. Arcagni, R. Juncos, A. Rizzo, M. Pavlin, V. Fajon, M.A. Arribére, M. Horvat, S. Ribeiro Guevara, Species- and habitat-specific bioaccumulation of total mercury and methylmercury in the food web of a deep oligotrophic lake, *Science of The Total Environment*. 612 (2018) 1311–1319. <https://doi.org/10.1016/j.scitotenv.2017.08.260>.
- [3] Q. Xu, L. Zhao, Y. Wang, Q. Xie, D. Yin, X. Feng, D. Wang, Bioaccumulation characteristics of mercury in fish in the Three Gorges Reservoir, China, *Environmental Pollution*. 243 (2018) 115–126. <https://doi.org/10.1016/j.envpol.2018.08.048>.
- [4] H.M. Amos, J.E. Sonke, D. Obrist, N. Robins, N. Hagan, H.M. Horowitz, R.P. Mason, M. Witt, I.M. Hedgecock, E.S. Corbitt, E.M. Sunderland, Observational and Modeling Constraints on Global Anthropogenic Enrichment of Mercury, *Environmental Science & Technology*. 49 (2015) 4036–4047. <https://doi.org/10.1021/es5058665>.
- [5] C.T. Driscoll, R.P. Mason, H.M. Chan, D.J. Jacob, N. Pirrone, Mercury as a Global Pollutant: Sources, Pathways, and Effects, *Environmental Science & Technology*. 47 (2013) 4967–4983. <https://doi.org/10.1021/es305071v>.
- [6] P.A. Ariya, M. Amyot, A. Dastoor, D. Deeds, A. Feinberg, G. Kos, A. Poulain, A. Ryjkov, K. Semeniuk, M. Subir, K. Toyota, Mercury Physicochemical and Biogeochemical Transformation in the Atmosphere and at Atmospheric Interfaces: A Review and Future Directions, *Chemical Reviews*. 115 (2015) 3760–3802. <https://doi.org/10.1021/cr500667e>.
- [7] A. Saiz-Lopez, S.P. Sitkiewicz, D. Roca-Sanjuán, J.M. Oliva-Enrich, J.Z. Dávalos, R. Notario, M. Jiskra, Y. Xu, F. Wang, C.P. Thackray, E.M. Sunderland, D.J. Jacob, O. Travnikov, C.A. Cuevas, A.U. Acuña, D. Rivero, J.M.C. Plane, D.E. Kinnison, J.E. Sonke, Photoreduction of gaseous oxidized mercury changes global atmospheric mercury speciation, transport and deposition, *Nature Communications*. 9 (2018). <https://doi.org/10.1038/s41467-018-07075-3>.
- [8] A. Saiz-Lopez, A.U. Acuña, T. Trabelsi, J. Carmona-García, J.Z. Dávalos, D. Rivero, C.A. Cuevas, D.E. Kinnison, S.P. Sitkiewicz, D. Roca-Sanjuán, J.S. Francisco, Gas-Phase Photolysis of Hg(I) Radical Species: A New Atmospheric Mercury Reduction Process, *Journal of the American Chemical Society*. 141 (2019) 8698–8702. <https://doi.org/10.1021/jacs.9b02890>.
- [9] UNEP, 2013, *Global Mercury Assessment 2013: Sources, Emissions, Releases and Environmental Transport*, (n.d.).
- [10] D.R. Engstrom, W.F. Fitzgerald, C.A. Cooke, C.H. Lamborg, P.E. Drevnick, E.B. Swain, S.J. Balogh, P.H. Balcom, Atmospheric Hg Emissions from Preindustrial Gold and Silver Extraction in the Americas: A Reevaluation from Lake-Sediment Archives, *Environmental Science & Technology*. 48 (2014) 6533–6543. <https://doi.org/10.1021/es405558e>.
- [11] H. Biester, R. Bindler, A. Martinez-Cortizas, D.R. Engstrom, Modeling the Past Atmospheric Deposition of Mercury Using Natural Archives, *Environmental Science & Technology*. 41 (2007) 4851–4860. <https://doi.org/10.1021/es0704232>.
- [12] S.A. Beal, E.C. Osterberg, C.M. Zdanowicz, D.A. Fisher, Ice Core Perspective on Mercury Pollution during the Past 600 Years, *Environmental Science & Technology*. 49 (2015) 7641–7647. <https://doi.org/10.1021/acs.est.5b01033>.
- [13] P.F. Schuster, D.P. Krabbenhoft, D.L. Naftz, L.D. Cecil, M.L. Olson, J.F. Dewild, D.D. Susong, J.R. Green, M.L. Abbott, Atmospheric Mercury Deposition during the Last 270 Years: A Glacial Ice Core Record of Natural and Anthropogenic Sources, *Environmental Science & Technology*. 36 (2002) 2303–2310. <https://doi.org/10.1021/es0157503>.
- [14] A. Martínez-Cortizas, Mercury in a Spanish Peat Bog: Archive of Climate Change and Atmospheric Metal Deposition, *Science*. 284 (1999) 939–942. <https://doi.org/10.1126/science.284.5416.939>.

- [15] C.A. Cooke, A. Martínez-Cortizas, R. Bindler, M. Sexauer Gustin, Environmental archives of atmospheric Hg deposition – A review, *Science of The Total Environment*. 709 (2020) 134800. <https://doi.org/10.1016/j.scitotenv.2019.134800>.
- [16] J.P. Corella, A. Saiz-Lopez, M.J. Sierra, M.P. Mata, R. Millán, M. Morellón, C.A. Cuevas, A. Moreno, B.L. Valero-Garcés, Trace metal enrichment during the Industrial Period recorded across an altitudinal transect in the Southern Central Pyrenees, *Science of The Total Environment*. 645 (2018) 761–772. <https://doi.org/10.1016/j.scitotenv.2018.07.160>.
- [17] A. Martínez Cortizas, E. Peiteado Varela, R. Bindler, H. Biester, A. Cheburkin, Reconstructing historical Pb and Hg pollution in NW Spain using multiple cores from the Chao de Lamoso bog (Xistral Mountains), *Geochimica et Cosmochimica Acta*. 82 (2012) 68–78. <https://doi.org/10.1016/j.gca.2010.12.025>.
- [18] M. Enrico, G.L. Roux, N. Maruszczak, L.-E. Heimbürger, A. Claustres, X. Fu, R. Sun, J.E. Sonke, Atmospheric Mercury Transfer to Peat Bogs Dominated by Gaseous Elemental Mercury Dry Deposition, *Environmental Science & Technology*. 50 (2016) 2405–2412. <https://doi.org/10.1021/acs.est.5b06058>.
- [19] S. Osterwalder, K. Bishop, C. Alewell, J. Fritsche, H. Laudon, S. Åkerblom, M.B. Nilsson, Mercury evasion from a boreal peatland shortens the timeline for recovery from legacy pollution, *Scientific Reports*. 7 (2017). <https://doi.org/10.1038/s41598-017-16141-7>.
- [20] J. Rydberg, V. Gälman, I. Renberg, R. Bindler, L. Lambertsson, A. Martínez-Cortizas, Assessing the Stability of Mercury and Methylmercury in a Varved Lake Sediment Deposit, *Environmental Science & Technology*. 42 (2008) 4391–4396. <https://doi.org/10.1021/es7031955>.
- [21] J.D. Blum, L.S. Sherman, M.W. Johnson, Mercury Isotopes in Earth and Environmental Sciences, *Annual Review of Earth and Planetary Sciences*. 42 (2014) 249–269. <https://doi.org/10.1146/annurev-earth-050212-124107>.
- [22] B.A. Bergquist, J.D. Blum, Mass-Dependent and -Independent Fractionation of Hg Isotopes by Photoreduction in Aquatic Systems, *Science*. 318 (2007) 417–420. <https://doi.org/10.1126/science.1148050>.
- [23] J. Chen, H. Hintelmann, X. Feng, B. Dimock, Unusual fractionation of both odd and even mercury isotopes in precipitation from Peterborough, ON, Canada, *Geochimica et Cosmochimica Acta*. 90 (2012) 33–46. <https://doi.org/10.1016/j.gca.2012.05.005>.
- [24] A.Y. Kurz, J.D. Blum, S.J. Washburn, M. Baskaran, Changes in the mercury isotopic composition of sediments from a remote alpine lake in Wyoming, USA, *Science of The Total Environment*. 669 (2019) 973–982. <https://doi.org/10.1016/j.scitotenv.2019.03.165>.
- [25] C.A. Cooke, H. Hintelmann, J.J. Ague, R. Burger, H. Biester, J.P. Sachs, D.R. Engstrom, Use and Legacy of Mercury in the Andes, *Environmental Science & Technology*. 47 (2013) 4181–4188. <https://doi.org/10.1021/es3048027>.
- [26] S. Guédron, D. Amouroux, P. Sabatier, C. Desplanque, A.-L. Develle, J. Barre, C. Feng, F. Guiter, F. Arnaud, J.L. Reyss, L. Charlet, A hundred year record of industrial and urban development in French Alps combining Hg accumulation rates and isotope composition in sediment archives from Lake Luitel, *Chemical Geology*. 431 (2016) 10–19. <https://doi.org/10.1016/j.chemgeo.2016.03.016>.
- [27] T.A. Jackson, Stratigraphic variations in the $\delta^{201}\text{Hg}/\delta^{199}\text{Hg}$ ratio of mercury in sediment cores as historical records of methylmercury production in lakes, *Journal of Paleolimnology*. 61 (2019) 387–401. <https://doi.org/10.1007/s10933-019-00066-4>.
- [28] T.A. Jackson, Historical variations in the stable isotope composition of mercury in a sediment core from a riverine lake: Effects of dams, pulp and paper mill wastes, and mercury from a chlor-alkali plant, *Applied Geochemistry*. 71 (2016) 86–98. <https://doi.org/10.1016/j.apgeochem.2016.06.001>.
- [29] T.A. Jackson, D.C.G. Muir, W.F. Vincent, Historical Variations in the Stable Isotope Composition of Mercury in Arctic Lake Sediments, *Environmental Science & Technology*. 38 (2004) 2813–2821. <https://doi.org/10.1021/es0306009>.

- [30] R. Yin, R.F. Lepak, D.P. Krabbenhoft, J.P. Hurley, Sedimentary records of mercury stable isotopes in Lake Michigan, *Elementa: Science of the Anthropocene*. 4 (2016) 000086. <https://doi.org/10.12952/journal.elementa.000086>.
- [31] R. Yin, X. Feng, J.P. Hurley, D.P. Krabbenhoft, R.F. Lepak, S. Kang, H. Yang, X. Li, Historical Records of Mercury Stable Isotopes in Sediments of Tibetan Lakes, *Scientific Reports*. 6 (2016). <https://doi.org/10.1038/srep23332>.
- [32] C.M. Zdanowicz, E.M. Krümmel, A.J. Poulain, E. Yumvihoze, J. Chen, M. Štok, M. Scheer, H. Hintelmann, Historical variations of mercury stable isotope ratios in Arctic glacier firn and ice cores: Mercury Stable Isotopes in Glacier Ice, *Global Biogeochemical Cycles*. 30 (2016) 1324–1347. <https://doi.org/10.1002/2016GB005411>.
- [33] M. Enrico, G. Le Roux, L.-E. Heimbürger, P. Van Beek, M. Souhaut, J. Chmeleff, J.E. Sonke, Holocene Atmospheric Mercury Levels Reconstructed from Peat Bog Mercury Stable Isotopes, *Environmental Science & Technology*. 51 (2017) 5899–5906. <https://doi.org/10.1021/acs.est.6b05804>.
- [34] X. Fu, N. Maruszczak, X. Wang, F. Gheusi, J.E. Sonke, Isotopic Composition of Gaseous Elemental Mercury in the Free Troposphere of the Pic du Midi Observatory, France, *Environmental Science & Technology*. 50 (2016) 5641–5650. <https://doi.org/10.1021/acs.est.6b00033>.
- [35] D. Obrist, Y. Agnan, M. Jiskra, C.L. Olson, D.P. Colegrove, J. Hueber, C.W. Moore, J.E. Sonke, D. Helmig, Tundra uptake of atmospheric elemental mercury drives Arctic mercury pollution, *Nature*. 547 (2017) 201–204. <https://doi.org/10.1038/nature22997>.
- [36] J.P. Corella, B.L. Valero-Garcés, F. Wang, A. Martínez-Cortizas, C.A. Cuevas, A. Saiz-Lopez, 700 years reconstruction of mercury and lead atmospheric deposition in the Pyrenees (NE Spain), *Atmospheric Environment*. 155 (2017) 97–107. <https://doi.org/10.1016/j.atmosenv.2017.02.018>.
- [37] J.P. Corella, M.J. Sierra, A. Garralón, R. Millán, J. Rodríguez-Alonso, M.P. Mata, A.V. de Vera, A. Moreno, P. González-Sampériz, B. Duval, D. Amouroux, P. Vivez, C.A. Cuevas, J.A. Adame, B. Wilhelm, A. Saiz-Lopez, B.L. Valero-Garcés, Recent and historical pollution legacy in high altitude Lake Marboré (Central Pyrenees): A record of mining and smelting since pre-Roman times in the Iberian Peninsula, *Science of The Total Environment*. 751 (2021) 141557. <https://doi.org/10.1016/j.scitotenv.2020.141557>.
- [38] M. Morellón, B. Valero-Garcés, T. Vegas-Vilarrúbia, P. González-Sampériz, Ó. Romero, A. Delgado-Huertas, P. Mata, A. Moreno, M. Rico, J.P. Corella, Lateglacial and Holocene palaeohydrology in the western Mediterranean region: The Lake Estanya record (NE Spain), *Quaternary Science Reviews*. 28 (2009) 2582–2599. <https://doi.org/10.1016/j.quascirev.2009.05.014>.
- [39] B. Valero-Garcés, B. Oliva-Urcia, A. Moreno, M. Herrero, M. del Pi. Mata, Á. Salazar, M. Rieradevall, J.M. García-Ruiz, J. Cía, P. Gonzalez Samperiz, A. Sanz, A. Salabarnada, A. Pardo, C. Sancho, F. Barreiro-Lostres, M. Bartolomé, E. Garcia-Prieto, G. Gil-Romera, L. Merino, P. Tarrats, Dinámica glacial, clima y vegetación en el Parque Nacional de Ordesa y Monte Perdido durante el Holoceno, (2013) 7–37.
- [40] M. Leunda, P. González-Sampériz, G. Gil-Romera, J. Aranbarri, A. Moreno, B. Oliva-Urcia, M. Sevilla-Callejo, B. Valero-Garcés, The Late-Glacial and Holocene Marboré Lake sequence (2612 m a.s.l., Central Pyrenees, Spain): Testing high altitude sites sensitivity to millennial scale vegetation and climate variability, *Global and Planetary Change*. 157 (2017) 214–231. <https://doi.org/10.1016/j.gloplacha.2017.08.008>.
- [41] P.M. Nicolás-Martínez, Morfología del circo de Tucarroya (Macizo de Monte Perdido, Pirineo Aragonés), *Cuadernos de Investigación Geográfica*. 7 (1981) 51. <https://doi.org/10.18172/cig.884>.
- [42] J. Sánchez-España, M.P. Mata, J. Vegas, M. Morellón, J.A. Rodríguez, Á. Salazar, I. Yusta, Limnochemistry of the remote, high mountain Lake Marboré (Ordesa and Monte Perdido National Park, Central Pyrenees): Stratification dynamics and trace metal anomalies, *Limnetica*. (2018) 85–103. <https://doi.org/10.23818/limn.37.08>.
- [43] C. Sancho, El polje de Saganta (Sierras Exteriores Pirenaicas, Provincia de Huesca), (2012).
- [44] M. Morellón, B. Valero-Garcés, P. González-Sampériz, T. Vegas-Vilarrúbia, E. Rubio, M. Rieradevall, A. Delgado-Huertas, P. Mata, Ó. Romero, D.R. Engstrom, M. López-Vicente, A.

- Navas, J. Soto, Climate changes and human activities recorded in the sediments of Lake Estanya (NE Spain) during the Medieval Warm Period and Little Ice Age, *J Paleolimnol.* 46 (2011) 423–452. <https://doi.org/10.1007/s10933-009-9346-3>.
- [45] P. González-Sampériz, J. Aranbarri, A. Pérez-Sanz, G. Gil-Romera, A. Moreno, M. Leunda, M. Sevilla-Callejo, J.P. Corella, M. Morellón, B. Oliva, B. Valero-Garcés, Environmental and climate change in the southern Central Pyrenees since the Last Glacial Maximum: A view from the lake records, *CATENA.* 149 (2017) 668–688. <https://doi.org/10.1016/j.catena.2016.07.041>.
- [46] B. Oliva-Urcia, A. Moreno, M. Leunda, B. Valero-Garcés, P. González-Sampériz, G. Gil-Romera, M.P. Mata, Last deglaciation and Holocene environmental change at high altitude in the Pyrenees: the geochemical and paleomagnetic record from Marboré Lake (N Spain), *Journal of Paleolimnology.* 59 (2018) 349–371.
- [47] N. Givelet, F. Roos-Barraclough, W. Shotyk, Predominant anthropogenic sources and rates of atmospheric mercury accumulation in southern Ontario recorded by peat cores from three bogs: comparison with natural “background” values (past 8000 years), *J. Environ. Monit.* 5 (2003) 935–949. <https://doi.org/10.1039/B307140E>.
- [48] M. Jiménez-Moreno, J.P.G. Barre, V. Perrot, S. Bérail, R.C. Rodríguez Martín-Doimeadios, D. Amouroux, Sources and fate of mercury pollution in Almadén mining district (Spain): Evidences from mercury isotopic compositions in sediments and lichens, *Chemosphere.* 147 (2016) 430–438. <https://doi.org/10.1016/j.chemosphere.2015.12.094>.
- [49] J.D. Blum, B.A. Bergquist, Reporting of variations in the natural isotopic composition of mercury, *Analytical and Bioanalytical Chemistry.* 388 (2007) 353–359. <https://doi.org/10.1007/s00216-007-1236-9>.
- [50] L.S. Sherman, J.D. Blum, Mercury stable isotopes in sediments and largemouth bass from Florida lakes, USA, *Science of The Total Environment.* 448 (2013) 163–175. <https://doi.org/10.1016/j.scitotenv.2012.09.038>.
- [51] J.E. Sonke, J. Schäfer, J. Chmeleff, S. Audry, G. Blanc, B. Dupré, Sedimentary mercury stable isotope records of atmospheric and riverine pollution from two major European heavy metal refineries, *Chemical Geology.* 279 (2010) 90–100. <https://doi.org/10.1016/j.chemgeo.2010.09.017>.
- [52] J. Ma, H. Hintelmann, J.L. Kirk, D.C.G. Muir, Mercury concentrations and mercury isotope composition in lake sediment cores from the vicinity of a metal smelting facility in Flin Flon, Manitoba, *Chemical Geology.* 336 (2013) 96–102. <https://doi.org/10.1016/j.chemgeo.2012.10.037>.
- [53] A. Biswas, J.D. Blum, B.A. Bergquist, G.J. Keeler, Z. Xie, Natural Mercury Isotope Variation in Coal Deposits and Organic Soils, *Environmental Science & Technology.* 42 (2008) 8303–8309. <https://doi.org/10.1021/es801444b>.
- [54] P.L.H. Higuera, L.M. Plaza, S.L. Álvarez, J.M.E. Víctor, The Almadén mercury mining district, (n.d.) 15.
- [55] J. Chételat, M. Amyot, P. Arp, J.M. Blais, D. Depew, C.A. Emmerton, M. Evans, M. Gamberg, N. Gantner, C. Girard, J. Graydon, J. Kirk, D. Lean, I. Lehnher, D. Muir, M. Nasr, A. J. Poulain, M. Power, P. Roach, G. Stern, H. Swanson, S. van der Velden, Mercury in freshwater ecosystems of the Canadian Arctic: Recent advances on its cycling and fate, *Science of The Total Environment.* 509–510 (2015) 41–66. <https://doi.org/10.1016/j.scitotenv.2014.05.151>.
- [56] N. Maruszczak, C. Larose, A. Dommergue, E. Yumvihoze, D. Lean, R. Nedjai, C. Ferrari, Total mercury and methylmercury in high altitude surface snow from the French Alps, *Science of The Total Environment.* 409 (2011) 3949–3954. <https://doi.org/10.1016/j.scitotenv.2011.06.040>.
- [57] L.D. Hylander, M. Meili, 500 years of mercury production: global annual inventory by region until 2000 and associated emissions, *Science of The Total Environment.* 304 (2003) 13–27. [https://doi.org/10.1016/S0048-9697\(02\)00553-3](https://doi.org/10.1016/S0048-9697(02)00553-3).
- [58] R.F. Lepak, S.E. Janssen, D.R. Engstrom, D.P. Krabbenhoft, M.T. Tate, R. Yin, W.F. Fitzgerald, S.A. Nagorski, J.P. Hurley, Resolving Atmospheric Mercury Loading and Source Trends from Isotopic Records of Remote North American Lake Sediments, *Environmental Science & Technology.* 54 (2020) 9325–9333. <https://doi.org/10.1021/acs.est.0c00579>.

- [59] R. Sun, D.G. Streets, H.M. Horowitz, H.M. Amos, G. Liu, V. Perrot, J.-P. Toutain, H. Hintelmann, E.M. Sunderland, J.E. Sonke, Historical (1850–2010) mercury stable isotope inventory from anthropogenic sources to the atmosphere, *Elementa: Science of the Anthropocene*. 4 (2016) 000091. <https://doi.org/10.12952/journal.elementa.000091>.
- [60] J.M. Esbrí, P. Higuera, Mercury Contents in Waters from the Valdeazogues Watershed (Almadén, Spain), (n.d.) 7.
- [61] M. Garcia Gomez, J. Diego Caballero Klink, P. Boffetta, S. Espanol, G. Sallsten, J. Gomez Quintana, Exposure to mercury in the mine of Almaden, *Occupational and Environmental Medicine*. 64 (2006) 389–395. <https://doi.org/10.1136/oem.2006.030940>.
- [62] J.E. Gray, M.J. Pribil, P.L. Higuera, Mercury isotope fractionation during ore retorting in the Almadén mining district, Spain, *Chemical Geology*. 357 (2013) 150–157. <https://doi.org/10.1016/j.chemgeo.2013.08.036>.
- [63] J.P.G. Barre, G. Deletraz, C. Sola-Larrañaga, J.M. Santamaria, S. Bérail, O.F.X. Donard, D. Amouroux, Multi-element isotopic signature (C, N, Pb, Hg) in epiphytic lichens to discriminate atmospheric contamination as a function of land-use characteristics (Pyrénées-Atlantiques, SW France), *Environmental Pollution*. 243 (2018) 961–971. <https://doi.org/10.1016/j.envpol.2018.09.003>.
- [64] J. Chen, H. Hintelmann, W. Zheng, X. Feng, H. Cai, Z. Wang, S. Yuan, Z. Wang, Isotopic evidence for distinct sources of mercury in lake waters and sediments, *Chemical Geology*. 426 (2016) 33–44. <https://doi.org/10.1016/j.chemgeo.2016.01.030>.
- [65] M.D. Cohen, R.R. Draxler, R.S. Artz, P. Blanchard, M.S. Gustin, Y.-J. Han, T.M. Holsen, D.A. Jaffe, P. Kelley, H. Lei, C.P. Loughner, W.T. Luke, S.N. Lyman, D. Niemi, J.M. Pacyna, M. Pilote, L. Poissant, D. Ratte, X. Ren, F. Steenhuisen, A. Steffen, R. Tordon, S.J. Wilson, Modeling the global atmospheric transport and deposition of mercury to the Great Lakes, *Elementa: Science of the Anthropocene*. 4 (2016) 000118. <https://doi.org/10.12952/journal.elementa.000118>.
- [66] S. Guédron, D. Point, D. Acha, S. Bouchet, P.A. Baya, E. Tessier, M. Monperrus, C.I. Molina, A. Groleau, L. Chauvaud, J. Thebault, E. Amice, L. Alanoca, C. Duwig, G. Uzu, X. Lazzaro, A. Bertrand, S. Bertrand, C. Barbraud, K. Delord, F.M. Gibon, C. Ibanez, M. Flores, P. Fernandez Saavedra, M.E. Ezpinoza, C. Heredia, F. Rocha, C. Zepita, D. Amouroux, Mercury contamination level and speciation inventory in Lakes Titicaca & Uru-Uru (Bolivia): Current status and future trends, *Environmental Pollution*. 231 (2017) 262–270. <https://doi.org/10.1016/j.envpol.2017.08.009>.
- [67] C.R. Hammerschmidt, W.F. Fitzgerald, Methylmercury in Freshwater Fish Linked to Atmospheric Mercury Deposition, *Environmental Science & Technology*. 40 (2006) 7764–7770. <https://doi.org/10.1021/es061480i>.
- [68] R.P. Mason, K.A. Sullivan, Mercury in Lake Michigan, *Environmental Science & Technology*. 31 (1997) 942–947. <https://doi.org/10.1021/es960656i>.
- [69] C. Meuleman, M. Leermakers, W. Baeyens, Mercury speciation in Lake Baikal, *Water, Air, & Soil Pollution*. 80 (1995) 539–551. <https://doi.org/10.1007/BF01189704>.
- [70] A. Økelsrud, E. Lydersen, E. Fjeld, Biomagnification of mercury and selenium in two lakes in southern Norway, *Science of The Total Environment*. 566–567 (2016) 596–607. <https://doi.org/10.1016/j.scitotenv.2016.05.109>.
- [71] K.R. Rolfhus, H.E. Sakamoto, L.B. Cleckner, R.W. Stoor, C.L. Babiarz, R.C. Back, H. Manolopoulos, J.P. Hurley, Distribution and Fluxes of Total and Methylmercury in Lake Superior, *Environmental Science & Technology*. 37 (2003) 865–872. <https://doi.org/10.1021/es026065e>.
- [72] J. Wiener, D. Krabbenhoft, G. Heinz, A. Scheuhammer, Ecotoxicology Of Mercury, in: D. Hoffman, B. Rattner, G. Allen Burton Jr, J. Cairns Jr (Eds.), *Handbook of Ecotoxicology*, Second Edition, CRC Press, 2002. <https://doi.org/10.1201/9781420032505.ch16>.
- [73] J.D. Demers, J.D. Blum, D.R. Zak, Mercury isotopes in a forested ecosystem: Implications for air-surface exchange dynamics and the global mercury cycle: MERCURY ISOTOPES IN A FORESTED ECOSYSTEM, *Global Biogeochemical Cycles*. 27 (2013) 222–238. <https://doi.org/10.1002/gbc.20021>.

- [74] M. Morellón, A. Pérez-Sanz, J.P. Corella, U. Büntgen, J. Catalán, P. González-Sampériz, J.J. González-Trueba, J.A. López-Sáez, A. Moreno, S. Pla-Rabes, M.Á. Saz-Sánchez, P. Scussolini, E. Serrano, F. Steinhilber, V. Stefanova, T. Vegas-Vilarrúbia, B. Valero-Garcés, A multi-proxy perspective on millennium-long climate variability in the Southern Pyrenees, *Clim. Past.* 8 (2012) 683–700. <https://doi.org/10.5194/cp-8-683-2012>.
- [75] S. Desprat, M.F. Sánchez Goñi, M.-F. Loutre, Revealing climatic variability of the last three millennia in northwestern Iberia using pollen influx data, *Earth and Planetary Science Letters.* 213 (2003) 63–78. [https://doi.org/10.1016/S0012-821X\(03\)00292-9](https://doi.org/10.1016/S0012-821X(03)00292-9).
- [76] A. Spolaor, E. Barbaro, D. Cappelletti, C. Turetta, M. Mazzola, F. Giardi, M.P. Björkman, F. Lucchetta, F. Dallo, K.A. Pfaffhuber, H. Angot, A. Dommergue, M. Maturilli, A. Saiz-Lopez, C. Barbante, W.R.L. Cairns, Diurnal cycle of iodine, bromine, and mercury concentrations in Svalbard surface snow, *Atmospheric Chemistry and Physics.* 19 (2019) 13325–13339. <https://doi.org/10.5194/acp-19-13325-2019>.
- [77] W. Yuan, J. Sommar, C.-J. Lin, X. Wang, K. Li, Y. Liu, H. Zhang, Z. Lu, C. Wu, X. Feng, Stable Isotope Evidence Shows Re-emission of Elemental Mercury Vapor Occurring after Reductive Loss from Foliage, *Environmental Science & Technology.* 53 (2019) 651–660. <https://doi.org/10.1021/acs.est.8b04865>.